

AD-764 986

EXPERIMENTAL PROGRAM FOR THE DEVELOPMENT OF IMPROVED HELICOPTER STRUCTURAL CRASHWORTHINESS ANALYTICAL AND DESIGN TECHNIQUES. VOLUME II. TEST DATA AND DESCRIPTION OF AN UNSYMMETRICAL CRASH ANALYSIS COMPUTER PROGRAM, INCLUDING A USER'S GUIDE AND SAMPLE CASE

Gilbert Wittlin, et al

Lockheed-California Company

Prepared for:

Army Air Mobility Research and Development  
Laboratory

May 1973

DISTRIBUTED BY:

**NTIS**

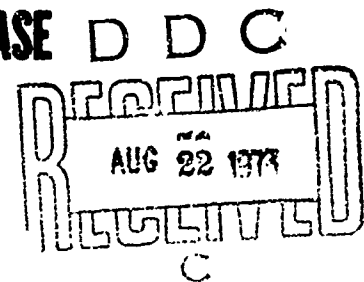
National Technical Information Service  
U. S. DEPARTMENT OF COMMERCE  
5285 Port Royal Road, Springfield Va. 22151

AD

**USAAMRDL TECHNICAL REPORT 72-72B**  
**EXPERIMENTAL PROGRAM FOR THE DEVELOPMENT OF IMPROVED**  
**HELICOPTER STRUCTURAL CRASHWORTHINESS**  
**ANALYTICAL AND DESIGN TECHNIQUES**

**VOLUME II**

**AD 764986** **TEST DATA AND DESCRIPTION OF AN UNSYMMETRICAL**  
**CRASH ANALYSIS COMPUTER PROGRAM, INCLUDING**  
**A USER'S GUIDE AND SAMPLE CASE**



By  
E. Wittlin  
M. A. Gamon

May 1973

**EUSTIS DIRECTORATE**  
**U. S. ARMY AIR MOBILITY RESEARCH AND DEVELOPMENT LABORATORY**  
**FORT EUSTIS, VIRGINIA**

**CONTRACT DAAJ02-71-C-0066**  
**LOCKHEED-CALIFORNIA COMPANY**  
**BURLAND, CALIFORNIA**

Approved for public release;  
distribution unlimited.



Reproduced by  
**NATIONAL TECHNICAL**  
**INFORMATION SERVICE**  
U S Department of Commerce  
Springfield VA 22151

7027

### DISCLAIMERS

The findings in this report are not to be construed as an official Department of the Army position unless so designated by other authorized documents.

When Government drawings, specifications, or other data are used for any purpose other than in connection with a definitely related Government procurement operation, the U.S. Government thereby incurs no responsibility nor any obligation whatsoever; and the fact that the Government may have formulated, furnished, or in any way supplied the said drawings, specifications, or other data is not to be regarded by implication or otherwise as in any manner licensing the holder or any other person or corporation, or conveying any rights or permission, to manufacture, use, or sell any patented invention that may in any way be related thereto.

Trade names cited in this report do not constitute an official endorsement or approval of the use of such commercial hardware or software.

### DISPOSITION INSTRUCTIONS

Destroy this report when no longer needed. Do not return it to the originator.

FORM 107-107	
FILE	CLASSIFIED <input checked="" type="checkbox"/>
1	EXCLUDED <input type="checkbox"/>
2	EXCLUDED <input type="checkbox"/>
BY	
AVAILABILITY CODES	
SPECIAL	
A	AE

Unclassified  
Security Classification

DOCUMENT CONTROL DATA - R & D

(Security classification of title, body of abstract and indexing annotation must be entered when the overall report is classified)

1. ORIGINATING ACTIVITY (Corporate author) Lockheed-California Company Burbank, California		2a. REPORT SECURITY CLASSIFICATION Unclassified	
		2b. GROUP	
3. REPORT TITLE EXPERIMENTAL PROGRAM FOR THE DEVELOPMENT OF IMPROVED HELICOPTER STRUCTURAL CRASH-WORTHINESS ANALYTICAL AND DESIGN TECHNIQUES, VOLUME II - TEST DATA AND DESCRIPTION OF AN UNSYMMETRICAL CRASH ANALYSIS COMPUTER PROGRAM, INCLUDING A USER'S GUIDE AND SAMPLE CASE			
4. DESCRIPTIVE NOTES (Type of report and inclusive dates)			
5. AUTHOR(S) (First name, middle initial, last name) Gilbert Wittlin Max A. Gamon			
6. REPORT DATE May 1973		7a. TOTAL NO. OF PAGES 448 249	7b. NO. OF REFS 48
8a. CONTRACT OR GRANT NO. DAAJ02-71-C-0066 8. PROJECT NO. Task 1F162203A52902 c. d.		9a. ORIGINATOR'S REPORT NUMBER(S) USAAHRDL Technical Report 72-72B 9b. OTHER REPORT NO(S) (Any other numbers that may be assigned this report)	
10. DISTRIBUTION STATEMENT Approved for public release; distribution unlimited.			
11. SUPPLEMENTARY NOTES Volume II of a 2-volume report		12. SPONSORING MILITARY ACTIVITY Eustis Directorate, U.S. Army Air Mobility Research and Development Laboratory, Fort Eustis, Virginia	
13. ABSTRACT Volume II contains supporting data for the details presented in Volume I. This volume contains abstracts for the 32 technical reports reviewed during the program. Included in the literature survey section is a matrix categorization of the reports by subject and applicable areas of interest. A brief description is presented on STAGS, the LMSC computer program used to perform the analysis of the P2V-4 fuselage bumper. A comprehensive description of program KRASH is presented, including the theory, initial conditions, the User's Guide, and a sample problem. Twenty-six channels of recorded test data and film data are presented in another section. Additional analytical data are presented in the last section.			

DD FORM 1473

REPLACES DD FORM 1473, 1 JAN 64, WHICH IS OBSOLETE FOR ARMY USE

1a

Unclassified

Security Classification



14. KEY WORDS	LINK A		LINK B		LINK C	
	ROLE	WT	ROLE	WT	ROLE	WT
nonlinear behavior dynamic response crashworthiness impact dynamics structural dynamics design criteria and concepts crash environment analytical techniques experimental program accident analysis human tolerance survivable accident load deflection energy absorption mathematical simulation Dynamic Response Index structural deformation design tradeoff						

12

Unclassified  
Security Classification



DEPARTMENT OF THE ARMY  
U. S. ARMY AIR MOBILITY RESEARCH & DEVELOPMENT LABORATORY  
EUSTIS DIRECTORATE  
FORT EUSTIS, VIRGINIA 23604

This report was prepared by Lockheed-California Company under the terms of Contract DAAJ02-71-C-0066. The Eustis Directorate technical monitor for this effort was Mr. G. T. Singley III of the Military Operations Technology Division.

The purpose of this effort was to develop (1) a computerized mathematical simulation which can predict the dynamic response of U.S. Army helicopters exposed to a crash environment with combined vertical and lateral impact velocity components, and (2) design techniques which, when implemented, will enhance occupant survival and reduce materiel losses during severe yet survivable helicopter accidents. The contractor achieved these objectives by (1) conducting literature, accident data, and organizational surveys, (2) developing a 40-mass, 240-degree-of-freedom, nonlinear lumped mass mathematical model, (3) tailoring the model to represent the UH-1D/H aircraft, (4) correlating the computerized UH-1D/H mathematical model with the results of a full-scale UH-1D/H drop test, and (5) conducting parametric studies to analyze the effect of design changes on system crashworthiness. This report contains a description of the state-of-the-art surveys, mathematical model, parametric studies, supporting testing, and results obtained.

The conclusions and recommendations submitted by the contractor are considered to be valid.

The report is divided into two volumes. Volume I contains a description of the state-of-the-art surveys, mathematical model, testing, parametric study, and results obtained. Volume II contains abstracts of literature reviewed, a comprehensive description of the mathematical model, a user's guide for the computer program, and the full-scale crash test instrumentation and photographic data.

Task 1F162203A52902  
Contract DAAJ02-71-C-0066  
USAMRD Technical Report 72-728  
May 1973

EXPERIMENTAL PROGRAM FOR THE DEVELOPMENT OF IMPROVED  
HELICOPTER STRUCTURAL CRASHWORTHINESS  
ANALYTICAL AND DESIGN TECHNIQUES

VOLUME II

TEST DATA AND DESCRIPTION OF AN UNSYMMETRICAL  
CRASH ANALYSIS COMPUTER PROGRAM, INCLUDING A  
USER'S GUIDE AND SAMPLE CASE

by

G. Wittlin

M. A. Gannon

Prepared by

Lockheed-California Company

Rurbank, California

for

EUSTIS DIRECTORATE  
U. S. ARMY AIR MOBILITY RESEARCH AND DEVELOPMENT LABORATORY  
FORT EUSTIS, VIRGINIA

Approved for public release;  
distribution unlimited.

## SUMMARY

Volume II contains supporting data for the details presented in Volume I. This volume contains abstracts for the 32 technical reports reviewed during the program. Included in the literature survey section is a matrix categorization of the reports by subject and applicable areas of interest. A brief description is presented on STAGS, the LMSC computer program used to perform the analysis of the P2V-4 fuselage bumper. A comprehensive description of program KRASH is presented, including the theory, initial conditions, the User's Guide, and a sample problem. Twenty-six channels of recorded test data, 13 channels of filtered data, and 48 channels of integrated test data and film data are presented in another section. Additional analytical data are presented in the last section.

## TABLE OF CONTENTS

	<u>Page</u>
SUMMARY . . . . .	iii
LIST OF ILLUSTRATIONS . . . . .	vii
LIST OF TABLES . . . . .	xiii
LIST OF SYMBOLS . . . . .	xiv
INTRODUCTION . . . . .	1
LITERATURE SURVEY . . . . .	2
Literature Synopsis . . . . .	2
DESCRIPTION OF STAGS (STRUCTURAL ANALYSIS OF GENERAL SKELLS) PROGRAM . . . . .	21
MATHEMATICAL MODEL DESCRIPTION . . . . .	23
Program KRASH Description . . . . .	23
Theory . . . . .	25
Mathematical Model of Helicopter . . . . .	25
Coordinate Systems . . . . .	25
Relations Between Coordinate Systems . . . . .	27
Sign Conventions . . . . .	29
Forces Acting on Each Mass . . . . .	29
Total Forces and Moments at $m_1$ ( $X_1, Y_1, Z_1, L_1, M_1$ , and $N_1$ ) . . . . .	68
Rigid Body Equations of Motion of Each Mass . . . . .	69
Control Volume Mass Penetration Calculations . . . . .	75
Dynamic Response Index (DRI) . . . . .	73
Integration Routine . . . . .	75
Initial Conditions . . . . .	76
User's Guide . . . . .	87
Input . . . . .	87
Print Output . . . . .	96
Sample Case . . . . .	99
Program Listing . . . . .	99

	<u>Page</u>
TEST DATA . . . . .	153
Recorded Data . . . . .	153
100 cps Low-Pass Filtered Test Data . . . . .	153
Time Histories of Integrated Data . . . . .	176
Impact Velocity Data . . . . .	176
Calculated Test Impact Velocities . . . . .	205
ANALYTICAL DATA . . . . .	208
Computer Output Correlation Run . . . . .	208
Comparison of Analytical and Test Results - Axial Responses . . . . .	208
LITERATURE CITED . . . . .	225
DISTRIBUTION . . . . .	229

# LIST OF ILLUSTRATIONS

<u>Figure</u>		<u>Page</u>
1	Mathematical Model of Helicopter . . . . .	26
2	Beam Deflections . . . . .	33
3	Beam Loads . . . . .	40
4	Loading - Unloading Model . . . . .	41
5	Internal Load Algorithm . . . . .	42
6	Beam Internal Load Static Balance . . . . .	44
7	External Spring Compression Geometry . . . . .	50
8	External Spring Load-Stroke Curve . . . . .	57
9	External Load Calculation . . . . .	59
10	Crash Forces and Moments . . . . .	61
11	Numerical Integration Flow Diagram . . . . .	77
12	Euler Angles $\Theta_{ij}$ and $\Psi_{ij}$ . . . . .	85
13	Computation of $\Theta_{ij}$ and $\Psi_{ij}$ . . . . .	86
14	Input Data Format . . . . .	91
15	Output Data Format . . . . .	97
16	Sample 31 Mass Case Input Data . . . . .	100
17	Sample Case, Engine Vertical Velocity Time History Plot. .	111
18	Sample Case, Engine Vertical Acceleration Time History Plot . . . . .	112
19	Sample Case, Engine Mount Vertical Deflection Time History Plot . . . . .	113
20	Program Listing . . . . .	114
21	Recorded Time History, Pilot Seat Pan, Vertical Acceleration (Channel 07) . . . . .	154

<u>Figure</u>		<u>Page</u>
22	Recorded Time History, Pilot Seat Pan, Lateral Acceleration (Channel 08) . . . . .	154
23	Recorded Time History, Copilot Seat Pan, Vertical Acceleration (Channel 09) . . . . .	155
24	Recorded Time History, Copilot Seat Pan, Lateral Acceleration (Channel 10) . . . . .	155
25	Recorded Time History, Floor Copilot Location, Vertical Acceleration (Channel 30) . . . . .	156
26	Recorded Time History, Floor Copilot Location, Lateral Acceleration (Channel 31) . . . . .	156
27	Recorded Time History, Floor Pilot Location, Vertical Acceleration (Channel 32) . . . . .	157
28	Recorded Time History, Floor Pilot Location, Lateral Acceleration (Channel 33) . . . . .	157
29	Recorded Time History, Cargo Floor Forward Right, Vertical Acceleration (Channel 34) . . . . .	158
30	Recorded Time History, Cargo Floor Forward Right, Lateral Acceleration (Channel 35) . . . . .	158
31	Recorded Time History, PAX Floor Rear Left, Vertical Acceleration (Channel 36) . . . . .	159
32	Recorded Time History, PAX Floor Rear Left, Lateral Acceleration (Channel 37) . . . . .	159
33	Recorded Time History, Cargo Floor Forward Left, Vertical Acceleration (Channel 38) . . . . .	160
34	Recorded Time History, Cargo Floor Forward Left, Lateral Acceleration (Channel 39) . . . . .	161
35	Recorded Time History, Transmission Rotor Housing, Vertical Acceleration (Channel 40) . . . . .	162
36	Recorded Time History, Transmission Rotor Housing, Lateral Acceleration (Channel 41) . . . . .	162



<u>Figure</u>		<u>Page</u>
37	Recorded Time History, Transmission Rotor Housing, Axial Acceleration (Channel 42) . . . . .	163
38	Recorded Time History, Engine, Vertical Acceleration (Channel 43) . . . . .	163
39	Recorded Time History, Engine, Lateral Acceleration (Channel 44) . . . . .	164
40	Recorded Time History, Engine, Axial Acceleration (Channel 45) . . . . .	164
41	Recorded Time History, Tail Rotor Gearbox, Vertical Acceleration (Channel 46) . . . . .	165
42	Recorded Time History, Tail Rotor Gearbox, Lateral Acceleration (Channel 47) . . . . .	165
43	Recorded Time History, Passenger Pelvic, Vertical Acceleration (Channel 48) . . . . .	166
44	Recorded Time History, Passenger Pelvic, Lateral Acceleration (Channel 60) . . . . .	166
45	Recorded Time History, Forward Strut, Left Side Strain Gage (Channel 61) . . . . .	167
46	Recorded Time History, Rear Strut, Left Side Strain Gage (Channel 62) . . . . .	168
47	100-CPS Low-Pass Filtered Test Data, Pilot Seat Pan, Vertical Acceleration (Channel 07) . . . . .	169
48	100-CPS Low-Pass Filtered Test Data, Pilot Seat Pan, Lateral Acceleration (Channel 08) . . . . .	170
49	100-CPS Low-Pass Filtered Test Data, Copilot Seat Pan, Vertical Acceleration (Channel 09) . . . . .	170
50	100-CPS Low-Pass Filtered Test Data, Copilot Seat Pan, Lateral Acceleration (Channel 10) . . . . .	171
51	100-CPS Low-Pass Filtered Test Data, Copilot Floor, Vertical Acceleration (Channel 30) . . . . .	171

<u>Figure</u>		<u>Page</u>
52	100-CPS Low-Pass Filtered Test Data, Copilot Floor, Lateral Acceleration (Channel 31) . . . . .	172
53	100-CPS Low-Pass Filtered Test Data, Passenger Floor, Vertical Acceleration (Channel 36) . . . . .	172
54	100-CPS Low-Pass Filtered Test Data, Transmission Rotor Housing, Vertical Acceleration (Channel 40) . . . . .	173
55	100-CPS Low-Pass Filtered Test Data, Transmission Rotor Housing, Lateral Acceleration (Channel 41) . . . . .	173
56	100-CPS Low-Pass Filtered Test Data, Transmission Rotor Housing, Axial Acceleration (Channel 42) . . . . .	174
57	100-CPS Low-Pass Filtered Test Data, Engine, Vertical Acceleration (Channel 43) . . . . .	174
58	100-CPS Low-Pass Filtered Test Data, Engine, Lateral Acceleration (Channel 44) . . . . .	174
59	100-CPS Low-Pass Filtered Test Data, Engine, Axial Acceleration (Channel 45) . . . . .	175
60	Integrated Velocities, Pilot Seat Pan . . . . .	177
61	Integrated Velocities, Copilot Seat Pan . . . . .	178
62	Integrated Velocities, Floor, Copilot Location . . . . .	179
63	Integrated Velocities, Floor, Pilot Location . . . . .	180
64	Integrated Velocities, Cargo Floor, Forward Right . . . . .	181
65	Integrated Velocities, Passenger Floor, Rear Left . . . . .	182
66	Integrated Velocities, Cargo Floor, Forward Left . . . . .	183
67	Integrated Velocities, Transmission Rotor Housing . . . . .	184
68	Integrated Velocities, Engine . . . . .	185
69	Integrated Velocities, Tail Rotor Gearbox . . . . .	186

<u>Figure</u>		<u>Page</u>
70	Integrated Velocities, Passenger Pelvic . . . . .	187
71	Integrated Displacements, Pilot Seat Pan . . . . .	188
72	Integrated Displacements, Copilot Seat Pan . . . . .	189
73	Integrated Displacements, Floor, Copilot Location . . . .	190
74	Integrated Displacements, Floor, Pilot Location . . . . .	191
75	Integrated Displacements, Cargo Floor Forward Right . . .	192
76	Integrated Displacements, Passenger Floor Rear Left . . .	193
77	Integrated Displacements, Cargo Floor Forward Left . . . .	194
78	Integrated Displacements, Transmission Rotor Housing . . .	195
79	Integrated Displacements, Engine . . . . .	196
80	Integrated Displacement, Tail Rotor Gearbox, Vertical, Channel 46 . . . . .	197
81	Integrated Displacement, Tail Rotor Gearbox, Lateral, Channel 47 . . . . .	198
82	Integrated Displacement, Passenger Pelvic . . . . .	199
83	Sequence of Events - Film Data . . . . .	200
84	Vertical Impact Velocity - Film Data . . . . .	201
85	Lateral Impact Velocity - Film Data . . . . .	202
86	Vertical Displacement - Film Data . . . . .	203
87	Lateral Displacement - Film Data . . . . .	204
88	Correlation Run Analysis Output, Aft Floor, Lateral Velocity Time History . . . . .	209
89	Correlation Run Analysis Output, Forward Floor, Lateral Velocity Time History . . . . .	210

<u>Figure</u>		<u>Page</u>
90	Correlation Run Analysis Output, Aft Floor, Vertical Velocity Time History . . . . .	211
91	Correlation Run Analysis Output, Forward Floor, Vertical Velocity Time History . . . . .	212
92	Correlation Run Analysis Output, Engine, Lateral Acceleration Time History . . . . .	213
93	Correlation Run Analysis Output, Transmission Rotor Housing, Lateral Acceleration Time History . . . . .	214
94	Correlation Run Analysis Output, Mid-Floor, Lateral Acceleration Time History . . . . .	215
95	Correlation Run Analysis Output, Engine, Vertical Acceleration Time History . . . . .	216
96	Correlation Run Analysis Output, Transmission Rotor Housing, Vertical Acceleration Time History . . . . .	217
97	Correlation Run Analysis Output, Mid-Floor, Vertical Acceleration Time History . . . . .	218
98	Correlation Run Analysis Output, Engine Mount, Vertical Deflection Time History . . . . .	219
99	Correlation Run Analysis Output, Transmission Mount, Vertical Deflection Time History . . . . .	220
100	Correlation Run Analysis Output, Forward Seated Occupant, Vertical Deflection Time History . . . . .	221
101	Correlation, Transmission Rotor Housing Axial Acceleration . . . . .	222
102	Correlation, Engine Axial Acceleration . . . . .	222
103	Correlation, Transmission Rotor Housing Axial Velocity . . . . .	223
104	Correlation, Engine Axial Velocity . . . . .	223

<u>Figure</u>		<u>Page</u>
105	Correlation, Transmission Rotor Housing Axial Displacement . . . . .	224
106	Correlation, Engine Axial Displacement . . . . .	224

#### LIST OF TABLES

<u>Table</u>		<u>Page</u>
I	Literature Survey Subject Index . . . . .	20
II	Transformation Matrices . . . . .	28

## LIST OF SYMBOLS

### MATHEMATICAL MODEL

$A_i, B_i, C_i$	Terms used in Euler's equations of motion (68)
$[A_i]$	Rotation transformation matrix from body axes to ground axes
$[\bar{A}_i]$	Matrix relating $(\phi_i, \theta_i, \psi_i)$ to $(p_i, q_i, r_i)$ in equation (92)
$[\dot{A}_i]$	Time derivative of $[A_i]$
$[A_i'']$	Rotation transformation matrix from ith body axes to c.g. axes
$[A_{ij}]$	Rotation transformation matrix from beam ij axes to body i axes
$[A']$	Rotation transformation matrix from c.g. axes to ground axes
$[\bar{A}']$	Matrix relating $(\phi', \theta', \psi')$ to $(p', q', r')$ in equation (88)
$C_{ik}$	End point of kth spring on ith mass
$C_{ik}^i$	Ground contact point of kth spring on ith mass
$dvc_{ijk}$	Ground axes components of vector from $m_i$ to $C_{ik}$
$dvc_{ijk}^i$	Ground axes components of vector for $C_{ik}^i$ to $C_{ik}$
$[D_i]$	Derivative matrix used in equation (2)
$[D']$	Derivative matrix used in equation (86)
$FM_{ijkl}$	Running time sum of $\Delta FM_{ijkl}$
$\overline{FM}_{ijkl}$	Value of $FM_{ijkl}$ at time of loading reversal
$FSP_{ijk}$	Body i axes components of spring force at ground contact point $C_{ik}$
$FSP_{0,ik}$	Axial compressive force in kth spring on ith mass
$\overline{FSP}_{0,ik}$	Value of $FSP_{0,ik}$ at time of loading reversal

# LIST OF SYMBOLS

## MATHEMATICAL MODEL

$FSPO_{Fik}$	Final value of $FSPO_{ik}$ in input table of $s_{ik}$ vs. $FSPO_{ik}$
G	Center-of-gravity of total vehicle
H	Origin of helicopter coordinate system (F.S.O, B.L.O, W.L.O)
$He_{xi}, He_{yi}, He_{zi}$	Angular momenta of $m_i$ due to rotation of masses internal to $m_i$
$I_{xi}, I_{yi}, I_{zi}$	Moments of inertia of lumped mass $m_i$ , about $i$ th body fixed axes
$I_{xyi}, I_{yzi}, I_{zxi}$	Products of inertia of lumped mass $m_i$ , about $i$ th body fixed axes
$ke_{ik}$	Linear unloading stiffness for $k$ th spring
$[K_{ij}]$	Six by six linear stiffness matrix for beam $ij$
$[KR_{ij}]$	Six by six diagonal stiffness reduction matrix for beam $ij$ .
$l_{ik}$	Length of vector from $m_i$ to ground contact point $C'_{ik}$
$\bar{l}_{xi}, \bar{l}_{yi}, \bar{l}_{zi}(\bar{l}_{ik})$	Free length of $k$ th spring on $i$ th mass
$l_{ci}$	Aerodynamic lift constant
$LIFT_i$	Aerodynamic lift on $m_i$ , positive up, in ground axes
$m_i$	$i$ th lumped mass
$\mu_{ik}$	Ground-spring friction coefficient for $k$ th spring on $i$ th mass
N	Total number of lumped masses
$\bar{n}_{ik}$	Unit vector triad fixed in $i$ th body coordinate system
$\bar{n}_x, \bar{n}_y, \bar{n}_z$	Unit vector triad fixed in ground coordinate system
O	Origin of ground coordinate system

## LIST OF SYMBOLS




### MATHEMATICAL MODEL

$p_i, q_i, r_i$	$i$ th body axes components of absolute angular velocity vector of mass $i$
$p', q', r'$	c.g. axes components of initial( $t=0$ ) vehicle angular velocity vector
$[p]_i$	Contact point velocity matrix used in equation (60)
$s_{ik}$	Axial external spring compression, $k$ th spring on $i$ th mass
$\bar{s}_{ik}$	Value of $s_{ik}$ at time of loading reversal
$s_{fik}$	Final value of $s_{ik}$ in input table of $s_{ik}$ vs. $FSPO_{ik}$
$s_{ik}$	$k$ th spring axial compression measured relative to current load stroke curve origin
$s''_{ik}$	Horizontal shift of $s_{ik}$ coordinates with respect to $S_{ik}$ coordinates
$t$	Time
$[T]_{ij}$	Static balance matrix used in equation (30b)
$u_i, v_i, w_i$	Body $i$ axes components of absolute translational velocity vector of point $a_i$
$va_{ij}$	$x_i, y_i, z_i$
$vb_{ij}$	Running time sum of $\Delta vb_{ij}$
$\bar{vb}_{ijl}$	Value of $vb_{ijl}$ at time of loading reversal
$\bar{v}_{ik}$	Magnitude of ground plane contact point velocity
$vb^i_{ijl}$	$i$ th total beam deflection measured relative to current load-stroke curve origin
$vb''_{ijl}$	Horizontal shift of $vb^i_{ijl}$ coordinates with respect to $vb_{ijl}$ coordinates
$vc_{ijk}$	Ground coordinates of point $C_{ik}$



## LIST OF SYMBOLS

### MATHEMATICAL MODEL

$\dot{v}_{CP_{1jk}}$	Ground axes components of absolute velocity of ground contact point $C_{1k}$
	Velocity vector of $C_{1k}$ with respect to $m_1$
	Velocity vector of $C_{1k}$ with respect to ground
	Velocity vector of $m_1$ with respect to ground
$W_1$	Weight of $i$ th lumped mass
$W_{TOT}$	Total vehicle weight
$x_{b1j}, y_{b1j}, z_{b1j}$	Beam $ij$ coordinates
$x_G, y_G, z_G$ ( $v_{Gj}$ )	Ground coordinates of initial ( $t = 0$ ) c.g. position
$\dot{x}_G, \dot{y}_G, \dot{z}_G$	Ground axes components of initial ( $t = 0$ ) c.g. velocity vector
$x_G'', y_G'', z_G''$ ( $v_{GPP_{1j}}$ )	Helicopter axes coordinates of vehicle c.g. (point G)
$x_1, y_1, z_1$ ( $v_{a1j}$ )	Ground coordinates of $m_1$
$x_1^i, y_1^i, z_1^i$ ( $v_{iP_{1j}}$ )	Coordinates of $m_1$ in center-of-gravity coordinate system
$x_1'', y_1'', z_1''$ ( $v_{iPP_{1j}}$ )	Coordinates of $m_1$ in helicopter coordinate system
$x_{1j}, y_{1j}, z_{1j}$	Ground coordinates of vector from point $i$ to point $j$
$\dot{x}_{1j}, \dot{y}_{1j}, \dot{z}_{1j}$	$i$ th body coordinates of vector from point $i$ to point $j$
$\begin{pmatrix} X_{1j}^i & Y_{1j}^i & Z_{1j}^i \\ L_{1j}^i & M_{1j}^i & N_{1j}^i \end{pmatrix}^0$	Total (summed over time) internal forces and moments at point $i$ due to beam $ij$ , body $i$ axes
$\begin{pmatrix} X_{j1}^i & Y_{j1}^i & Z_{j1}^i \\ L_{j1}^i & M_{j1}^i & N_{j1}^i \end{pmatrix}$	Total (summed over time) internal forces and moments at point $j$ due to beam $ij$ , body $j$ axes

# LIST OF SYMBOLS

## MATHEMATICAL MODEL

$\begin{pmatrix} X_1, Y_1, Z_1 \\ L_1, M_1, N_1 \end{pmatrix}$	Total forces and moments on mass 1, in 1th body axes
$X_{A1}, Y_{A1}, Z_{A1}$	Aerodynamic forces, body 1 axes
$\begin{pmatrix} X_{C1}, Y_{C1}, Z_{C1} \\ L_{C1}, M_{C1}, N_{C1} \end{pmatrix}$	Crash (external) forces and moments, body 1 axes
$X_{G1}, Y_{G1}, Z_{G1}$	Gravity forces, body 1 axes
$\begin{pmatrix} X_{I1}, Y_{I1}, Z_{I1} \\ L_{I1}, M_{I1}, N_{I1} \end{pmatrix}$	Internal forces and moments, body 1 axes
$XVOC_{ijk}$	Ground axes components of spring force at ground contact point $C_{ik}$ , positive up, left and aft
$z_{MAX}^c$	Vertical distance from c.g. to lowest $C_{ik}$
$\Delta_i$	Determinate expression used in equation (58)
$\Delta F_{ijk}$	Incremental forces and moments at point j due to beam ij
$\Delta F_{ijk}^{FM}$	kth incremental load due to lth incremental deflection for beam ij
$\Delta \phi_{1j}, \Delta \theta_{1j}, \Delta \psi_{1j}$	Incremental rotations of point j with respect to point 1, in beam ij axes
$\Delta \phi_1, \Delta \theta_1, \Delta \psi_1$	Incremental change in 1th mass Euler angles
$\Delta t$	Numerical integration time interval
$\Delta v_{bij}$	Six element vector made up of $\Delta x_{bij}, \Delta y_{bij}, \Delta z_{bij}, \Delta \phi_{bij}, \Delta \theta_{bij}, \Delta \psi_{bij}$
$\overrightarrow{\Delta v_{bij}}$	Incremental displacement vector of point j with respect to point 1, due to deformation of beam ij
$\overrightarrow{\Delta v_{dij}}$	Incremental displacement vector of point j with respect to point i

# LIST OF SYMBOLS

## MATHEMATICAL MODEL

$$\overrightarrow{\Delta \mathbf{r}_{ij}}$$

Incremental displacement vector of point j with respect to point i, due to rotation of mass i

$$\Delta x_{bij}, \Delta y_{bij}, \Delta z_{bij}$$

Coordinates of  $\overrightarrow{\Delta \mathbf{r}_{bij}}$  in beam ij axes

$$\Delta x_i, \Delta y_i, \Delta z_i$$

incremental displacement of point i, ground axes

$$\Delta x_{ij}, \Delta y_{ij}, \Delta z_{ij}$$

Incremental displacement of point j with respect to point i in ground axes

$$\begin{pmatrix} \Delta X_{ij}, \Delta Y_{ij}, \Delta Z_{ij} \\ \Delta L_{ij}, \Delta M_{ij}, \Delta N_{ij} \end{pmatrix}$$

Incremental internal forces and moments at point j due to beam ij, in beam ij axes (elements of  $\Delta \mathbf{F}_{ij}$  vector)

$$\begin{pmatrix} \Delta X_{ij}^o, \Delta Y_{ij}^o, \Delta Z_{ij}^o \\ \Delta L_{ij}^o, \Delta M_{ij}^o, \Delta N_{ij}^o \end{pmatrix}$$

Incremental internal forces and moments at point j due to beam ij, ground axes

$$\begin{pmatrix} \overline{\Delta X_{ij}^o}, \overline{\Delta Y_{ij}^o}, \overline{\Delta Z_{ij}^o} \\ \overline{\Delta L_{ij}^o}, \overline{\Delta M_{ij}^o}, \overline{\Delta N_{ij}^o} \end{pmatrix}$$

Incremental internal forces and moments at point i due to beam ij, ground axes

$$\begin{pmatrix} \Delta X_{ij}^i, \Delta Y_{ij}^i, \Delta Z_{ij}^i \\ \Delta L_{ij}^i, \Delta M_{ij}^i, \Delta N_{ij}^i \end{pmatrix}$$

Incremental internal forces and moments at point i due to beam ij, body i axes

$$\begin{pmatrix} \Delta X_{ji}^i, \Delta Y_{ji}^i, \Delta Z_{ji}^i \\ \Delta L_{ji}^i, \Delta M_{ji}^i, \Delta N_{ji}^i \end{pmatrix}$$

Incremental internal forces and moments at point j due to beam ij, body j axes

$$\phi_i, \theta_i, \psi_i$$

Euler angles from ground axes to body axes (time varying)

$$\phi_{ij}, \theta_{ij}, \psi_{ij}$$

Euler angles from ith body axes to beam ij axes (constant)

$$\phi^i, \theta^i, \psi^i$$

Euler angles from ground axes to c.g. axes (constant); initial (t=0) attitude of vehicle

$$\phi_i'', \theta_i'', \psi_i''$$

Euler angles from c.g. axes to ith body axes (constant)

## INTRODUCTION

This report contains test and analysis data in support of the detailed discussions presented in Volume I. The format in this volume is consistent with the order of the major sections of Volume I.

The 32 technical reports and specifications reviewed during the study are briefly summarized and then tabulated in a Literature Survey Subject Index. Program STAGS is briefly described in the next section. This is followed by a comprehensive description of Program KRASH, including input and output data formats and a sample problem.

The test data is presented in the form of:

- recorded acceleration and strain gage time histories
- 100-cps low-pass filtered acceleration histories
- integrated velocity time histories
- integrated displacement time histories
- film data
- calculated test impact velocities

The analytical data consists of sample output plots obtained with program KRASH during the correlation analysis.

## LITERATURE SURVEY

### LITERATURE SYNOPSIS

1. Reed, William, Avery, James Ph.D., PRINCIPLES FOR IMPROVING STRUCTURAL CRASHWORTHINESS FOR STOL AND CTOL AIRCRAFT, Aviation Safety Engineering and Research; USAAVLABS Technical Report 66-39, U. S. Army Aviation Materiel Laboratories, Fort Eustis, Virginia, June 1966, AD 637133.

In this report, the area of crash behavior analysis of aircraft structures is investigated. The investigation begins with the definition of two indices of crashworthiness of basic aircraft structures and the analysis of the influence of several general types of structural modifications upon these two indices. This analysis, using fundamental principles of mechanics, contains several simplifying assumptions, which are explained as they are introduced.

Design concepts to improve the ability of the "protective container" to maintain living space for occupants during a crash or to attenuate the accelerations experienced by occupants during a crash are developed for crash conditions which are either primarily longitudinal in nature or primarily vertical in nature. Analytical methods are then provided to show how and when to apply these design concepts to any particular aircraft. Principles are presented which are considered to be suitable for use during design of new aircraft as well as modifications of existing aircraft.

The results are presented from three full-scale crash tests of small twin-engine airplanes which were conducted as a part of this investigation.

Among the pertinent conclusions of the report are: (1) improvements in crashworthiness can be achieved via minor changes in structural design or modification of existing structure, (2) vertical and longitudinal impact environments offer significantly different problems in designing for improved crashworthiness, and (3) analysis of aircraft behavior is hampered by the lack of adequate knowledge of the relationships which apply to the determination of the reaction force which decelerates the aircraft upon contact with the ground.

2. Turnbow, J. W., Carroll, D. F., Haley, J. L., Jr. Robertson, S. N. CRASH SURVIVAL DESIGN GUIDE, Dynamic Science; USAAVLABS Technical Report 70-22, U. S. Army Aviation Materiel Laboratories, Fort Eustis, Virginia, August 1969, AD 695648. (Most recent revision is USAAMRDL TR 71-22, AD 733358)

This report is a design guide that has been assembled to provide the engineer with an understanding of the basic problems associated with the development of crashworthy U. S. Army aircraft. Where possible, solutions to specific problems are indicated. In areas in which little design data are available, only the general philosophy appropriate to the problem solution is presented; the details of such solutions as well as the degree of crashworthiness to be achieved must be left, at present, to the ingenuity of the designer.

This guide presents, in a condensed form, the data, design techniques, and criteria that are presently available in eight areas: (1) aircraft crash kinematic and survival envelope, (2) airframe crashworthiness design criteria, (3) aircraft seat design criteria (crew and troop/passenger), (4) restraint system design criteria (crew, troop/passenger, and cargo), (5) occupant environment design criteria, (6) aircraft ancillary equipment stowage design criteria, (7) emergency escape provisions, and (8) postcrash fire design criteria.

It is intended that both airframe and component designers and manufacturers use this guide to extend the "region of survivability" in aircraft accidents to a maximum level.

3. Gatlin, Clifford; Goebel, Donald; and Larsen, Stuart; ANALYSIS OF HELICOPTER STRUCTURAL CRASHWORTHINESS, Dynamic Science; USAAVLABS Technical Report 70-71, Eustis Directorate U. S. Army Air Mobility Research and Development Laboratory, Fort Eustis, Virginia, January 1971, AD 880680 and AD 880678.

This report describes the development of a mathematical model that will simulate the response of a UH-1D/H helicopter airframe to vertical crash loading and the full-scale crash test performed to verify the validity of the model.

In the initial phase of the model development, a study was made of 43 major accidents involving the UH-1D/H aircraft to determine what types of structural failure were contributing to injuries in helicopter accidents.

Based on the results of this accident study, a nonlinear lumped-mass model of 23 degrees of freedom was developed and programmed for computer solution. This model was then used in a parametric study of the UH-1D/H to evaluate potential areas of crashworthiness improvement.

At the conclusion of the parametric study, a full-scale, instrumented drop test of a UH-1D/H airframe was conducted. The data generated in this test were correlated with the model data to determine the ability of the model to predict airframe accelerations and deflections under crash conditions.

The results of this program indicate that:

- The structural weaknesses contributing to most impact injuries in UH-1D/H helicopter accidents are lack of resistance to failure in lateral rollover and lack of energy-absorbing capability to reduce vertical accelerations.
- The mathematical model is capable of accurately predicting the floor and engine accelerations and deflections.
- In its present form, the model does not accurately predict the transmission accelerations and deflections.

It is recommended in the report that further research in the field of mathematical modeling for structural crashworthiness be conducted.

4. Greer, D. L., et al, CRASHWORTHY DESIGN PRINCIPLES, General Dynamics, Convair; FAA Technical Report ADS-24, Federal Aviation Administration, Washington, D. C., November 1965, AD 623575.

The primary areas of study in the investigation of transport aircraft crashworthiness, presented in this report, are as follows:

- Mechanisms of failure and energy absorption structure:
  - To retain habitable shell structure.
- Delethalization:
  - To improve occupant retention system and occupant safety
- Evacuation:
  - Structural integrity on evacuation efficiency

The study indicates that crashworthiness improvements can be realized by increased fuselage strength, redistribution of load-carrying materials in the structure, and the use of more ductile materials in local areas. It is stated in the report that no appreciable weight or cost increase is necessary to improve survivability in a transport aircraft if consideration is given to crashworthy principles at the preliminary design level.

Investigations into occupant retention and safety indicate that seat failures and occupant injuries are probably more often the result of seat and support structure design inadequacies and relative velocity between seat and occupant than of excessive airplane deceleration.

The primary parameters affect the assumptions regarding the crash environment are terrain, descent angle, impact angle and approach velocity.

Although ductility is an important property of airframe structure for crashworthiness design, it is difficult to measure. Elongation, tear resistance, crack propagation, and stress or strain concentration effects are all needed to determine the material best suited to a crashworthy design.

5. Reed, W. H., et al, FULL SCALE DYNAMIC CRASH TEST OF A DOUGLAS DC-7 AIRCRAFT, Aviation Safety Engineering and Research; FAA Technical Report ADS-37, Federal Aviation Administration, Washington, D. C., April 1965, AD 624051.

This report describes a test program designed to obtain crash environment data regarding fuel containment and to collect data on the behavior of various components and equipment aboard the aircraft using a DC-7 as the test vehicle.

The test involved a DC-7 aircraft which was guided into a series of crash barriers with a monorail nose gear guidance system. The aircraft was accelerated under its own power by remote control for a distance of 4000 feet, reaching a velocity of 110 knots. At the end of this acceleration run, the aircraft impacted against a specially designed barrier which removed the landing gear, permitting the aircraft to become airborne until the moment of impact with wing and fuselage crash barriers.

The wing and fuselage barriers were designed to provide the following crash sequence: The left wing was to impact against an earthen mound shaped to produce a simulated wing-low accident. Simultaneously, the right wing was to impact telephone poles implanted vertically to simulate trees. Next, the main fuselage was to impact against an 8-degree slope. The slope was designed so that the aircraft could become airborne after sliding a short distance along the ground. Finally the aircraft was to impact against a 20-degree slope to simulate a crash with a steeper angle of impact.

The test occurred as planned except that the aircraft, instead of coming to rest on the 20-degree slope, bounced over the hill on which the slope was formed and landed at the base of the backside of the hill. A failure of the voltage control regulator, in the data recording system, prevented the program from reaching all its objectives.

6. Reed, W. H., et al, FULL-SCALE DYNAMIC CRASH TEST OF A LOCKHEED CONSTELLATION MODEL 1649 AIRCRAFT, Aviation Safety Engineering and Research; FAA Technical Report ADS-38, Federal Aviation Administration, Washington, D. C., October 1965.

This report provides the details of a full-scale crash test of a large transport aircraft. The purpose of the test was to obtain crash environment data of the test aircraft and the various experiments installed aboard the aircraft.



The Federal Aviation Agency sponsored the test program with the participation of several other organizations who provided data recording equipment and special experiments on board the test aircraft. The participating organizations included the U. S. Navy, the U. S. Army, the U. S. Air Force, the Society of Automotive Engineers, and the Flight Safety Foundation, which conducted the test under contract to and with the guidance of the FAA. The special experiments consisted of military crew and commercial passenger seats, cargo restraint systems, postcrash locator beacons, baby and child restraint systems, radioactive material containers, a military litter system, and provisions for emergency lighting.

The test involved a Lockheed Constellation Model 1649A aircraft, which was guided into a series of crash barriers with a monorail nose gear guidance system. The aircraft was accelerated under its own power by remote control for a distance of 4,000 feet, reaching a velocity of 112 knots. Initial impact occurred against barriers which removed the landing gear, permitting the airplane to become airborne until the moment of impact with the wing and fuselage crash barriers.

The wing fuel tanks were ripped open by the wing barriers, allowing simulated fuel to spill out in a heavy mist during the crash sequence. The fuselage was broken in two places during the crash, just aft of the cockpit between fuselage stations 370 and 380 and just aft of the galley between fuselage stations 1020 and 1030. Peak longitudinal accelerations on the order of 25 G's were measured at the cockpit floor when the aircraft impacted the 20-degree slope. Most of the on-board experiments remained in their relative locations throughout the test.

7. Fitzgibbon, Donald P., et al, CRASH LOADS ENVIRONMENT STUDY, Mechanics Research, Inc.; FAA Technical Report DS-67-2, Federal Aviation Administration, Washington, D. C., February 1967, AD 655920.

This report presents a study of the survivable crash environment for commercial type aircraft. The study includes an analysis both of the results of previous crash tests of full-scale aircraft components and of the data from actual commercial aircraft crashes during the period of 1955 through 1965.

The severity of each crash test has been determined by relating the characteristics of the measured acceleration time histories to the characteristics of human tolerance to acceleration. The results of this analysis show that the severity of a crash for a given set of crash parameters is highly dependent upon the configuration, structural design, and weight of the aircraft.

The determination of the crash environment is accomplished through the use of the shock spectra of acceleration time histories from the crash tests. Shock spectra were obtained for all the pertinent acceleration time

histories, and the methods determining equivalent pulses are presented. The application of this method to the specification of component test environment is discussed.

The data from actual commercial crashes is presented and analyzed. It was found that the most common survivable accident can be described as occurring during the landing phase of the flight, with null, pitch, roll and yaw angles, with an angle of impact of less than 5 degrees, and with an impact velocity of 166 feet per second. The most common obstacle encountered during the crash was trees. It was also found that there were no strong correlations between the crash parameters and the severity measured in terms of the percentage of the occupants killed.

Methods for generalizing the crash environments relative to the treatment of fuel tank locations and components attached to fuselage floor structure are presented. Idealization of the acceleration time history curves is considered to be adequate for fuel tank locations because of the large dampening effect of the fuel. For components attached to the structure, use of the shock spectra is advocated for generalizing the crash environment in order to include significant high-frequency loads in the selection of design criteria.

Based on the results of the study, the requirements for future full-scale tests are presented. The crash parameters are presented for a modern jet aircraft to produce a marginally survivable accident.

The instrumentation requirements are described and a data acquisition system is recommended.

8. Greer, D. L., et al, DESIGN STUDY AND MODEL STRUCTURES TEST PROGRAM TO IMPROVE FUSELAGE CRASHWORTHINESS, General Dynamics, Convair; FAA Report DS-67-20, Federal Aviation Administration, Washington, D. C., October 1967.

This report presents the results of a study to evaluate methods to improve crashworthiness by retaining transport cabin integrity during crash impact loadings.

The study includes analyses of the effects of strengthening, redistribution of bending material, and incorporation of energy dissipating features on the ability of the fuselage to provide a protective shell around the occupants. Analytical results were substantiated by a test program.

The test program included compression tests of plate-stringer panels and drop tests of representative fuselage structure. Tests were made on three 100-inch-diameter cylindrical sections dropped axially, four segments of 100-inch-diameter cylinders dropped laterally, and a structurally complete nose section of a jet transport dropped in a 10-degree nose-down attitude.

The requirement for a plastically deforming structure is important for both axial and vertical collapse characteristics of a fuselage. Plastic collapse provides the most efficient energy-absorbing capability and also reduces the possibility of excessive tearing or complete disintegration of the structure.

The portion of the longitudinal kinetic energy that can be absorbed by structural crushing is not a significant part of the energy produced at the existing takeoff and landing speeds.

Both energy-absorbing capacity and failure mode are important for vertical crushing conditions. The recommended manner of reinforcement for the fuselage lower frame segments strengthens the bottom centerline portion and the floor beam to frame area. No significant weight or cost penalty is involved since the crash requirement reinforcement occurs at the most critical areas for existing design conditions.

An analytical approach, using a digital computer program to simulate the response of fuselage impact, is included. The mathematical model for this program consists of a beam with 10 mass items to represent the fuselage. Each mass is supported on a variable, partially restoring spring to simulate the vertical crushing characteristics of the lower fuselage structure. This analysis indicates that fuselage bending strength is of primary concern in crashworthy considerations.

9. Bigham, James P., and Bingham, William W., THEORETICAL DETERMINATION OF CRASH LOADS FOR A LOCKHEED 1649 AIRCRAFT IN A CRASH TEST PROGRAM, Boeing Airplane Company; FAA Technical Report ADS-15, Federal Aviation Administration, Washington, D. C., July 1964.

This report presents the results of an analytical study to theoretically predict the loads to be experienced by a Lockheed Model 1649 Super Constellation during a controlled crash. Acceleration time histories in directions normal and parallel to the fuselage cabin floor are given at three positions along the length of the fuselage for impact velocities of 140, 160, 180, and 200 feet per second. Results of investigations of the effects of variations in important problem parameters are also presented.

It is concluded that during the initial impact at 180 feet per second, peak normal accelerations of 11, 0, and -3 times that of gravity (G's) will be developed 0.03 second after impact at Body Stations 180, 682, and 1176. Maximum normal and longitudinal accelerations during the 6-degree ramp crash will occur at 0.24 second. Maximum normal accelerations at Body Stations 180, 682, and 1176 will be -17, 8, and 35 G's, respectively. Maximum longitudinal accelerations will be 4 G's.

It is further concluded that the nose of the airplane will bend upward 10 inches relative to the center section of the fuselage 0.14 second after impact. This deflection will probably be of sufficient magnitude to exceed the ultimate strength of the fuselage above the cabin floor. If the fuselage should fail, all analytical results beyond the time of failure will be questionable to a degree dependent on the type of failure that occurs.

10. Turnbow, J. W., Ph.D., A DYNAMIC TEST OF AN H-25 HELICOPTER, Aviation Crash Injury Research Division; SAE Report 517A, National Aeronautic Meeting, April 1962.

This paper describes the first test conducted as an exploratory study to (1) provide a "first" look at the acceleration environment in helicopter accidents and (2) evaluate certain problems inherent in the dynamic crash testing of full-scale helicopter and VTOL aircraft.

An H-25A Piasecki helicopter was employed in recreating a "typical" accident occurring with both longitudinal and vertical velocity components at impact. Acceleration patterns at various stations in the aircraft and in the dummy occupants were found to be incomparable with the results of similar tests conducted for fixed-wing aircraft by NACA. For the helicopter, large-magnitude, short-duration accelerations were observed. By contrast, accelerations of smaller magnitude but with relatively longer duration were found for transport-type aircraft by NACA. When the acceleration environment for the H-25 is compared with known tolerance limits for human subjects, evidence of the need for modification in crew and passenger seats to provide better crash protection for the aircraft's occupants becomes apparent.

11. Leredaht, B. H., et al, SOME NOTES ON THE PHYSIOLOGICAL TOLERANCE TO ACCELERATION, Douglas Aircraft Company, Report ES 40253, February 1961.

This report presents a compilation of data concerning human and animal tolerance to acceleration. Longitudinal and transverse accelerations, both positive and negative, are covered. The effects of rate and duration of acceleration are discussed.

12. Stech, Ernest, and Payne, Peter, DYNAMIC MODELS OF THE HUMAN BODY, Frost Engineering Development Company; AMRL-TR-66-157, Aerospace Medical Research Laboratory, Wright-Patterson Air Force Base, Ohio, November 1969, AD 701 383.

This report covers the analytical modeling of the human body as a single-degree-of-freedom system. Sources of body dynamic data include drop tests, sled tests, vibration tests, structural tests, animal tests, accident data and ejection seat data. Estimates of human body mass and

spring stiffness, natural frequency, damping, and critical force levels are included. The effect of age on natural frequency and critical forces is estimated, as is the nonlinearity of the spinal column.

13. PERSONNEL RESTRAINT SYSTEMS STUDY, BASIC CONCEPTS, Flight Safety Foundation; TCREC Technical Report 62-94, Task 9R95-20-001-01, U.S. Army Transportation Research Command, Fort Eustis, Virginia, December 1962.

This report covers the basic concepts, applicable to all U. S. Army aircraft, that are pertinent to a personnel restraint system study. Man's limits of tolerance to decelerative loads are reviewed and related to the existing restraint harnesses currently being used in Army aircraft. The magnitude of decelerative loads to which airframes of various aircraft have been dynamically tested, while still maintaining a livable volume in the cabin, is also reviewed, and it is noted that man's limits are, in general, higher than airframe limits.

Several practical harness configurations are discussed, the load distribution between the various components of the harness is explored, and design strength values are recommended. The dynamic strength of restraint systems is also discussed and related to the static strength.

14. Coleman, Rolf R., THE MECHANICAL IMPEDANCE OF THE HUMAN BODY IN SITTING AND STANDING POSITION AT LOW FREQUENCIES, Biomedical Laboratory; ASD technical Report 61-492, Aeronautical Systems Division, Wright-Patterson Air Force Base, Ohio, September 1961.

This report discusses the application of the theory of the mechanical impedance of systems with one or more degrees of freedom to the human body. A method of measuring mechanical impedance and determining the parameters of the vibrating systems is developed. Impedance curves for longitudinal vibrations of a sitting and standing subject are established for the frequency range of 1 to 20 cps. The influence of varied posture and restraining systems is investigated. Dynamic movements of body parts are measured, directly or indirectly, and compared with the impedance curves. The responsible elements in the body for the apparent resonances are identified. Correlations between the impedance function of the body and the subjective tolerance curve to vibration are found, and the reasons for the tolerance limits are explained. The variability of subjective tolerances due to varying posture, restraining systems, cushions, duration of exposure, and vibrations is discussed, and conclusions for the development of protective devices are drawn. The correlation between the steady-state response of the human body system and the effects of impact is discussed.

15. Eiband, Martin A., HUMAN TOLERANCE TO RAPIDLY APPLIED ACCELERATIONS: A SUMMARY OF THE LITERATURE, Lewis Research Center, NASA Memo 5-19-59E, National Aeronautics and Space Administration, Washington, D. C., June 1959.

The report describes a survey of the literature to determine human tolerance to rapidly applied accelerations. Pertinent human and animal experiments applicable to space flight and to crash impact forces are analyzed and discussed. These data are compared and presented on the basis of a trapezoidal pulse. The effects of body restraint and of acceleration direction, onset rate, and plateau duration on the maximum tolerable and survivable rapidly applied accelerations are shown.

Results of the survey indicate that adequate torso and extremity restraint is the primary variable in tolerance to rapidly applied accelerations. The harness, or restraint system, must be arranged to transmit the major portion of the accelerating force directly to the pelvic structure and not via the vertebral column. When the conditions of adequate restraint have been met, then the other variables -- direction, magnitude, and onset rate of rapidly applied accelerations -- govern maximum tolerance and injury limits.

The results also indicate that adequately stressed aft-facing passenger seats offer maximum complete body support with minimum objectionable harnessing. Such a seat, whether designed for 20-, 30-, or 40-G dynamic loading, would include lap strap, chest (axillary) strap, and winged-back seat to increase headward and lateral G protection, full-height integral head rest, arm rests (load-bearing) with recessed handholds and provisions to prevent arms from slipping either laterally or beyond the seat back, and leg support to keep the legs from being wedged under the seat.

For crew members and others whose duties require forward-facing seats, maximum complete body support requires lap, shoulder, and thigh straps, lap-belt tie-down strap, and full-height seat back with integral head support.

16. O'Bryan, Thomas, and Hatch, Howard, Jr., LIMITED INVESTIGATION OF CRUSHABLE STRUCTURES FOR ACCELERATION PROTECTION OF OCCUPANTS OF VEHICLES AT LOW IMPACT SPEEDS, Langley Research Center, NASA-TN-D-158, National Aeronautics and Space Administration, Washington, D.C., October 1959.

The report describes the results of a limited investigation to determine the characteristics of three materials to see how they can be applied for human protection against accelerations encountered at low impact speeds. As a result, if given man's physiological tolerance to abrupt acceleration, which has not yet been well defined, an alleviation system can be designed.

Foamed plastics require considerable depth to provide a given stopping distance for impact alleviation, and their use would require some control of rebound. They can be made soft enough to obtain the low onset of acceleration that may be necessary for man where depth is not limited.

Aluminum honeycomb is an efficient material for impact load alleviation from the standpoint of usable material depth, and it exhibits very little rebound. The stiffness of the material results in a very high initial onset rate of acceleration. For many installations, this can be controlled by reducing the initial loading area of contact to get the material to start failing.

17. UH-1 ACCIDENT SUMMARY, USABAAR Report, U. S. Army Board for Aviation Accident Research, Ft. Rucker, Alabama, 1963.

The report contains a summary of all Army UH-1 accident, incident, and forced-landing experiences for the 5-year period ending 27 September 1963. Percentage pie charts for major and minor accidents, incidents, and forced landings are given in percentages of total cause factors and are not directly related to the total number of mishaps in each category, as these mishaps often involve multiple cause factors.

Except for forced landings, pilot cause factors account for the giant's share of each pie chart. This points to a need for greater quality control in personnel selection, training, and supervision.

It is noted that many incidents and forced landings are recorded in this summary with cause factors not reported. This results from reporting units failing to provide supplemental information as it becomes available. Reports of this nature, without supplemental data, are of little use to the aviation safety program.

18. Mattox, Kenneth L., INJURY EXPERIENCE IN ARMY HELICOPTER ACCIDENTS, U. S. Army Board for Aviation Accident Research, Ft. Rucker, Alabama, September 1967, AD 658079.

The gross pattern of injury site, frequency, and seriousness in U. S. Army helicopter accidents is presented in this report. Although 95 percent of the major helicopter accidents are survivable, 22 percent of the deaths in all helicopter accidents occur under survivable conditions. The mechanisms of these avoidable deaths are discussed as well as the steps that should be taken to reduce the morbidity and mortality rate.

Correlation of accidents in Army helicopter experience to injuries incurred in them requires an analysis of the operational envelope. Most U. S. Army aircraft fly in and out of confined areas at relatively slow speed and low altitudes. Operational areas are frequently complicated by wires, tires, towers, and rough terrain at the landing site. Helicopters are not equipped with ejection seats, and because of the



altitudes and missions flown, parachutes are not worn by the aviators. U. S. Army helicopters operate in an environment that nears the extreme both in density of traffic and operational terrain (versus commercial airlines flying in and out of London International). Therefore, although the helicopter has the capability to autorotate in case of in-flight emergency, the aviator must always ride the helicopter in.

19. Turnbow, James W., and Haley, J. L., Jr., A REVIEW OF CRASHWORTHY SEAT DESIGN PRINCIPLES, Arizona State University and AVSER Flight Safety Foundation, SAE Paper 851A, Air Transport and Space Meeting, April 1964.

This paper briefly reviews the known factors pertinent to the design of crashworthy aircraft seats. Ultimate design load factors, based upon human tolerance to decelerative load and the anticipated loads in accident situations for fixed-wing transport aircraft, light fixed-wing aircraft, and military helicopters are presented. The use of energy-absorbing devices is discussed. In this paper it is concluded that energy absorbers would not be practical to reduce longitudinal acceleration levels involving large velocity changes in a single deceleration pulse. However, it is deemed possible to provide energy absorption to limit vertical accelerations to the order of 20 to 25 G's in accidents occurring at rates of 50 to 50 fps, assuming some vertical deformation of the structure.

20. Rich, M. J., VULNERABILITY AND CRASHWORTHINESS IN THE DESIGN OF ROTARY WING VEHICLE STRUCTURES, SAE Paper 680673, 1968.

This paper indicates that the problem of crash survivability capability resolves to the following areas of considerations:

- Absorption of the forward velocities through ground friction and structural elastic/plastic structural energy.
- Absorption of the vertical impact through elastic/plastic structural energy.
- Provision of local strength and living space for the occupants.

The paper states that the 95th percentile potentially survivable accident environment (vertical = 47 fps, horizontal = 60 fps, lateral = 25 fps) appears to be a rational and conservative criterion. The 95th percentile crash acceleration data appears to be potentially within human tolerance limits. Peak loads, however, are very dependent on the amount of sub-structure to absorb the crash. Significant improvements can be achieved by considering the failure modes such that living space for survival is provided. This report also discusses the use of auxiliary landing gear energy absorption in addition to airframe crushing and seat energy absorption.



21. Moseley, Harry, Colonel, et al, RELATION OF INJURY TO FORCES AND DIRECTION OF DECELERATION IN AIRCRAFT ACCIDENTS, Journal of Aviation Medicine, Vol. 29, October 1958.

The article reviews all major cargo and transport-type aircraft accidents in the U. S. Air Force during a 2-year period to determine the path that such aircraft follow during actual crashes and to relate this to variations in aircraft attitude and to injury of occupants. The results indicate that the airframe tends to follow its established path and to remain stable around its own axis. At high velocities, the airframe continues in its established course even though major components are destroyed. With decreased velocity, major course and attitude deviations may result primarily from striking impeding objects. Most injuries are sustained when the aircraft is experiencing little deviation from its established path. The most obvious and most easily effected remedial measures would involve improvement of structural and retention strength of aircraft seats and moorings. These should be designed to provide maximum protection against fore and aft deceleration with additional consideration being given to designing for relatively small yaw deviation.

22. Brinkley, James W., DEVELOPMENT OF AEROSPACE ESCAPE SYSTEMS, Air University Review, July-August 1968.

This article reviews the development of aerospace escape systems from the aeromedical standpoint and describes recent advances that have made it possible to define more completely the human factors limiting the escape system performance envelope. The parameters which directly or indirectly determine if the ejectee will be injured by the ejection acceleration are the maximum acceleration, duration of maximum acceleration, and rate and duration of the entire acceleration. Within the last 5 to 10 years, there has been improvement in the methodology to describe human systems. The use of the Dynamic Response Index (DRI) to model the critical mode of injury when accelerations are applied parallel to the vertebrae is discussed.

23. Weinberg, L. W. T., CRASHWORTHINESS EVALUATION OF AN ENERGY ABSORPTION EXPERIMENTAL TROOP SEAT CONCEPT, Aviation Safety Engineering and Research; USATRECOM Technical Report 65-6, U. S. Army Transportation Research Command, Fort Eustis, Virginia, February 1965, AD614582.

This report describes an evaluation of an experimental troop seat concept that was progressively developed and dynamically tested. The seats were installed and tested along with other equipment in four full-scale crashes of CH-21 helicopters.

The designs represented progressive steps in the development of a troop seat using strut-type energy attenuation. The basic concept was a single-passenger, side-facing, bucket seat. Anthropomorphic dummies, restrained by lap belts and single diagonal chest straps, were placed in the seats to provide simulated human loading characteristics during impact. Accelerometers were mounted in the pelvic cavity of the dummies to permit recording of the impact decelerations. Floor accelerations were also measured near the seat installations. Tensiometers recorded the belt forces. High-speed cameras positioned in the helicopters recorded the reaction of the dummies and experimental seats during the crash sequences.

The seats were divided into two basic functional units: first, a seat base incorporating an energy-absorbing strut to provide the vertical support; and second, a curved nylon seat back that was designed to provide the occupant with restraint in the lateral and longitudinal directions, in addition to the restraint provided by the lap belt and chest strap. The test series demonstrated the effectiveness of strut-type energy absorption as a method of attenuating crash forces.

The report is presented such that each test involved is discussed as well as the overall analysis and evaluation. Photographs, acceleration records, and kinematic sketches are included where pertinent.

24. Bruggink, G. M., and Schneider, D. J., M.D., LIMITS OF SEAT BELT PROTECTION DURING CRASH DECELERATIONS, Aviation Crash Injury Research; TCRC 61-115, U. S. Army Transportation Research Command, Fort Eustis, Virginia, September 1961, AD 265868.

This report reviews three accidents in which aircraft occupants, restrained only by seat belts, received serious or fatal decelerative injuries. The study indicates some of the trauma that may be expected when the tolerable and injurious limits of seat-belt protection are exceeded.

The results indicate that full protection of seat-belt restraint can be realized only when the occupant has an unobstructed path for his flailing extremities and upper torso. If this condition does not exist, the protection offered by seat-belt restraint may not be limited by G factors but by the injurious aspects of the occupant's environment.

Seat-belt-caused injuries, in general, should not be considered as proof against a seat belt's usefulness, but as evidence of its necessarily limited protective value when compared to restraint systems that offer better load distribution over the entire skeleton.

To provide maximum protection, the strength of the occupant tie-down chain (seat, seat belt, floor) should be determined by the threshold between the injurious and fatal limits of seat-belt restraint.

An aircraft seat-belt restraint system with an energy-absorbing capability of 25 G's (occupant weight, 200 pounds) for a duration of at least 0.2 second may form a realistic compromise between the ideal and the practical dynamic strength of such a system.

25. Haley, J. L., HELICOPTER STRUCTURAL DESIGN FOR IMPACT SURVIVAL, U.S. Army Board of Aviation Accident Research, Ft. Rucker, Ala., November 1970.

This paper discusses the factors pertinent to crashworthiness design to enable occupants to survive the impact forces developed during a survivable crash. The paper presents results from a crash performance study of 71 utility helicopter accidents. In the paper it is concluded that:

- impact type injuries cause more fatalities than thermal injuries
- inadequate tie-down of transmission and rotor mast was the most severe structural weakness
- the most severe design weakness was the absence of suitable restraint harness or troop compartment doors to prevent ejection of occupants
- rollover and sideward type impact is a significant cause of occupant injury
- there is a lack of detailed specifications that has hindered crashworthiness design

The paper presents recommendations regarding crash environment, structural loads, and design concepts.

26. Smith, H. G., and McDermott, J. M., DESIGNING FOR CRASHWORTHINESS AND SURVIVABILITY, Hughes Tool Co., American Helicopter Society Proceedings, November 1968.

This paper discusses the prospects of intentionally designing for helicopter crashworthiness and survivability. Rotary-wing aircraft damage photographs are related to crash survivability design. The paper discusses the crash design survivability indices and human tolerance levels. Load factor versus deformation for equal crash energy absorption is compared, and the desirability of large deformation and correspondingly low load factors is explained. Several of the pertinent factors in designing for vertical impacts are presented. Present design practice is stated and future design objectives are presented.

27. Thompson, A. B., A PROPOSED NEW CONCEPT FOR ESTIMATING THE LIMIT OF HUMAN TOLERANCE TO IMPACT ACCELERATION, Aerospace Medical Journal, Vol. 33, No. 11, November 1962.

This article suggests that although mathematical techniques are being developed to determine human whole-body response to various impact accelerations, no satisfactory method is available for defining the human tolerance limit to impact loads resulting from abrupt accelerations. Limits set by total G vs. time, rate of onset, and velocity change are ill-defined and variable. A concept is proposed whereby limits are set by the force exerted per unit area on the body by the restraint or support system at maximum deceleration. Correlation is made between blast tolerance, sled test tolerance, and automobile accident and fall impact survivals, which indicates that 28 to 32 pounds per square inch is the onset level for shock and 45 to 55 pounds per square inch is the level for 50 percent mortality for transverse accelerations of less than 0.07 second duration. In this concept, G, rate of onset, and duration time are all dependent variables, while impact force per unit area, delta velocity change, and impact pulse time define the tolerance envelope.

28. MIL S-9749, A GENERAL SPECIFICATION FOR AIRCRAFT UPWARD EJECTION SEAT SYSTEM, Amended December 1969.

The following sections pertaining to crash loads are excerpted from the specifications:

"3.6.2.6 Crash loads

"3.6.2.6.1.1 Forward crash loads. The restraint subsystem and ejection seat installation shall be capable of withstanding the following loads.

"3.6.2.6.1.2 Seat installation. The ejection seat installation shall withstand a load of 40G ultimate applied in a forward direction through the seat structure to the seat attachment. The load shall be applied through the center of gravity of the seat/man combination, and the seat shall be in the most structurally critical position of adjustment during the load application. (One "G" equals 215 pounds plus the weight of the entire ejection seat system.)

"3.6.2.6.2 Side crash loads. The restraint subsystem and ejection seat installation shall withstand the loads specified in 3.6.2.6.1 applied in a direction of 20° to either side of the forward direction.

"3.6.2.6.3 Vertical crash loads. The restraint subsystem and ejection seat installation shall be capable of withstanding the following loads:

- "a. Restraint subsystem - A load of 1,750 pounds ultimate applied to the restraint subsystem in a vertical upward direction and through

the center of gravity of the occupant. The seat shall be in the most structurally critical position during the load application.

"b. Seat bucket - A load of 4,300 pounds ultimate applied downward perpendicular to the seat bucket bottom and through the center of gravity of the seat occupant. The load shall be distributed over the seat bucket bottom. The seat shall be adjusted to the upper limit of vertical adjustment during the load application.

"c. Seat installation - A load of 20G ultimate applied in a vertical downward direction perpendicular to and uniformly distributed over the seat bucket. (one G equals 215 pounds plus weight of the entire ejection seat system.)

"3.6.2.6.4 Back crash loads. The ejection seat shall be capable of withstanding a load of 1,500 pounds ultimate (1,000 pounds proof) distributed thereon below the headrest. The seat shall be adjusted to the most structurally critical vertical adjustment position for the application of this load."

29. MIL-T-27422B AIRCRAFT CRASH RESISTANT FUEL TANK MILITARY SPECIFICATION, Amended February 1970.

Paragraph 4.6.6.2 applies to crash impact design and reads as follows:

"The No. 2 test cube with cover plate attached to the fitting and filled with 770 pounds of water (no air in the cube) and held loosely with a sling made of webbing in accordance with Figure 9 shall be lifted to a height of 65 feet, measured from the bottom of the cube. With the bottom of the cube in a horizontal position, the release mechanism shall be actuated and the cube allowed to drop freely on a nondeforming surface. Any rupture resulting in spillage shall constitute failure."

30. MIL S-8698, HELICOPTER STRUCTURAL DESIGN REQUIREMENTS MILITARY SPECIFICATION, July 1954.

Paragraph 3.4.7 applies to design for crash loads and reads as follows:

"Sufficient strength shall be provided in the seat installation and attachments of engines, transmissions, equipment, and useful load items (including fuel tanks one-half full) and their carry-through structure to prevent failure of such attachments which would result in injury to personnel. The ultimate inertia-load factors shall be those specified by the procuring activity."

31. MIL S-58095, GENERAL MILITARY SPECIFICATION FOR AIRCREW NON EJECTION CRASHWORTHY SEAT SYSTEM, August 1971.

This specification describes a 95th percentile potentially survivable accident which specifies the time period, peak G values, and velocity change for a triangular pulse shape. The pulse parameters are obtained from USAAVLABS Technical Report 70-22. The specifications consider designing for human tolerance to vertical accelerations. The specification describes the seat system requirements necessary to provide occupant protection and survival in aircraft accidents.

Longitudinal, lateral, and upward seat structural strength and deformation requirements stated are based on the 95th percentile clothes occupant weight plus the weight of the seat and any equipment attached to or carried by the seat. Downward seat structural strength and deformation requirements are based on the effective weight of the 50th percentile clothed occupant plus the weight of that portion of the seat which must stroke during vertical crash force attenuation.

32. Haley, J., PRELIMINARY DRAFT, COST EFFECTIVENESS OF CRASHWORTHY STRUCTURAL FEATURES IN A 9-13 PLACE HELICOPTER, USAAAVS, TN 72-1, U.S. Army Agency for Aviation Safety, Ft. Rucker, Ala.

This report discusses the results of a cost-effectiveness study of crashworthy structural features for a 9-13 place helicopter. The study takes into consideration the following:

- accident history of the UH-1
- cost to the government of personnel injuries and fatalities
- savings potential on aircraft damage repair and replacement costs
- increased operating costs as a result of increased empty weight

The preliminary draft concludes that the crashworthy features intended for the UTTAS will be cost effective in 5.4 years on the basis of (1) an estimated initial cost increase of \$15,000 per aircraft and (2) an accident rate equal to half that of the UH-1 series in FY 69.

TABLE I. LITERATURE SURVEY SUBJECT INDEX

Subject	1	2	3	4	5	6	7	8	9	10	11	12	13	14	15	16	17	18	19	20	21	22	23	24	25	26	27	28	29	30	31	32
Rotary Wing Aircraft	•	•	•	•	•	•	•	•	•	•	•	•	•	•	•	•	•	•	•	•	•	•	•	•	•	•	•	•	•	•	•	•
Fixed Wing Aircraft	•	•	•	•	•	•	•	•	•	•	•	•	•	•	•	•	•	•	•	•	•	•	•	•	•	•	•	•	•	•	•	•
Design Principles	•	•	•	•	•	•	•	•	•	•	•	•	•	•	•	•	•	•	•	•	•	•	•	•	•	•	•	•	•	•	•	•
Structural Design Criteria	•	•	•	•	•	•	•	•	•	•	•	•	•	•	•	•	•	•	•	•	•	•	•	•	•	•	•	•	•	•	•	•
IL Specification Requirements	•	•	•	•	•	•	•	•	•	•	•	•	•	•	•	•	•	•	•	•	•	•	•	•	•	•	•	•	•	•	•	•
Man Environment	•	•	•	•	•	•	•	•	•	•	•	•	•	•	•	•	•	•	•	•	•	•	•	•	•	•	•	•	•	•	•	•
Aircraft Loads and Accelerations	•	•	•	•	•	•	•	•	•	•	•	•	•	•	•	•	•	•	•	•	•	•	•	•	•	•	•	•	•	•	•	•
Structural Behavior	•	•	•	•	•	•	•	•	•	•	•	•	•	•	•	•	•	•	•	•	•	•	•	•	•	•	•	•	•	•	•	•
Airframe Structure & Materials	•	•	•	•	•	•	•	•	•	•	•	•	•	•	•	•	•	•	•	•	•	•	•	•	•	•	•	•	•	•	•	•
Energy Absorption	•	•	•	•	•	•	•	•	•	•	•	•	•	•	•	•	•	•	•	•	•	•	•	•	•	•	•	•	•	•	•	•
Gas-Phase Systems	•	•	•	•	•	•	•	•	•	•	•	•	•	•	•	•	•	•	•	•	•	•	•	•	•	•	•	•	•	•	•	•
Seat and Harness Design	•	•	•	•	•	•	•	•	•	•	•	•	•	•	•	•	•	•	•	•	•	•	•	•	•	•	•	•	•	•	•	•
Posture and Design Criteria	•	•	•	•	•	•	•	•	•	•	•	•	•	•	•	•	•	•	•	•	•	•	•	•	•	•	•	•	•	•	•	•
Avionics Equipment	•	•	•	•	•	•	•	•	•	•	•	•	•	•	•	•	•	•	•	•	•	•	•	•	•	•	•	•	•	•	•	•
Analytical Methods	•	•	•	•	•	•	•	•	•	•	•	•	•	•	•	•	•	•	•	•	•	•	•	•	•	•	•	•	•	•	•	•
Test Methods	•	•	•	•	•	•	•	•	•	•	•	•	•	•	•	•	•	•	•	•	•	•	•	•	•	•	•	•	•	•	•	•
Test Data	•	•	•	•	•	•	•	•	•	•	•	•	•	•	•	•	•	•	•	•	•	•	•	•	•	•	•	•	•	•	•	•
Analytical/Test Correlation	•	•	•	•	•	•	•	•	•	•	•	•	•	•	•	•	•	•	•	•	•	•	•	•	•	•	•	•	•	•	•	•
Accident Data	•	•	•	•	•	•	•	•	•	•	•	•	•	•	•	•	•	•	•	•	•	•	•	•	•	•	•	•	•	•	•	•
Failure Modes and Sequence	•	•	•	•	•	•	•	•	•	•	•	•	•	•	•	•	•	•	•	•	•	•	•	•	•	•	•	•	•	•	•	•
Failure Analysis	•	•	•	•	•	•	•	•	•	•	•	•	•	•	•	•	•	•	•	•	•	•	•	•	•	•	•	•	•	•	•	•
Human Tolerance Levels	•	•	•	•	•	•	•	•	•	•	•	•	•	•	•	•	•	•	•	•	•	•	•	•	•	•	•	•	•	•	•	•
Injury Data	•	•	•	•	•	•	•	•	•	•	•	•	•	•	•	•	•	•	•	•	•	•	•	•	•	•	•	•	•	•	•	•
Dynamic Response	•	•	•	•	•	•	•	•	•	•	•	•	•	•	•	•	•	•	•	•	•	•	•	•	•	•	•	•	•	•	•	•
Structural Systems	•	•	•	•	•	•	•	•	•	•	•	•	•	•	•	•	•	•	•	•	•	•	•	•	•	•	•	•	•	•	•	•
Human Systems	•	•	•	•	•	•	•	•	•	•	•	•	•	•	•	•	•	•	•	•	•	•	•	•	•	•	•	•	•	•	•	•
Escape Systems	•	•	•	•	•	•	•	•	•	•	•	•	•	•	•	•	•	•	•	•	•	•	•	•	•	•	•	•	•	•	•	•
Cost Effectiveness	•	•	•	•	•	•	•	•	•	•	•	•	•	•	•	•	•	•	•	•	•	•	•	•	•	•	•	•	•	•	•	•

## DESCRIPTION OF STAGS (STRUCTURAL ANALYSIS OF GENERAL SHELLS) PROGRAM

STAGS is a computer program developed to analyze the behavior of general shells under arbitrary static thermal and mechanical loading. Nonlinearities caused by material behavior and finite deformations are accounted for. The STAGS analysis is based on an energy formulation. Derivatives which appear in the energy expression are replaced by their two-dimensional finite difference approximations. Minimization of the energy results in a system of nonlinear algebraic equations which are solved by use of a modified Newton-Raphson method.

The computer program STAGS (Structural Analysis of General Shells) performs a nonlinear analysis of shells by use of a two-dimensional finite difference approach. Displacement and stress histories are computed corresponding to a given history of applied load, displacement, or temperature. Two versions of STAGS are described in this report. The first version provides an elastic nonlinear collapse analysis. In addition to the basic nonlinear branch, there are two special branches: the first is for linear analysis, and the second is for buckling analysis based on the classical bifurcation approach with a linear prebuckling analysis. Collapse loads are found as limit points in the nonlinear load displacement curve. The program is useful for postbuckling analysis of shells which behave according to classical buckling theory and for studies of the influence of imperfections.

STAGS applies to any shell for which a reference surface and a suitable set of grid lines can be mathematically defined. In general, the user of the program provides a subroutine describing the geometry, but several such routines for standard geometries are permanently included in the program. For the elastic version, the shell wall thickness can be varied, and elastic properties are allowed to vary with the shell coordinates and through the thickness. Cutouts in the shell wall and discrete eccentric stiffeners are included. The program is also general relative to boundary conditions and to loading. The loading can be applied in terms of variable surface tractions, point forces, or line loads. Displacements, such as uniform end shortening of a cylindrical shell, can be applied if desired rather than fixed loading, and provision is made for thermal loading.

Stiffeners and cutout edges must follow coordinate lines, or rather the coordinate lines must be chosen so that they follow boundaries, internal or external, and the direction of internal stiffeners. This is not a severe program limitation because the capability of handling nonorthogonal grids has been included. However, analysis of more complicated shells will require some user skill.

On each of the boundaries, the input parameters can be used to specify restraint on either of the three displacement components or on the rotation about the tangent to the edge. If displacement restraint is not



specified for one or more of these qualities, the analysis will be based on appropriate natural boundary conditions (stress free). If more complicated boundary conditions are used, it will be necessary to modify the program in an area which is not easily accessible to the user. However, displacement restraints off the boundary lines can be introduced by using specified displacement in the load routine.

Two items are of special importance relative to the problem of computer run time. One is the transformation of the structure into a model which is suitable for analysis; the other is the choice of strategy in the non-linear analysis. Often, it is impossible to model the structure in a straightforward manner, and considerable engineering skill may be needed. Eventually a few different models must be analyzed, all reflecting different types of local behavior. The strategy in the analysis involves choice of such items as step size and convergence criterion; it also involves the use of initial imperfections and the use of the results from the application of the bifurcation analysis. The choice of a proper strategy is very important for computer economy.

The basic problem dimensions (number of nodal points in each direction) are restricted only by the availability of mass storage. Some program limitations are imposed by dimension statements. In each direction, there can be as many as 80 stiffeners but only of 20 different types. The number of points for integration through the thickness must be an odd number, and it may not exceed 9. In the plasticity analysis, as many as 10 material components may be used.

A comprehensive description of STAGS can be found in Reference 42.

## MATHEMATICAL MODEL DESCRIPTION

### PROGRAM KRASH

Program KRASH was developed during Phase II of the study described herein. Program KRASH computes the time history response of  $N$  arbitrarily interconnected lumped masses. Each mass is allowed six degrees of freedom defined by inertial coordinates  $x_i$ ,  $y_i$ ,  $z_i$  and Eulerian angles  $\phi_i$ ,  $\theta_i$ ,  $\psi_i$ ,  $i = 1, 2, \dots, N$ . Euler's equations of motion are written for each mass. The equations of motion are integrated numerically to obtain velocities and displacements and rotations. Angular momentum terms due to rotor angular velocity are included in the equations of motion.

The following loads (forces and moments) act on each lumped mass:

1. Gravity forces
2. Aerodynamic forces
3. Internal forces and moments
4. External forces and moments

The gravity forces are self-explanatory. The aerodynamic forces consist of the simple lift force on each mass held constant throughout the run. This lift force is computed for each mass as an input fraction of the total vehicle weight.

The internal forces and moments result from the deformation of structural members, termed "beams", which interconnect the various lumped masses. The degree of interconnectivity, i.e., which of the  $N$  masses are interconnected, is specified in the input. Each beam's properties are specified in terms of a  $6 \times 6$  linear stiffness matrix relating the forces and moments at mass  $j$  to the relative deflections and rotations of mass  $j$  with respect to mass  $i$ .

The actual internal forces are computed on an incremental basis. Each increment is just the incremental linear force determined from the stiffness matrix, times the incremental deflection, multiplied by a stiffness reduction factor  $KR$ . For each beam element there are six different  $KR$ 's, one for each relative deflection. For a given relative deflection, say, axial deflection, the corresponding  $KR$  applies to all six possible loads due to this deflection. Each  $KR$  is input as a tabular function of the corresponding deflection. For small deflections,  $KR = 1$ , so that a linear analysis is obtained; for larger deflections,  $KR \neq 1$ , so that general plastic deformations are allowed. Since the forces are computed incrementally,  $KR$  is simply the slope of the appropriate load-stroke curve.

The structural element is assumed to behave the same under the influence of positive and negative loads.

In addition to the above, the internal load computation is written such that unloading and subsequent reloading occur along a linear elastic line. Once any of the six deflections exceeds an input value, the member is assumed to have failed completely (fracture) and the interconnecting forces are set to zero for the remainder of the run. Linear (viscous) damping is included in the calculation of the internal loads.

The external forces result from the crushing of structure which is external to the lumped masses. Each lumped mass is allowed to have as many as three mutually perpendicular "springs" which radiate outward from the mass. Obviously, only those masses on the exterior of the vehicle will utilize these springs. When any spring contacts the ground, an axial spring compression load is calculated from an input table of spring axial load versus axial compression.

This table can be input in any form to allow for general elastic-plastic deformation. Unloading (extending) and reloading follow an elastic line whose stiffness is input, so that energy is absorbed in permanent deformation. In addition, beyond an input maximum deflection, further loading-unloading proceeds along a steep elastic line (input constant). This is to represent the finite crushing distance available, beyond which the stiffness increases drastically. The external springs do not develop tensile loads, and they do not fracture as do the internal "beams".

A ground drag load is computed at the ground contact point for each spring. This load is just a constant input friction coefficient times the normal component of the axial spring load. The direction of the drag load is opposite to the velocity vector of the contact point. The contact surface (ground) is assumed to be flat and rigid.

Program KRASH has a built-in routine which will determine when an identified mass penetrates a defined occupiable volume. In addition, the program will obtain the Dynamic Response Index (DRI) for desired personnel locations. Program KRASH uses a modified predictor-corrector integration routine and includes an initial condition subroutine which provides for a balanced vehicle at the start of the analysis.

## THEORY

### Mathematical Model of Helicopter

The helicopter is modeled as a series of interconnected lumped masses. Each mass is allowed six degrees of freedom, three translations, and three rotations. The masses are connected internally by nonlinear beam elements. Each mass is allowed up to three external nonlinear "springs", which radiate outward from the mass and contact the ground, providing external crash forces. The helicopter model is shown in Figure 1.

$m_i$ ,  $m_j$  and  $m_k$  are three lumped masses, interconnected by beams  $ij$  and  $ik$ . Three external springs are shown radiating outward from  $m_k$ . The end points of these springs are denoted by  $C_{ik}$ ,  $C_{jk}$  and  $C_{sk}$ . The center-of-gravity of the entire helicopter is denoted by  $G$ . (In general, there will be no lumped mass exactly at  $G$ .)

### Coordinate Systems

#### Definition of Coordinate Systems

1. Ground Coordinate System ( $O, x, y, z$ ). This is a right-handed coordinate system fixed in the ground with origin at point  $O$  in Figure 1. The  $x$  axis is positive forward, the  $y$  axis positive to the right, and the  $z$  axis positive downward. The  $xy$  plane ( $z = 0$ ) corresponds to the ground surface. The ground coordinate system is considered an inertial coordinate system for writing the dynamic equations of motion.
2. Helicopter Coordinate System ( $H, x'', y'', z''$ ). This is a left-handed coordinate system fixed in the helicopter with origin at point  $H$  in Figure 1. The  $x''$  axis is positive aft,  $y''$  is positive left, and  $z''$  is positive upward. The origin, point  $H$ , corresponds to F.S.O., B.L.O, W.L.O. This coordinate system is used only to input the coordinates of the lumped mass points, since the coordinates of the points are usually available in terms of F.S., B.L. and W.L.
3. Center-of-Gravity Coordinate System ( $G, x', y', z'$ ). This is a right-handed system fixed in the helicopter with the origin at the c.g. of the helicopter (Point  $G$ ). The  $x'$  axis is positive forward,  $y'$  positive right, and  $z'$  positive downward. These axes are parallel to the  $H, x'', y'', z''$  axes.
4. Body Coordinate System ( $m_i, x_i, y_i, z_i$ ). Each lumped mass has its right-handed coordinate system fixed in the mass. The orientation of each of these coordinate systems is arbitrary, and it is specified by means of three input Euler angles for each mass, relating its orientation to the  $G, x', y', z'$  center-of-gravity coordinate system.

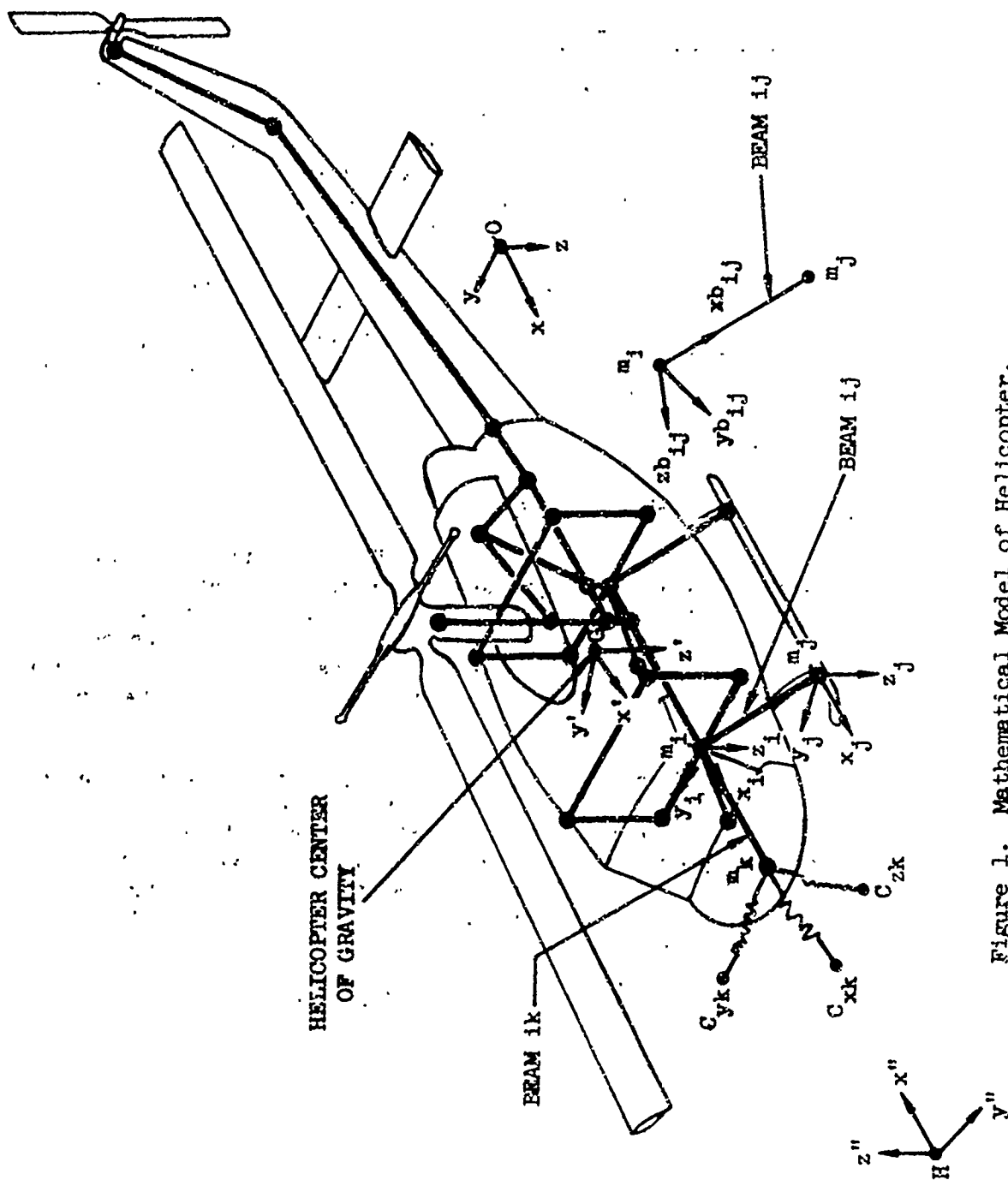


Figure 1. Mathematical Model of Helicopter.

Normally the body coordinate system is taken parallel to the center-of-gravity coordinate system (and hence, the three input Euler angles are set = 0), since the inertia data is generally available about these axes. The body coordinate system is the system used in writing Euler's equations of motion for each lumped mass  $m_1$ .

5. Beam Coordinate System ( $m_1, x_{b1j}, y_{b1j}, z_{b1j}$ ). This is a right-handed coordinate system fixed in mass  $m_1$ , with its origin at  $m_1$ . The  $x_{b1j}$  is along a straight line from  $m_1$  to  $m_j$ , with the helicopter in its original undeformed configuration. As the helicopter deforms, this coordinate system remains fixed in mass  $m_1$ , so that  $x_{b1j}$  will no longer point to  $m_j$ . The direction of  $y_{b1j}$  and  $z_{b1j}$  (they are mutually perpendicular) is arbitrary and is input to the program. Each beam  $ij$  has a beam coordinate system, used to compute the beam forces and moments.

#### Relations Between Coordinate Systems

Any quantity which can be expressed as a vector in one coordinate system (forces, moments, displacements, velocities, accelerations, but not large rotations) can be, likewise, specified in another coordinate system by use of an Eulerian transformation matrix relating the two coordinate systems. Thus, for example, if we have a force vector at  $m_1$  expressed in its body axes components as  $(X_1, Y_1, Z_1)$ , this can be expressed in ground axes as simply

$$\begin{Bmatrix} X_{o1} \\ Y_{o1} \\ Z_{o1} \end{Bmatrix} = [A_1] \begin{Bmatrix} X_1 \\ Y_1 \\ Z_1 \end{Bmatrix}$$

where  $\{X_{o1}, Y_{o1}, Z_{o1}\}$  are the ground axes components of the force vector and  $[A_1]$  is a  $3 \times 3$  Eulerian transformation matrix. The form of  $[A_1]$  depends on the sequence in which rotations from one axis system to the other are performed. In this program, the following sequence is employed:

1. Starting with the  $O, x, y, z$  coordinate system, perform a clockwise (right-hand rule) rotation about the  $O_z$  axis, through an angle  $\psi_1$ .
2. Next, perform a clockwise rotation about the new  $O_y$  axis, through an angle  $\theta_1$ .

3. Finally, perform a clockwise rotation about the final  $O_x$  axis, through an angle  $\phi_1$ .

The resulting transformation matrix is then inverted to obtain a transformation from body axes to ground axes. The resulting transformation matrix is given by

$$A_1 = \begin{bmatrix} \cos\theta_1 \cos\psi_1 & -\cos\phi_1 \sin\psi_1 + \sin\phi_1 \sin\theta_1 \cos\psi_1 & \sin\phi_1 \sin\psi_1 + \cos\phi_1 \sin\theta_1 \cos\psi_1 \\ \cos\theta_1 \sin\psi_1 & \cos\phi_1 \cos\psi_1 + \sin\phi_1 \sin\theta_1 \sin\psi_1 & -\sin\phi_1 \cos\psi_1 + \cos\phi_1 \sin\theta_1 \sin\psi_1 \\ -\sin\theta_1 & \sin\phi_1 \cos\theta_1 & \cos\phi_1 \cos\theta_1 \end{bmatrix}$$

(1)

Similar transformation matrices are formed to relate various other coordinate systems. These are summarized in Table II.

TABLE II. TRANSFORMATION MATRICES				
Matrix	Transforms From	To	Using Angles	Angles Constant or Varying
$[A_1]$	ith body axes	ground axes	$\phi_1, \theta_1, \psi_1$	varying
$[A_{1j}]$	beam ij axes	ith body axes	$\phi_{1j}, \theta_{1j}, \psi_{1j}$	constant
$[A''_1]$	ith body axes	c.g. axes	$\phi''_1, \theta''_1, \psi''_1$	constant
$[A']$	c.g. axes	ground axes	$\phi', \theta', \psi'$	constant

All the above matrices utilize equation (1) with the appropriate angles from the above table.  $[A''_1]$  and  $[A']$  are used only in initial conditions determination, so that their Euler angles are indicated as constant.

These "constants" are really the time zero values of the angles which actually vary but are not used in the time history computations.  $\phi'$ ,  $\theta'$ ,  $\psi'$  are input constants defining the initial attitude of the overall vehicle. The  $[A_i]$  matrices are constant since, as mentioned above, the  $i$ j beam axes are fixed in the  $i$ th body axes. Hence, the only time varying Euler angles are  $\phi_i$ ,  $\theta_i$ , and  $\psi_i$  in the  $[A_i]$  matrices. These obviously are the three rotational degrees-of-freedom of the  $i$ th lumped mass.

We also will require the time derivative of the  $[A_i]$  matrix, denoted  $[\dot{A}_i]$ . It can be shown that this is given by postmultiplying  $[A_i]$  by a matrix  $[D_i]$  so that

$$[\dot{A}_i] = [A_i] [D_i] \quad (2)$$

where  $[D_i]$  is given by

$$[D_i] = \begin{bmatrix} 0 & \dot{\theta}_1 \sin \phi_1 - \dot{\psi}_1 \cos \phi_1 \cos \theta_1 & \dot{\theta}_1 \cos \phi_1 + \dot{\psi}_1 \sin \phi_1 \cos \theta_1 \\ -\dot{\theta}_1 \sin \phi_1 + \dot{\psi}_1 \cos \phi_1 \cos \theta_1 & 0 & -\dot{\phi}_1 + \dot{\psi}_1 \sin \theta_1 \\ -\dot{\theta}_1 \cos \phi_1 - \dot{\psi}_1 \sin \phi_1 \cos \theta_1 & \dot{\phi}_1 - \dot{\psi}_1 \sin \theta_1 & 0 \end{bmatrix} \quad (3)$$

### Sign Conventions

The basic sign convention used for all displacements, rotations, velocities, accelerations, forces and moments is that all quantities are positive in the positive direction of the axes shown in Figure 1. Rotation and moments utilize a right-hand rule to define the positive direction. The few exceptions to this rule are indicated in the theoretical development.

### Forces Acting on Each Mass

The following forces and moments act on each lumped mass:

1. Gravity forces
2. Aerodynamic forces
3. Internal forces and moments
4. External forces and moments



### 5. Damping forces and moments (internal)

All forces and moments are positive when they act in the positive direction of the  $m_1, x_1, y_1, z_1$  axes.

Gravity Forces ( $X_{G_1}, Y_{G_1}$ , and  $Z_{G_1}$ )

The gravity force for the  $i$ th lumped mass is evidently just the weight  $W_1$  acting along the ground fixed  $O_z$  axis. Transforming this force into body axes gives the gravity forces as

$$\begin{Bmatrix} X_{G_1} \\ Y_{G_1} \\ Z_{G_1} \end{Bmatrix} = [A_1]^T \begin{Bmatrix} 0 \\ 0 \\ W_1 \end{Bmatrix} \quad (4)$$

where  $[A_1]^T$  indicates the transpose of  $[A_1]$ . Note that the transpose rather than the inverse is used, since for rotation transformation matrices the two are equal.

Aerodynamic Forces ( $X_{A_1}, Y_{A_1}$ , and  $Z_{A_1}$ )

The only aerodynamic forces considered are a constant lift force, in ground axes, positive upward, acting on each lumped mass. This lift force is expressed as a constant fraction of the total vehicle weight, times the vehicle weight:

$$\text{LIFT}_1 = l_{c_1} W_{\text{TOT}} \quad (5)$$

where

$$W_{\text{TOT}} = \sum_{i=1}^N W_i \quad (6)$$

and  $N$  is the total number of lumped masses. Transforming this lift into  $i$ th body axes gives the desired aerodynamic forces as

$$\begin{Bmatrix} x_{A_i} \\ y_{A_i} \\ z_{A_i} \end{Bmatrix} = [A_i]^T \begin{Bmatrix} 0 \\ 0 \\ -\text{LIFT}_i \end{Bmatrix} \quad (7)$$

where the minus sign is necessary because the lift is positive upward (in the negative direction of the  $O_z$  ground axis.)

Inputting all  $lc_i = 0$  gives a zero lift case, generally the most common. If a 100% lift case is desired, and it is assumed that all the lift is from the rotor, then input  $lc_i = 1$  for the  $i$ th mass corresponding to the rotor.

#### Internal Forces and Moments ( $X_{I_i}$ , $Y_{I_i}$ , $Z_{I_i}$ , $M_{I_i}$ , and $N_{I_i}$ )

These forces and moments result from the deformations of the interconnecting beams as the lumped masses move. First, for beam  $ij$ , the deflections and rotations of point  $j$  with respect to point  $i$  are computed in beam  $ij$  axes. These are then used to calculate the three forces and three moments at point  $j$ , utilizing a  $6 \times 6$  stiffness matrix relating the loads to the deformations. Nonlinear effects are also included in computing the loads. The loads at point  $j$  in beam axes are then transformed into ground axes, and the loads at point  $i$  in ground axes are computed from static equilibrium equations (the beams are assumed massless). Then the loads at  $i$  and  $j$  are transformed into  $i$ th and  $j$ th mass body axes, respectively. Finally, for each mass the contributions from the various beams that attach to that mass are summed to obtain the total internal force for the mass. All the internal force calculations are performed on an incremental basis, i.e., incremental deflections are used to compute incremental forces, since a tangent modulus is utilized for computing nonlinear effects.

1. Beam Deformations - This section calculates the deflections and rotations of point  $j$  with respect to point  $i$ , for beam  $ij$ , in beam  $ij$  axes. First, the incremental deflections of point  $j$  with respect to point  $i$ , in ground axes, are clearly given by

$$\begin{Bmatrix} \Delta x_{ij} \\ \Delta y_{ij} \\ \Delta z_{ij} \end{Bmatrix} = \begin{Bmatrix} \Delta x_j \\ \Delta y_j \\ \Delta z_j \end{Bmatrix} - \begin{Bmatrix} \Delta x_i \\ \Delta y_i \\ \Delta z_i \end{Bmatrix} \quad (8)$$

$\Delta x_i$  and  $\Delta x_j$  are the incremental displacements of points  $i$  and  $j$ , from one time interval to the next, obtained by numerical integration of the velocities. The running time sums of these quantities give the total coordinate positions,  $x_i$ ,  $y_i$ ,  $z_i$ :

$$\begin{aligned} x_i &= x_i + \Delta x_i & i = 1, 2, \dots, N & \quad (9) \\ y_i &= y_i + \Delta y_i \\ \begin{array}{c} \nearrow z_i \\ \text{current} \\ \text{value} \end{array} &= \begin{array}{c} \nearrow z_i \\ \text{previous} \\ \text{value} \end{array} + \Delta z_i \end{aligned}$$

$x_i$ ,  $y_i$ ,  $z_i$  are the three translational degrees of freedom of mass  $i$ . Referring to Figure 1, they give the position of the  $i$ th mass in the ground ( $O_{x,y,z}$ ) coordinate system. Similarly, the three Euler angles  $\phi_i$ ,  $\theta_i$ ,  $\psi_i$  mentioned earlier are the three rotational degrees of freedom of mass  $i$ . Since incremental values of these are also used, we have

$$\begin{aligned} \phi_i &= \phi_i + \Delta \phi_i \\ \theta_i &= \theta_i + \Delta \theta_i & i = 1, 2, \dots, N & \quad (10) \\ \begin{array}{c} \nearrow \psi_i \\ \text{current} \\ \text{value} \end{array} &= \begin{array}{c} \nearrow \psi_i \\ \text{previous} \\ \text{value} \end{array} + \Delta \psi_i \end{aligned}$$

Figure 2 illustrates beam  $ij$  in two positions, at time  $t$  and time  $t + \Delta t$ , where  $\Delta t$  is the numerical integration time interval. Mass  $i$  is shown as not moving during  $\Delta t$ , which is done only to clarify

the figure. Mass  $j$  moves from  $m_{jt}$  to  $m_{jt+\Delta t}$  during the  $\Delta t$  time interval. This motion can be viewed as resulting from two vector motions.

$$\overrightarrow{\Delta d}_{ij} = \overrightarrow{\Delta r}_{ij} + \overrightarrow{\Delta b}_{ij} \quad (11)$$

$\overrightarrow{\Delta d}_{ij}$  is clearly given by equation (8) in ground axes, i.e.,

$$\overrightarrow{\Delta d}_{ij} = \begin{Bmatrix} \Delta x_{ij} \\ \Delta y_{ij} \\ \Delta z_{ij} \end{Bmatrix} \quad (12)$$

The first component of  $\overrightarrow{\Delta d}_{ij}$ ,  $\overrightarrow{\Delta r}_{ij}$ , is the deflection of point  $j$  due solely to rotation of mass  $m_i$  during  $\Delta t$ . In Figure 2, the coordinate axis  $(x_{b_{ij}})$  is shown rotating clockwise to its new position, due to rotation of mass  $m_i$  (recall that the beam axes are fixed in mass  $i$ ).

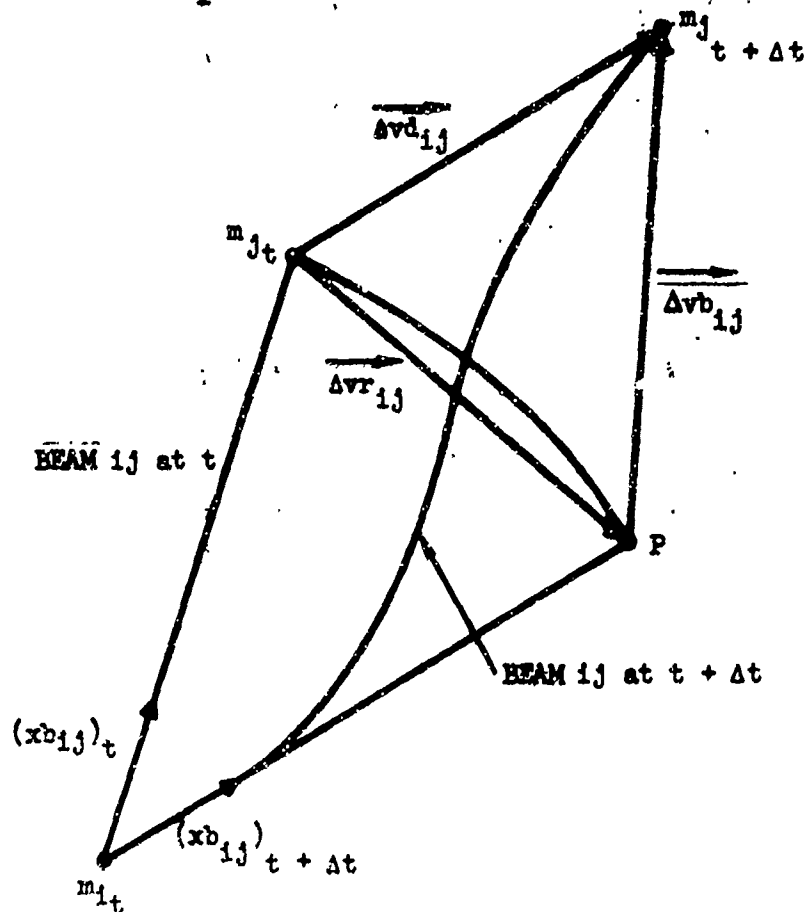


Figure 2. Beam Deflections.

This motion alone moves point  $m_{jt}$  over to point P in Figure 2.

However, this motion alone would induce no loading in beam ij. The fact that point j actually moves to  $m_{jt+\Delta t}$  causes the beam loads. Thus, it is clearly the vector  $\overline{\Delta v}_{ij}$  that gives the incremental beam deformations that cause incremental beam loads. Solving equation (11) for the desired deflections  $\overline{\Delta v}_{ij}$ :

$$\overline{\Delta v}_{ij} = \overline{\Delta d}_{ij} - \overline{\Delta r}_{ij} \quad (13)$$

$\overline{\Delta d}_{ij}$  is already known, in ground axes, from equation (12).

$\overline{\Delta r}_{ij}$  is now determined. At time t, a vector from i to j in ground axes, defined as  $\{x_{ij}, y_{ij}, z_{ij}\}$ , is given by

$$\begin{pmatrix} x_{ij} \\ y_{ij} \\ z_{ij} \end{pmatrix} = \begin{pmatrix} x_j - x_i \\ y_j - y_i \\ z_j - z_i \end{pmatrix} \quad (14)$$

This vector in ith body axes (denoted ') is just

$$\begin{pmatrix} x'_{ij} \\ y'_{ij} \\ z'_{ij} \end{pmatrix}_t = [A_1]_t^T \begin{pmatrix} x_{ij} \\ y_{ij} \\ z_{ij} \end{pmatrix}_t \quad (15)$$

where the subscript t denotes at time t. This same vector at time  $t + \Delta t$ , where mass i has now rotated but the vector remains unchanged in inertial space, is given by

$$\begin{Bmatrix} x'_{ij} \\ y'_{ij} \\ z'_{ij} \end{Bmatrix}_{t+\Delta t} = [A_i]_{t+\Delta t}^T \begin{Bmatrix} x_{ij} \\ y_{ij} \\ z_{ij} \end{Bmatrix}_t \quad (16)$$

where  $[A_i]_{t+\Delta t}^T$  is now evaluated with the new rotated angles.

The desired  $\overrightarrow{\Delta vr}_{ij}$  is evidently just (15) minus (16),

$$\overrightarrow{\Delta vr}_{ij} = \left\{ [A_i]_t^T - [A_i]_{t+\Delta t}^T \right\} \begin{Bmatrix} x_{ij} \\ y_{ij} \\ z_{ij} \end{Bmatrix}_t \quad (17)$$

Substituting "previous" for values at  $t$ , and not denoting the values at  $t + \Delta t$  (since the new  $[A_i]$  is evaluated before these calculations), we have

$$\overrightarrow{\Delta vr}_{ij} = \left\{ [A_i]_{\text{prev.}}^T - [A_i]^T \right\} \begin{Bmatrix} x_{ij} \\ y_{ij} \\ z_{ij} \end{Bmatrix}_{\text{prev.}} \quad (18)$$

in current  $i$ th mass axes. Rotating into beam  $ij$  axes, we obtain

$$\overrightarrow{\Delta vr}_{ij} = [A_{ij}]^T \left\{ [A_i]_{\text{prev.}}^T - [A_i]^T \right\} \begin{Bmatrix} x_{ij} \\ y_{ij} \\ z_{ij} \end{Bmatrix}_{\text{prev.}} \quad (19)$$

Returning to equation (13), we still require  $\overrightarrow{\Delta vd}_{ij}$ , in beam  $ij$  axes. This is evidently given by

$$\overline{\Delta v}_{1j} = [A_{1j}]^T [A_1]^T \begin{Bmatrix} \Delta x_{1j} \\ \Delta y_{1j} \\ \Delta z_{1j} \end{Bmatrix} \quad (20)$$

Finally, combining (19) and (20) into (13), we obtain the desired  $\overline{\Delta v}_{1j}$  in beam  $ij$  axes:

$$\overline{\Delta v}_{1j} = \begin{Bmatrix} \Delta x_{b_{1j}} \\ \Delta y_{b_{1j}} \\ \Delta z_{b_{1j}} \end{Bmatrix} = [A_{1j}]^T \left[ [A_1]^T \begin{Bmatrix} \Delta x_{1j} \\ \Delta y_{1j} \\ \Delta z_{1j} \end{Bmatrix} - \left( [A_1]^T \begin{Bmatrix} x_{1j} \\ y_{1j} \\ z_{1j} \end{Bmatrix} \right)_{\text{prev.}} - [A_1]^T \begin{Bmatrix} x_{1j} \\ y_{1j} \\ z_{1j} \end{Bmatrix}_{\text{prev.}} \right] \quad (21)$$

Equation (21) gives the three incremental beam deflections (point  $j$  relative to point  $i$ ); the incremental rotations are now derived. The incremental rotations of point  $j$  relative to point  $i$ , in  $i$ th mass axes, are evidently given by

$$\begin{Bmatrix} \Delta \phi_{b_{1j}} \\ \Delta \theta_{b_{1j}} \\ \Delta \psi_{b_{1j}} \end{Bmatrix}_{i \text{ axes}} = [A_1]^T [A_j] \begin{Bmatrix} \Delta \text{inp}_j \\ \Delta \text{inq}_j \\ \Delta \text{inr}_j \end{Bmatrix} - \begin{Bmatrix} \Delta \text{inp}_1 \\ \Delta \text{inq}_1 \\ \Delta \text{inr}_1 \end{Bmatrix} \quad (22)$$

where the incremental angles on the right-hand side of the equation are the incremental changes in the integral of the angular velocities for masses  $i$  and  $j$ .

This equation assumes that the incremental rotations can be treated as vectors, which is true only for small angles. However, since  $\Delta t$  for the numerical integration is normally chosen quite small, these angles are sufficiently small to treat as vectors. Transforming (22) into beam  $ij$  axes, we obtain

$$\begin{Bmatrix} \Delta \phi_{b_{1j}} \\ \Delta \theta_{b_{1j}} \\ \Delta \psi_{b_{1j}} \end{Bmatrix} = [A_{1j}]^T \left[ [A_1]^T [A_j] \begin{Bmatrix} \Delta \text{inp}_j \\ \Delta \text{inq}_j \\ \Delta \text{inr}_j \end{Bmatrix} - \begin{Bmatrix} \Delta \text{inp}_1 \\ \Delta \text{inq}_1 \\ \Delta \text{inr}_1 \end{Bmatrix} \right] \quad (23)$$

Equations (21) and (23) give us the three deflections and three rotations of point  $j$  with respect to point  $i$ , in beam  $ij$  axes. These are now utilized to compute the forces and moments at point  $j$  due to these deflections and rotations.

2. Beam Forces and Moments at Point j - The forces and moments at point j, in beam ij axes, denoted  $\Delta F_{ijk}$  ( $k = x, y, z, \phi, \theta, \psi$ ), are indicated in Figure 3. These are the loads acting on the beam; the loads acting on mass j are equal in magnitude and opposite in direction. Positive loads acting on the beam at point j are in the same direction as the six relative deflections (j with respect to i) calculated in the previous section.

The incremental loads at j are calculated from the incremental deflections utilizing a  $6 \times 6$  stiffness matrix for beam ij. This linear relationship is then modified by a diagonal stiffness reduction ( $KR_{ij}$ ) matrix, resulting in the following governing equation for the incremental loads at point j:

$$\{\Delta F_{ij}\} = [K_{ij}][KR_{ij}]\{\Delta v_{ij}\} \quad (24)$$

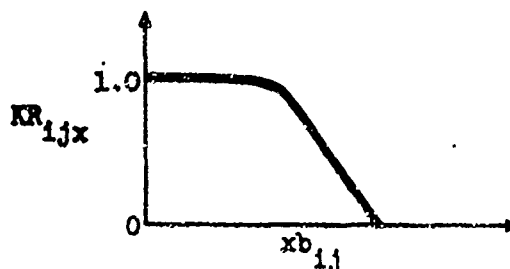
where  $\{\Delta v_{ij}\}$  is now defined as a six-element vector as follows:

$$\{\Delta v_{ij}\} = \begin{Bmatrix} \Delta x_{b_{ij}} \\ \Delta y_{b_{ij}} \\ \Delta z_{b_{ij}} \\ \Delta \phi_{b_{ij}} \\ \Delta \theta_{b_{ij}} \\ \Delta \psi_{b_{ij}} \end{Bmatrix} \quad (25)$$

The elements of  $\{\Delta v_{ij}\}$  come from equations (21) and (23) from the previous section. Each element of  $[KR_{ij}]$  is input to the program as a tabular function of the corresponding element of  $\{v_{ij}\}$ , where  $\{v_{ij}\}$  is just the total beam deflection given by

$$\underbrace{\{v_{ij}\}}_{\text{current}} = \underbrace{\{v_{ij}\}}_{\text{previous}} + \{\Delta v_{ij}\} \quad (26)$$

A typical  $KR_{ij}$  input table is shown in the following sketch:





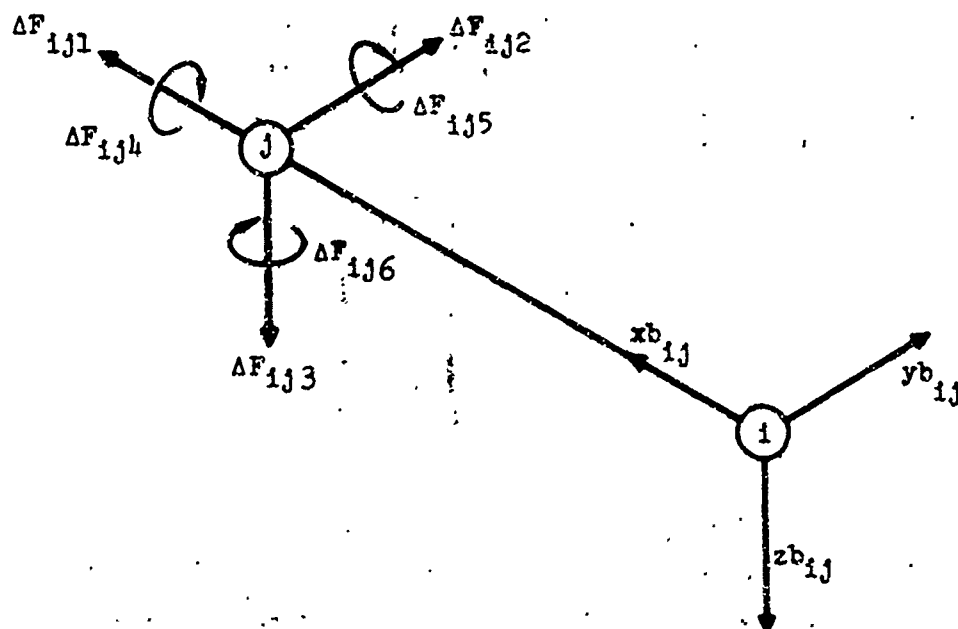
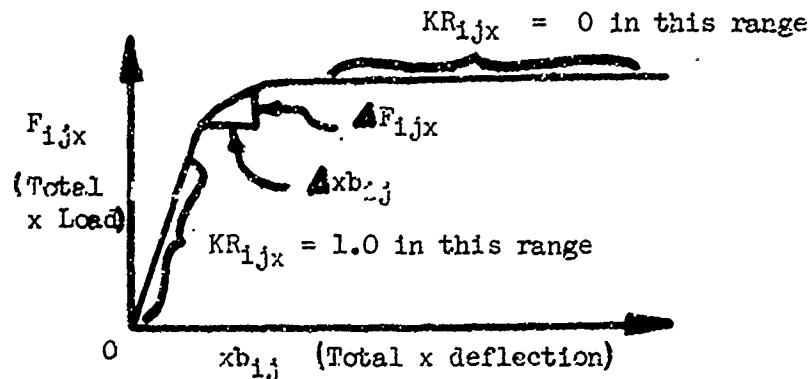


Figure 3. Beam Loads.

$KR_{ijx}$  starts out at 1.0 for small deflections  $xb_{ij}$ , corresponding to a linear analysis. Beyond a certain limiting deflection,  $KR_{ijx}$  becomes less than 1.0, representing nonlinear softening of beam  $ij$  in the axial ( $x$ ) direction. Since equation (24) is written on an incremental basis, each increment varies according to  $KR_{ij}$  so that a total load versus total deflection curve would look like the following:



Obviously the total loads are just the time sums of the incremental loads in (24):

$$\begin{matrix} \{F_{ij}\} \\ \text{current} \end{matrix} = \begin{matrix} \{F_{ij}\} \\ \text{previous} \end{matrix} + \{\Delta F_{ij}\} \quad (27)$$

The above illustration shows the  $x$  load varying only with the  $x$  deflection. In general, equation (24) shows each of the 6 loads varying with all 6 deflections, via the  $6 \times 6$   $[K_{ij}]$  linear stiffness matrix. Thus, in general, any load depends on all 6 deflections and also all 6  $KR_{ij}$  input tables. In practice, the stiffness matrix  $[K_{ij}]$  would seldom be fully populated.

In addition to the nonlinear load capability just described, the program also allows for unloading and subsequent reloading to proceed along an elastic line. This is illustrated in Figure 4. The ordinate  $FM_{ijkl}$  is the total (over time)  $k$ th load due to the  $l$ th deflection  $vb_{ijl}$  for beam  $ij$ . Also shown is a typical incremental load  $\Delta FM_{ijkl}$  due to the incremental deflection  $\Delta vb_{ijl}$ . The  $\Delta FM_{ijkl}$  are the six individual terms that make up each  $\Delta F_{ijk}$  in equation (24), i.e.,

$$\Delta F_{ijk} = \sum_{l=1}^6 \Delta F_{M_{ijkl}} \quad (28)$$

Thus, for example, Figure 4 could represent the total (over time) y force due to  $\psi$  rotations plotted against  $\psi$  rotation, for beam ij.

Loading proceeds along the solid line O-F-A. Unloading then proceeds along dashed line A-B, parallel to the original linear loading line O-F. Subsequent reloading then proceeds along B-A, until point A is reached. At this point, further loading proceeds along A-C. At point C, fracture occurs and the load drops to zero.

Note that if unloading occurs along the original elastic portion of the curve (O-F), unloading will be along F-O. The intent of this loading-unloading model is to represent crushing structure with elastic rebound.

The important feature represented here is the energy absorbed by the structure in a loading-unloading-reloading cycle such as O-F-A-B-C. It is felt that under the large deformation crash conditions that this program is intended to investigate, this energy absorption is far more significant than the small structural damping generally present.

A flow diagram for the calculation of the loading-unloading forces is shown in Figure 5. The equation for  $\Delta F_{M_{ijkl}}$  is just each term of equation (24); the summation over l gives the  $\Delta F_{ijk}$  of (24). In Figure 5, if  $K_{ijkl} \neq 0$ , then the sign of  $\Delta v_{b_{ijl}}$  is compared to the sign of  $(v_{b_{ijl}} + \Delta v_{b_{ijl}})$ , i.e., the sign of the current incremental deflection is compared to the sign of the current total deflection. If these are equal, then loading is occurring. (This may be in either the upper right hand or lower left-hand quadrants in Figure 4, but is always proceeding away from the origin O.) Then the magnitude of the total deflection is compared to the magnitude of  $v_{b_{ijl}}$ . This is the deflection corresponding to point A of Figure 4, except that it is initially set to zero. Therefore the center path termed "LOADING" will be followed initially. KR is read from an input table and  $\Delta F_{M_{ijkl}}$  is computed.

When point A of Figure 4 is reached and unloading begins, the sign of  $\Delta v_{b_{ijl}}$  will not be equal to the sign of  $(v_{b_{ijl}} + \Delta v_{b_{ijl}})$ . The left-hand branch of Figure 5 will then be followed. The first time through this branch,  $v_{b_{ijl}}$  is set equal to the last  $v_{b_{ijl}}$ , which is point A of Figure 4. Then KR is set equal to 1 for the unloading and  $\Delta F_{M_{ijkl}}$  is computed. As long as unloading proceeds, the left-hand branch is followed and  $KR = 1$ .

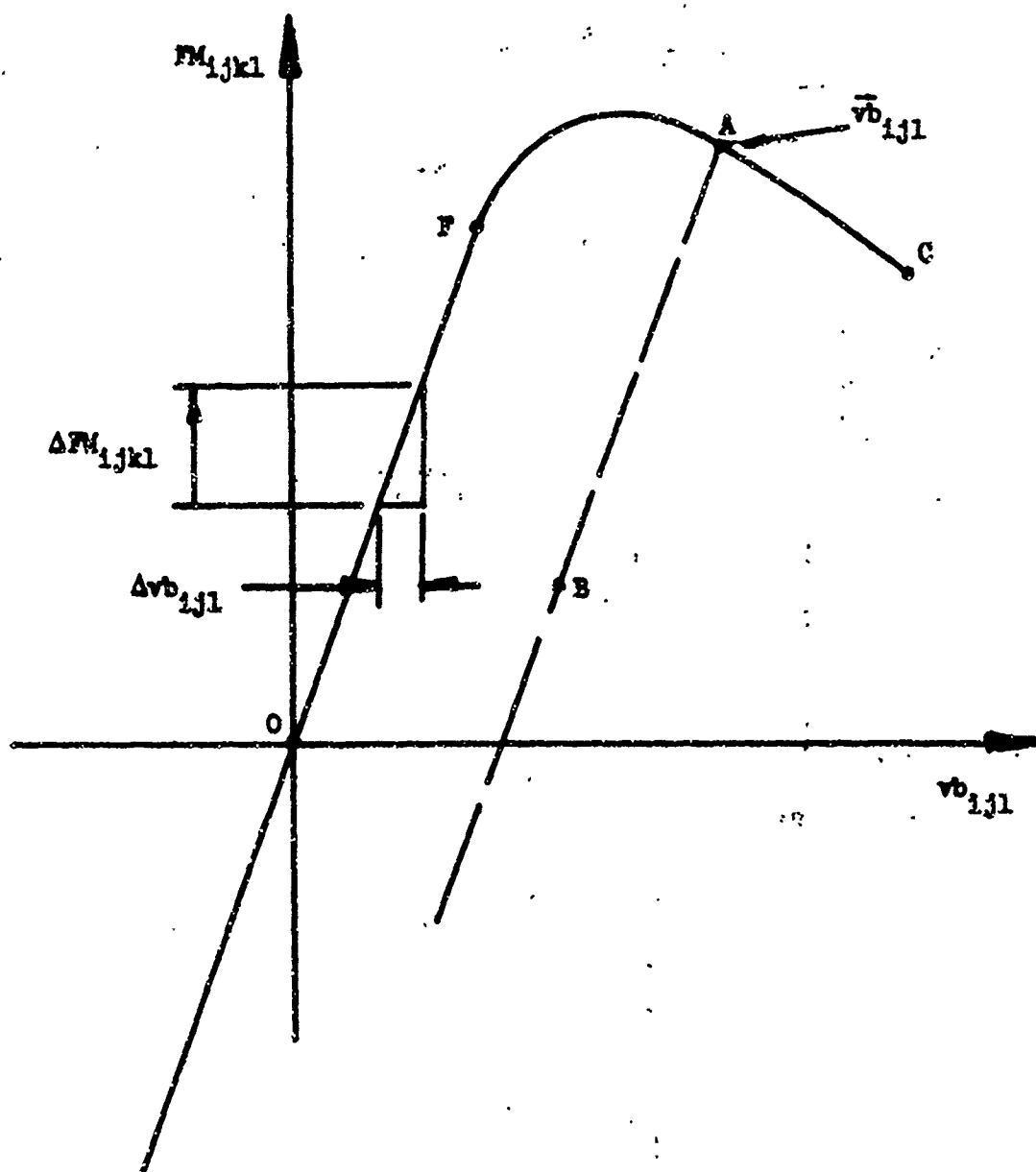


Figure 4. Loading - Unloading Model.

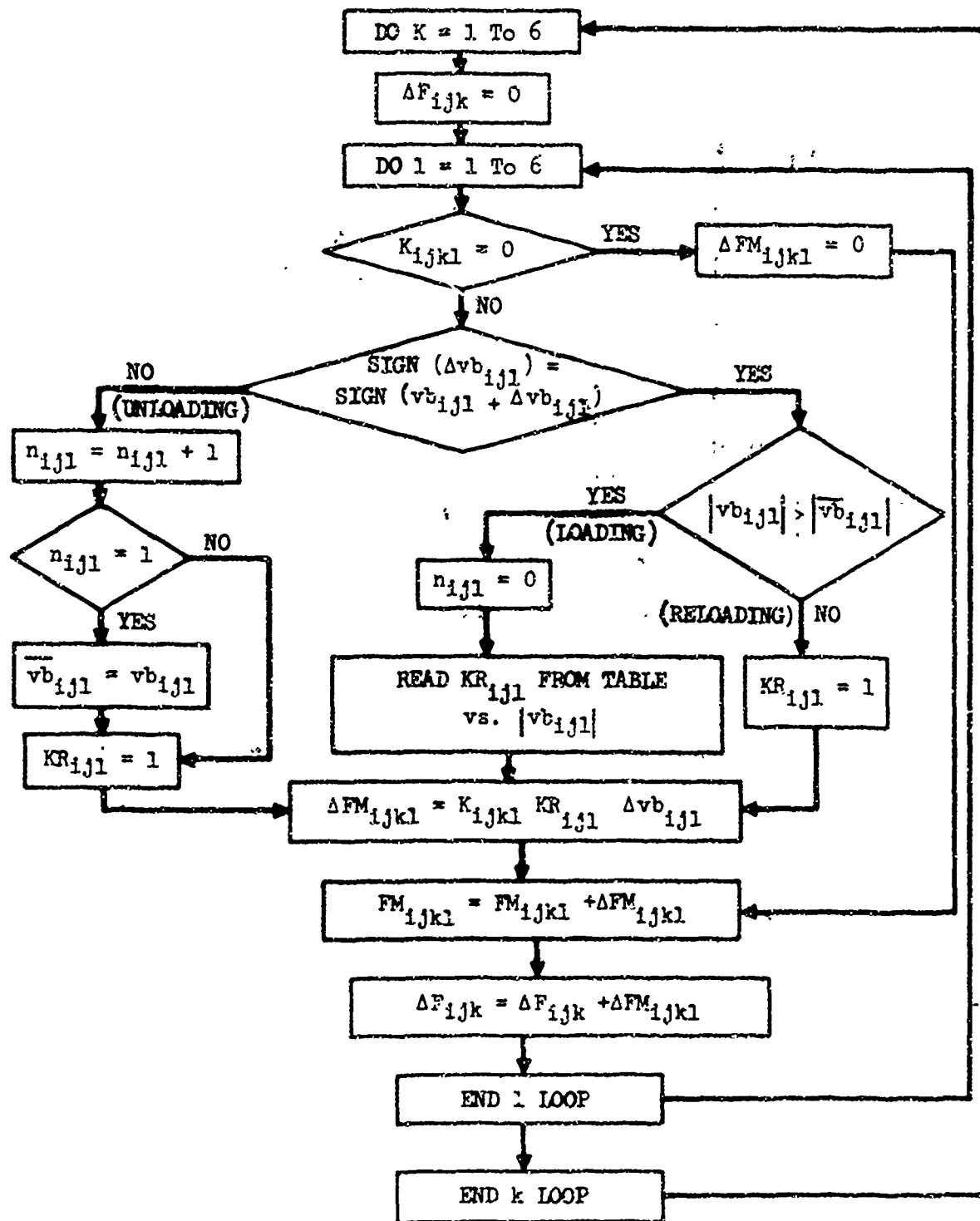


Figure 5. Internal Load Algorithm.

Subsequent reloading occurs along the right-hand branch; the sign of the incremental deflection equals the sign of the total deflection and the magnitude of the deflection is less than  $\bar{v}_{ijl}$ . This corresponds to reloading along B-A in Figure 4. For this situation KR is still 1. Finally, once point A is again reached, further loading proceeds along the original curve A-C. The center branch is again followed since  $|v_{ijl}| > |\bar{v}_{ijl}|$ , and KR is again read from the input table.

Equation (26), updating  $v_{ijl}$ , follows immediately after the coding shown in Figure 5; this also includes a test for fracture of beam ij. Thus, if any one of the six  $v_{ijl}$ 's for beam ij is greater in magnitude than an input constant,  $v_{MAX_{ijl}}$ , beam ij fractures and its internal forces are set to zero for the remainder of the run.

Thus, the algorithm shown in Figure 5 computes the six forces and moments at point j,  $\Delta F_{ijk}$ , in beam ij axes, according to the sign convention in Figure 3.

3. Internal Forces and Moments Acting on Mass 1 - The  $\Delta F_{ijk}$  just computed are transformed into ground axes as follows:

$$\begin{Bmatrix} \Delta X_{ij}^o \\ \Delta Y_{ij}^o \\ \Delta Z_{ij}^o \end{Bmatrix} = [A_1][A_{ij}] \begin{Bmatrix} \Delta X_{ij} \\ \Delta Y_{ij} \\ \Delta Z_{ij} \end{Bmatrix} \quad (28a)$$

where the superscript o refers to ground axes and the right-hand vector is made up of the first three elements of  $\Delta F_{ijk}$ . Similarly, for the three moments, we have

$$\begin{Bmatrix} \Delta L_{ij}^o \\ \Delta M_{ij}^o \\ \Delta N_{ij}^o \end{Bmatrix} = [A_1][A_{ij}] \begin{Bmatrix} \Delta L_{ij} \\ \Delta M_{ij} \\ \Delta N_{ij} \end{Bmatrix} \quad (28b)$$

Next, a static balance is performed on the beam (since the beam is assumed massless, it has no inertia forces) to obtain the loads at point i, acting on the beam, in ground axes. These are denoted the same as those at j except with a bar. Figure 6 shows the

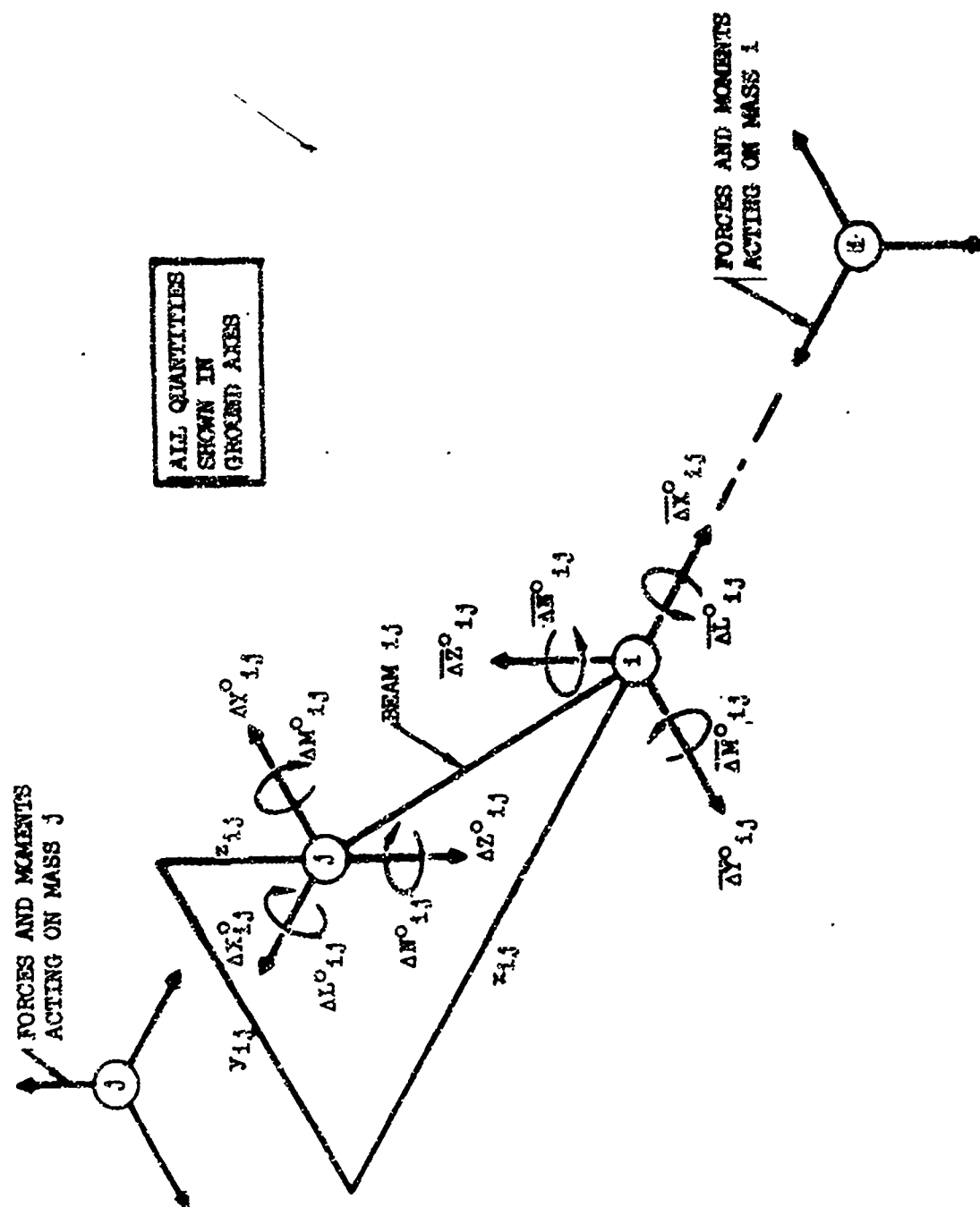


Figure 6. Beam Internal Load Static Balance.

positive loads, in ground axes, at i and j acting on the beam.  $x_{ij}$ ,  $y_{ij}$ ,  $z_{ij}$  are simply the current distances between j and i in ground axes, shown in Figure 6. These are given by

$$\begin{Bmatrix} x_{ij} \\ y_{ij} \\ z_{ij} \end{Bmatrix} = \begin{Bmatrix} x_j - x_i \\ y_j - y_i \\ z_j - z_i \end{Bmatrix} \quad (29)$$

The static balance equations, from Figure 6, yield simply

$$\begin{Bmatrix} \Delta \bar{X}_{ij}^0 \\ \Delta \bar{Y}_{ij}^0 \\ \Delta \bar{Z}_{ij}^0 \end{Bmatrix} = \begin{Bmatrix} \Delta X_{ij}^0 \\ \Delta Y_{ij}^0 \\ \Delta Z_{ij}^0 \end{Bmatrix} \quad (30a)$$

and

$$\begin{Bmatrix} \Delta \bar{L}_{ij}^0 \\ \Delta \bar{M}_{ij}^0 \\ \Delta \bar{N}_{ij}^0 \end{Bmatrix} = \begin{Bmatrix} \Delta L_{ij}^0 \\ \Delta M_{ij}^0 \\ \Delta N_{ij}^0 \end{Bmatrix} + [T_{ij}] \begin{Bmatrix} \Delta X_{ij}^0 \\ \Delta Y_{ij}^0 \\ \Delta Z_{ij}^0 \end{Bmatrix} \quad (30b)$$

The matrix  $[T_{ij}]$  is given simply by

$$[T_{ij}] = \begin{bmatrix} 0 & -z_{ij} & y_{ij} \\ z_{ij} & 0 & -x_{ij} \\ -y_{ij} & x_{ij} & 0 \end{bmatrix} \quad (31)$$

Finally, these loads at point i are transformed back into ith mass axes, since it is in these axes that the internal forces are desired for Euler's equations of motion. (They were transformed from beam to ground axes only to simplify the static balance equations.) Thus, we have

$$\begin{Bmatrix} \Delta X'_{ij} \\ \Delta Y'_{ij} \\ \Delta Z'_{ij} \end{Bmatrix} = [A_i]^T \begin{Bmatrix} \Delta \bar{X}_{ij}^0 \\ \Delta \bar{Y}_{ij}^0 \\ \Delta \bar{Z}_{ij}^0 \end{Bmatrix} \quad (32a)$$



$$\begin{Bmatrix} \Delta L_{ij} \\ \Delta M_{ij} \\ \Delta N_{ij} \end{Bmatrix} = [A_i]^T \begin{Bmatrix} \Delta L_{ij}^o \\ \Delta M_{ij}^o \\ \Delta N_{ij}^o \end{Bmatrix} \quad (32b)$$

The loads acting on mass  $j$ , in  $j$ th mass axes, are similarly obtained from the loads at point  $j$  acting on the beam (equation (28)) in ground axes, by

$$\begin{Bmatrix} \Delta X_{ji} \\ \Delta Y_{ji} \\ \Delta Z_{ji} \end{Bmatrix} = -[A_j]^T \begin{Bmatrix} \Delta X_{ij}^o \\ \Delta Y_{ij}^o \\ \Delta Z_{ij}^o \end{Bmatrix} \quad (33a)$$

$$\begin{Bmatrix} \Delta L_{ji} \\ \Delta M_{ji} \\ \Delta N_{ji} \end{Bmatrix} = -[A_j]^T \begin{Bmatrix} \Delta L_{ij}^o \\ \Delta M_{ij}^o \\ \Delta N_{ij}^o \end{Bmatrix} \quad (33b)$$

The minus sign is necessary because the sense of the loads acting on mass  $j$  is opposite the sign convention for the loads acting on mass  $j$  (see Figure 6). The minus signs in equations (33) and none in equations (32) are the result of the opposite definitions for the loads acting on the beam at points  $i$  and  $j$  shown in Figure 6.

The incremental loads from equations (32) and (33) are now summed over time to obtain the total loads:

$$\begin{Bmatrix} X_{ij} \\ Y_{ij} \\ Z_{ij} \\ L_{ij} \\ M_{ij} \\ N_{ij} \end{Bmatrix} = \begin{Bmatrix} X_{ij} \\ Y_{ij} \\ Z_{ij} \\ L_{ij} \\ M_{ij} \\ N_{ij} \end{Bmatrix} + \begin{Bmatrix} \Delta X_{ij} \\ \Delta Y_{ij} \\ \Delta Z_{ij} \\ \Delta L_{ij} \\ \Delta M_{ij} \\ \Delta N_{ij} \end{Bmatrix} \quad (34a)$$

↑ current      ↑ previous

$$\begin{pmatrix} X'_{ji} \\ Y'_{ji} \\ Z'_{ji} \\ L'_{ji} \\ M'_{ji} \\ N'_{ji} \end{pmatrix} = \begin{pmatrix} X'_{ji} \\ Y'_{ji} \\ Z'_{ji} \\ L'_{ji} \\ M'_{ji} \\ N'_{ji} \end{pmatrix} + \begin{pmatrix} \Delta X'_{ji} \\ \Delta Y'_{ji} \\ \Delta Z'_{ji} \\ \Delta L'_{ji} \\ \Delta M'_{ji} \\ \Delta N'_{ji} \end{pmatrix} \quad (34b)$$

$\uparrow$                        $\uparrow$   
 current                  previous

The total internal forces and moments acting on mass  $i$  are now computed by summing equations (34) over the second subscript, holding the first subscript constant:

$$\begin{aligned}
 X_{I_i} &= \sum_{j=1}^N X'_{ij} & Y_{I_i} &= \sum_{j=1}^N Y'_{ij} & Z_{I_i} &= \sum_{j=1}^N Z'_{ij} \\
 L_{I_i} &= \sum_{j=1}^N L'_{ij} & M_{I_i} &= \sum_{j=1}^N M'_{ij} & N_{I_i} &= \sum_{j=1}^N N'_{ij}
 \end{aligned} \quad (35)$$

where  $N$  is the total number of masses. As an example, assume a four-mass system fully interconnected. Equation (34a) gives the

$F'_{12}$   
 $13$   
 $14$   
 $23$   
 $24$   
 $34$                   loads.

Equation (34b) gives the

$F'_{21}$   
 $31$   
 $41$   
 $32$   
 $42$   
 $43$                   loads.

Thus, equation (35) sums over the second subscript, holding the first subscript constant, to obtain the total internal loads from all the beams:

$$F_{I_1} = F_{12}' + F_{13}' + F_{14}'$$

$$F_{I_2} = \textcircled{F_{21}'} + F_{23}' + F_{24}'$$

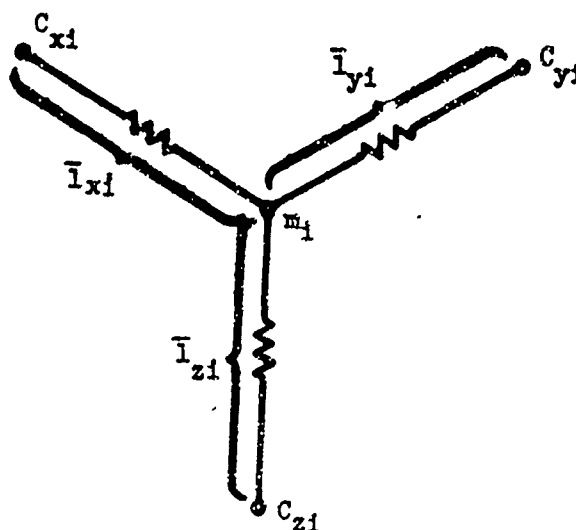
$$F_{I_3} = \textcircled{F_{31}'} + \textcircled{F_{32}'} + F_{34}'$$

$$F_{I_4} = \textcircled{F_{41}'} + \textcircled{F_{42}'} + \textcircled{F_{43}'}$$

The circled terms come from equation (34b); the others, from (34a).  $F_{ij}' = 0$  for  $i = j$  (there is no beam from  $i$  to  $i$ ). The above scheme is used so that the loads at each end of the beam  $ij$  are not computed twice (once for mass  $i$  and again for mass  $j$ ). Equation (35) gives the desired total internal loads to be used later to determine the total loads acting on mass  $i$ .

Crash (External) Forces and Moments ( $X_{ci}$ ,  $Y_{ci}$ ,  $Z_{ci}$ ,  $L_{ci}$ ,  $M_{ci}$ , and  $N_{ci}$ )

The crash forces result from the compression of external springs radiating from each mass, when these springs contact the ground plane ( $z = 0$ ). The following sketch shows the three springs radiating outward from mass  $i$ :



The free (uncompressed) lengths of the three springs are denoted  $\bar{l}_{xi}$ ,  $\bar{l}_{yi}$ , and  $\bar{l}_{zi}$ . These springs lie along the body axes for the  $i$ th mass.  $\bar{l}_{xi}$ ,  $\bar{l}_{yi}$ , and  $\bar{l}_{zi}$  are input either positive or negative, depending upon whether the spring radiates outward along the positive or negative body axis. Those shown above are all positive springs.  $C_{xi}$ ,  $C_{yi}$ , and  $C_{zi}$  are the end points of the fully extended springs. Only data for those springs desired in the analysis need be input; if no spring is input, its crash forces are set to zero. Typically, only those masses at the extremities of the vehicle likely to contact the ground would have crash springs. The intent of these springs is to represent crushable external structure such as found on the lower fuselage and nose sections.

The first step in the calculation is to determine which of the  $C_{xi}$ ,  $C_{yi}$ , and  $C_{zi}$  spring end points are below the ground. Only these springs are further analyzed to determine their crash forces. For these springs, the spring compression along the spring axis is determined, as well as the compression velocity and the ground contact point velocity. Then the spring force along the spring axis is calculated, from which the vertical load in ground axes at the ground contact point is obtained. From this vertical load and input friction coefficients, the ground drag load is computed. The direction of this load is opposite the ground contact point velocity vector. Finally, the three forces at the ground contact point are rotated into  $i$ th mass body axes, and the resulting forces and moments at mass  $i$  are calculated.

1. Spring Compression - Figure 7 shows a typical spring contacting the ground at an oblique angle. Point  $C'_i$  is the ground contact point. Treating the fully extended spring as a vector, that portion of the vector below the ground represents the spring compression. This is the distance from point  $C'_i$  to point  $C_i$ . The coordinates of point  $C_i$ , in ground axes, are given simply by

$$\begin{bmatrix} x_{C_{xi}} & x_{C_{yi}} & x_{C_{zi}} \\ y_{C_{xi}} & y_{C_{yi}} & y_{C_{zi}} \\ z_{C_{xi}} & z_{C_{yi}} & z_{C_{zi}} \end{bmatrix} = \begin{bmatrix} x_i & x_i & x_i \\ y_i & y_i & y_i \\ z_i & z_i & z_i \end{bmatrix} + [A_i] \begin{bmatrix} \bar{l}_{xi} \\ \bar{l}_{yi} \\ \bar{l}_{zi} \end{bmatrix} \quad (36)$$

The above equation gives the coordinates of all three  $C_i$  for mass  $i$ ; these points are denoted  $C_{xi}$ ,  $C_{yi}$ , and  $C_{zi}$ . Figure 7 shows only one of the three springs, so the nomenclature in Figure 7 is

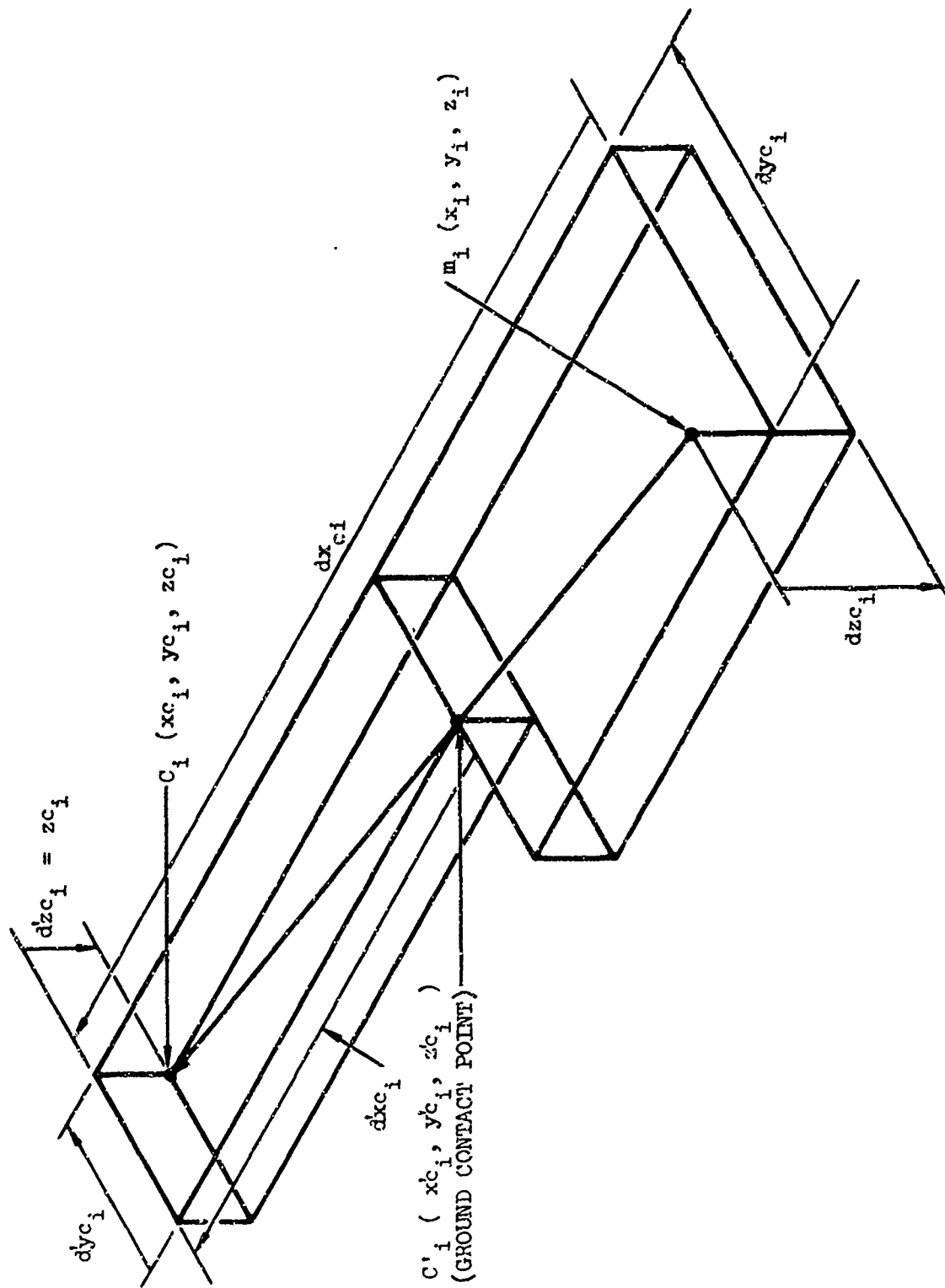


Figure 7. External Spring Compression Geometry.

not subscripted to indicate whether an x, y or z spring is shown. The second term in the above equation is equal to  $dx_{ci}$ ,  $dy_{ci}$ , and  $dz_{ci}$  in Figure 7:

$$\begin{bmatrix} dxc_{xi} & dxc_{yi} & dxc_{zi} \\ dyc_{xi} & dyc_{yi} & dyc_{zi} \\ dzc_{xi} & dzc_{yi} & dzc_{zi} \end{bmatrix} = [A_i] \begin{bmatrix} \bar{l}_{xi} \\ \bar{l}_{yi} \\ \bar{l}_{zi} \end{bmatrix} \quad (37)$$

The  $dxc_i$ ,  $dyc_i$ , and  $dzc_i$  in Figure 7 can be determined from proportionality considerations as

$$\begin{Bmatrix} dxc_{xi} \\ dyc_{xi} \\ dzc_{xi} \end{Bmatrix} = \frac{zc_{xi}}{dzc_{xi}} \begin{Bmatrix} dxc_{xi} \\ dyc_{xi} \\ dzc_{xi} \end{Bmatrix} \quad (38)$$

and similarly for the y and z springs,

$$\begin{Bmatrix} dxc_{yi} \\ dyc_{yi} \\ dzc_{yi} \end{Bmatrix} = \frac{zc_{yi}}{dzc_{yi}} \begin{Bmatrix} dxc_{yi} \\ dyc_{yi} \\ dzc_{yi} \end{Bmatrix} \quad (38)$$

$$\begin{Bmatrix} dxc_{zi} \\ dyc_{zi} \\ dzc_{zi} \end{Bmatrix} = \frac{zc_{zi}}{dzc_{zi}} \begin{Bmatrix} dxc_{zi} \\ dyc_{zi} \\ dzc_{zi} \end{Bmatrix}$$

From these ground axes components of the vector from  $C_i'$  to  $C_i$ , the magnitude of this vector (equal to the spring compression) is given simply by

$$\begin{aligned}
s_{xi} &= \left[ (\dot{dxc}_{xi})^2 + (\dot{dyc}_{xi})^2 + (\dot{dzc}_{xi})^2 \right]^{1/2} \\
s_{yi} &= \left[ (\dot{dxc}_{yi})^2 + (\dot{dyc}_{yi})^2 + (\dot{dzc}_{yi})^2 \right]^{1/2} \\
s_{zi} &= \left[ (\dot{dxc}_{zi})^2 + (\dot{dyc}_{zi})^2 + (\dot{dzc}_{zi})^2 \right]^{1/2}
\end{aligned} \tag{39}$$

In order to simplify the notation, the following vectors and matrices are defined ( $i = 1, 2, \dots, N$  indicates the mass;  $j = 1, 2, 3$  indicates the direction;  $k = 1, 2, 3$  indicates which spring):

$$\bar{l}_{ik} \triangleq \begin{Bmatrix} \bar{l}_{xi} \\ \bar{l}_{yi} \\ \bar{l}_{zi} \end{Bmatrix}, \quad va_{ij} \triangleq \begin{Bmatrix} x_i \\ y_i \\ z_i \end{Bmatrix}, \quad s_{ik} \triangleq \begin{Bmatrix} s_{xi} \\ s_{yi} \\ s_{zi} \end{Bmatrix} \tag{40}$$

$$dvc_{ijk} \triangleq_j \begin{bmatrix} dxc_{xi} & dxc_{yi} & dxc_{zi} \\ dyc_{xi} & dyc_{yi} & dyc_{zi} \\ dzc_{xi} & dzc_{yi} & dzc_{zi} \end{bmatrix}_k \tag{41}$$

$$vc_{ijk} \triangleq_j \begin{bmatrix} xc_{xi} & xc_{yi} & xc_{zi} \\ yc_{xi} & yc_{yi} & yc_{zi} \\ zc_{xi} & zc_{yi} & zc_{zi} \end{bmatrix}_k \tag{42}$$

$$\dot{dvc}_{ijk} \triangleq_j \begin{bmatrix} \dot{dxc}_{xi} & \dot{dxc}_{yi} & \dot{dxc}_{zi} \\ \dot{dyc}_{xi} & \dot{dyc}_{yi} & \dot{dyc}_{zi} \\ \dot{dzc}_{xi} & \dot{dzc}_{yi} & \dot{dzc}_{zi} \end{bmatrix}_k \tag{43}$$

Using this nomenclature, equations (36) through (39) become simply

$$vc_{ijk} = va_{ij} + dvc_{ijk} \tag{44}$$

$$dvc_{ijk} = A_{ijk} \bar{l}_{ik} \quad (45)$$

$$\dot{dvc}_{ijk} = \frac{vc_{13k}}{dvc_{13k}} dvc_{ijk} \quad (46)$$

$$s_{ik} = \left[ \sum_{j=1}^3 (\dot{dvc}_{ijk})^2 \right]^{1/2} \quad (47)$$

We shall also require the spring compression velocity,  $\dot{s}_{ik}$ . This is given by differentiating equation (47) as

$$\dot{s}_{ik} = \frac{1}{2s_{ik}} \sum_{j=1}^3 2 \dot{dvc}_{ijk} (\dot{dvc}_{ijk}) \quad (48)$$

where the last term is obtained from (46) as

$$\dot{dvc}_{ijk} = \frac{vc_{13k}}{dvc_{13k}} dvc_{ijk} + dvc_{ijk} \frac{dvc_{13k} \dot{vc}_{13k} - vc_{13k} \dot{dvc}_{13k}}{(dvc_{13k})^2} \quad (49)$$

The time derivatives in (49) are given by

$$\dot{dvc}_{ijk} = \dot{A}_{ijk} \bar{l}_{ik} \quad j = 1, 2, 3 \quad (50)$$

$$\dot{vc}_{13k} = \dot{z}_1 + \dot{dvc}_{13k} \quad (51)$$

2. Ground Contact Point Velocity - The next computation required is to determine the ground contact point velocity in the ground plane. This is necessary to determine the line of action of the ground plane drag load, which is opposite to the contact point velocity vector. The velocity of point C' with respect to ground is given in vector notation as

$$\vec{0} \rightarrow C' = \vec{m}_1 \rightarrow C' + \vec{0} \rightarrow m_1 \quad (52)$$



where  $0 \xrightarrow{\quad} C'$

$\nabla$  = velocity of  $C'$  with respect to ground

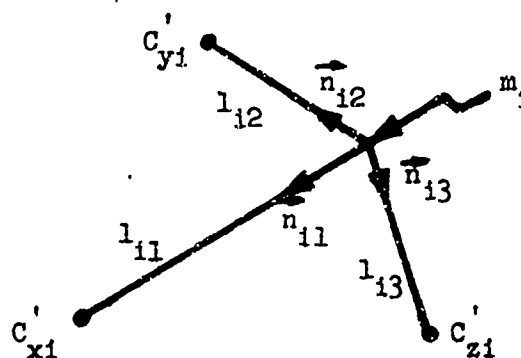
$m_i \xrightarrow{\quad} C'$

$\nabla$  = velocity of  $C'$  with respect to point  $m_i$

$0 \xrightarrow{\quad} m_i$

$\nabla$  = velocity of point  $m_i$  with respect to ground

Define  $\bar{n}_{ik}$  as a unit vector radiating from  $m_i$  parallel to the  $i$ th mass body fixed axes, as shown in the following sketch:



Also define  $l_{ik}$  as the length from  $m_i$  to point  $C'$ . This is given by

$$l_{ik} = \text{SIGN}(\bar{l}_{ik}) \left| |\bar{l}_{ik}| - s_{ik} \right| \quad (53)$$

This form is used so that  $l_{ik}$  has the same sign as the input  $\bar{l}_{ik}$ , which as mentioned earlier can be negative to allow springs in the negative direction of the body axes. Returning to equation (52),  $0 \xrightarrow{\quad} m_i$  is given by

$$0 \xrightarrow{\quad} m_i = \dot{x}_i \bar{n}_x + \dot{y}_i \bar{n}_y + \dot{z}_i \bar{n}_z \quad (54)$$

where  $\bar{n}_x$ ,  $\bar{n}_y$ , and  $\bar{n}_z$  are unit vectors fixed in the ground coordinate system.  $m_i \xrightarrow{\quad} C'$  is given by

$$\underset{\vee}{m_i \rightarrow C'} = -\dot{s}_{ik} \bar{n}_{ik} + \overset{0 \rightarrow m_i}{\omega} \times l_{ik} \bar{n}_{ik} \quad k = 1, 2, 3 \quad (55)$$

where  $\overset{0 \rightarrow m_i}{\omega}$  is the angular velocity vector of  $m_i$  with respect to the ground. This is defined as

$$\overset{0 \rightarrow m_i}{\omega} \triangleq p_i \bar{n}_{i1} + q_i \bar{n}_{i2} + r_i \bar{n}_{i3} \quad (56)$$

in body fixed axes. Equation (55), therefore, becomes

$$\underset{\vee}{m_i \rightarrow C'} = -\dot{s}_{ik} \bar{n}_{ik} + (p_i \bar{n}_{i1} + q_i \bar{n}_{i2} + r_i \bar{n}_{i3}) \times l_{ik} \bar{n}_{ik} \quad (57)$$

$k = 1, 2, 3$

Expanding the cross product and combining terms, we obtain

$$\underset{\vee}{m_i \rightarrow C'} = \begin{aligned} & -\dot{s}_{i1} \bar{n}_{i1} + r_i l_{i1} \bar{n}_{i2} - q_i l_{i1} \bar{n}_{i3} & k = 1 \\ & -r_i l_{i2} \bar{n}_{i1} - \dot{s}_{i2} \bar{n}_{i2} + p_i l_{i2} \bar{n}_{i3} & k = 2 \\ & q_i l_{i3} \bar{n}_{i1} - p_i l_{i3} \bar{n}_{i2} - \dot{s}_{i3} \bar{n}_{i3} & k = 3 \end{aligned} \quad (58)$$

Denoting the transpose of the above terms by the matrix  $[p l_i]$ , we can obtain  $\underset{\vee}{m_i \rightarrow C'}$  in ground axes simply by premultiplying the  $k$ th column of  $[p l_i]$  by  $[A_i]$ :

$$\underset{\substack{\vee \\ \text{ground} \\ \text{axes}}}{m_i \rightarrow C'} = [A_i] \begin{Bmatrix} p l_{i1k} \\ p l_{i2k} \\ p l_{i3k} \end{Bmatrix} \quad k = 1, 2, 3 \quad (59)$$

Combining (54) and (59), recalling definition (40) for  $v_{ij}$ , we obtain the desired contact velocities as simply

$$v_{cp_{ijk}} = v_{a_{ij}} + \sum_{l=1}^3 A_{ijl} p_{ilk}^l \quad \begin{array}{l} i = 1, 2, \dots, M \\ j = 1, 2, 3, \\ k = 1, 2, 3 \end{array} \quad (60)$$

where

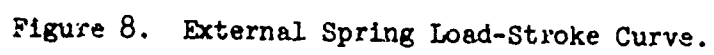
$$[p_i^l] = \frac{1}{k} \begin{bmatrix} -\dot{s}_{i1} & -r_{i12}^l & q_{i13}^l \\ r_{i11}^l & -\dot{s}_{i2} & -p_{i13}^l \\ -q_{i11}^l & p_{i12}^l & -\dot{s}_{i3} \end{bmatrix} \quad (61)$$

Equation (60) gives the desired velocities of the pavement contact points, in ground axes. Only the x and y components are used later; the z component should be zero. Recall that i refers to the ith mass, j the jth direction, and k the kth spring or contact point.

3. External Spring Axial Force - This section discusses the calculation of the external spring force along the spring axis. The axial force in the spring, denoted  $FSPO_{ik}$ , is input as a tabular function of the spring compression  $s_{ik}$ . As with the internal forces, unloading along an elastic line is included. However, unlike the internal forces, an extension load is not allowed; positive  $FSPO_{ik}$  is a compressive load acting at the ground contact point along the axis of spring  $ik$ .

Figure 8 illustrates a typical load-stroke curve for an external spring. The basic loading curve O-A-B-C is input in tabular form vs  $s_{ik}$ , and this curve is followed during the initial loading. During unloading, say, from point B, the dashed line B-D is followed. The slope of this line,  $ke_{ik}$ , is input to the program. During subsequent reloading, curve D-E-F is followed; this is merely the original curve transposed to the right by the amount  $s_{ik}''$ . The dashed coordinate system always contains the original input curve, but the location of the system varies with each unloading cycle. Once  $\bar{s}_{ik}$  goes negative,  $\bar{s}_{ik}$  and  $\bar{FSPO}_{ik}$  are assigned the latest values of  $s_{ik}$  and  $FSPO_{ik}$  (the values at point B). These barred quantities are then used with  $ke_{ik}$  to define  $s_{ik}''$ . The barred quantities are initially set to zero, so that until the first unloading, the dashed coordinates coincide with the solid coordinates.

When the spring compresses beyond point C, a stiff spring  $ke_{ik}$  takes effect (this is the same spring constant as is used for unloading), as shown by line C-F-C in Figure 8. This is intended



to represent the finite crushing distance available, beyond which the spring becomes very stiff. There is no fracture of an external spring, as there is with the internal beams.

The flow diagram for the calculation of the spring force  $FSPO_{ik}$  is shown in Figure 9. The calculations are performed within nested  $i$  and  $k$  loops. The first test on  $SP_{ik}$  is to tell if there is an external spring. If there is, then  $vc_{3k}$  is checked. This is  $zc_{ik}$ , the vertical position of the end of spring  $ik$ . If this is greater than zero, then there will be a spring force. The next test is to see if  $s_{ik} > S_{fik}$ , the final value input in the table of  $s_{ik}$  vs  $FSPO_{ik}$  (point C in Figure 8). If it is greater, the force is computed as  $FSPO_{fik}$  plus an increment due to the  $ke_{ik}$  spring. Then if this is less than zero, it is set to zero.

If  $s_{ik} < S_{fik}$ , then we test  $BS_{ik}$ . This is simply an indicator to see if the bottoming spring has been hit ( $BS_{ik} = 0$  initially). If it has been hit ( $BS_{ik} = 1$ ), then from then on the force is computed along line C-F-G, and its extension downward. If the bottoming spring has not been hit, then  $s'_{ik}$  is computed from  $\bar{s}_{ik}$  and  $FSPO_{ik}$ . During the first loading cycle these will be zero, but after unloading they will be nonzero.  $S'_{ik}$  is then calculated, and  $FSPO_{ik}$  is read from the input table unless  $s'_{ik} < 0$ , in which case  $FSPO_{ik} = 0$ . Then  $\dot{s}_{ik}$  is checked to see if loading or unloading is taking place. The first time unloading occurs,  $nn_{ik} = 0$  and  $FSPO_{ik}$  and  $\bar{s}_{ik}$  are assigned the latest values of  $FSPO_{ik}$  and  $s_{ik}$ . These correspond to point B in Figure 8. During continued unloadings,  $nn_{ik} \neq 0$  so these values are not reassigned until a loading cycle occurs and  $nn_{ik}$  is reset to zero. This completes the calculation of the axial spring force  $FSPO_{ik}$ .

4. Crash Forces at Ground Contact Point - The three components of the ground interaction force at the ground contact point are denoted by  $XVOC_{ijk}$ , where, as before,  $i$  refers to the  $i$ th mass,  $j$  to the force direction, and  $k$  to the  $k$ th spring for mass  $i$ . First the component of the axial spring force perpendicular to the ground is computed. This is positive upward acting on the spring. This is given simply by resolving  $FSPO_{ik}$  into ground axes and retaining only the vertical component. Thus, we have

$$XVOC_{i3k} = A_{i3k} FSPO_{ik} \quad k = 1, 2, 3 \quad (62)$$

since  $FSPO_{ik}$  acts along the  $k$ th body axis for mass  $i$ . The ground plane components of the axial force  $FSPO_{ik}$  are ignored, since these values are next computed on the assumption that they are

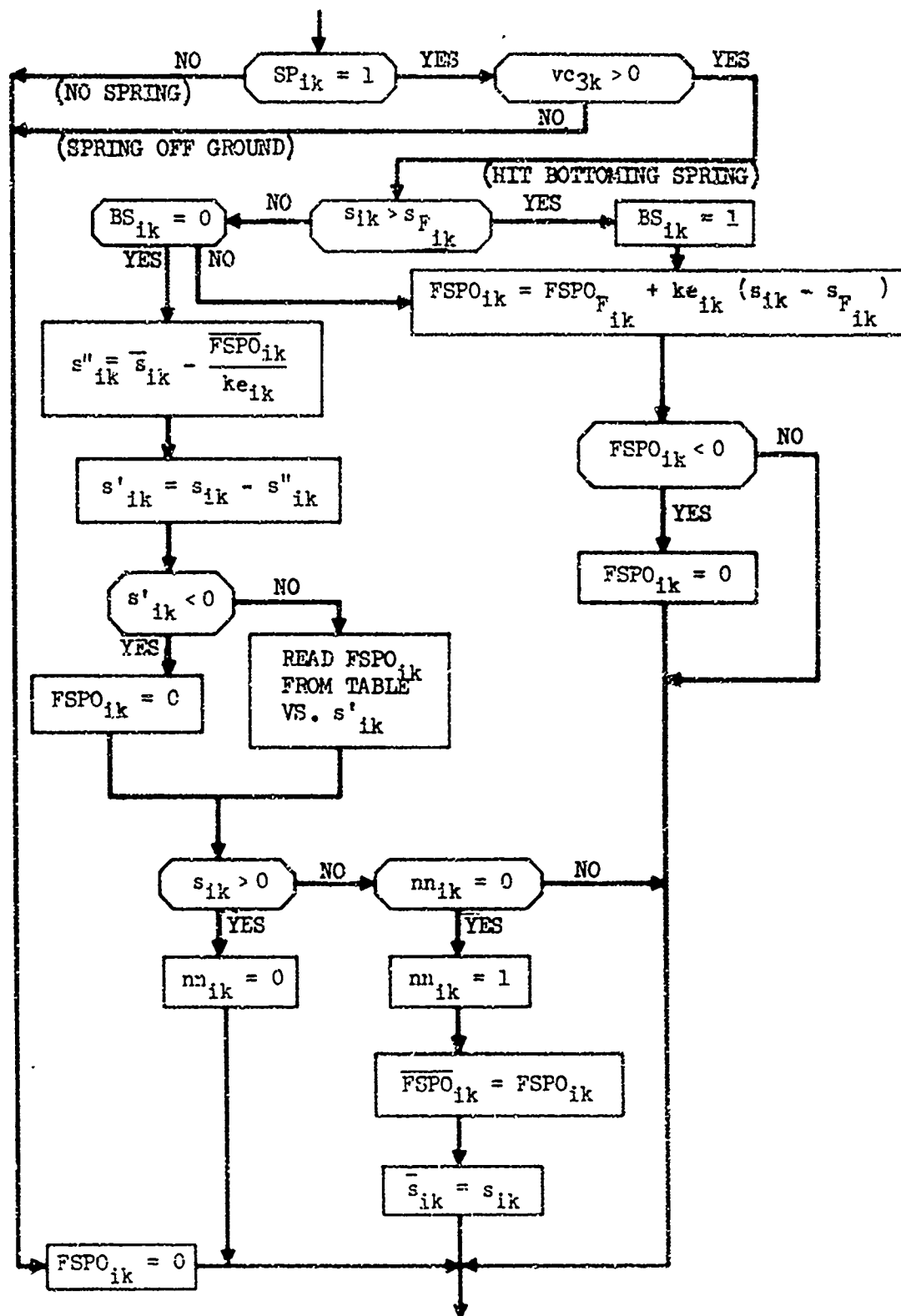
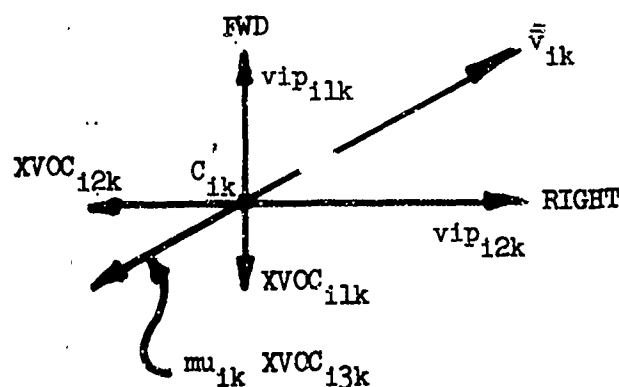


Figure 9. External Load Calculation.

functions of the ground-spring friction coefficient. The ground plane velocity vector, from equation (60), has the magnitude

$$\bar{v}_{ik} = \left[ (\dot{v}_{cp_{11k}})^2 + (\dot{v}_{cp_{12k}})^2 \right]^{1/2} \quad (63)$$

This is shown in the following sketch, a plan view looking downward at ground contact point  $C'_{ik}$ :



The magnitude of the resultant ground plane load is assumed to be given by  $\mu_{ik} XVO_{i3k}$ , i.e., an input friction coefficient times the vertical load perpendicular to the ground plane. The direction of this ground plane load is assumed to be opposite to the contact point velocity vector  $\bar{v}_{ik}$ , as shown in the above sketch. Therefore, the drag and side loads at point  $C'_{ik}$ , in ground axes, are given by

$$XVO_{ijk} = \mu_{ik} XVO_{i3k} \frac{\dot{v}_{cp_{ijk}}}{\bar{v}_{ik}} \quad j = 1, 2 \quad (64)$$

These are illustrated in the above sketch. These forces are now resolved back into ith mass body axes; these resolved forces are denoted by  $FSP_{ijk}$ .

We have

$$\begin{pmatrix} FSP_{11k} \\ FSP_{12k} \\ FSP_{13k} \end{pmatrix} = -[A_i]^T \begin{pmatrix} XVOC_{11k} \\ XVOC_{12k} \\ XVOC_{13k} \end{pmatrix} \quad k = 1, 2, 3 \quad (65)$$

The minus sign is used so that these forces have the same sense as the basic body axis convention, since  $XVOC_{ijk}$  were positive aft, left and upward.

These forces are illustrated in Figure 10.

5. Crash Forces and Moments at Point  $m_i$  - Now we are in a position to obtain the crash forces and moments acting at point  $m_i$ . Figure 10 shows these forces and moments, which are just the resultant of the  $FSP_{ijk}$  also shown in Figure 10; i.e., the  $FSP_{ijk}$  are just moved to point  $m_i$  and compensating moments at  $m_i$  added.

Thus, we have

$$\begin{aligned} X_{c_i} &= \sum_{k=1}^3 FSP_{11k} \\ Y_{c_i} &= \sum_{k=1}^3 FSP_{12k} \quad i = 1, 2, \dots, N \quad (66a) \\ Z_{c_i} &= \sum_{k=1}^3 FSP_{13k} \end{aligned}$$

$$\begin{aligned} L_{c_i} &= FSP_{132} l_{12} - FSP_{123} l_{13} \\ M_{c_i} &= FSP_{113} l_{13} - FSP_{131} l_{11} \quad i = 1, 2, \dots, N \quad (66b) \\ N_{c_i} &= FSP_{121} l_{11} - FSP_{112} l_{12} \end{aligned}$$



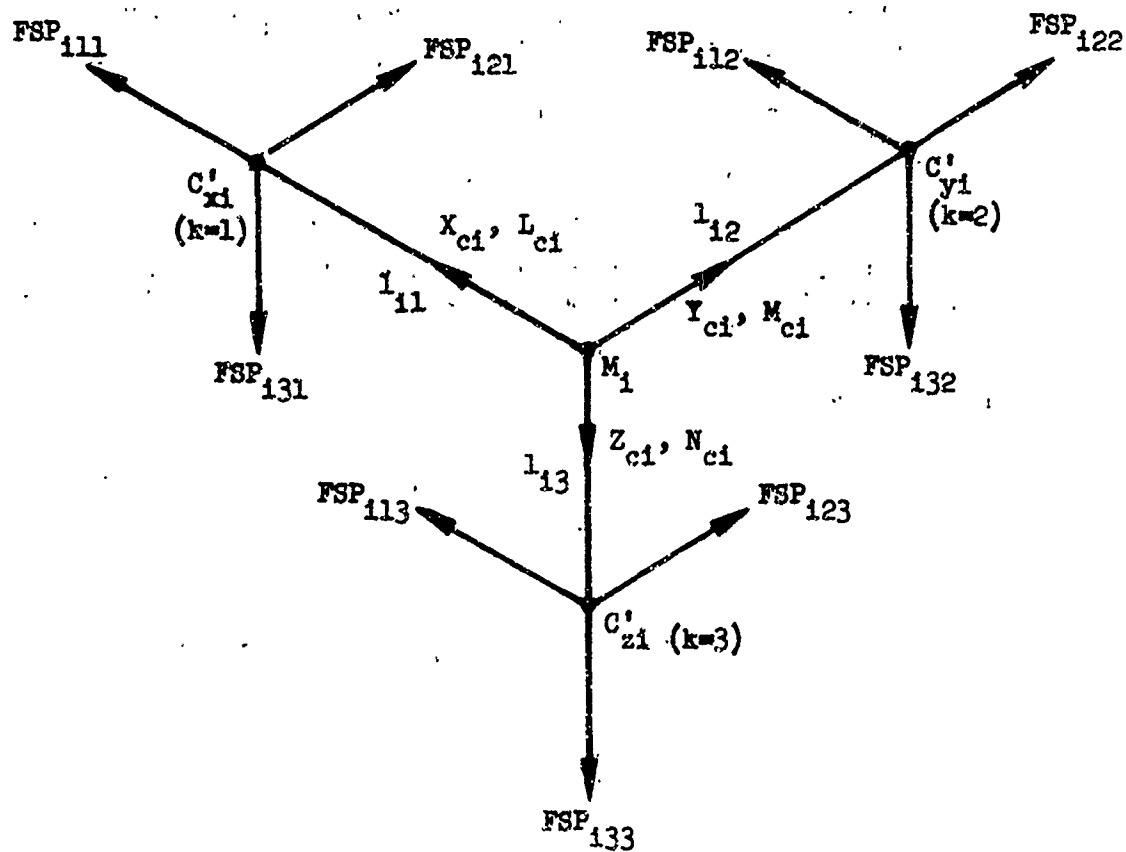


Figure 10. Crash Forces and Moments.

The  $l_{ik}$  are from equation (53); recall that they may be plus or minus to allow for springs in the negative direction of the mass body axes. Figure 10 shows all  $l_{ik}$  positive. Equations (66) give the desired crash forces acting at  $m_i$  in  $i$ th mass body axes.

Damping Forces and Moments (Internal) ( $X_{D_i}$ ,  $Y_{D_i}$ ,  $Z_{D_i}$ ,  $L_{D_i}$ ,  $M_{D_i}$ , and  $N_{D_i}$ )

The damping forces and moments are internal loads in that they act at masses  $i$  and  $j$  due to the damping associated with beam  $ij$ . This damping results from the friction of the joints in the structure that comprises beam  $ij$ , and from the damping inherent in the structural material. For simplicity, the damping is modeled as linear (viscous). Experience with the program indicates that this structural damping, although believed to be small, must be represented in order to control high-frequency structural vibrations.

First, for beam  $ij$ , the linear and angular velocities of point  $j$  with respect to point  $i$  are computed in beam  $ij$  axes. These are then pre-multiplied by a  $6 \times 6$  diagonal damping coefficient matrix to obtain damping forces and moments in beam axes. The damping loads at point  $j$  in beam axes are then transformed into ground axes, and the loads at point  $i$  in ground axes are computed from static equilibrium equations. Then, the loads at  $i$  and  $j$  are transformed into  $i$ th and  $j$ th mass body axes, respectively. Finally, for each mass, the contributions from the various beams that attach to that mass are summed to obtain the total damping loads for the mass. The damping forces calculated are instantaneous total values, rather than incremental loads as were used for the internal loads.

The linear velocities of point  $j$  with respect to point  $i$ , resolved into beam  $ij$  axes, are clearly given by

$$\begin{Bmatrix} \dot{x}_{b_{ij}} \\ \dot{y}_{b_{ij}} \\ \dot{z}_{b_{ij}} \end{Bmatrix} = [A_{ij}]^T \left[ [A_i]^T [A_j] \begin{Bmatrix} u_j \\ v_j \\ w_j \end{Bmatrix} - \begin{Bmatrix} u_i \\ v_i \\ w_i \end{Bmatrix} \right] \quad (67e)$$

where  $u_i$ ,  $v_i$ , and  $w_i$  are the body axes components of the absolute linear velocity of mass  $i$ . Similarly for the angular velocities, we have

$$\begin{Bmatrix} \dot{\phi}_{ij} \\ \dot{\theta}_{ij} \\ \dot{\psi}_{ij} \end{Bmatrix} = [A_{ij}]^T \left[ [A_i]^T [A_j] \begin{Bmatrix} p_j \\ q_j \\ r_j \end{Bmatrix} - \begin{Bmatrix} p_i \\ q_i \\ r_i \end{Bmatrix} \right] \quad (67b)$$

where  $p_i$ ,  $q_i$ , and  $r_i$  are the body axes components of the absolute angular velocity of mass  $i$ . The damping forces, in beam axes, are now computed simply as

$$\{FD_{ij}\} = [C_{ij}] \{\dot{v}_{ij}\} \quad (68)$$

where the velocity and load vectors  $\{\dot{v}_{ij}\}$  and  $\{FD_{ij}\}$  are defined as

$$\{\dot{v}_{ij}\} \triangleq \begin{Bmatrix} \dot{x}_{bij} \\ \dot{y}_{bij} \\ \dot{z}_{bij} \\ \dot{\phi}_{bij} \\ \dot{\theta}_{bij} \\ \dot{\psi}_{bij} \end{Bmatrix} \quad \{FD_{ij}\} \triangleq \begin{Bmatrix} X_{Dij} \\ Y_{Dij} \\ Z_{Dij} \\ L_{Dij} \\ M_{Dij} \\ N_{Dij} \end{Bmatrix} \quad (69)$$

The  $6 \times 6$  damping coefficient matrix  $[C_{ij}]$  is a diagonal matrix, since it is felt that the actual damping values are so poorly known that the inclusion of off-diagonal terms is not justified. The calculation of the  $[C_{ij}]$  matrix is discussed later.

The loads in equation (68) are those acting at mass  $j$ , in beam  $ij$  axes. These are transformed to ground axes as follows:

$$\begin{pmatrix} X_{D1j}^o \\ Y_{D1j}^o \\ Z_{D1j}^o \end{pmatrix} = [A_1][A_{1j}] \begin{pmatrix} X_{D1j} \\ Y_{D1j} \\ Z_{D1j} \end{pmatrix} \quad (70a)$$

and

$$\begin{pmatrix} L_{D1j}^o \\ M_{D1j}^o \\ N_{D1j}^o \end{pmatrix} = [A_1][A_{1j}] \begin{pmatrix} L_{D1j} \\ M_{D1j} \\ N_{D1j} \end{pmatrix} \quad (70b)$$

Now the forces and moments at point i, in ground axes, are computed from static equilibrium in the same manner as in equation (30):

$$\begin{pmatrix} \bar{X}_{D1j}^o \\ \bar{Y}_{D1j}^o \\ \bar{Z}_{D1j}^o \end{pmatrix} = \begin{pmatrix} X_{D1j}^o \\ Y_{D1j}^o \\ Z_{D1j}^o \end{pmatrix} \quad (71a)$$

and

$$\begin{pmatrix} \bar{L}_{D1j}^o \\ \bar{M}_{D1j}^o \\ \bar{N}_{D1j}^o \end{pmatrix} = \begin{pmatrix} L_{D1j}^o \\ M_{D1j}^o \\ N_{D1j}^o \end{pmatrix} + [T_{1j}] \begin{pmatrix} X_{D1j}^o \\ Y_{D1j}^o \\ Z_{D1j}^o \end{pmatrix} \quad (71b)$$

Now, transforming these loads into ith mass axes gives the loads acting on mass  $m_1$  due to beam ij, in ith mass body axes.

$$\begin{Bmatrix} X'_{D1j} \\ Y'_{D1j} \\ Z'_{D1j} \end{Bmatrix} = [A_i]^T \begin{Bmatrix} \bar{X}^o_{D1j} \\ \bar{Y}^o_{D1j} \\ \bar{Z}^o_{D1j} \end{Bmatrix} \quad (72a)$$

and

$$\begin{Bmatrix} L'_{D1j} \\ M'_{D1j} \\ N'_{D1j} \end{Bmatrix} = [A_i]^T \begin{Bmatrix} \bar{L}^o_{D1j} \\ \bar{M}^o_{D1j} \\ \bar{N}^o_{D1j} \end{Bmatrix} \quad (72b)$$

The loads at mass  $m_j$ , in  $j$ th body axes, are obtained from equation (70) as

$$\begin{Bmatrix} X'_{Dj1} \\ Y'_{Dj1} \\ Z'_{Dj1} \end{Bmatrix} = -[A_j]^T \begin{Bmatrix} X^o_{D1j} \\ Y^o_{D1j} \\ Z^o_{D1j} \end{Bmatrix} \quad (73a)$$

and

$$\begin{Bmatrix} L'_{Dj1} \\ M'_{Dj1} \\ N'_{Dj1} \end{Bmatrix} = -[A_j]^T \begin{Bmatrix} L^o_{D1j} \\ M^o_{D1j} \\ N^o_{D1j} \end{Bmatrix} \quad (73b)$$

The minus sign is necessary because the sense of the loads acting on mass  $j$  is opposite the sign convention for the loads acting on mass  $j$ , as shown in Figure 6.

We now obtain the total forces and moments acting on mass  $i$  by summing the contributions from equations (72) and (73) over the second subscript. This is the same method as employed for the internal forces,

equation (35), and explained earlier.

$$\begin{aligned} X_{Di} &= \sum_{j=1}^N X'_{Dij} & Y_{Di} &= \sum_{j=1}^N Y'_{Dij} & Z_{Di} &= \sum_{j=1}^N Z'_{Dij} \\ L_{Di} &= \sum_{j=1}^N L'_{Dij} & M_{Di} &= \sum_{j=1}^N M'_{Dij} & N_{Di} &= \sum_{j=1}^N N'_{Dij} \end{aligned} \quad (74)$$

These are the total damping forces and moments acting on mass  $m_i$ , in  $i$ th body axes.

We now digress briefly to discuss the determination of the diagonal damping matrix  $[C_{ij}]$  used in equation (68). The first three diagonal elements of this matrix are given simply by

$$C_{ijk} = 2\bar{C}_{ij} [K_{ijkk} (m_i + m_j)]^{1/2} \quad k = 1, 2, 3 \quad (75)$$

where  $K_{ijkk}$  is the  $k$ th diagonal element of the  $6 \times 6$  stiffness matrix  $[K_{ij}]$  for beam  $ij$ .  $\bar{C}_{ij}$  is an input constant giving the damping ratio used for beam  $ij$ . Equation (75) gives the viscous damping constant corresponding to the input damping  $\bar{C}_{ij}$ , for the isolated system consisting of masses  $i$  and  $j$  connected by beam  $ij$ . A separate  $\bar{C}_{ij}$  is input for each beam  $ij$ .

For the rotational degrees of freedom, we must first rotate the inertia matrix for  $m_j$  into  $i$ th mass axes. This is evidently given by

$$[I_j]_{\text{axes } i} = [A_i]^T [A_j] [I_j] [A_j]^T [A_i] \quad (76)$$

where  $[I_j]$  is the  $3 \times 3$  inertia matrix for mass  $m_j$ .

$$[I_j] = \begin{bmatrix} I_{xj} & I_{xyj} & I_{xzj} \\ I_{xyj} & I_{yj} & I_{yzj} \\ I_{xzj} & I_{yzj} & I_{zj} \end{bmatrix} \quad (77)$$

The last three elements of  $[C_{ij}]$  are now given simply by

$$C_{ijk} = 2\bar{C}_{ij} [K_{ijk} I_{ij(k-3)(k-3)}]^{1/2} \quad k = 4, 5, 6 \quad (78)$$

where  $I_{ij(k-3)(k-3)}$  are the diagonal elements of the  $I_{ij}$  inertia sum matrix defined as

$$[I_{ij}] \triangleq [A_{ij}]^T \left[ [I_i] + [I_j] \right]_{\text{axes}} [A_{ij}] \quad (79)$$

Note that  $I_{ij}$  is just the sum of  $I_i$  and  $I_j$ , rotated into beam  $ij$  axes. This rotation must be performed because  $K_{ijk}$  in equation (78) is associated with beam  $ij$  axes. Equations (75) and (78) give the six  $[C_{ij}]$  terms necessary for equation (68). These terms are computed prior to the main time loop in the program, since they involve no time-varying quantities. This completes the discussion of the damping forces and moments.

#### Total Forces and Moments at $m_i$ ( $X_i$ , $Y_i$ , $Z_i$ , $L_i$ , $M_i$ , and $N_i$ )

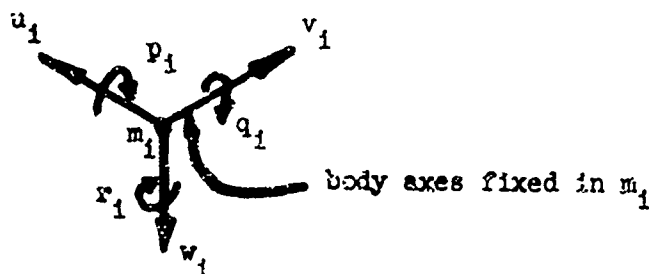
The total forces and moments at  $m_i$ , in  $i$ th body axes, are used to drive the six rigid-body degrees of freedom of lumped mass  $m_i$ . These total forces and moments are just the sum of the components, i.e., the gravity, aerodynamic, internal, crash and damping forces and moments. The total loads are given by

$$\begin{aligned}
X_i &= X_{G_i} + X_{A_i} + X_{I_i} + X_{C_i} + X_{D_i} \\
Y_i &= Y_{G_i} + Y_{A_i} + Y_{I_i} + Y_{C_i} + Y_{D_i} \\
Z_i &= Z_{G_i} + Z_{A_i} + Z_{I_i} + Z_{C_i} + Z_{D_i} \\
L_i &= L_{I_i} + L_{C_i} + L_{D_i} \\
M_i &= M_{I_i} + M_{C_i} + M_{D_i} \\
N_i &= N_{I_i} + N_{C_i} + N_{D_i}
\end{aligned} \tag{80}$$

There are no gravity and aerodynamic moments. The terms of equation (80) come from equations (4), (7), (35), (66), and (74).

#### Rigid-Body Equations of Motion of Each Mass

Having obtained all the forces and moments acting on each mass  $m_i$ , we can now write the rigid-body equations of motion for mass  $m_i$ . Euler's equations of motion are used. These are derived in Reference 43; the derivation is not repeated here. The body axis components of the absolute (relative to ground) translational velocity of mass  $m_i$  are denoted by  $u_i$ ,  $v_i$ , and  $w_i$ . The corresponding rotational velocities are designated  $p_i$ ,  $q_i$ , and  $r_i$ . These velocities are shown in the following sketch:





Euler's equations of motion are six equations for the time derivatives of the six velocities, in terms of the six total forces and moments from the preceding section, the velocities themselves, and the inertia properties of mass  $m_i$ . These equations are (from Reference 43):

$$\dot{u}_i = \frac{X_i g}{W_i} - q_i w_i + r_i v_i$$

$$\dot{v}_i = \frac{Y_i g}{W_i} - r_i u_i + p_i w_i$$

$$\dot{w}_i = \frac{Z_i g}{W_i} - p_i v_i + q_i u_i$$

$$\begin{aligned} p_i &= \frac{1}{\Delta_i} \left[ (L_i - A_i) (I_{y_i} I_{z_i} - I_{yz_i}^2) + (M_i - B_i) (I_{xy_i} I_{z_i} + I_{yz_i} I_{xz_i}) \right. \\ &\quad \left. + (N_i - C_i) (I_{xy_i} I_{yz_i} + I_{y_i} I_{xz_i}) \right] \\ q_i &= \frac{1}{\Delta_i} \left[ (L_i - A_i) (I_{xy_i} I_{z_i} + I_{yz_i} I_{xz_i}) + (M_i - B_i) (I_{x_i} I_{z_i} - I_{xz_i}^2) \right. \\ &\quad \left. + (N_i - C_i) (I_{x_i} I_{yz_i} + I_{xz_i} I_{xy_i}) \right] \\ r_i &= \frac{1}{\Delta_i} \left[ (L_i - A_i) (I_{xy_i} I_{yz_i} + I_{y_i} I_{xz_i}) + (M_i - B_i) (I_{x_i} I_{yz_i} + I_{xz_i} I_{xy_i}) \right. \\ &\quad \left. + (N_i - C_i) (I_{x_i} I_{y_i} - I_{xy_i}^2) \right] \end{aligned} \quad (81)$$

where

$$\begin{aligned}
 \Delta_i &= I_{x_i} \left( I_{y_i} I_{z_i} - I_{yz_i}^2 \right) - I_{xy_i} \left( I_{xy_i} I_{z_i} + I_{xz_i} I_{yz_i} \right) - I_{xz_i} \left( I_{xy_i} I_{yz_i} + I_{y_i} I_{xz_i} \right) \\
 A_i &= q_i \left( H_{e_{z_i}} - I_{xz_i} p_i - I_{yz_i} q_i + I_{z_i} r_i \right) - r_i \left( H_{e_{y_i}} - I_{xy_i} p_i + I_{y_i} q_i - I_{yz_i} r_i \right) \\
 B_i &= r_i \left( H_{e_{x_i}} + I_{x_i} p_i - I_{xy_i} q_i - I_{xz_i} r_i \right) - p_i \left( H_{e_{z_i}} - I_{xz_i} p_i - I_{yz_i} q_i + I_{z_i} r_i \right) \\
 C_i &= p_i \left( H_{e_{y_i}} - I_{xy_i} p_i + I_{y_i} q_i - I_{yz_i} r_i \right) - q_i \left( H_{e_{x_i}} + I_{x_i} p_i - I_{xy_i} q_i - I_{xz_i} r_i \right)
 \end{aligned} \tag{82}$$

$X_i, Y_i, Z_i, L_i, M_i$ , and  $N_i$  are the total forces and moments from equation (80).  $I_{x_i}, I_{y_i}$ , and  $I_{z_i}$  are the moments of inertia of mass  $m_i$  about its body fixed axes.  $I_{xy_i}, I_{yz_i}$ , and  $I_{zx_i}$  are the products of inertia, e.g.,  $I_{xy_i} = \int x_i y_i dm_i$ , etc.  $H_{ex_i}, H_{ey_i}$ , and  $H_{ez_i}$  are the angular momenta of masses  $m_i$ , due to rotation of internal masses within  $m_i$ , such as propellers, rotors, and engine turbines. These terms are used only for a few selected masses, such as the rotor disk, the engine, and the tail boom. They are input constants.

The above equations of motion are integrated numerically to yield  $u_i, v_i, w_i$ , and  $p_i, q_i, r_i$ . We obtain the translational velocities in ground axes by a simple transformation.

$$\begin{pmatrix} \dot{x}_i \\ \dot{y}_i \\ \dot{z}_i \end{pmatrix} = [A_i] \begin{pmatrix} u_i \\ v_i \\ w_i \end{pmatrix} \tag{83}$$

Similarly, the angular velocities  $p_i, q_i$ , and  $r_i$  are the body axes components of the instantaneous absolute rotation rate  $\vec{\omega}_i$  of mass  $m_i$ . These variables do not correspond to any set of coordinates which specify the orientation of the airplane. Therefore, in order to solve for the orientation, it is necessary to transform the  $p', q', r'$  to

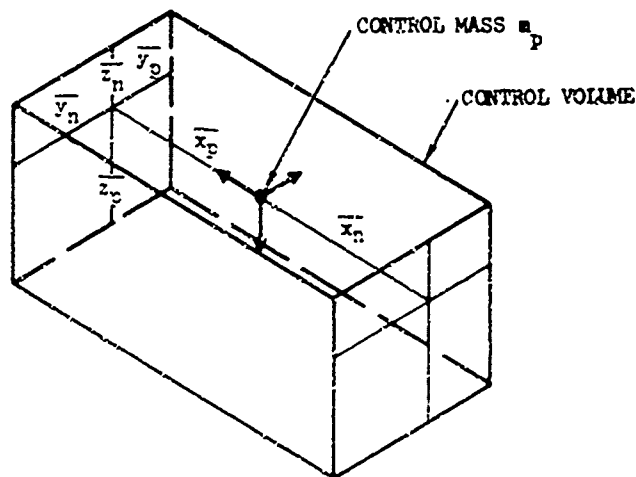
the time derivatives  $\dot{\phi}_i$ ,  $\dot{\theta}_i$ ,  $\dot{\psi}_i$  of the Euler angles. By summing the orthogonal projections of  $\dot{\phi}_i$ ,  $\dot{\theta}_i$ ,  $\dot{\psi}_i$  onto each of the body fixed axes, the following kinematic relations are obtained (Reference 43):

$$\begin{aligned}\dot{\phi}_i &= p_i + (q_i \sin \phi_i + r_i \cos \phi_i) \tan \theta_i \\ \dot{\theta}_i &= q_i \cos \phi_i - r_i \sin \phi_i \\ \dot{\psi}_i &= (q_i \sin \phi_i + r_i \cos \phi_i) \sec \theta_i\end{aligned}\tag{84}$$

Equations (83) and (84) are integrated numerically to obtain  $x_i$ ,  $y_i$ ,  $z_i$  and  $\phi_i$ ,  $\theta_i$ ,  $\psi_i$ . Also,  $p_i$ ,  $q_i$ , and  $r_i$  are integrated to obtain the quantities  $\text{inp}_i$ ,  $\text{inq}_i$ , and  $\text{inr}_i$ . The incremental changes in these integrals are used in equation (23). They represent the incremental rotations of mass  $m_i$  in body fixed axes.

#### Control Volume Mass Penetration Calculations

The computer program includes the calculation of whether or not any of the  $N$  lumped masses have penetrated into an input control volume. The purpose of these calculations is to determine if a major mass item (such as the transmission) has moved into a position where it threatens the vehicle's passengers. Therefore, the control volume input is intended to define the volume of the vehicle in which human occupants are present. The rectangular control volume is located with respect to one of the lumped masses, which is specified in the input. The following sketch shows a typical rectangular control volume defined with respect to mass  $m_p$ .



The six walls of the control volume are always perpendicular to the three body axes fixed in mass  $m_p$ . Thus, the spatial orientation of the control volume varies as mass  $m_p$  rotates.  $\bar{x}_p, \bar{x}_n, \bar{y}_p, \bar{y}_n, \bar{z}_p$ , and  $\bar{z}_n$ , all positive, are the input constants defining the distances from  $m_p$  to the six walls, measured in the positive and negative directions along the body fixed axes of  $m_p$ .

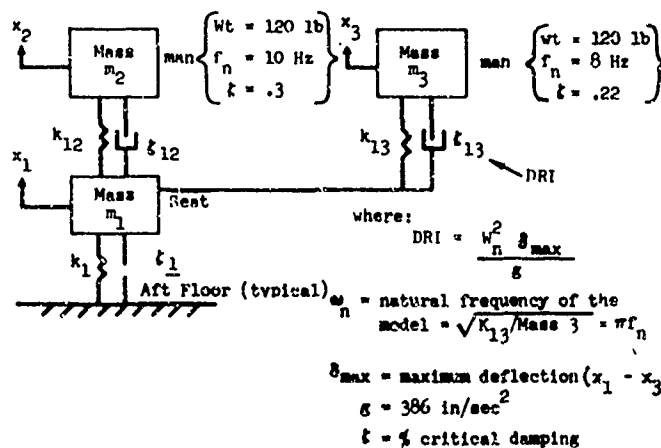
Mass penetration is determined by merely examining the pth body axes components of a vector from control mass  $m_p$  to mass  $m_i$ ,  $i = 1, 2, \dots, N$  ( $i \neq p$ ). These components are given simply by

$$\begin{pmatrix} x_{p_i} \\ y_{p_i} \\ z_{p_i} \end{pmatrix} = [A_p]^T \begin{pmatrix} x_i - x_p \\ y_i - y_p \\ z_i - z_p \end{pmatrix} \quad i = 1, 2, \dots, N (i \neq p) \quad (85)$$

where  $[A_p]$  is the transformation matrix  $[A_i]$  for  $i = p$ . These vector components are then tested against the control volume dimensions. If all three vector components lie within the corresponding pairs of control volume walls, then the ith point has penetrated inside the control volume. Whenever a mass penetration occurs, the program prints out the time and mass that penetrated. These data are repeated in a summary table at the end of the run, showing all the mass penetrations for that run.

#### Dynamic Response Index (DRI)

The program also includes the capability of computing Dynamic Response Index (DRI) for certain selected masses. DRI is a nondimensionalized measure of the compression of the human spinal column, and statistical data is available relating DRI to the probability of spinal injury. References 35 and 36 describe DRI's in detail. Basically, all that is involved is the following mathematical model:



Mass  $m_1$  is the occupant's seat. Mass  $m_2$  is the upper torso of the occupant; the frequency and damping ratio given are intended to properly model the dynamic response of the upper torso to the seat's excitation. Mass  $m_3$  is also the upper torso, but the stiffness and damping are slightly different. This is done to obtain a response number (DRI) for mass  $m_3$  that correlates well with statistical injury data. The important point is that mass  $m_3$  is driven by mass  $m_1$ , but the interconnecting forces only drive mass  $m_3$ , not mass  $m_1$ . Thus, the coupled systems of  $m_1$  and  $m_2$  determine the response of  $m_1$ , and this response drives  $m_3$ . The Dynamic Response Index is defined in the previous sketch by

$$DRI = \frac{\omega_n^2 \delta}{g}$$

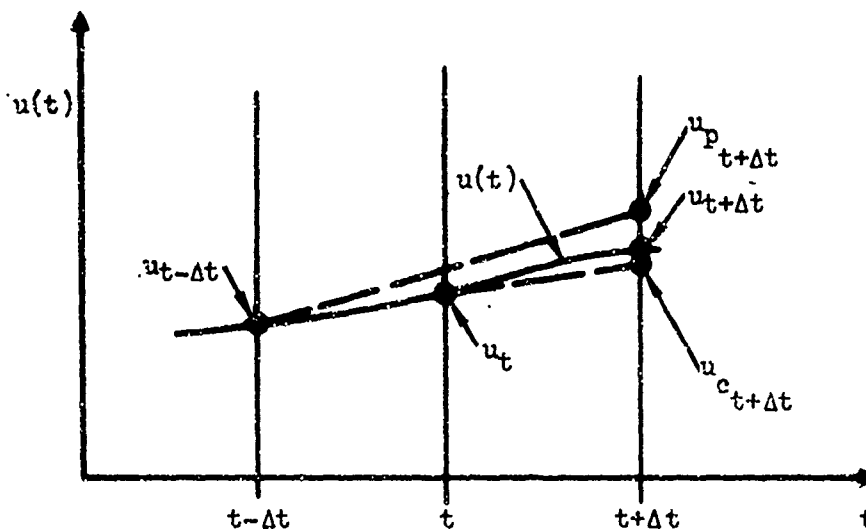
Plugging in the constants, we obtain

$$DRI = 6.558$$

If the damping were zero, the DRI would be the acceleration of mass  $m_3$ . With damping, it is a nondimensionalized measure of spring compression. In the computer program,  $\delta$  is taken as  $-vb_1$  (Equation 26) for the  $ij$  element corresponding to the beam between mass 1 and 3. The program is coded so that for selected  $ij$  pairs (specified by the input), the internal force acts only on mass  $j$ , not on mass  $i$ . In the above sketch, beam 1-3 would be treated in this way, with its internal forces acting only on mass 3. The only restriction is in the numbering of the masses; the mass representing the torso must be assigned a larger number than the mass representing the seat.

### Integration Routine

The equations of motion derived earlier are integrated numerically in the computer program KRASH. The integration scheme employed is a modified predictor-corrector method. The following sketch shows a time history of a typical response quantity, say,  $u$ . Assume that  $u$  and  $\dot{u}$  are



known at time  $t$  and all previous times. The predicted value of  $u$  at  $t + \Delta t$ ,  $u_{p,t+\Delta t}$  is computed as

$$u_{p,t+\Delta t} = u_{t-\Delta t} + 2\Delta t \dot{u}_t \quad (86)$$

This is shown in the above sketch by the upper dashed line of slope  $\dot{u}_t$ . Using this predicted value of  $u$  at  $t + \Delta t$ , the derivative  $\dot{u}$  at  $t + \Delta t$  is

computed from the equations derived in the theory. This derivative is then averaged with  $\dot{u}$  at  $t$  to determine a corrected value of  $u$  at  $t + \Delta t$ :

$$u_{c_{t+\Delta t}} = u_t + \frac{\Delta t}{2}(\dot{u}_{t+\Delta t} + \dot{u}_t) \quad (87)$$

This is shown by the lower dashed line in the above sketch. The final value used for  $u_{t+\Delta t}$  is a weighted average of the predicted and corrected values. For the present program, the weighting used is 4 to 1 in favor of the corrected value. Hence

$$u_{t+\Delta t} = 0.8u_{c_{t+\Delta t}} + 0.2u_{p_{t+\Delta t}} \quad (88)$$

A computational flow diagram for this scheme is shown in Figure 11. Since the technique is not self-starting (due to the  $u_{t-\Delta t}$  term in equation (86)), a simple Euler integration is used for the first step. The subroutine DERIV encompasses all the equations derived in the theory, and is used to compute the derivatives of all the variables, knowing the variables themselves.

The iteration shown by the dashed line in Figure 11 is often employed with this scheme, the iteration continuing until the predicted and corrected values agree to within a specified tolerance. However, the iteration is not used in the program KRASH. Due to the large number of computations in the subroutine DERIV, it is more efficient to go through DERIV only once per time step, and to choose a sufficiently small time step  $\Delta t$  to obtain the desired accuracy.

The subroutine IC computes all the initial values (at  $t = 0$ ) of the variables necessary for the integration to proceed. The following section discusses the calculations of these initial conditions.

#### Initial Conditions

Initial values (at  $t = 0$ ) are required for the following quantities:

$$\left. \begin{array}{ll} x_i, y_i, z_i & \phi_i, \theta_i, \psi_i \\ u_i, v_i, w_i & p_i, q_i, r_i \\ \dot{x}_i, \dot{y}_i, \dot{z}_i & \dot{\phi}_i, \dot{\theta}_i, \dot{\psi}_i \end{array} \right\} \quad i = 1, 2, \dots, N$$

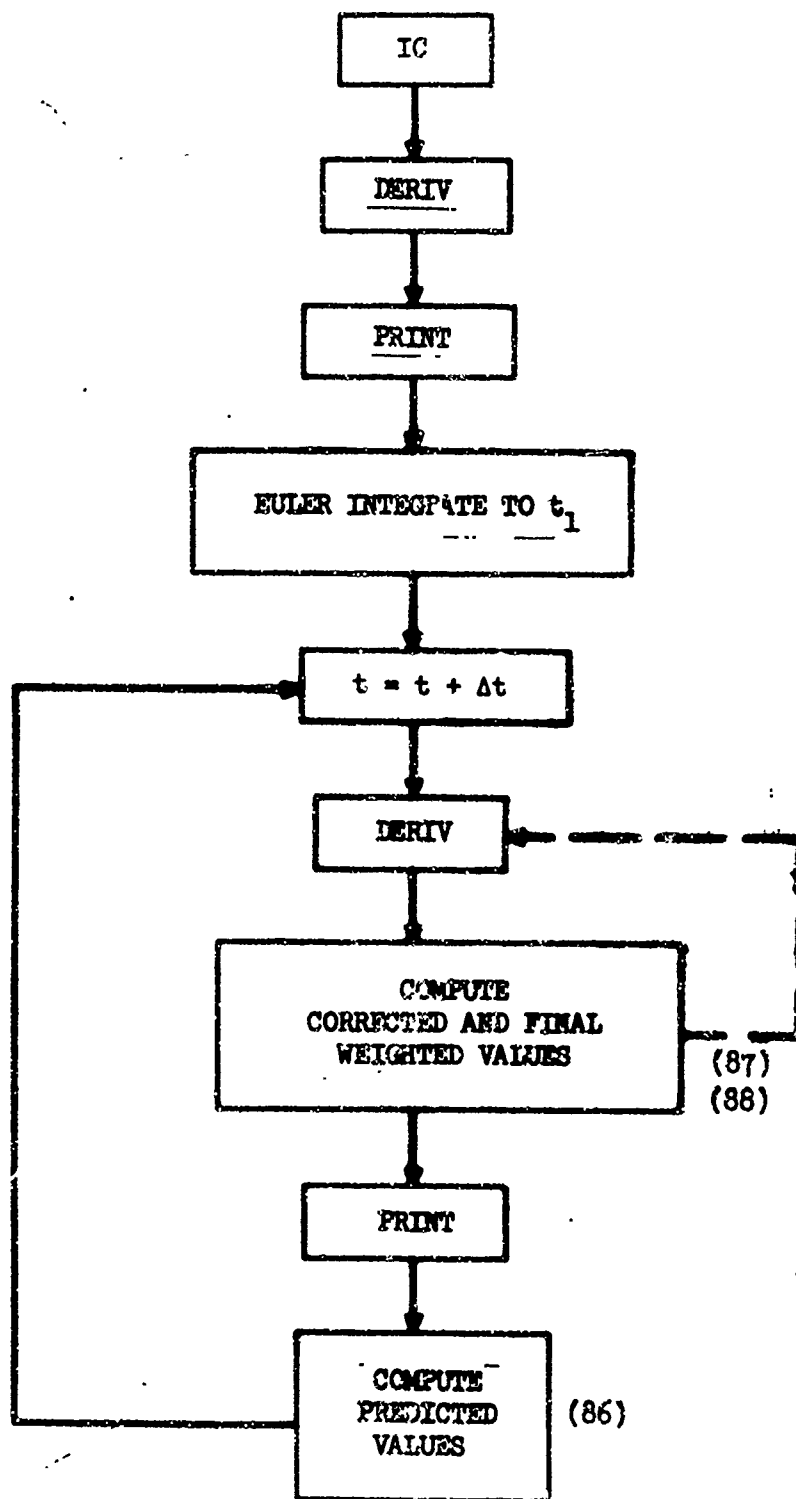


Figure 11. Numerical Integration Flow Diagram.



$vb_{ijl}$  all input ij pairs  $l = 1-6$

$FM_{ijkl}$  all input ij pairs  $k = 1-6$   $l = 1-6$

$\left. \begin{array}{l} X'_{ij}, Y'_{ij}, \dots, N'_{ij} \\ X'_{ji}, Y'_{ji}, \dots, N'_{ji} \end{array} \right\}$  all input ij pairs

The initial conditions which are input to the program are the following:

$\dot{x}_g, \dot{y}_g, \dot{z}_g$  vehicle c.g. velocity in ground axes

$p', q', r'$  vehicle angular velocity in body axes

$\phi', \theta', \psi'$  vehicle attitude, Euler angles of vehicle relative to ground

First the total vehicle weight is computed from the individual mass weights (input):

$$W_{TOT} = \sum_{i=1}^N W_i \quad (89)$$

Next, the location of the overall vehicle c.g., in the  $H, x'', y'', z''$  coordinate system, is determined. We have

$$\begin{aligned}
 x''_G &= \frac{1}{W_{TOT}} \sum_{i=1}^N W_i x''_i \\
 y''_G &= \frac{1}{W_{TOT}} \sum_{i=1}^N W_i y''_i \\
 z''_G &= \frac{1}{W_{TOT}} \sum_{i=1}^N W_i z''_i
 \end{aligned} \quad (90)$$

We now write an expression for the ground coordinates of  $m_1$ :

$$\begin{pmatrix} x_i \\ y_i \\ z_i \end{pmatrix} = \begin{pmatrix} x_G \\ y_G \\ z_G \end{pmatrix} + [A'] \begin{pmatrix} x'_i \\ y'_i \\ z'_i \end{pmatrix} \quad (91)$$

or

$$va_{ij} = vg_j + \sum_{l=1}^3 A'_{jl} vip_{il} \quad j = 1, 2, 3$$

where  $x_G$ ,  $y_G$ , and  $z_G$  are currently unknown, and

$$\begin{pmatrix} x'_i \\ y'_i \\ z'_i \end{pmatrix} = - \begin{pmatrix} x''_i - x''_G \\ y''_i - y''_G \\ z''_i - z''_G \end{pmatrix} \quad (92)$$

or

$$vip_{ij} = -(vip_{ij} - gpp_{ij}) \quad j = 1, 2, 3$$

The  $vipp_{ij}$  are the input coordinates of the  $m_i$ , and the  $vgpp_{ij}$  were computed in (90), so the  $vip_{ij}$  are known. In equation (91),  $[A']$  is known from the input Euler angles  $\phi'$ ,  $\theta'$ , and  $\psi'$ . The only unknowns in (91) are  $x_G$ ,  $y_G$ ,  $z_G$  (defined as  $vg_j$ ). Clearly, the x and y ground coordinates of the initial c.g. position are arbitrary, so these are set to zero. It remains only to determine the initial c.g. height,  $z_G$  ( $vg_3$ ). This height is either input to the program or, if zero is input, is chosen so that the lowest crash point ( $C_{xk}$ ,  $C_{yk}$ ,  $C_{zk}$  in Figure 1) is initially 0.001 inch above the ground. From equations (44) and (45), we have the z coordinate of the kth spring for the itn mass

$$vc_{13k} = va_{13} + A_{13k} \bar{l}_{1k} \quad (93)$$

From equation (91), we know  $va_{i3}$  to be

$$va_{i3} = vg_3 + \sum_{l=1}^3 A'_{3l} vip_{il} \quad (94)$$

once  $vg_3(z_G)$  is known. Combining (93) and (94), we have

$$vc_{i3k} = vg_3 + \sum_{l=1}^3 A'_{3l} vip_{il} + A_{i3k} \bar{z}_{ik} \quad (95)$$

Now set  $vg_3(z_G) = 0$ , and determine the largest value of  $vc_{i3k}$ , varying over  $i$  and  $k$  to test all crash springs. Denote this largest value by  $z_{cmax}$ ; this is the vertical location of the lowest spring if  $z_G$  were equal to zero. Finally,  $z_G$  is determined by

$$z_G = -z_{cmax} - 0.001 \quad (96)$$

This results in the lowest spring being 0.001 inch above the ground. Now we can use (91) to determine the initial  $x_i, y_i, z_i$ :

$$\begin{pmatrix} x_i \\ y_i \\ z_i \end{pmatrix} = \begin{pmatrix} 0 \\ 0 \\ -z_{cmax} - 0.001 \end{pmatrix} + [A'] \begin{pmatrix} x'_i \\ y'_i \\ z'_i \end{pmatrix} \quad (97)$$

where  $x'_i, y'_i, z'_i$  are known from (92). If a nonzero  $z_G$  is input, then (95) and (96) are ignored and (91) is used directly instead of (97).

$$[A_1] = [A'] [A''] \quad i = 1, 2, \dots, N \quad (98)$$
$$\theta_1 = -\sin^{-1} A_{131} \quad (99)$$
$$\phi_2 = \sin^{-1} \left( \frac{\Lambda_{132}}{\cos \theta_1} \right) \quad (100)$$
$$\psi_1 = \sin^{-1} \left( \frac{A_{121}}{\cos \theta_1} \right) \quad (101)$$

Next the linear and angular velocities are calculated. Differentiating equation (91), we obtain

$$\begin{Bmatrix} \dot{x}_1 \\ \dot{y}_1 \\ \dot{z}_1 \end{Bmatrix} = \begin{Bmatrix} \dot{x}_G \\ \dot{y}_G \\ \dot{z}_G \end{Bmatrix} + [A'] \begin{Bmatrix} x'_1 \\ y'_1 \\ z'_1 \end{Bmatrix} \quad (102)$$

where the first vector is input and the second vector is given by (92).  $[\dot{A}']$  is treated the same as  $[A_i]$  was earlier in the theory:

$$[\dot{A}'] = [A'] [\dot{D}'] \quad (103)$$

where

$$[D'] = \begin{bmatrix} 0 & \dot{\theta}' \sin \phi' - \dot{\psi}' \cos \phi' \cos \theta' & \dot{\theta}' \cos \phi' + \dot{\psi}' \sin \phi' \cos \theta' \\ -\dot{\theta}' \sin \phi' + \dot{\psi}' \cos \phi' \cos \theta' & 0 & -\dot{\phi}' + \dot{\psi}' \sin \theta' \\ -\dot{\theta}' \cos \phi' - \dot{\psi}' \sin \phi' \cos \theta' & \dot{\phi}' - \dot{\psi}' \sin \theta' & 0 \end{bmatrix} \quad (104)$$

$\phi'$ ,  $\theta'$ , and  $\psi'$  are input, and  $\dot{\phi}'$ ,  $\dot{\theta}'$ , and  $\dot{\psi}'$  are calculated from the input  $p'$ ,  $q'$ , and  $r'$  by (refer to equation (84)):

$$\begin{Bmatrix} \dot{\phi}' \\ \dot{\theta}' \\ \dot{\psi}' \end{Bmatrix} = [\bar{A}'] \begin{Bmatrix} p' \\ q' \\ r' \end{Bmatrix} \quad (105)$$

where

$$[\bar{A}'] = \begin{bmatrix} 1 & \sin \phi' \tan \theta' & \cos \phi' \tan \theta' \\ 0 & \cos \phi' & -\sin \phi' \\ 0 & \sin \phi' \sec \theta' & \cos \phi' \sec \theta' \end{bmatrix} \quad (106)$$

Once  $\dot{x}_i$ ,  $\dot{y}_i$ , and  $\dot{z}_i$  are known from (102), these are simply transformed into body axes to obtain  $u_i$ ,  $v_i$ , and  $w_i$ :

$$\begin{Bmatrix} u \\ v \\ w \end{Bmatrix} = [A_i]^T \begin{Bmatrix} \dot{x}_i \\ \dot{y}_i \\ \dot{z}_i \end{Bmatrix} \quad (107)$$

The angular velocities in body axes ( $p_i$ ,  $q_i$ , and  $r_i$ ) are equal to the vehicle angular velocity ( $p'$ ,  $q'$ , and  $r'$ ), transformed from c.g. axes to  $i$ th mass axes:

$$\begin{pmatrix} p_i \\ q_i \\ r_i \end{pmatrix} = [A_i'']^T \begin{pmatrix} p' \\ q' \\ r' \end{pmatrix} \quad (108)$$

Next we determine  $\dot{\phi}_i$ ,  $\dot{\theta}_i$ , and  $\dot{\psi}_i$  by equations analogous to (105) and (106), only using angles  $\phi_i$  and  $\theta_i$  this time:

$$\begin{pmatrix} \dot{\phi}_i \\ \dot{\theta}_i \\ \dot{\psi}_i \end{pmatrix} = [\bar{A}_i] \begin{pmatrix} p_i \\ q_i \\ r_i \end{pmatrix} \quad (109)$$

where

$$[\bar{A}_i] = \begin{bmatrix} 1 & \sin\phi_i \tan\theta_i & \cos\phi_i \tan\theta_i \\ 0 & \cos\phi_i & -\sin\phi_i \\ 0 & \sin\phi_i \sec\theta_i & \cos\phi_i \sec\theta_i \end{bmatrix} \quad (110)$$

The only remaining initial conditions to be determined are the beam deflections and forces  $v_{ijl}$ ,  $F_{ijkl}$  and  $X'_{ij}, \dots, N'_{ij}$ . At present, the program is written so that the initial values for all these quantities are zero. This is only true for the case where there are no aerodynamic loads, so that all masses are uniformly accelerating downward at  $g$ . Therefore, if aerodynamic loads are used in the program, the initial conditions will not be correct since internal forces would be required to balance the aerodynamic and gravity forces. However, this is not considered a serious limitation since the vast majority of accident cases involve loss of aerodynamic lift.

Also computed in the initial condition subroutine, although not truly initial conditions, are the Euler angles  $\theta''_{ij}$  and  $\psi''_{ij}$ . These angles are used in  $[A_{ij}]$ , which transforms vectors from beam  $ij$  axes to  $i$ th body axes. This computation is performed only if the input angles  $\phi''_i$ ,  $\theta''_i$ , and  $\psi''_i$  are all zero. This means that all the  $i$ th body axes are parallel to the vehicle c.g. axes. This is normally the case, since the inertia properties for the masses are usually available in these axes. Figure 11 shows beam  $ij$  connecting points  $m_i$  and  $m_j$ . The distances from  $m_i$  to  $m_j$ , measured along vehicle c.g. ( $'$ ) axes, are given by

$$\begin{pmatrix} x'_{ij} \\ y'_{ij} \\ z'_{ij} \end{pmatrix} = \begin{pmatrix} x'_j - x'_i \\ y'_j - y'_i \\ z'_j - z'_i \end{pmatrix} \quad (111)$$

where the terms on the right-hand side are computed in equation (92). Figure 12 shows the Euler angles  $\psi_{ij}$  and  $\theta_{ij}$ . The basic equations for these can be seen from Figure 12 to be

$$\psi_{ij} = \tan^{-1} \frac{y'_{ij}}{x'_{ij}} \quad (112)$$

$$\theta_{ij} = \tan^{-1} \frac{z'_{ij}}{(x'^2_{ij} + y'^2_{ij})^{1/2}}$$

However, due to the problems encountered in calculating these angles in various quadrants, as well as in calculating  $90^\circ$  angles, the algorithm shown in Figure 13 is actually used to compute these angles. The arc tangent functions used give angles between  $+180^\circ$  and  $-180^\circ$ .

The function also automatically gives  $\psi_{ij} = \text{SIGN}(y'_{ij}) \times \frac{\pi}{2}$  if  $x'_{ij} = 0$  in the right-hand equation for  $\psi_{ij}$ . The test for  $y'_{ij} = 0$  is necessary to avoid the indeterminate  $0/0$  for  $\psi_{ij}$  if both  $y'_{ij}$  and  $x'_{ij}$  are zero.

The remaining Euler angle  $\phi_{ij}$  is always input, since it is not a function of the locations of  $m_i$  and  $m_j$ . This "roll" angle is chosen so that the resultant beam  $ij$  axes coincide with convenient structural axes.  $\phi_{ij}$  is usually zero. This completes the computation of the initial conditions.

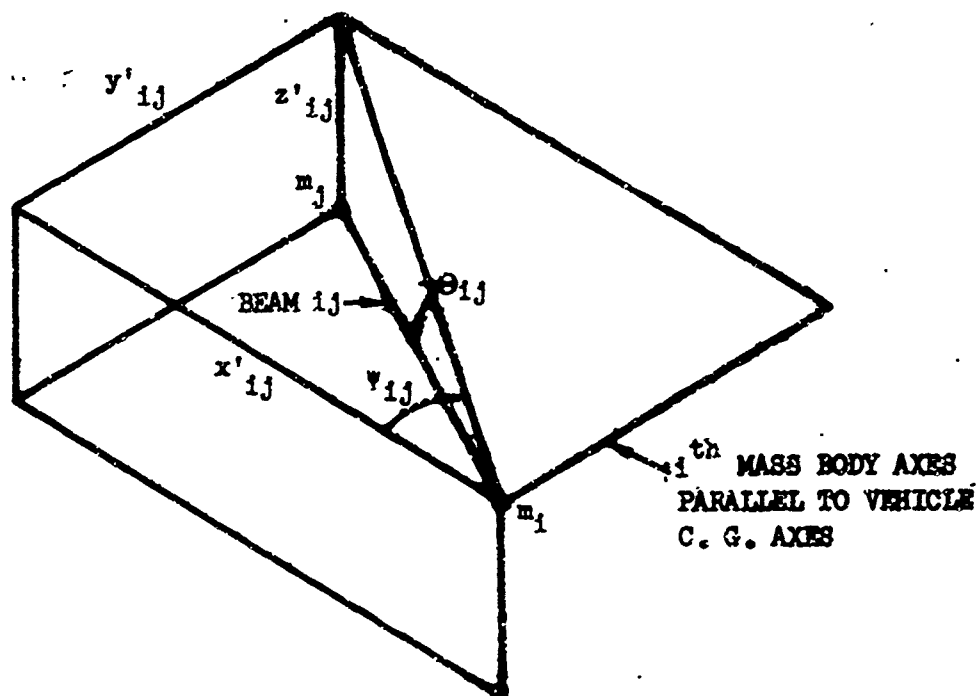


Figure 12. Euler Angles  $\Theta_{ij}$  and  $\psi_{ij}$ .



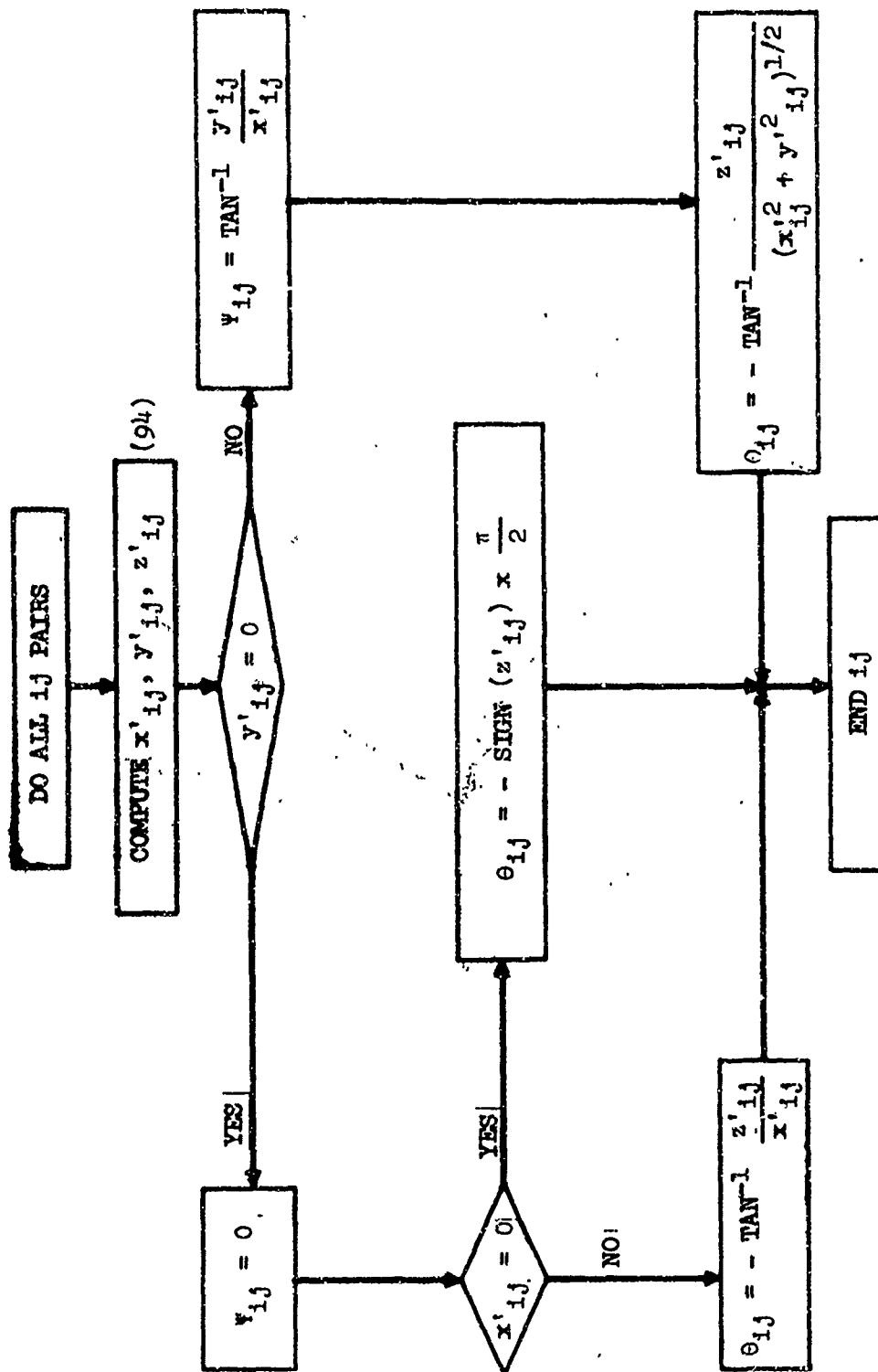


Figure 13. Computation of  $\theta_{ij}$  and  $\psi_{ij}$ .

This section describes all the input necessary to run the program, and the output available from the program.

The input data format is described in detail in this section and is shown in Figure 14. Unless otherwise specified, all quantities are input in inch, pound, second, and radian units. For cards 0300 and on, the input format is 6E12.0 unless otherwise noted. Each card has 6 fields; each field is 12 columns wide. As an example of this format, the number 126.08 can be input in the following ways:

			1	2	6	.	0	8		
			1	2	6	.		8		

	1.2608		E2
	12608.		E-2

Card 0100 - This card contains the title for the case being analyzed. All text material on card 0100 is reproduced at the top of every page of the output and on every plot.

Cards 0200 thru 02XX - These cards contain the Euler angles  $\phi_{ij}$ ,  $\theta_{ij}$ , and  $\psi_{ij}$  for all beams  $ij$ . The beam interconnections are defined by the  $i$ 's and  $j$ 's input.  $i$  must be less than  $j$ , but there is no other requirement on the ordering of the  $ij$  pairs.  $\phi_{ij}$  is always input;  $\theta_{ij}$  and  $\psi_{ij}$  need not be input if  $\phi_i$ ,  $\theta_i$ , and  $\psi_i$  on cards 0500-05XX are all zero. In the latter case,  $\theta_{ij}$  and  $\psi_{ij}$  are computed in initial conditions.  $\phi_{ij}$  will normally be zero. There must be a blank card following all the  $ij$  pairs input.

87

Cards 0310 thru 03XX -  $N$  of these cards are required. Each card inputs the six moments and products of inertia for the  $i$ th mass,  $i = 1, 2, \dots, N$ .

Cards 0400 thru 04XX -  $He_{xi}$ ,  $He_{yi}$ , and  $He_{zi}$  are the body axes components of the angular moments of masses  $m_i$ , due to rotation of internal masses within  $m_i$ . These are normally zero.

Cards 0450 thru 045X -  $l_{ci}$  are the aerodynamic lift constants used in equation (5).

Cards 0460 thru 0462 - The cards contain the overall vehicle initial conditions.  $x_G$ ,  $y_G$ , and  $z_G$  are the ground axes components of the initial c.g. velocity.  $p'$ ,  $q'$ , and  $r'$  are the c.g. coordinate system components of the initial angular velocity of the vehicle.  $p'$  is the roll velocity,  $q'$  the pitch velocity, and  $r'$  the yaw velocity.  $\phi'$ ,  $\theta'$ , and  $\psi'$  are the Euler angles relating the initial position of the vehicle to ground coordinates.  $\phi'$  is the roll angle,  $\theta'$  the pitch angle, and  $\psi'$  the yaw angle.  $z_G$  is the negative of the initial vehicle c.g. height above ground. If this is input as zero (blank), the initial condition subroutine computes a value of  $z_G$  so that the lowest extremity of the vehicle is .1 inch above the ground.

Cards 0470 thru 04XX - These cards are used to input the coordinates of the  $N$  lumped masses.  $x_i''$  is the Fuselage Station (increasing aft),  $y_i''$  is the Butt Line (positive left), and  $z_i''$  is the Water Line (increasing upward).

Cards 0500 thru 05XX -  $\phi_i''$ ,  $\theta_i''$ ,  $\psi_i''$ ,  $i = 1, 2, \dots, N$  are the Euler angles from the c.g. axes to the  $i$ th mass axes. If the  $i$ th mass body-fixed axes are parallel to the vehicle c.g. coordinate axes, which is usually the case, these are all input as zero. Note that if any nonzero values are input, then  $\phi_{ij}$  and  $\psi_{ij}$  on cards 0200 thru 02XX must be input.

Cards 0600 thru 06XX -  $I_{ik}$ ,  $i = 1, 2, \dots, N$ ;  $k = 1, 2, 3$  are the free lengths of the external springs. Zeros are input if no spring is utilized.  $I_{ik}$  is positive if it radiates out from mass  $m_i$  in the positive direction of the  $i$ th mass body axes;  $I_{ik}$  is negative if it radiates in the opposite direction. Springs in both directions are not allowed.

Cards 0700 thru 07XX - Integer format I3 is used to define the  $SP_{ik}$ . If  $SP_{ik} = 1$ , there is a  $k$ th spring on the  $i$ th mass; if  $SP_{ik} = 0$ , there is no spring.

Cards 0710 thru 07XX -  $\mu_{ik}$  are the friction coefficients between ground and the end of the  $ik$  spring.

Cards 0750 thru 07XX -  $ke_{ik}$  are the linear unloading stiffnesses and also bottoming stiffnesses for the  $ik$  spring.

Cards 0800 thru 0805 - These six cards are used to input the  $6 \times 6$  linear stiffness matrix  $[K_{ij}]$  for the first  $ij$  beam, listed on card 0200. Each card inputs one row of the matrix.

Cards 0806 thru 1999 - As many cards as necessary are used to input all the remaining  $6 \times 6$   $[K_{ij}]$  matrices. These matrices must be ordered the same as the  $ij$  pairs are ordered on cards 0200 thru 02XX.

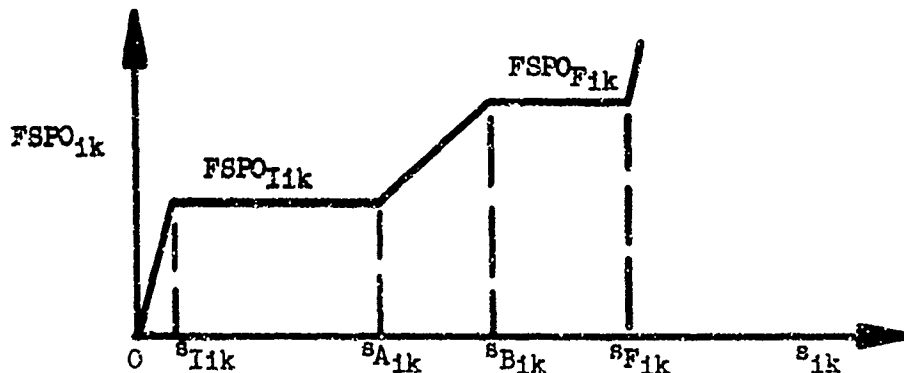
Cards 2000 thru 20XX -  $v_{\max ij}$ ,  $k = 1-6$  are the maximum beam deflections and rotations for beam  $ij$ . These are ordered the same as cards 0200 thru 02XX. When any one of the six maximum deflections or rotations is exceeded (either positive or negative), element  $ij$  fractures and its internal forces are set to zero for the remainder of the run. The deflections and rotations are of point  $j$  with respect to point  $i$ , in beam  $ij$  axes. They are ordered  $x, y, z, \phi, \theta, \psi$ .

Cards 2100 thru 21XX -  $DX_{ijl}$  are the spacings for the six equally spaced abscissa values in the following table of  $KR_{ijl}$  vs  $vb_{ijl}$ , for  $l = 1$  thru 6.

Cards 2100 thru 2206 - Each card inputs the six  $KR_{ijl}$  values defining the table of  $KR_{ijl}$  vs  $vb_{ijl}$ , for the first  $ij$  pair. The first value corresponds to  $vb_{ijl} = 0$ , the remaining five are spaced  $DX_{ijl}$ , to the right. Six cards are input, one for each  $l$  deflection or rotation, ordered  $x, y, z, \phi, \theta, \psi$ .  $KR_{ijl}$  are the diagonal elements of a  $6 \times 6$  diagonal stiffness reduction matrix. It is initially 1.0, corresponding to a linear system, and then increases or decreases with  $vb_{ijl}$ , depending on whether the nonlinear beam gets stiffer or softer. Refer to the THEORY section on internal forces for the usage of  $KR_{ijl}$ .

Cards 2207 thru 2XXX - As many cards as necessary are used to input the  $KR_{ijl}$  tables for the remaining  $ij$  pairs. Six cards per  $ij$  pair are used. The  $ij$  pairs are ordered as on cards 0200 thru 02XX.

Cards 3000 thru 30XX - These cards are used to input tables of  $FSPO_{ik}$  vs  $s_{ik}$ , the axial load in the external springs versus the spring compression. The program is currently written so that a table of the following form must be input:



This table is defined by six parameters  $S_{Iik}$ ,  $S_{Aik}$ ,  $S_{Bik}$ ,  $S_{Tik}$ ,  $FSPO_{Iik}$  and  $FSPO_{Fik}$ . These parameters are input in order for  $k = 1, 2, 3$  and  $i = 1, 2, \dots, N$ . Zeros are input if no spring exists ( $SP_{ik} = 0$ ).

Cards 3200 thru 32XX - These cards are used to input the  $\bar{C}_{ij}$  for all the  $ij$  pairs defined on cards 0200 thru 02XX.  $\bar{C}_{ij}$  is the damping ratio (damping/critical damping) for the isolated system consisting of masses  $m_i$  and  $m_j$  connected by beam  $ij$ . Values of  $\bar{C}_{ij}$  between .01 and .05 are generally representative of the structural damping.

Cards 5001 thru 5024 - These cards are used to specify the time history output plots desired. The only input for these cards is either a 1 or a blank. A 1 results in the output of a time history plot for the response quantity indicated; a blank results in no plot for that item. For example, a 1 in the 13th column of card 5003 specifies that a time history plot of  $z_{13}$  is to be generated. For cards 5001 thru 5012, the column number in which the 1 is input indicates which mass  $i$  is desired. For cards 5013 thru 5024, the column number in which the 1 is input indicates which  $ij$  pair is desired, where the  $ij$  pairs are ordered as on cards 0200 thru 02XX.

Plots are available for the displacements, velocities and accelerations of all the lumped masses, all the external spring compressions  $S_{ik}$ , and all the beam  $ij$  total deflections/rotations ( $vb_{ij}$ ) and forces/moments ( $F_{ij}$ ). The latter two items are in beam  $ij$  axes. Also available are plots of the DRI (Dynamic Response Index). These are identified by the DRI  $ij$  element, as described on card 7000 below. The plot variables are labelled automatically, and the plot scales are chosen automatically. The user merely has to specify which plots are desired. Up to 150 plots can be requested per run. Thirty thousand data points are stored for plotting, with the plot time interval depending on run time and number of plots requested. Thus, if the maximum of 150 plots are requested, 200 points will be saved to generate each plot. If the maximum run time is .2 second, this will give one data point every .001 second. For the types of problems analyzed, this appears to be a marginally acceptable resolution. Requesting fewer plots automatically increases the number of points per plot and, hence, the resolution.

Card 6000 -  $P$  is the mass to be used to locate the mass penetration control volume. The format is I2. If no mass penetration calculations are required, this card is input blank and card 6001 is not required.

Card 6001 -  $\bar{x}_n$ ,  $\bar{x}_p$ ,  $\bar{y}_n$ ,  $\bar{y}_p$ ,  $\bar{z}_n$ , and  $\bar{z}_p$  are the six distances (all positive), measured from the control mass  $P$  to the six sides of the control volume. These are measured along the positive ( $p$ ) and negative ( $n$ ) body-fixed axes for mass  $m_p$ .

# REAL PURPOSE DATA SHEET

LOCKHEED-CALIFORNIA COMPANY  
A DIVISION OF LOCKHEED AIRCRAFT CORPORATION

TITLE:		PREPARED BY	DATE	CHECKED BY	DATE	JOB NO.	GROUP	PAGE	OF
								1	5
								ID	SEQ
1	2	3	4	5	6	7	8	9	10
11	12	13	14	15	16	17	18	19	20
21	22	23	24	25	26	27	28	29	30
31	32	33	34	35	36	37	38	39	40
41	42	43	44	45	46	47	48	49	50
51	52	53	54	55	56	57	58	59	60
61	62	63	64	65	66	67	68	69	70
71	72	73	74	75	76	77	78	79	80
81	82	83	84	85	86	87	88	89	90
91	92	93	94	95	96	97	98	99	100
101	102	103	104	105	106	107	108	109	110
111	112	113	114	115	116	117	118	119	120
121	122	123	124	125	126	127	128	129	130
131	132	133	134	135	136	137	138	139	140
141	142	143	144	145	146	147	148	149	150
151	152	153	154	155	156	157	158	159	160
161	162	163	164	165	166	167	168	169	170
171	172	173	174	175	176	177	178	179	180
181	182	183	184	185	186	187	188	189	190
191	192	193	194	195	196	197	198	199	200
201	202	203	204	205	206	207	208	209	210
211	212	213	214	215	216	217	218	219	220
221	222	223	224	225	226	227	228	229	230
231	232	233	234	235	236	237	238	239	240
241	242	243	244	245	246	247	248	249	250
251	252	253	254	255	256	257	258	259	260
261	262	263	264	265	266	267	268	269	270
271	272	273	274	275	276	277	278	279	280
281	282	283	284	285	286	287	288	289	290
291	292	293	294	295	296	297	298	299	300
301	302	303	304	305	306	307	308	309	310
311	312	313	314	315	316	317	318	319	320
321	322	323	324	325	326	327	328	329	330
331	332	333	334	335	336	337	338	339	340
341	342	343	344	345	346	347	348	349	350
351	352	353	354	355	356	357	358	359	360
361	362	363	364	365	366	367	368	369	370
371	372	373	374	375	376	377	378	379	380
381	382	383	384	385	386	387	388	389	390
391	392	393	394	395	396	397	398	399	400
401	402	403	404	405	406	407	408	409	410
411	412	413	414	415	416	417	418	419	420
421	422	423	424	425	426	427	428	429	430
431	432	433	434	435	436	437	438	439	440
441	442	443	444	445	446	447	448	449	450
451	452	453	454	455	456	457	458	459	460
461	462	463	464	465	466	467	468	469	470
471	472	473	474	475	476	477	478	479	480
481	482	483	484	485	486	487	488	489	490
491	492	493	494	495	496	497	498	499	500
501	502	503	504	505	506	507	508	509	510
511	512	513	514	515	516	517	518	519	520
521	522	523	524	525	526	527	528	529	530
531	532	533	534	535	536	537	538	539	540
541	542	543	544	545	546	547	548	549	550
551	552	553	554	555	556	557	558	559	560
561	562	563	564	565	566	567	568	569	570
571	572	573	574	575	576	577	578	579	580
581	582	583	584	585	586	587	588	589	590
591	592	593	594	595	596	597	598	599	600
601	602	603	604	605	606	607	608	609	610
611	612	613	614	615	616	617	618	619	620
621	622	623	624	625	626	627	628	629	630
631	632	633	634	635	636	637	638	639	640
641	642	643	644	645	646	647	648	649	650
651	652	653	654	655	656	657	658	659	660
661	662	663	664	665	666	667	668	669	670
671	672	673	674	675	676	677	678	679	680
681	682	683	684	685	686	687	688	689	690
691	692	693	694	695	696	697	698	699	700
701	702	703	704	705	706	707	708	709	710
711	712	713	714	715	716	717	718	719	720
721	722	723	724	725	726	727	728	729	730
731	732	733	734	735	736	737	738	739	740
741	742	743	744	745	746	747	748	749	750
751	752	753	754	755	756	757	758	759	760
761	762	763	764	765	766	767	768	769	770
771	772	773	774	775	776	777	778	779	780
781	782	783	784	785	786	787	788	789	790
791	792	793	794	795	796	797	798	799	800
801	802	803	804	805	806	807	808	809	810
811	812	813	814	815	816	817	818	819	820
821	822	823	824	825	826	827	828	829	830
831	832	833	834	835	836	837	838	839	840
841	842	843	844	845	846	847	848	849	850
851	852	853	854	855	856	857	858	859	860
861	862	863	864	865	866	867	868	869	870
871	872	873	874	875	876	877	878	879	880
881	882	883	884	885	886	887	888	889	890
891	892	893	894	895	896	897	898	899	900
901	902	903	904	905	906	907	908	909	910
911	912	913	914	915	916	917	918	919	920
921	922	923	924	925	926	927	928	929	930
931	932	933	934	935	936	937	938	939	940
941	942	943	944	945	946	947	948	949	950
951	952	953	954	955	956	957	958	959	960
961	962	963	964	965	966	967	968	969	970
971	972	973	974	975	976	977	978	979	980
981	982	983	984	985	986	987	988	989	990
991	992	993	994	995	996	997	998	999	1000

Figure 14. Input Data Format.

LOCKHEED-CALIFORNIA, CALIF.  
A DIVISION OF LOCKHEED AIRCRAFT CORPORATION

Figure 14. (Continued)

**LOCKHEED-CALIFORNIA COMPANY  
A DIVISION OF LOCKHEED AIRCRAFT CORPORATION**

**Figure 14. (Continued)**



# GENERAL PURPOSE DATA SHEET

LOCKHEED-CALIFORNIA COMPANY  
A DIVISION OF LOCKHEED AIRCRAFT CORPORATION

TITLE:		PREPARED BY	DATE	CHECKED BY	DATE	JOB NO. (W.O.)	DATE	OFFICE	IN	PAGE	OF													
PLOT OUTPUT CARDS										4	5													
1	5	7	10	15	20	25	30	35	40	45	50	55	60	65	70	75	80	85	90	95	100			
<p>1 in 10th column means plot that item for miss <math>i = m</math></p> <p>1 in 11th column means plot that item for 11th pair</p>																								
5001	5002	5003	5004	5005	5006	5007	5008	5009	5010	5011	5012	5013	5014	5015	5016	5017	5018	5019	5020	5021	5022	5023	5024	5025

Figure 14. (Continued)

LOCKHEED-CALIFORNIA COMPANY  
A DIVISION OF LOCKHEED AIRCRAFT CORPORATION

**Figure 14. (Continued)**

### Print Output

First, all the input data is printed out, with self-explanatory identifying titles. Next, at each print time ( $= \Delta \text{Print} / \Delta t \times \Delta t$ ), the data shown in Figure 15 is printed out. At the top of each page, the case identification data is printed out (from input card 0100). Then the current value of time  $t$  is printed.

Next, for each of the  $N$  masses, five lines of data are output.  $x_i, y_i,$  and  $z_i$  are the ground coordinates of  $m_i$ .  $\dot{x}_i, \dot{y}_i,$  and  $\dot{z}_i$  are the ground axes components of the velocity of  $m_i$ .  $u_i, v_i,$  and  $w_i$  are the  $i$ th body axes components of the velocity of  $m_i$ .  $\dot{u}_i, \dot{v}_i,$  and  $\dot{w}_i$  are the time derivatives of  $u_i, v_i,$  and  $w_i$ . (These are not equal to the acceleration of  $m_i$ , as can be seen from equation (81).) XACCEL, YACCEL, ZACCEL are the body axes components of the acceleration of  $m_i$ .

$\phi_i, \theta_i,$  and  $\psi_i$  are the Euler angles defining the attitude of body  $m_i$ , in roll, pitch and yaw.  $\dot{\phi}_i, \dot{\theta}_i,$  and  $\dot{\psi}_i$  are the time derivatives of  $\phi_i, \theta_i,$  and  $\psi_i$ .  $p_i, q_i,$  and  $r_i$  are the body axes components of the angular velocity of  $m_i$ ; they are the velocities in roll, pitch, and yaw, respectively.  $\dot{p}_i, \dot{q}_i,$  and  $\dot{r}_i$  are the body axes components of the angular acceleration of  $m_i$ .

Following that output, the running time sums of the internal forces  $\{F_{ij}\}$  (Equation (27)) are printed out; the six forces and moments for each  $ij$  pair are printed on a line preceded by the identifying  $i$  and  $j$ . Next, the running time sums of the beam deflections  $\{v_{bij}\}$  (Equation (26)) are printed out in the same format.

Finally, the external spring compressions  $s_{ik}$  (Equation (47)) are printed out. Each line starts with the  $i$ , followed by the  $s_{ik}$  for  $k = 1, 2, 3$ . Only values of  $i$  for which a spring is input are shown.

During the course of the run, if any ruptures or control volume mass penetrations occur, the appropriate information is printed out. When a rupture occurs, the word RUPTURE is printed, followed by four items:

1. The  $ij$  pair that ruptured, where the numbering corresponds to the ordering of the  $ij$  pairs as input on cards 0200 thru 02XX.
2. The  $l$  (from 1 to 6) indicating in which direction (in beam axes) the rupture occurred. These are ordered  $x, y, z, \phi, \theta,$  and  $\psi$ . See Figure 24 for the directions of the beam axes.
3. The  $v_{bijl}$  at the time of rupture. This is the total deflection, in beam axes, in the direction that ruptured.
4. The  $v_{\max ij l}$  which defines the maximum allowable beam deflection in the  $l^{\text{th}}$  direction. This is an input constant.

TIME = 0.10000

		X DOOT U DOOT ACCEL	Y DOOT V DOOT TACCEL	Z DOOT W DOOT TACCEL	PHI PHIDOT P PHOT	THETA THETADOT Q THOT	PSI PSIDOT R PSHOT
MASS 25		5.009000 01 -1.001500 01 -2.000000 01 -9.107600 02 -2.200000 00	-7.501370 01 -1.000000 02 -1.000000 02 1.000000 03 0.000000 00	-0.750000 01 -0.000000 01 0.000000 01 -0.000000 03 -1.000000 01	-5.001170 02 -0.000000 00 -2.000000 00 1.000000 02	4.000000 02 0.000000 01 0.000000 01 1.000000 00	2.000000 02 -7.000000 03 2.000000 02 -5.000000 00
MASS 26		-2.000000 01 -1.000000 01 -1.000000 01 0.000000 02 0.000000 01	-2.000000 01 -1.000000 02 -1.000000 02 -0.000000 03 -1.000000 02	-2.000000 01 -1.000000 02 -1.000000 02 0.000000 03 0.000000 01	-2.000000 02 0.000000 01 0.000000 01 0.000000 01 0.000000 01	0.000000 01 0.000000 00 0.000000 00 0.000000 00 0.000000 01	2.000000 02 1.000000 01 1.000000 01 0.000000 00 0.000000 00
MASS 27		0.725730 01 1.000000 00 0.000000 01 0.000000 01 0.000000 00	-2.000000 01 -1.000000 02 -1.000000 02 1.000000 03 0.000000 01	-2.000000 01 -1.000000 02 -1.000000 02 0.000000 03 -1.000000 01	-0.000000 02 -0.000000 01 -0.000000 01 0.000000 01 0.000000 01	0.000000 02 0.000000 01 0.000000 01 0.000000 01 0.000000 01	2.000000 02 -1.000000 01 -1.000000 01 -1.000000 01 -1.000000 01
MASS 28		-0.372000 01 -0.000000 01 -0.000000 01 -0.000000 01 -1.000000 00	-0.000000 01 -1.000000 02 -1.000000 02 -0.000000 03 -1.000000 01	-0.000000 01 -1.000000 02 -1.000000 02 0.000000 03 -1.000000 01	-2.000000 02 0.000000 01 0.000000 01 0.000000 01 0.000000 01	0.000000 01 0.000000 00 0.000000 00 0.000000 00 0.000000 01	2.000000 02 0.000000 01 0.000000 01 0.000000 01 0.000000 01
MASS 29		0.000000 01 -1.000000 01 -1.000000 01 0.000000 02 0.000000 00	-2.000000 01 -1.000000 02 -1.000000 02 0.000000 03 0.000000 01	-2.000000 01 -1.000000 02 -1.000000 02 0.000000 03 0.000000 01	-2.000000 02 -0.000000 01 -0.000000 01 0.000000 01 0.000000 01	0.000000 01 0.000000 00 0.000000 00 0.000000 00 0.000000 01	2.000000 02 -1.000000 01 -1.000000 01 -1.000000 01 -1.000000 01
MASS 30		-2.000000 01 -0.000000 01 -0.000000 01 -0.000000 01 -0.000000 01	-0.000000 01 -1.000000 02 -1.000000 02 0.000000 03 -1.000000 01	-0.000000 01 -1.000000 02 -1.000000 02 0.000000 03 -1.000000 01	-2.000000 02 -0.000000 01 -0.000000 01 0.000000 01 0.000000 01	0.000000 01 0.000000 00 0.000000 00 0.000000 00 0.000000 01	2.000000 02 -1.000000 01 -1.000000 01 -1.000000 01 -1.000000 01
MASS 31		0.000000 01 -1.000000 01 -1.000000 01 0.000000 02 0.000000 00	-2.000000 01 -1.000000 02 -1.000000 02 0.000000 03 0.000000 01	-2.000000 01 -1.000000 02 -1.000000 02 0.000000 03 0.000000 01	-2.000000 02 -0.000000 01 -0.000000 01 0.000000 01 0.000000 01	0.000000 01 0.000000 00 0.000000 00 0.000000 00 0.000000 01	2.000000 02 -1.000000 01 -1.000000 01 -1.000000 01 -1.000000 01
1	2	0.000000 01	0.000000 01	0.000000 01	0.00	0.00	0.00
2	2	0.000000 01	0.000000 01	0.000000 01	0.00	0.00	0.00
3	2	0.000000 01	0.000000 01	0.000000 01	0.00	0.00	0.00
4	2	0.000000 01	0.000000 01	0.000000 01	0.00	0.00	0.00
5	2	0.000000 01	0.000000 01	0.000000 01	0.00	0.00	0.00
6	2	0.000000 01	0.000000 01	0.000000 01	0.00	0.00	0.00
7	2	0.000000 01	0.000000 01	0.000000 01	0.00	0.00	0.00
8	2	0.000000 01	0.000000 01	0.000000 01	0.00	0.00	0.00
9	2	0.000000 01	0.000000 01	0.000000 01	0.00	0.00	0.00
10	2	0.000000 01	0.000000 01	0.000000 01	0.00	0.00	0.00
11	2	0.000000 01	0.000000 01	0.000000 01	0.00	0.00	0.00
12	2	0.000000 01	0.000000 01	0.000000 01	0.00	0.00	0.00
13	2	0.000000 01	0.000000 01	0.000000 01	0.00	0.00	0.00
14	2	0.000000 01	0.000000 01	0.000000 01	0.00	0.00	0.00
15	2	0.000000 01	0.000000 01	0.000000 01	0.00	0.00	0.00
16	2	0.000000 01	0.000000 01	0.000000 01	0.00	0.00	0.00
17	2	0.000000 01	0.000000 01	0.000000 01	0.00	0.00	0.00
18	2	0.000000 01	0.000000 01	0.000000 01	0.00	0.00	0.00
19	2	0.000000 01	0.000000 01	0.000000 01	0.00	0.00	0.00
20	2	0.000000 01	0.000000 01	0.000000 01	0.00	0.00	0.00
21	2	0.000000 01	0.000000 01	0.000000 01	0.00	0.00	0.00
22	2	0.000000 01	0.000000 01	0.000000 01	0.00	0.00	0.00
23	2	0.000000 01	0.000000 01	0.000000 01	0.00	0.00	0.00
24	2	0.000000 01	0.000000 01	0.000000 01	0.00	0.00	0.00
25	2	0.000000 01	0.000000 01	0.000000 01	0.00	0.00	0.00
26	2	0.000000 01	0.000000 01	0.000000 01	0.00	0.00	0.00
27	2	0.000000 01	0.000000 01	0.000000 01	0.00	0.00	0.00
28	2	0.000000 01	0.000000 01	0.000000 01	0.00	0.00	0.00
29	2	0.000000 01	0.000000 01	0.000000 01	0.00	0.00	0.00
30	2	0.000000 01	0.000000 01	0.000000 01	0.00	0.00	0.00
31	2	0.000000 01	0.000000 01	0.000000 01	0.00	0.00	0.00

Figure 15. Output Data Format.



If a control volume mass penetration occurs, the mass which penetrates and the time are printed out. At the end of the run, the ruptures and mass penetrations that occurred during the run are summarized in tables for ready reference.

#### Sample Case

A sample 31 mass case is presented. Figure 16 represents the input data and follows the User's Guide input format (Figure 14). The representative output for one time period is shown in Figure 15 and follows the format described under the User's Guide output format.

Sample output plots are presented in Figures 17, 18, and 19 for the engine vertical velocity, vertical acceleration and vertical mount deflection respectively.

#### Program Listing

A complete listing of the computer program KRASH, including subroutines, is presented in Figure 20.

RUN 31-52 OF 100 TEST CORRELATION 206/186 ENGINE  
 NM, SPINT, ITABLL, DELTAT, TMAX  
 31 100 2.000000-05 2.000000-01  
 I,J,PHITJ,THEIJ,PTIJJ

100

CARD 100  
 CARD 101

1	2	0.0	0.0	0.0
2	3	0.0	0.0	0.0
3	4	0.0	0.0	0.0
4	5	0.0	0.0	0.0
4	7	0.0	0.0	0.0
5	6	0.0	0.0	0.0
5	7	0.0	0.0	0.0
5	20	0.0	0.0	0.0
5	21	0.0	0.0	0.0
5	22	0.0	0.0	0.0
5	23	0.0	0.0	0.0
6	9	0.0	0.0	0.0
6	11	0.0	0.0	0.0
7	9	0.0	0.0	0.0
8	9	0.0	0.0	0.0
10	11	0.0	0.0	0.0
10	14	0.0	0.0	0.0
10	15	0.0	0.0	0.0
10	24	0.0	0.0	0.0
10	23	0.0	0.0	0.0
11	16	0.0	0.0	0.0
12	16	0.0	0.0	0.0
12	24	0.0	0.0	0.0
13	16	0.0	0.0	0.0
13	25	0.0	0.0	0.0
16	17	0.0	0.0	0.0
16	18	0.0	0.0	0.0
16	15	0.0	0.0	0.0
20	21	0.0	0.0	0.0
22	24	0.0	0.0	0.0
31	23	0.0	0.0	0.0
24	25	0.0	0.0	0.0
10	26	0.0	0.0	0.0
16	27	0.0	0.0	0.0
26	28	0.0	0.0	0.0
27	29	0.0	0.0	0.0
28	30	0.0	0.0	0.0
27	31	0.0	0.0	0.0

CARDS 200-238

NET

1.390000 02	8.500000 01	6.200000 01	1.720000 02	2.780000 02	9.320000 02
7.310000 02	1.412000 03	9.000000 01	2.570000 02	1.821000 03	1.730000 02
1.750000 02	2.400000 01	2.400000 01	9.500000 02	2.400000 01	2.400000 01
3.070000 02	2.100000 01	3.100000 01	1.400000 02	1.400000 02	2.000000 01
2.600000 01	3.500000 01	7.000000 01	1.200000 02	1.200000 02	1.200000 02
1.200000 02					

CARDS 300-305

I,XI(1),YI(1),ZI(1),XI(1),YI(1),ZI(1)					
1	2.000000 02	1.730000 02	0.0	0.0	0.0
2	1.000000 01	2.050000 02	2.000000 02	0.0	0.0
3	1.500000 01	1.470000 02	1.320000 02	0.0	0.0
4	2.400000 01	3.400000 01	1.000000 01	0.0	0.0
5	2.500000 02	2.500000 02	2.500000 02	0.0	0.0
6	1.000000 03	1.000000 03	1.000000 03	0.0	0.0
7	3.000000 02	6.000000 02	4.200000 02	0.0	0.0
8	3.900000 03	3.900000 03	3.100000 02	0.0	0.0
9	3.700000 01	4.700000 01	4.000000 01	0.0	0.0
10	2.500000 02	2.500000 02	2.500000 02	0.0	0.0
11	2.010000 03	5.000000 03	3.290000 03	0.0	0.0
12	4.300000 01	2.500000 02	2.300000 02	0.0	0.0
13	4.300000 01	2.500000 02	4.300000 02	0.0	0.0
14	3.570000 01	3.570000 01	2.400000 01	0.0	0.0
15	3.570000 01	2.570000 01	2.400000 01	0.0	0.0
16	1.000000 03	1.100000 03	1.100000 03	0.0	0.0
17	3.420000 01	2.470000 01	2.400000 01	0.0	0.0
18	3.420000 01	2.470000 01	2.400000 01	0.0	0.0
19	1.710000 02	2.470000 02	7.600000 01	0.0	0.0
20	1.200000 02	1.200000 02	3.900000 01	0.0	0.0
21	1.200000 02	1.200000 02	3.900000 01	0.0	0.0
22	4.400000 01	7.000000 01	7.000000 01	0.0	0.0
23	4.400000 01	7.000000 01	7.000000 01	0.0	0.0
24	1.350000 02	2.400000 02	1.500000 02	0.0	0.0
25	1.350000 02	2.400000 02	1.500000 02	0.0	0.0
26	1.000000 02	1.000000 02	1.000000 02	0.0	0.0
27	1.000000 02	1.000000 02	1.000000 02	0.0	0.0
28	1.000000 02	1.000000 02	1.000000 02	0.0	0.0
29	1.000000 02	1.000000 02	1.000000 02	0.0	0.0
30	1.000000 02	1.000000 02	1.000000 02	0.0	0.0
31	1.000000 02	1.000000 02	1.000000 02	0.0	0.0

CARDS 310-340

I,XI(1),YI(1),ZI(1)			
1	0.0	0.0	0.0
2	0.0	0.0	0.0
3	0.0	0.0	0.0
4	0.0	0.0	0.0
5	0.0	0.0	0.0
6	0.0	0.0	0.0
7	0.0	0.0	0.0
8	0.0	0.0	0.0
9	0.0	0.0	0.0
10	0.0	0.0	0.0
11	0.0	0.0	0.0
12	0.0	0.0	0.0
13	0.0	0.0	0.0
14	0.0	0.0	0.0
15	0.0	0.0	0.0
16	0.0	0.0	0.0
17	0.0	0.0	0.0

CARDS 400-415

Figure 16. Sample 31 Mars Case Input Data.





5	0.0	0.0	0.0
6	0.0	0.0	0.0
7	0.0	0.0	0.0
8	0.0	0.0	0.0
9	0.0	0.0	0.0
10	0.0	0.0	1.700000 01
11	0.0	0.0	1.700000 01
12	0.0	1.000000 01	1.700000 01
13	0.0	0.0	1.700000 01
14	0.0	1.000000 00	2.250000 00
15	0.0	0.0	2.250000 00
16	0.0	0.0	1.700000 01
17	0.0	3.000000 00	2.250000 00
18	0.0	0.0	2.250000 00
19	0.0	0.0	0.0
20	0.0	1.000000 01	0.0
21	0.0	0.0	0.0
22	0.0	1.000000 01	1.700000 01
23	0.0	0.0	1.700000 01
24	0.0	1.000000 01	0.0
25	0.0	0.0	0.0
26	0.0	0.0	0.0
27	0.0	0.0	0.0
28	0.0	0.0	0.0
29	0.0	0.0	0.0
30	0.0	0.0	0.0
31	0.0	0.0	0.0

CARDS 600-615

1, SP (1,1), SP (1,2), SP (1,3)

1	0	0	0
2	0	0	0
3	0	0	0
4	0	0	0
5	0	0	0
6	0	0	0
7	0	0	0
8	0	0	0
9	0	0	0
10	0	0	1
11	0	0	1
12	0	0	1
13	0	0	1
14	0	0	1
15	0	0	1
16	0	0	1
17	0	0	1
18	0	0	1
19	0	0	0
20	0	0	0
21	0	0	0
22	0	0	1
23	0	0	1
24	0	0	0
25	0	0	0
26	0	0	0
27	0	0	0
28	0	0	0
29	0	0	0
30	0	0	0
31	0	0	0

CARDS 700-703

1, MU (1,1), MU (1,2), MU (1,3)

1	0.0	0.0	0.0
2	0.0	0.0	0.0
3	0.0	0.0	0.0
4	0.0	0.0	0.0
5	0.0	0.0	0.0
6	0.0	0.0	0.0
7	0.0	0.0	0.0
8	0.0	0.0	0.0
9	0.0	0.0	0.0
10	0.0	0.0	3.000000-01
11	0.0	0.0	3.000000-01
12	0.0	3.000000-01	3.000000-01
13	0.0	0.0	3.000000-01
14	0.0	1.000000-01	3.000000-01
15	0.0	0.0	3.000000-01
16	0.0	0.0	3.000000-01
17	0.0	1.000000-01	3.000000-01
18	0.0	0.0	3.000000-01
19	0.0	0.0	0.0
20	0.0	3.000000-01	0.0
21	0.0	0.0	0.0
22	0.0	1.000000-01	3.000000-01
23	0.0	0.0	3.000000-01
24	0.0	1.000000-01	0.0
25	0.0	0.0	0.0
26	0.0	0.0	0.0
27	0.0	0.0	0.0
28	0.0	0.0	0.0
29	0.0	0.0	0.0
30	0.0	0.0	0.0
31	0.0	0.0	0.0

CARDS 710-725

Figure 16. (Continued)

CARDS 800-1027

103

12	1	3.040000 04	0.0	0.0	0.0	0.0	0.0
12	2	0.0	4.010000 05	0.0	0.0	0.0	-5.780000 04
12	3	0.0	0.0	3.250000 05	0.0	4.890000 04	0.0
12	4	0.0	0.0	0.0	2.340000 07	0.0	0.0
12	5	0.0	0.0	4.890000 04	0.0	8.950000 07	0.0
12	6	0.0	-5.780000 04	0.0	0.0	0.0	1.140000 06
13	1	4.890000 04	0.0	0.0	0.0	0.0	0.0
13	2	0.0	4.227000 04	0.0	0.0	0.0	-3.477000 07
13	3	0.0	0.0	3.420000 06	0.0	2.816000 07	0.0
13	4	0.0	0.0	0.0	8.767000 07	0.0	0.0
13	5	0.0	0.0	2.816000 07	0.0	3.080000 08	0.0
13	6	0.0	-3.477000 07	0.0	0.0	0.0	3.813000 08
14	1	0.0	0.0	0.0	0.0	0.0	0.0
14	2	0.0	0.0	0.0	0.0	0.0	0.0
14	3	0.0	0.0	0.0	0.0	0.0	0.0
14	4	0.0	0.0	0.0	2.190000 06	0.0	0.0
14	5	0.0	0.0	0.0	0.0	0.0	0.0
14	6	0.0	0.0	0.0	0.0	0.0	0.0
15	1	2.030000 06	0.0	0.0	0.0	0.0	0.0
15	2	0.0	1.051000 05	0.0	0.0	0.0	-2.422000 06
15	3	0.0	0.0	1.911000 04	0.0	4.404000 05	0.0
15	4	0.0	0.0	0.0	2.250000 04	0.0	0.0
15	5	0.0	0.0	4.404000 05	0.0	1.354000 07	0.0
15	6	0.0	-2.422000 06	0.0	0.0	0.0	7.443000 07
16	1	3.450000 05	0.0	0.0	0.0	0.0	0.0
16	2	0.0	4.890000 05	0.0	0.0	0.0	-5.550000 06
16	3	0.0	0.0	1.003000 05	0.0	1.703000 06	0.0
16	4	0.0	0.0	0.0	2.340000 04	0.0	0.0
16	5	0.0	0.0	1.983000 04	0.0	2.409000 07	0.0
16	6	0.0	-3.550000 04	0.0	0.0	0.0	7.855000 07
17	1	4.795000 05	0.0	0.0	0.0	0.0	0.0
17	2	0.0	3.697000 03	0.0	0.0	0.0	-4.637000 04
17	3	0.0	0.0	2.497000 03	0.0	4.637000 04	0.0
17	4	0.0	0.0	0.0	5.587000 07	0.0	0.0
17	5	0.0	0.0	4.637000 04	0.0	2.170000 04	0.0
17	6	0.0	-4.637000 04	0.0	0.0	0.0	2.170000 04
18	1	4.795000 05	0.0	0.0	0.0	0.0	0.0
18	2	0.0	2.497000 03	0.0	0.0	0.0	-4.637000 04
18	3	0.0	0.0	2.497000 03	0.0	4.637000 04	0.0
18	4	0.0	0.0	0.0	5.587000 07	0.0	0.0
18	5	0.0	0.0	4.637000 04	0.0	2.170000 04	0.0
18	6	0.0	-4.637000 04	0.0	0.0	0.0	2.170000 04
19	1	8.807000 04	0.0	0.0	0.0	0.0	0.0
19	2	0.0	2.230000 04	0.0	0.0	0.0	-5.037000 05
19	3	0.0	0.0	1.317000 05	0.0	2.963000 06	0.0
19	4	0.0	0.0	0.0	0.0	0.0	0.0
19	5	0.0	0.0	2.963000 06	0.0	8.807000 07	0.0
19	6	0.0	-5.037000 05	0.0	0.0	0.0	1.951000 07
20	1	8.807000 04	0.0	0.0	0.0	0.0	0.0
20	2	0.0	2.230000 04	0.0	0.0	0.0	-5.037000 05
20	3	0.0	0.0	1.317000 05	0.0	2.963000 06	0.0
20	4	0.0	0.0	0.0	0.0	0.0	0.0
20	5	0.0	0.0	2.963000 06	0.0	8.807000 07	0.0
20	6	0.0	-5.037000 05	0.0	0.0	0.0	1.951000 07
21	1	1.730000 02	0.0	0.0	0.0	0.0	0.0
21	2	0.0	1.545000 04	0.0	0.0	0.0	-4.350000 07
21	3	0.0	0.0	5.700000 03	0.0	1.944000 05	0.0
21	4	0.0	0.0	0.0	7.500000 05	0.0	0.0
21	5	0.0	0.0	1.944000 05	0.0	9.225000 04	0.0
21	6	0.0	-5.350000 07	0.0	0.0	0.0	2.470000 04
22	1	1.770000 06	0.0	0.0	0.0	0.0	0.0
22	2	0.0	1.275000 05	0.0	0.0	0.0	-2.040000 06
22	3	0.0	0.0	2.123000 04	0.0	4.776000 05	0.0
22	4	0.0	0.0	0.0	1.367000 04	0.0	0.0
22	5	0.0	0.0	4.776000 05	0.0	1.433000 07	0.0
22	6	0.0	-2.040000 06	0.0	0.0	0.0	3.604000 07
23	1	1.481000 05	0.0	0.0	0.0	0.0	0.0
23	2	0.0	5.611000 03	0.0	0.0	0.0	-1.441000 05
23	3	0.0	0.0	7.377000 04	0.0	1.792000 04	0.0
23	4	0.0	0.0	0.0	2.981000 05	0.0	0.0
23	5	0.0	0.0	1.792000 04	0.0	7.170000 07	0.0
23	6	0.0	-1.441000 05	0.0	0.0	0.0	3.250000 06
24	1	1.770000 06	0.0	0.0	0.0	0.0	0.0
24	2	0.0	1.275000 05	0.0	0.0	0.0	-2.040000 06
24	3	0.0	0.0	2.123000 04	0.0	4.776000 05	0.0
24	4	0.0	0.0	0.0	1.367000 04	0.0	0.0
24	5	0.0	0.0	4.776000 05	0.0	1.433000 07	0.0
24	6	0.0	-2.040000 06	0.0	0.0	0.0	3.604000 07
25	1	1.481000 05	0.0	0.0	0.0	0.0	0.0
25	2	0.0	5.611000 03	0.0	0.0	0.0	-1.441000 05
25	3	0.0	0.0	7.377000 04	0.0	1.792000 04	0.0
25	4	0.0	0.0	0.0	2.981000 05	0.0	0.0
25	5	0.0	0.0	1.792000 04	0.0	7.170000 07	0.0
25	6	0.0	-1.441000 05	0.0	0.0	0.0	3.250000 06
26	1	2.397000 04	0.0	0.0	0.0	0.0	0.0
26	2	0.0	1.429000 03	0.0	0.0	0.0	-3.316000 04
26	3	0.0	0.0	1.429000 03	0.0	3.316000 04	0.0
26	4	0.0	0.0	0.0	2.944000 07	0.0	0.0
26	5	0.0	0.0	3.316000 04	0.0	1.154000 06	0.0
26	6	0.0	-3.316000 04	0.0	0.0	0.0	1.154000 06
27	1	2.397000 04	0.0	0.0	0.0	0.0	0.0
27	2	0.0	1.429000 03	0.0	0.0	0.0	-3.316000 04
27	3	0.0	0.0	1.429000 03	0.0	3.316000 04	0.0
27	4	0.0	0.0	0.0	2.944000 07	0.0	0.0
27	5	0.0	0.0	3.316000 04	0.0	1.154000 06	0.0
27	6	0.0	-3.316000 04	0.0	0.0	0.0	1.154000 06

CARDS 800-1027

Figure 16. (Continued)

CARDS 800-1027

CARDS 2000-2037

105

74	1.000000 01	1.000000 01	1.000000 01	1.000000 01	1.000000 01	1.000000 01
75	1.000000 01	1.000000 01	1.000000 01	1.000000 01	1.000000 01	1.000000 01
76	1.000000 01	1.000000 01	1.000000 01	1.000000 01	1.000000 01	1.000000 01
77	1.000000 01	1.000000 01	1.000000 01	1.000000 01	1.000000 01	1.000000 01
78	1.000000 01	1.000000 01	1.000000 01	1.000000 01	1.000000 01	1.000000 01

[illegible][illegible]

CARDS 2100-2137

CARDS 2201-2428

Figure 16. (Continued)

CARDS 2201-2428

107







1, J, C, B, A, I, J

1	2	5.000000-02
2	2	5.000000-02
3	4	5.000000-02
4	5	5.000000-02
5	7	5.000000-02
6	6	5.000000-02
7	7	5.000000-02
8	20	5.000000-02
9	21	5.000000-02
10	22	1.000000-01
11	23	1.000000-01
12	4	5.000000-02
13	11	1.000000-01
14	5	5.000000-02
15	4	5.000000-02
16	11	1.000000-01
17	14	1.000000-01
18	15	1.000000-01
19	22	1.000000-01
20	23	1.000000-01
21	14	1.000000-01
22	14	1.000000-01
23	24	5.000000-02
24	16	1.000000-01
25	25	5.000000-02
26	17	1.000000-01
27	16	1.000000-01
28	19	1.000000-01
29	21	5.000000-02
30	22	5.000000-02
31	23	5.000000-02
32	25	5.000000-02
33	26	5.000000-02
34	21	5.000000-02
35	28	2.000000-01
36	29	2.000000-01
37	33	1.000000-01
38	31	1.000000-01

CARDS 3200-3206

1, J, C, B, A, I, J, P, C, I, J, I, J, I, J

1	-0.375000-01	0.0
2	-1.431810-01	0.0
3	-2.963290-01	0.0
4	0.0	0.0
5	1.000000 00	0.0
6	0.0	0.0
7	2.107750 00	0.0
8	6.953940-01	1.570000 00
9	6.953940-01	-1.570000 00
10	-5.504650-01	1.570000 00
11	-5.504650-01	-1.570000 00
12	1.570000 00	0.0
13	-1.570000 00	0.0
14	-2.497790-01	0.0
15	-1.764500 00	0.0
16	0.0	0.0
17	-5.167220-01	1.570000 00
18	-5.167220-01	-1.570000 00
19	0.0	1.570000 00
20	0.0	-1.570000 00
21	0.0	0.0
22	3.0	-1.570000 00
23	1.570000 00	0.0
24	0.0	1.570000 00
25	1.570000 00	0.0
26	-5.167220-01	1.570000 00
27	-5.167220-01	-1.570000 00
28	0.0	0.0
29	0.0	-1.570000 00
30	-1.570000 00	0.0
31	-1.570000 00	0.0
32	0.0	-1.570000 00
33	1.570000 00	0.0
34	1.570000 00	0.0
35	1.570000 00	0.0
36	1.570000 00	0.0
37	1.570000 00	0.0
38	1.570000 00	0.0

Figure 16. (Continued)

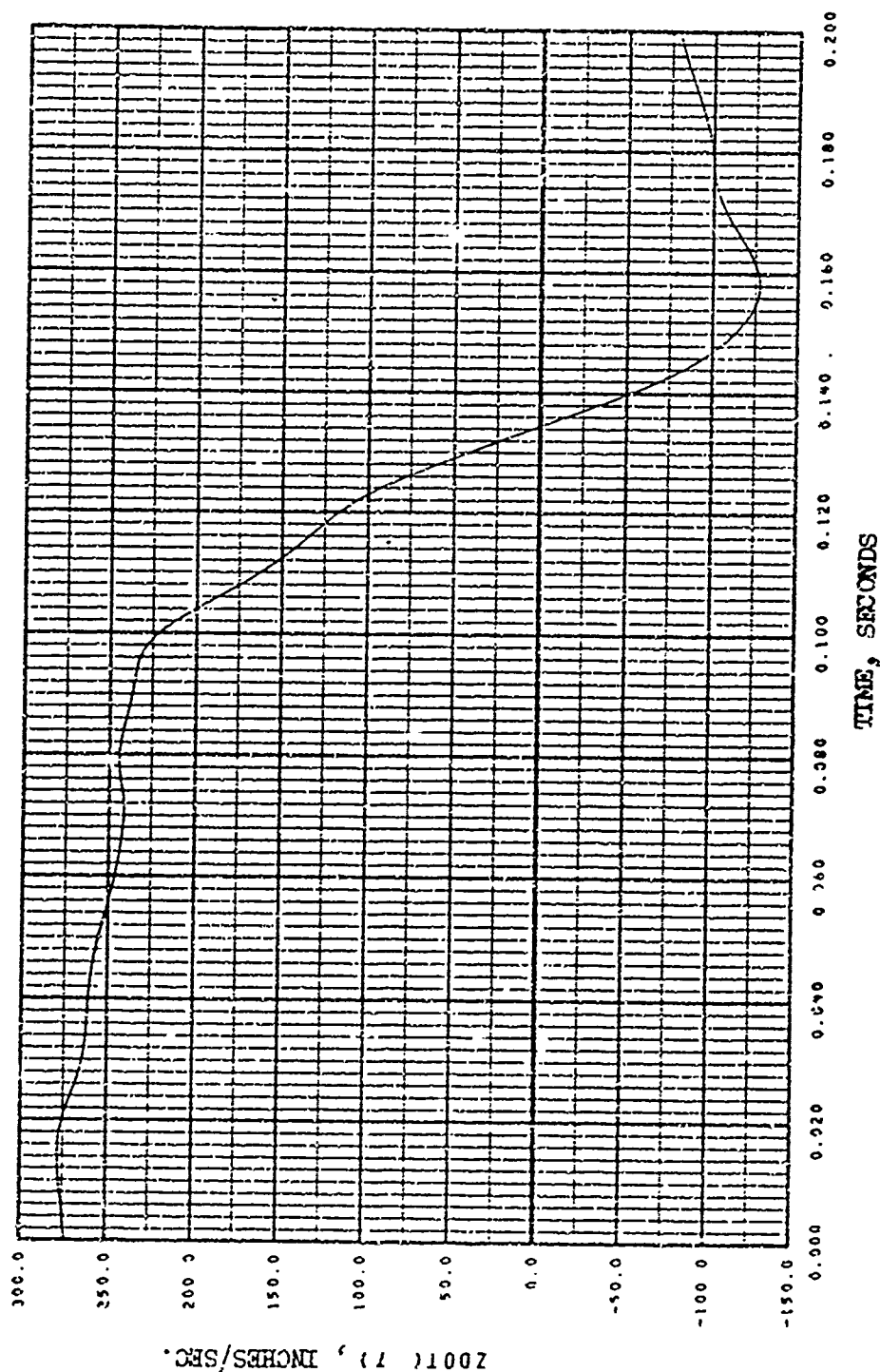
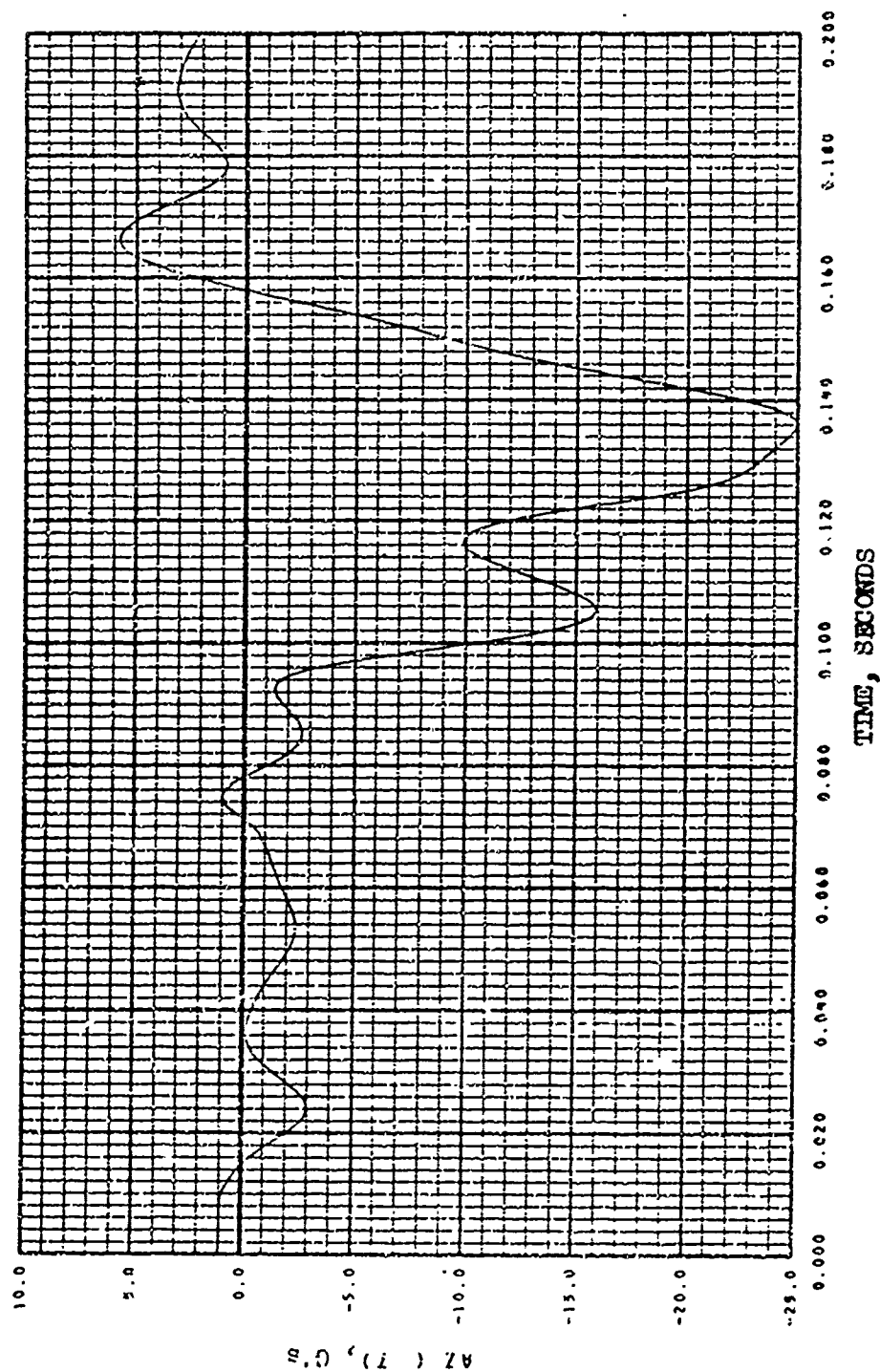
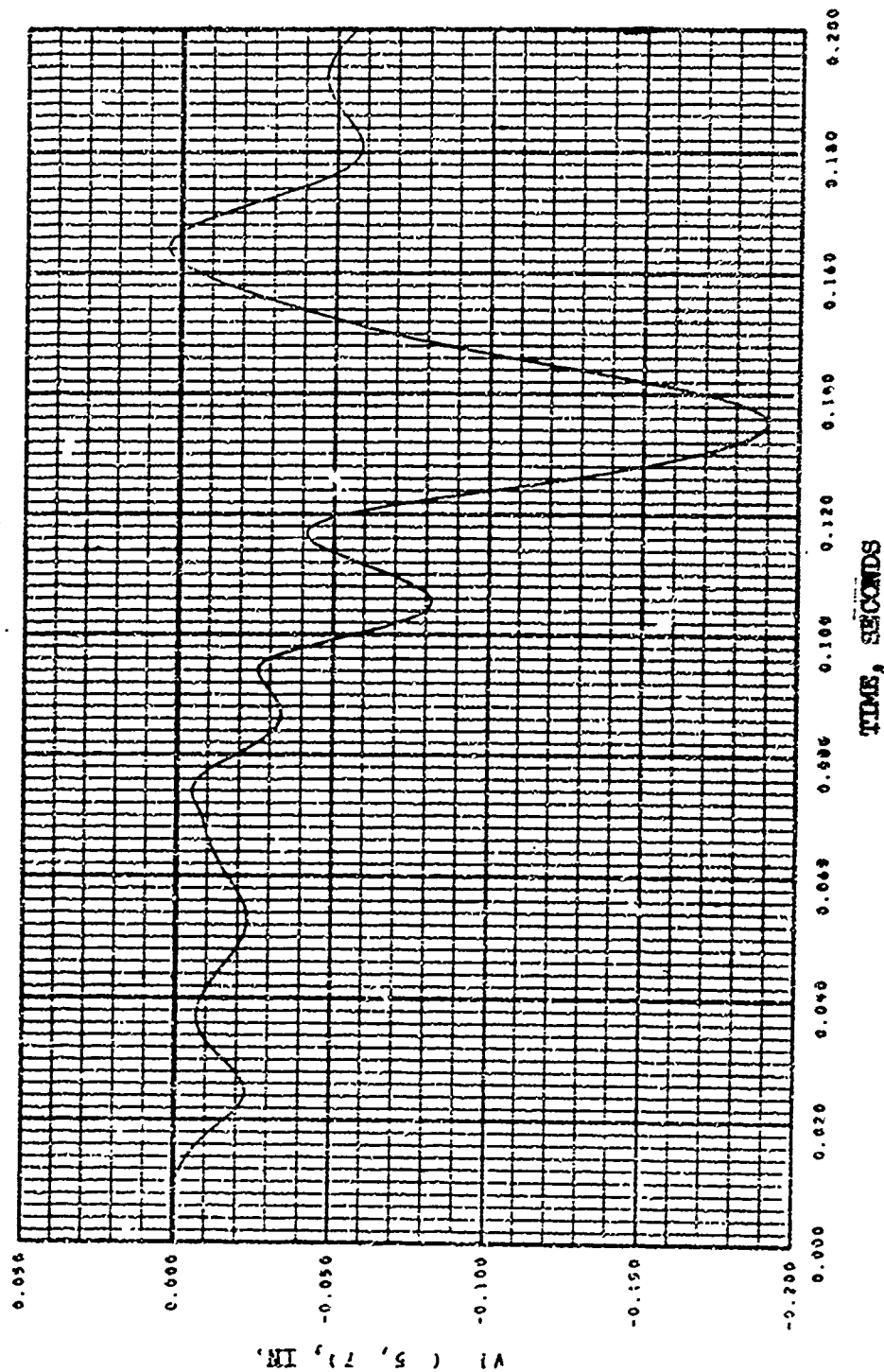


Figure 1.7. Sample Case, Engine Vertical Velocity Time History Plot.



RUN 31-52 DROP TEST CORRELATION 200/18G ENGINE

Figure 16. Sample Case, Engine Vertical Acceleration Time History Plot.



RUN 31-52 DROP TEST CORRELATION 203/180 ENGINE

Figure 19. Sample Case, Engine Mount Vertical Deflection Time History Plot.

```

IMPLICIT REAL*8 (A-H,O-Z)
PEA, #4 PLDT(30000),ZAR,TMPLDT(500)
DIMENSION SC(40,3),ZAR(200),IPLOT(150),IDPLDT(150)
DIMENSION IG(80),JJ(80),PHIJ(80),THEIJ(80),PSIJ(80),WGT(40),
1 XI(40),YI(40),ZI(40),XYI(40),YZI(40),XZI(40),HEX(40),HEY(40),
2 HFZ(40),ALIFT(40),XI(40),YI(40),ZI(40),PHI(40),THETA(40),PSI(40),
3 JI(40),VI(40),W(40),PI(40),C(40),R(40),XDOT(40),YDOT(40),ZDOT(40),
4 PHIDOT(40),THEDOT(40),PSIDOT(40),UDOT(40),VDOT(40),WDOT(40)
DIMENSION AIJ(5),AI(9),AJI(9),AIDOT(9),DX(40),DY(40),DZ(40),
1 DPHI(40),DTHETA(40),DPSI(40),D(6),DF(5),XX(40),XY(40),XZ(40),
2 XL(40),XM(40),XN(40),DELT(40),XI1(40),XI2(40),XI3(40),
3 XI4(40),XI5(40),XI6(40),XK(2880),FMBAR(2880),FMBAR3(6,6,80),
4 FM(2880),XXRIN(10,6,80),VEE(480),VMAX(480),NN(40,3),NN2(40,3)
DIMENSION XKI(219,6,80),AIJ(360),CIJ(360),DIJ(720),XLBAR(40,3),
1 XLBAR(3),ISPI(40,3),IISI(3),XMI(40,3),XPE(40,3),CAI(360),
2 ISS(40,3),ISS2(40,3),SI(40,3),SF(40,3),FSPDF(40,3),PHIDP(40),
3 THEDP(40),PSIDP(40),FSPBAR(40,3),FSPBA2(40,3),XLNGTH(3),XC(6),
4 XDP(40),YDP(40),ZDP(40),FM3(6,6,80),VEE2(6,80),VFEDOT(3,3)
DIMENSION PDD(40),QDD(40),RDD(40),N(480),N3(90,6),DVSIGN(6),
1 XCS(4320),XKS(9,6,80),XKI(4320),TITLE(10)
DIMENSION XOLD(40),YOLD(40),ZOLD(40),PHIOLD(40),THEOLD(40),
1 PSIOLD(40),POLD(40),QOLD(40),ROLD(40),UOLD(40),VOLD(40),WOLD(40)
DIMENSION XXX(80),XXJ(80),XYK(80),XYJ(80),XZK(80),XZJ(80),
1 XL(80),XLJ(80),XMK(80),XMJ(80),XNK(80),XNJ(80)
DIMENSION CXIJ(80),CYIJ(80),CZIJ(80)
DIMENSION PIN(40),QIN(40),RIN(40),PINO(40),QINO(40),RINO(40),
1 DIN(40),DQIN(40),DRIN(40)
DIMENSION DD(6),DPX(40),DPY(40),DPZ(40),DPL(40),DPM(40),DPN(40)
DIMENSION C(6,80),ZAR(80),DXDA(6,80)
DIMENSION XACC(40),YACC(40),ZACC(40)
DIMENSION SUMDF(6,80),TRUPT(80),IRUPT(80),JRUPT(80)
DIMENSION TPEN(80),IPFN(80)
DIMENSION IJPR(76)
DIMENSION AITAJ(9)
DIMENSION FSPDI(40,3),SA(40,3),SB(40,3)
DIMENSION DRI(76)
CJ44JN DRI
CJ44JN FSPDI,SA,SB
CJ44JN AITAJ
CJ44JN XNBAR,XPBAR,YNBAR,YPBAR,ZNBAR,ZPBAR,TPEN
CJ44JN SUMDF,TRUPT,DXDA,SC
CJ44JN XACC,YACC,ZACC
CJ44JN C,CBAR
CJ44JN DD,DPX,DPY,DPZ,DPL,DPM,DPN
CJ44JN PIN,QIN,RIN,PINO,QINO,RINO,DPIN,DQIN,DRIN
CJ44JN CXIJ,CYIJ,CZIJ,ZG
CJ44JN XXX,XXJ,XYK,XYJ,XZK,XZJ,XLK,XLJ,XMK,XMJ,XNK,XNJ
CJ44JN XOLD,YOLD,ZOLD,PHIOLD,THEOLD,PSIOLD,POLD,GOLD,ROLD,UOLD,
1 VOLD,WOLD,DT2,DT4,LF
CJ44JN PHI,THETA,PSI
CJ44JN BIJ,PSIDOT,THEDOT,PHIDOT,CIJ,X,Y,Z,XIJ,YIJ,ZIJ,D,DF
CJ44JN AI,AIDOT,AJ,AIJ,DX,DY,DZ,DPHI,DTHETA,DPSI,DVSIGN
CJ44JN VEF,FMBAR,FM,XKS,XKI,VMAX
CJ44JN XX,XY,XZ,XL,XM,XN,WGT,ALIFT,XC,P,Q,R,U,V,W
CJ44JN UNDOT,VDDOT,WDDOT,XZI,YZI,ZI,HFZ,XI,XYI,HEX,YI,HEY,DELT
CJ44JN PDDOT,XI1,XI2,XI3,QDDOT,XI5,XI4,RDDOT,XI5,XDDOT,YDDOT,ZDDOT
CJ44JN XLBAR,SF,FSPDF,XKE,FSPBAR,XMI,VFEDOT
CJ44JN XGDDOT,YGDDOT,ZGDDOT,PPR,QPR,PPP,PHIPR,THEPR,PSIPK
CJ44JN PHIDP,THEDP,PSIDP,XR,XYP,ZDP,DAI,DELTAT,TMAX,TIME,TITLE
CJ44JN PHIJ,THEIJ,PSIJ,XK,DIJ,XXIHAR,SI,XLNGTH,IP

```

CRS00010

CRS00020

CRS00030

CRS00040

CRS00050

CRS00060

CRS00070

CRS00080

CRS00090

CRS00100

CRS00110

CRS00120

CRS00130

CRS00140

CRS00150

CRS00160

CRS00170

CRS00180

CRS00190

CRS00200

CRS00210

CRS00220

CRS00230

CRS00240

CRS00250

CRS00260

CRS00290

CRS00300

CRS00320

CRS00330

CRS00340

CRS00350

CRS00360

CRS00370

CRS00380

CRS00390

CRS00400

CRS00410

CRS00420

CRS00430

CRS00440

CRS00360

CRS00460

CRS00470

Figure 20. Program Listing.



YACC(I)=0.0	
ZACC(I)=0.0	
DJ 150 K = 1.3	CRS00990
IRS2(I,K) = 0	CRS01000
NV2(I,K) = 0	CRS01010
SC(I,K) = 0.0	
150 FSPBA2(I,K) = C.0	CRS01020
DJ 160 IJ = 1.IGS	CRS01030
XXK(IJ) = 0.0	CRS01040
XXJ(IJ) = 0.0	CRS01050
XYK(IJ) = 0.0	CRS01060
XYJ(IJ) = 0.0	CRS01070
XZK(IJ) = 0.0	CRS01080
XZJ(IJ) = 0.0	CRS01090
XLK(IJ) = 0.0	CRS01100
XLJ(IJ) = 0.0	CRS01110
XMK(IJ) = 0.0	CRS01120
XMJ(IJ) = 0.0	CRS01130
XNK(IJ) = 0.0	CRS01140
XNJ(IJ) = 0.0	CRS01150
OX(IJ,IJ) = 0.0	CRS01300
OY(IJ,IJ) = 0.0	CRS01310
OZ(IJ,IJ) = 0.0	CRS01320
DJ 160 L = 1.6	CRS01330
SUMDF(L,IJ) = C.0	
N3(IJ,L) = 0	CRS01340
VEE2(L,IJ) = 0.0	CRS01350
DJ 160 K = 1.6	CRS01360
F43(L,K,IJ) = C.0	CRS01370
160 F4BAR3(L,K,IJ) = 0.0	CRS01380
DJ 165 J = 1.3	CRS01390
DJ 165 K = 1.3	CRS01400
165 VEED3T(J,K) = C.0	CRS01410
C DO INITIAL CONDITIONS	CRS01420
CALL IC	CRS01430
C DO ALL THE (AIJ) INTO DIJ	CRS01440
CALL DOAIJ	CRS01450
CALL DERIV	CRS01470
CALL PRINT	CRS01500
IPC = 0	CRS01510
IF(NPLOT.NE.0) CALL SAVE	
DJ 200 I = 1,NH	CRS01520
C PRESET JLD VALUES	CRS01530
PIND(I) = 0.0	CRS01540
QIND(I) = 0.0	CRS01550
RIND(I) = 0.0	CRS01560
XJLD(I) = X(I)	CRS01570
YJLD(I) = Y(I)	CRS01580
ZJLD(I) = Z(I)	CRS01590
PHIJLD(I) = PHI(I)	CRS01600
THETAJLD(I) = THETA(I)	CRS01610
PSIJLD(I) = PSI(I)	CRS01620
PJLD(I) = P(I)	CRS01630
QJLD(I) = Q(I)	CRS01640
RJLD(I) = R(I)	CRS01650
UJLD(I) = U(I)	CRS01660
VJLD(I) = V(I)	CRS01670
WJLD(I) = W(I)	CRS01680
C DO 1ST STEP EULER	CRS01690
DPIN(I) = DELTAT*P(I)	CRS01700

Figure 20. (Continued)

QIN(I) = DELTAT*Q(I)	CRS01710
ORIN(I) = DELTAT*R(I)	CRS01720
PIN(I) = OPIN(I)	CRS01730
QIN(I) = QIN(I)	CRS01740
RIN(I) = ORIN(I)	CRS01750
P(I) = P(I)+DELTAT*PODOT(I)	CRS01760
Q(I) = Q(I)+DELTAT*QDOT(I)	CRS01770
R(I) = R(I)+DELTAT*RODOT(I)	CRS01780
U(I) = U(I)+DELTAT*UDOT(I)	CRS01790
V(I) = V(I)+DELTAT*VDOT(I)	CRS01800
W(I) = W(I)+DELTAT*WDOT(I)	CRS01810
DX(I) = DELTAT*XDOT(I)	CRS01820
X(I) = X(I)+DX(I)	CRS01830
DY(I) = DELTAT*YDOT(I)	CRS01840
Y(I) = Y(I)+DY(I)	CRS01850
DZ(I) = DELTAT*ZDOT(I)	CRS01860
Z(I) = Z(I)+DZ(I)	CRS01870
DPHI(I) = DELTAT*PHIDOT(I)	CRS01880
PHI(I) = PHI(I)+DPHI(I)	CRS01890
DTHEA(I) = DELTAT*THEDOT(I)	CRS01900
THETA(I) = THETA(I)+DTHEA(I)	CRS01910
DPSI(I) = DELTAT*PSIDOT(I)	CRS01920
PSI(I) = PSI(I)+DPSI(I)	CRS01930
200 CONTINUE	CRS01940
190 TIME = TIME+DELTAT	CRS01950
CALL DERIV	CRS02020
IPC = IPC+1	CRS02030
IF(IPC-IPRINT) 310,270,270	CRS02040
270 CALL PRINT	CRS02050
IPC = 0	CRS02060
310 IF(NPLOT.EQ.0) GO TO 280	
IPLC = IPLC+1	
IF(IPLC.EQ.1)PLOT) CALL SAVE	
C PREDICT, MOVE DOWN, AND DO DELTA'S	CRS02070
280 DO 300 I = 1,NM	CRS02080
T = PIN(I)+DT2*P(I)	CRS02090
PIN(I) = PIN(I)	CRS02100
PIN(I) = T	CRS02110
OPIN(I) = PIN(I)-PIN(I)	CRS02120
T = QIN(I)+DT2*Q(I)	CRS02130
QIN(I) = QIN(I)	CRS02140
QIN(I) = T	CRS02150
OPIN(I) = QIN(I)-QIN(I)	CRS02160
T = RIN(I)+DT2*R(I)	CRS02170
RIN(I) = RIN(I)	CRS02180
RIN(I) = T	CRS02190
ORIN(I) = RIN(I)-RIN(I)	CRS02200
T = XOLD(I)+DT2*XDOT(I)	CRS02210
XOLD(I) = X(I)	CRS02220
X(I) = T	CRS02230
DX(I) = X(I)-XOLD(I)	CRS02240
T = YOLD(I)+DT2*YDOT(I)	CRS02250
YOLD(I) = Y(I)	CRS02260
Y(I) = T	CRS02270
DY(I) = Y(I)-YOLD(I)	CRS02280
T = ZOLD(I)+DT2*ZDOT(I)	CRS02290
ZOLD(I) = Z(I)	CRS02300
Z(I) = T	CRS02310
DZ(I) = Z(I)-ZOLD(I)	CRS02320
T = PHID(I)+DT2*PHIDOT(I)	CRS02330

Figure 20. (Continued)



PHOLD(I) = PHI(I)	CRS02340
PHI(I) = T	CPS02350
DPHI(I) = PHI(I)-PHOLD(I)	CRS02360
T = THEOLD(I)+DT2*THEODT(I)	CRS02370
THEOLD(I) = THETA(I)	CRS02380
THETA(I) = T	CRS02390
OTHEA(I) = THETA(I)-THEOLD(I)	CRS02400
T = PSOLD(I)+DT2*PSIDGT(I)	CPS02410
PSOLD(I) = PSI(I)	CRS02420
PSI(I) = T	CRS02430
DPSI(I) = PSI(I)-PSOLD(I)	CRS02440
Y = POLD(I)+DT2*PDGT(I)	CRS02450
POLD(I) = P(I)	CRS02460
P(I) = T	CRS02470
T = QOLD(I)+DT2*QDGT(I)	CRS02480
QOLD(I) = Q(I)	CRS02490
Q(I) = T	CRS02500
Y = ROLD(I)+DT2*RDGT(I)	CRS02510
ROLD(I) = R(I)	CRS02520
R(I) = T	CRS02530
T = UOLD(I)+DT2*UDGT(I)	CRS02540
UOLD(I) = U(I)	CRS02550
U(I) = T	CRS02560
T = VOLD(I)+DT2*VDGT(I)	CRS02570
VOLD(I) = V(I)	CRS02580
V(I) = T	CRS02590
T = WOLD(I)+DT2*WDGT(I)	CPS02600
WOLD(I) = W(I)	CRS02610
W(I) = T	CRS02620
300 CONTINUE	CRS02630
IF(TIME-TMAX) 190,190,500	CPS02640
500 IF (LRUPY) 5500,5500,5000	
5000 PRINT 2000	
2000 FJRMAT(1H1,7X,15HRUPTYPE SUMMARY,/)	
PRINT 3000	
3000 FJRMAT(1H,9X,1H1,9X,1HJ,7X,4HTIME,/)	
PRINT 4000,(IRLPT(KRY),JRUP(T(KRT),TRUPT(KRT),KRT=1,KRUPT)	
4000 FJRMAT(1H,211C,F10.5)	
5500 IF (KPEN.LE.0) GO TO 6000	
PRINT 5501	
5501 FJRMAT(1H1,7X,'CONTROL VOLUME PENETRATIONS' //)	
PRINT 5502	
5502 FJRMAT(1H,13X,'TIME',10X,'MASS' //)	
PRINT 5503,(IPEN(K),IPEN(K),K=1,KPEN)	
5503 FJRMAT(1H,10X,F10.5,110)	
6000 IF(NPLOT.NE.0) CALL TOLP	
GO TO 1	
1000 IF(IPLSW.NE.0) CALL EXITG(ZAK)	
STOP	
END	CRS02650

Figure 20. (Continued)

SUBROUTINE DERIV	CRS02660
IMPLICIT REAL*8 (A-H,O-Z)	
REAL*4 PLOT(3000),ZAP,TMPLOT(500)	
DIMENSION SC(40,3),ZAR(200),IPLOT(150),IDPLOT(150)	
DIMENSION IG(80),JG(80),PHIJ(80),THEIJ(80),PSIJ(80),WGT(40),	CRS02140
1 XI(40),YI(40),ZI(40),XYI(40),YZI(40),XZI(40),HEX(40),HEY(40),	CRS02150
2 HEZ(40),ALIFT(40),X(40),Y(40),Z(40),PHI(40),THETA(40),PSI(40),	CRS02160
3 UI(40),VI(40),W(40),P(40),Q(40),R(40),XDOT(40),YDOT(40),ZDOT(40),	CRS02170
4 PHIDOT(40),THEDOT(40),PSIDOT(40),UDOT(40),VDOT(40),WDOT(40)	CRS02180
DIMENSION AIJ(5),AJ(9),AJ(9),AJ(9),AJ(9),DX(40),DY(40),DZ(40),	CRS02190
1 DTHI(40),DTHETA(40),DPSI(40),D(6),DF(6),XX(40),XY(40),XZ(40),	CRS02200
2 XL(40),XM(40),XN(40),DEL(40),XI(40),XJ(40),XK(40),	CRS02210
3 XI(40),XJ(40),XK(40),XL(40),XM(40),XN(40),XO(40),XP(40),XQ(40),XR(40),XS(40),XT(40),XU(40),XV(40),XW(40),	CRS02220
4 FM(2800),XKR(IN(10,6,80),VEE(480),VMAX(480),NNI(40,3),NNZ(40,3)	CRS02230
DIMENSION XKI(3,6,80),BIJ(360),CIJ(360),DIJ(720),XLSAR(40,3),	CRS02240
1 XLSAR(3),ISPI(40,3),ISPI(3),XHU(40,3),XKE(40,3),DAI(360),	CRS02250
2 IRS(40,3),IRS2(40,3),SI(40,3),SF(40,3),FSPDF(40,3),PHIDP(40),	CRS02260
3 THEDP(40),PSIDP(40),FSPBAR(40,3),FSPBAZ(40,3),XLNGTH(3),XC(6),	CRS02270
4 XDP(40),YDP(40),ZDP(40),FM3(6,6,80),VEE2(6,80),VEEDOT(3,3)	CRS02280
DIMENSION PDDT(40),QDDT(40),RDOT(40),N(480),N3(50,6),DVSIGN(6),	CRS02290
1 XCS(4320),XKS(9,6,80),XKI(4320),TITLE(10)	CRS00180
DIMENSION AIAIJ(9),DAI(9)	CRS02310
DIMENSION XNLD(40),YOLD(40),ZOLD(40),PHIOLD(40),THEOLD(40),	CRS02320
1 PSIOLD(40),POLD(40),POLD(40),ROLD(40),UOLD(40),VOLD(40),WOLD(40)	CRS02330
DIMENSION XX(80),XXJ(80),XYK(80),XYJ(80),XZK(80),XZJ(80),	CRS02340
1 XLK(80),XLJ(80),XMK(80),XMJ(80),XNK(80),XNJ(80)	CRS02350
DIMENSION OXIJ(80),OYIJ(80),OZIJ(80)	CRS02360
DIMENSION PIN(40),PIN(40),PIN(40),PIN(40),QIN(40),RIN(40),	CRS00230
1 DPIN(40),DOIN(40),DPIN(40)	CRS00240
DIMENSION SINCS(6)	CRS02920
DIMENSION AITAJ(9)	CRS02930
DIMENSION DDI(6),DPX(40),DPY(40),DPZ(40),DPL(60),DPM(40),DPN(40)	CRS00250
DIMENSION C(6,60),CBAR(80),DXDA(6,80)	CRS00280
DIMENSION XACC(40),YACC(40),ZACC(40)	
DIMENSION XK(3,6,6,20)	
DIMENSION SUMDF(6,60),TRUPT(80),IRUPT(80),JRUPT(80),IRUPT(80)	
DIMENSION IPENSW(80),AP(9)	
DIMENSION TPEN(80),IPFN(80)	
DIMENSION IJPR(76)	
DIMENSION FSPDI(40,3),SA(40,3),SB(40,3)	
DIMENSION ORI(76)	
CJ44J4 ORI	
CJ44J4 FSPDI,SA,SB	
CJ44J4 AITAJ	
CJ44J4 XNBAR,XPRAR,YNBAR,YPRAR,ZNBAR,ZPRAR,TPEN	
CJ44J4 SUMDF,TRUPT,IRUPT,IRUPT,IRUPT	
CJ44J4 XACC,YACC,ZACC	
CJ44J4 C,CBAR	CRS02960
CJ44J4 DD,DPX,DPY,DPZ,DPL,DPM,DPN	CRS00300
CJ44J4 PIN,QIN,RIN,PIN,QIN,RIN,OPIN,OPIN,OPIN	CRS03010
CJ44J4 OXIJ,OYIJ,OZIJ,ZG	CRS03020
CJ44J4 XX,XXJ,XYK,XYJ,XZK,XZJ,XLK,XLJ,XMK,XMJ,XNK,XNJ	CRS03030
CJ44J4 XOLD,YOLD,ZOLD,PHIOLD,THEOLD,PSIOLD,POLD,QOLD,ROLD,UOLD,	CRS03040
1 VOLD,WOLD,DZ,DTHALF	CRS03050
CJ44J4 PHI,THETA,PSI	CRS03060
CJ44J4 BIJ,PSIDOT,THEDOT,PHIDOT,CIJ,X,Y,Z,XIJ,YIJ,ZIJ,D,DF	CRS03070
CJ44J4 AI,AIDOT,AJ,ATJ,DX,DY,DZ,DPM,DTHETA,DPSI,DVSIGN	CRS03080
CJ44J4 VEE,FMBAR,FM,XKS,XKI,VMAX	CRS00400
CJ44J4 XX,XY,XZ,XL,XM,XN,WGT,ALIFT,XC,P,Q,R,U,V,W	CRS03100
CJ44J4 UDOT,VDOT,WDOT,XZI,YZI,ZI,HEZ,XI,XYI,HEX,YI,HEY,DEL	CRS03110

Figure 20. (Continued)

```

CJ44CN PDDT,XI1,XI2,XI3,QDDT,XI5,XI4,RDDT,XI6,XDOT,YDOT,ZDOT      CRS03120
CJ44CN      XLBAR,SF,FSPDF,XKE,FSPBAR,XMU,VEEDOT      CRS00440
CJ44CN XGDDT,YGDDT,ZGDDT,PPR,QPR,RPR,PHIPR,THEPR,PSIPR      CRS00360
CJ44CN PHIDP,THEDP,PSIDP,XDP,YDP,ZDP,OAI,DELTAT,TMAX,TIME,TITLE      CRS03150
CJ44CN PHIJ,THEIJ,PSIJ,XK,DIJ,XLBAR,SI,XLNGTH,IP      CRS00470
CJ44CN XM,I,J,ILAST,IYABIJ,IYAB6,IJLIJ,IJKLIJ,IJJK,IJL,IJG,JG,IYAR,CRS03170
1 IYABO,IJKL,IYABL,IYPRINT,IYTABLE,ILINES,NPR,IGS,IISP,ISP,IS,N,NCRS00490
CJ44CN KRUPT,IUPT,JRUPT
CJ44CN INDP,IPEN,KPEN
CJ44CN IJPR
CJ44CN PLOT,ZAR,TMPLOT,IPLLOT,IDPLOT,IPLSW,IPLC,JPLLOT,NPLOT,I7PLOT
EQUIVALENCE (XKS(1),XKS3(1,1,1)),(XKI(1),XKI3(1,1,1)),      CRS02540
1 (XCRIN(1,1,1),FMBAR(1)),(FM(1),FM3(1,1,1)),(VEE(1),VEE2(1,1))      CRS02550
EQUIVALENCE (FMBAR(1),FMBAR3(1,1,1)),(NM(1),NM3(1,1,1)),(NM(1,1),      CRS02560
1 YVZ(1,1)),(FSPBAR(1,1),FSPBAR2(1,1)),(IBS(1,1),IBS2(1,1))      CRS02570
EQUIVALENCE (XKS(1,1,1),XK(1))
EQUIVALENCE (S1,SINCOS(1)),(C1,SINCOS(2)),(S2,SINCOS(3))      CRS03220
EQUIVALENCE (C2,SINCOS(4)),(S3,SINCOS(5)),(C3,SINCOS(6))      CRS05230
SIN(X) = DSIN(X)      CRS02580
COS(X) = DCOS(X)      CRS02590
TT = .200
ET = .R00
IF(TIME,ME,0.0) GO TO 60
07 70 IJ = 1,IGS
75 TRUPSW(IJ) = 0
07 72 I=1,NM
72 IPENSW(I)=0
C DO ALL THE (AI)((AJ))
60 07 10 I = 1,NM
ARG = PHI(I)
S1 = SIN(ARG)
C1 = COS(ARG)
ARG = THETA(I)
S2 = SIN(ARG)
C2 = COS(ARG)
ARG = PSI(I)
S3 = SIN(ARG)
C3 = COS(ARG)
07 40 J = 1,6
T = SINCOS(J)
IF(T) 45,40,50
45 T = -T
50 IF(T-1.E-10) 55,40,40
55 SINCOS(J) = 0.0
40 CONTINUE
C
J = 9*(I-1)
C MOVE AI S TO OLD AI S
03 4 JJ = 1,9
4 0AI(I+JJ) = 8IJ(J+JJ)
S1S2 = S1*S2
C1S2 = C1*S2
AI(1) = C2*C3
8IJ(J+1) = AI(1)
AI(2) = C2*S3
8IJ(J+2) = AI(2)
AI(3) = -S2
8IJ(J+3) = AI(3)
AI(4) = -C1*S3+S1S2*C3
8IJ(J+4) = AI(4)

```

Figure 20. (Continued)

```

AI(5) = C1*C3+S1S2*S3
BIJ(J+5) = AI(5)
AI(6) = S1*C2
BIJ(J+6) = AI(6)
AI(7) = S1*S3+C1S2*C3
BIJ(J+7) = AI(7)
AI(8) = -S1*C3+C1S2*S3
BIJ(J+8) = AI(8)
AI(9) = C1*C2
BIJ(J+9) = AI(9)
C (27)
PP = P(I)
QQ = Q(I)
RR = R(I)
UU = U(I)
VV = V(I)
WW = W(I)
XDOTI = XDOT(I)
XDOT(I) = AI(1)*UU*AI(4)*VV+AI(7)*WW
YDOTI = YDOT(I)
YDOT(I) = AI(2)*UU*AI(5)*VV+AI(8)*WW
ZDOTI = ZDOT(I)
ZDOT(I) = AI(3)*UU*AI(6)*VV+AI(9)*WW
C (28), (29)
CS = S1/C2
CC = C1/C2
PHDOTI = PHDOT(I)
PHDOT(I) = PP*QQ*CS+S2*RR*CC*S2
THDOTI = THDOT(I)
THDOT(I) = QQ*CI-RR*S1
PSDOTI = PSDOT(I)
PSDOT(I) = QQ*CS+RR*CC
C DO AIDOT NOW
T = PSDOT(I)*C2
T1 = THDOT(I)*S1-T*CI
T2 = THDOT(I)*CI-T*S1
T3 = PHDOT(I)-PSDOT(I)*S2
CIJ(J+1) = -BIJ(J+4)*T1-BIJ(J+7)*T2
CIJ(J+4) = BIJ(J+1)*T1+BIJ(J+7)*T3
CIJ(J+7) = BIJ(J+1)*T2-BIJ(J+4)*T3
CIJ(J+2) = -BIJ(J+5)*T1-BIJ(J+8)*T2
CIJ(J+5) = BIJ(J+2)*T1+BIJ(J+8)*T3
CIJ(J+8) = BIJ(J+2)*T2-BIJ(J+5)*T3
CIJ(J+3) = -BIJ(J+6)*T1-BIJ(J+9)*T2
CIJ(J+6) = BIJ(J+3)*T1+BIJ(J+9)*T3
CIJ(J+9) = BIJ(J+3)*T2-BIJ(J+6)*T3
IF(7*TIME) 10,1C,5
C CORRECT X,Y,Z,PHI,THEYA,PSI,
5 X(I) = TT*X(I)+ET*(XOLD(I)+DTHALF*(XDOT(I)+XDOT(I)))
Y(I) = TT*Y(I)+ET*(YOLD(I)+DTHALF*(YDOT(I)+YDOT(I)))
Z(I) = TT*Z(I)+ET*(ZOLD(I)+DTHALF*(ZDOT(I)+ZDOT(I)))
PHI(I) = TT*PHI(I)+ET*(PHIOLD(I)+DTHALF*(PHIDOT(I)+PHIDOT(I)))
THEYA(I) = TT*THEYA(I)+ET*(THEYOLD(I)+DTHALF*(THEYDOT(I)+THEYDOT(I)))
PSI(I) = TT*PSI(I)+ET*(PSIOLD(I)+DTHALF*(PSIDOT(I)+PSIDOT(I)))
C CLEAR THE DAMPING TERMS.
DPX(I) = 0.0
DPY(I) = 0.0
DPZ(I) = 0.0
DPL(I) = 0.0
DPHI(I) = 0.0

```

CRS03930  
CRS03940  
CRS03950  
CRS03960  
CRS03970  
CRS03980  
CRS03990  
CRS04000  
CRS04010  
CRS04020  
CRS04030  
CRS04040  
CRS04050  
CRS04060  
CRS04070  
CRS04080  
CRS04090  
CRS04100  
CRS04110  
CRS04120  
CRS04130  
CRS04140  
CRS04150  
CRS04160  
CRS04170  
CRS04180  
CRS04190  
CRS04200  
CRS04210  
CRS04220  
CRS04230  
CRS04240  
CRS04250  
CRS04260  
CRS04270  
CRS04280  
CRS04290  
CRS04300  
CRS04310  
CRS04320  
CRS04330  
CRS04340  
CRS04350  
CRS04360  
CRS04370  
CRS04380  
CRS04390  
CRS04400  
CRS03340  
CRS03350  
CRS03360  
CRS03370  
CRS03380  
CRS03390

Figure 20. (Continued)

```

      DPN(I) = 0.0
10  CONTINUE
C  DO 1000 IS MAIN DO LOOP TO GET TOTAL INTERNAL FORCES AND MOMENTS
      ILAST = 0
      ITAB(I) = -ITAB(I)
      IJLIJ = 0
      IJKLIJ = -36
      DO 1000 IJ = 1, IGS
      IJKLIJ = IJKLIJ + 36
      IJKK = IJKLIJ - 36
      IJLIJ = IJLIJ + 6
      IJL = IJLIJ
      ITAB(IJ) = -ITAB(IJ) + ITAB(I)
      IF (IRIPSW(IJ), NE, 0) GO TO 1000
      I = IG(IJ)
      J = JG(IJ)
C  IF WE GET TO A NEW I WE MUST MOVE (AI) INTO AI AND (AI00) INTO AI00T
      IF (I - ILAST) 20, 30, 20
20  ILAST = I
      IS = 9*(I-1)
      DO 320 KS = 1, 5
      IS = IS + 1
      AI00T(KS) = C(IJ, KS)
      DAI(KS) = DAI(IS) - BIJ(IS)
320  AI(KS) = BIJ(IS)
30  XIJ = X(I) - X(I)
      YIJ = Y(I) - Y(I)
      ZIJ = Z(I) - Z(I)
      XIJO = OXIJ(IJ)
      YIJO = OYIJ(IJ)
      ZIJO = OZIJ(IJ)
      OXIJ(IJ) = XIJ
      OYIJ(IJ) = YIJ
      OZIJ(IJ) = ZIJ
C
      IS = 9*(J-1)
      IJS = 9*(IJ-1)
      DO 310 KS = 1, 5
      IS = IS + 1
      IJS = IJS + 1
      AIJ(KS) = DIJ(IJS)
310  AJ(KS) = BIJ(IJS)
C (4)
      T1 = OXIJ - OX(I)
      T2 = OYIJ - OY(I)
      T3 = OZIJ - OZ(I)
C (5)
      T4 = AI(1)*T1 + AI(2)*T2 + AI(3)*T3 - DAI(1)*OXIJO - DAI(2)*OYIJO - DAI(3)*OZIJO
      T5 = AI(4)*T1 + AI(5)*T2 + AI(6)*T3 - DAI(4)*OXIJO - DAI(5)*OYIJO - DAI(6)*OZIJO
      T6 = AI(7)*T1 + AI(8)*T2 + AI(9)*T3 - DAI(7)*OXIJO - DAI(8)*OYIJO - DAI(9)*OZIJO
      OI(1) = AIJ(1)*T4 + AIJ(2)*T5 + AIJ(3)*T6
      OI(2) = AIJ(4)*T4 + AIJ(5)*T5 + AIJ(6)*T6
      OI(3) = AIJ(7)*T4 + AIJ(8)*T5 + AIJ(9)*T6
C (9)
      AITAJ(1) = AI(1)*AJ(1) + AI(2)*AJ(2) + AI(3)*AJ(3)
      AITAJ(2) = AI(4)*AJ(1) + AI(5)*AJ(2) + AI(6)*AJ(3)
      AITAJ(3) = AI(7)*AJ(1) + AI(8)*AJ(2) + AI(9)*AJ(3)
      AITAJ(4) = AI(1)*AJ(4) + AI(2)*AJ(5) + AI(3)*AJ(6)
      AITAJ(5) = AI(4)*AJ(4) + AI(5)*AJ(5) + AI(6)*AJ(6)
      AITAJ(6) = AI(7)*AJ(4) + AI(8)*AJ(5) + AI(9)*AJ(6)

```

CRS04520  
 CRS04530  
 CRS04540  
 CRS04550  
 CRS04560  
 CRS04570  
 CRS04580  
 CRS04590  
 CRS04600  
 CRS04610  
 CRS04620  
 CRS04630  
 CRS04640  
 CRS04660  
 CRS04670  
 CRS04680  
 CRS04690  
 CRS04700  
 CRS04710  
 CRS04720  
 CRS04730  
 CRS04740  
 CRS04750  
 CRS04800  
 CRS04810  
 CRS04820  
 CRS04830  
 CRS04840  
 CRS04850  
 CRS04860  
 CRS04870  
 CRS04880  
 CRS04890  
 CRS04900  
 CRS04910  
 CRS04920  
 CRS04930  
 CRS04940  
 CRS04950  
 CRS04960  
 CRS04970  
 CRS04980  
 CRS04990  
 CRS05000  
 CRS05010  
 CRS05020  
 CRS05030  
 CRS05040  
 CRS05050  
 CRS05060  
 CRS05070  
 CRS05150  
 CRS05160  
 CRS05170  
 CRS05180  
 CRS05190  
 CRS05200  
 CRS05210

Figure 20. (Continued)

AITAJ(7) = AI(1)*AJ(7)+AI(2)*AJ(8)+AI(3)*AJ(9)	CRS05220
AITAJ(8) = AI(4)*AJ(7)+AI(5)*AJ(8)+AI(6)*AJ(9)	CRS05230
AITAJ(9) = AI(7)*AJ(7)+AI(8)*AJ(8)+AI(9)*AJ(9)	CRS05240
T1 = DPIN(J)	CRS05250
T2 = DQIN(J)	CRS05260
T3 = DRIN(J)	CRS05270
T4 = T1*AITAJ(1)+T2*AITAJ(4)+T3*AITAJ(7)-DPIN(I)	CRS05280
T5 = T1*AITAJ(2)+T2*AITAJ(5)+T3*AITAJ(8)-DQIN(I)	CRS05290
T6 = T1*AITAJ(3)+T2*AITAJ(6)+T3*AITAJ(9)-DRIN(I)	CRS05300
C (9R)	CRS05310
D(4) = AIJ(1)*T4+AIJ(2)*T5+AIJ(3)*T6	CRS05320
D(5) = AIJ(4)*T4+AIJ(5)*T5+AIJ(6)*T6	CRS05330
D(6) = AIJ(7)*T4+AIJ(8)*T5+AIJ(9)*T6	CRS05340
T1 = U(J)	CRS05390
T2 = V(J)	CRS05400
T3 = W(J)	CRS05410
T4 = T1*AITAJ(1)+T2*AITAJ(4)+T3*AITAJ(7)-U(I)	CRS05420
T5 = T1*AITAJ(2)+T2*AITAJ(5)+T3*AITAJ(8)-V(I)	CRS05430
T6 = T1*AITAJ(3)+T2*AITAJ(6)+T3*AITAJ(9)-W(I)	CRS05440
DD(1) = T4*AIJ(1)+T5*AIJ(2)+T6*AIJ(3)	CRS05450
DD(2) = T4*AIJ(4)+T5*AIJ(5)+T6*AIJ(6)	CRS05460
DD(3) = T4*AIJ(7)+T5*AIJ(8)+T6*AIJ(9)	CRS05470
T1 = P(J)	CRS05480
T2 = Q(J)	CRS05490
T3 = R(J)	CRS05500
T4 = T1*AITAJ(1)+T2*AITAJ(4)+T3*AITAJ(7)-P(I)	CRS05510
T5 = T1*AITAJ(2)+T2*AITAJ(5)+T3*AITAJ(8)-Q(I)	CRS05520
T6 = T1*AITAJ(3)+T2*AITAJ(6)+T3*AITAJ(9)-R(I)	CRS05530
DD(4) = T4*AIJ(1)+T5*AIJ(2)+T6*AIJ(3)	CRS05540
DD(5) = T4*AIJ(4)+T5*AIJ(5)+T6*AIJ(6)	CRS05550
DD(6) = T4*AIJ(7)+T5*AIJ(8)+T6*AIJ(9)	CRS05560
DJ 270 K = 1,6	CRS05570
270 DD(K) = C(K,J)*DD(K)	
C FORM VECTOR OF (+,-1.0 TO USE IN ABS(VPIJL)	CRS05590
DJ 360 K = 1,6	CRS05600
IF(D(K)) 370,380,380	CRS05610
370 DVSIGN(K) = -1.0	CRS05620
GJ TJ 360	CRS05630
380 DVSIGN(K) = 1.0	CRS05640
360 CONTINUE	CRS05650
DJ 150 K = 1,6	CRS05660
ITAB = ITABJ-ITABD	CRS05670
IJKK = IJKK+6	CRS05680
IJKL = IJKK	CRS05690
IJL = IJL-6	CRS05700
DF(K) = 0.0	CRS05710
DJ 150 L = 1,6	CRS05740
ITAB = ITAB+ITABD	CRS05750
IJKL = IJKL+1	CRS05760
IJL = IJL+1	CRS05770
T = XK(IJKL)	CRS05810
IF(T) 160,150,160	CRS05820
C THIS GFTS ABS(VP(IJL))	CRS05830
160 V2 = DVSIGN(L)*(VEE(IJL)-FMBAR(IJKL))	CRS05840
IF(V2) 170,210,210	CRS05890
C SIGNS NOT SAME	CRS05900
170 I=(V(IJL)) 180,180,190	CRS05910
150 H(IJL) = 1	CRS05920
F404(IJKL) = VEE(IJL)-FM(IJKL)/T	CRS05930
190 DELFM = T*OIL	CRS05980

Figure 20. (Continued)

GO TO 220	CRS05990
C SIGNS THE SAME	CRS06000
210 M(IJL) = 0	CRS06010
II = (VP*DXDA(L,IJ))/DXDA(L,IJ)	CRS06020
C CLAMP II BETWEEN 1 AND ITABL-1	CRS06030
IF(II-1) 211,215,213	CRS06040
211 II = 1	CRS06050
GO TO 215	CRS06060
213 IF(II-ITABL) 215,215,214	CRS06070
214 II = ITABL	CRS06080
215 II = II+ITAB	CRS06090
DELFM = (XKS(II)*VP+XKE(II))*7*O(L)	CRS06100
220 F(IJ,KI) = FM(IJ,KI)+DELFM	CRS06150
DF(K) = DF(K)+DELFM	CRS06160
150 CONTINUE	CRS06200
DO 630 K = 1,6	
630 SUMDF(X,YJ) = SUMDF(K,IJ)+DF(K)	
IJL = IJL-6	CRS06210
DO 230 L = 1,6	CRS06220
IJL = IJL+1	CRS06230
T = VEE(IJL)*O(L)	CRS06240
VEE(IJL) = T	CRS06250
C MOVE DF TO D FOR (13) ETC.	CRS06260
D(L) = DF(L)	CRS06270
IF(T) 240,250,250	CRS06280
240 T = -T	CRS06290
250 IF(T-VMAX(IJL)) 230,260,260	CRS06300
260 (RUP*SW(IJ)) = 1	
XX(I) = XX(I)-XX(IJ)	CRS06320
XY(I) = XY(I)-XY(IJ)	CRS06330
XZ(I) = XZ(I)-XZ(IJ)	CRS06340
XL(I) = XL(I)-XL(IJ)	CRS06350
XM(I) = XM(I)-XM(IJ)	CRS06360
XV(I) = XV(I)-XV(IJ)	CRS06370
XX(J) = XX(J)-XX(IJ)	CRS06380
XY(J) = XY(J)-XY(IJ)	CRS06390
XZ(J) = XZ(J)-XZ(IJ)	CRS06400
XL(J) = XL(J)-XL(IJ)	CRS06410
XM(J) = XM(J)-XM(IJ)	CRS06420
XV(J) = XV(J)-XV(IJ)	CRS06430
KRUPT = KRUPT+1	
IRUPT(KRUPT) = I	
JRUPT(KRUPT) = J	
TRUPT(KRUPT) = TIME	
PRINT 1040, IJL,VEE(IJL),VMAX(IJL)	
1040 FORMAT(1H'L'RUPTURE '215,192E15.6)	
GO TO 1000	
230 CONTINUE	CRS06590
IF (IJPR(IJ),NE,0) DM(IJ)=-6.5500*VEE(IJL-5)	CRS06600
AIATJT(1) = AI(1)*AIJ(1)+AI(4)*AIJ(2)+AI(7)*AIJ(3)	CRS06640
AIATJT(4) = AI(1)*AIJ(4)+AI(4)*AIJ(5)+AI(7)*AIJ(6)	CRS06650
AIATJT(7) = AI(1)*AIJ(7)+AI(4)*AIJ(8)+AI(7)*AIJ(9)	CRS06660
AIATJT(2) = AI(2)*AIJ(1)+AI(5)*AIJ(2)+AI(8)*AIJ(3)	CRS06670
AIATJT(5) = AI(2)*AIJ(4)+AI(5)*AIJ(5)+AI(8)*AIJ(6)	CRS06680
AIATJT(8) = AI(2)*AIJ(7)+AI(5)*AIJ(8)+AI(8)*AIJ(9)	CRS06690
AIATJT(3) = AI(3)*AIJ(1)+AI(6)*AIJ(2)+AI(9)*AIJ(3)	CRS06700
AIATJT(6) = AI(3)*AIJ(4)+AI(6)*AIJ(5)+AI(9)*AIJ(6)	CRS06710
AIATJT(9) = AI(3)*AIJ(7)+AI(6)*AIJ(8)+AI(9)*AIJ(9)	CRS06720
C (13A)	CRS06730
TI = AIATJT(1)*O(1)+AIATJT(4)*O(2)+AIATJT(7)*O(3)	CRS06740

Figure 20. (Continued)

```

T2 = AIAIJT(2)*D(1)+AIAIJT(5)*D(2)+AIAIJT(8)*D(3)
Y3 = AIAIJT(2)*D(1)+AIAIJT(6)*D(2)+AIAIJT(9)*D(3)
-----
D(1) = T1
D(2) = T2
D(3) = T3
C (126)
T1 = AIAIJT(1)*D(4)+AIAIJT(4)*D(5)+AIAIJT(7)*D(6)
T2 = AIAIJT(2)*D(4)+AIAIJT(5)*D(5)+AIAIJT(8)*D(6)
T3 = AIAIJT(3)*D(4)+AIAIJT(6)*D(5)+AIAIJT(9)*D(6)
D(4) = T1
D(5) = T2
D(6) = T3
C (17A)
DXX = -(AJ(1)*D(1)+AJ(2)*D(2)+AJ(3)*D(3))
DXY = -(AJ(4)*D(1)+AJ(5)*D(2)+AJ(6)*D(3))
DXZ = -(AJ(7)*D(1)+AJ(8)*D(2)+AJ(9)*D(3))
XX(IJ) = XX(IJ)+DXX
XY(IJ) = XY(IJ)+DXY
XZ(IJ) = XZ(IJ)+DXZ
XXJ(IJ) = XXJ(IJ)+DXX
XYJ(IJ) = XYJ(IJ)+DXY
XZJ(IJ) = XZJ(IJ)+DXZ
C (17B)
DXL = -(AJ(1)*D(4)+AJ(2)*D(5)+AJ(3)*D(6))
DXY = -(AJ(4)*D(4)+AJ(5)*D(5)+AJ(6)*D(6))
DXN = -(AJ(7)*D(4)+AJ(8)*D(5)+AJ(9)*D(6))
XL(IJ) = XL(IJ)+DXL
XN(IJ) = XN(IJ)+DXN
XV(IJ) = XV(IJ)+DXN
XLJ(IJ) = XLJ(IJ)+DXL
XNJ(IJ) = XNJ(IJ)+DXN
XVJ(IJ) = XVJ(IJ)+DXN
IF (IJP(IJ).EQ.1) GO TO 700
C (149)
D(4) = D(4)-Z(IJ)*D(2)+Y(IJ)*D(3)
D(5) = D(5)+Z(IJ)*D(1)-X(IJ)*D(3)
D(6) = D(6)-Y(IJ)*D(1)+X(IJ)*D(2)
C (16A)
DXX = A(1)*D(1)+A(2)*D(2)+A(3)*D(3)
DXY = A(4)*D(1)+A(5)*D(2)+A(6)*D(3)
DXZ = A(7)*D(1)+A(8)*D(2)+A(9)*D(3)
XX(IJ) = XX(IJ)+DXX
XY(IJ) = XY(IJ)+DXY
XZ(IJ) = XZ(IJ)+DXZ
XXK(IJ) = XXK(IJ)+DXX
XYK(IJ) = XYK(IJ)+DXY
XZK(IJ) = XZK(IJ)+DXZ
C (16B)
DXL = A(1)*D(4)+A(2)*D(5)+A(3)*D(6)
DXM = A(4)*D(4)+A(5)*D(5)+A(6)*D(6)
DXN = A(7)*D(4)+A(8)*D(5)+A(9)*D(6)
XL(IJ) = XL(IJ)+DXL
XM(IJ) = XM(IJ)+DXM
XN(IJ) = XN(IJ)+DXN
XLJ(IJ) = XLJ(IJ)+DXL
XMK(IJ) = XMK(IJ)+DXM
XNK(IJ) = XNK(IJ)+DXN
C (16A)
700 CONTINUE
T1 = AIAIJT(1)*D(1)+AIAIJT(4)*D(2)+AIAIJT(7)*D(3)

```

```

CRS06750
CRS06760
CRS06770
CRS06780
CRS06790
CRS06800
CRS06810
CRS06820
CRS06830
CRS06840
CRS06850
CRS06860
CRS06870
CRS06880
CRS06890
CRS06900
CRS06910
CRS06920
CRS06930
CRS06940
CRS06950
CRS06960
CRS06970
CRS06980
CRS06990
CRS07000
CRS07010
CRS07020
CRS07030
CRS07040
CRS07050
CRS07060
CRS07140
CRS07150
CRS07160
CRS07170
CRS07180
CRS07190
CRS07200
CRS07210
CRS07220
CRS07230
CRS07240
CRS07250
CRS07260
CRS07270
CRS07280
CRS07290
CRS07300
CRS07310
CRS07320
CRS07330
CRS07340
CRS07350
CRS07360
CRS07370
CRS07440
CRS07450

```

Figure 20. (Continued)



```

T2 = A1A1JT(2)*DD(1)+A1A1JT(5)*DD(2)+A1A1JT(8)*DD(3)
T3 = A1A1JT(3)*DD(1)+A1A1JT(6)*DD(2)+A1A1JT(9)*DD(3)
DD(1) = T1
DD(2) = T2
DD(3) = T3
C (68)
T1 = A1A1JT(1)*DD(4)+A1A1JT(4)*DD(5)+A1A1JT(7)*DD(6)
T2 = A1A1JT(2)*DD(4)+A1A1JT(5)*DD(5)+A1A1JT(8)*DD(6)
T3 = A1A1JT(3)*DD(4)+A1A1JT(6)*DD(5)+A1A1JT(9)*DD(6)
DD(4) = T1
DD(5) = T2
DD(6) = T3
C (94)
DXX = -(AJ(1)*DD(1)+AJ(2)*DD(2)+AJ(3)*DD(3))
DXY = -(AJ(4)*DD(1)+AJ(5)*DD(2)+AJ(6)*DD(3))
DXZ = -(AJ(7)*DD(1)+AJ(8)*DD(2)+AJ(9)*DD(3))
DPX(I) = DPX(I)+DXX
DPY(I) = DPY(I)+DXY
DPZ(I) = DPZ(I)+DXZ
C (98)
DXL = -(AJ(1)*DD(4)+AJ(2)*DD(5)+AJ(3)*DD(6))
DXM = -(AJ(4)*DD(4)+AJ(5)*DD(5)+AJ(6)*DD(6))
DXN = -(AJ(7)*DD(4)+AJ(8)*DD(5)+AJ(9)*DD(6))
DPL(I) = DPL(I)+DXL
DPM(I) = DPM(I)+DXM
DPN(I) = DPN(I)+DXN
IF (IJPR(IJ),EQ,1) GO TO 1000
C (7)
DU(4) = DU(4)-ZIJ*DD(2)+YIJ*DD(3)
DU(5) = DU(5)+ZIJ*DD(1)-XIJ*DD(3)
DU(6) = DU(6)-YIJ*DD(1)+XIJ*DD(2)
C (8A)
DXX = A1(1)*DD(1)+A1(2)*DD(2)+A1(3)*DD(3)
DXY = A1(4)*DD(1)+A1(5)*DD(2)+A1(6)*DD(3)
DXZ = A1(7)*DD(1)+A1(8)*DD(2)+A1(9)*DD(3)
DPX(I) = DPX(I)+DXX
DPY(I) = DPY(I)+DXY
DPZ(I) = DPZ(I)+DXZ
C (8B)
DXL = A1(1)*DD(4)+A1(2)*DD(5)+A1(3)*DD(6)
DXM = A1(4)*DD(4)+A1(5)*DD(5)+A1(6)*DD(6)
DXN = A1(7)*DD(4)+A1(8)*DD(5)+A1(9)*DD(6)
DPL(I) = DPL(I)+DXL
DPM(I) = DPM(I)+DXM
DPN(I) = DPN(I)+DXN
C000 CONTINUE
IS=9*(IND*-1)
DO 1010 KS=1,5
IS=IS+1
1010 AP(KS)=R(J(IS)
C FINISH COMPUTING DERIVATIVES
DO 2000 I = 1,AM
IS = 0*(I-1)
DO 330 XS = 1,5
IS = IS+1
A1D(J(KS) = C1J(IS)
330 A1(KS) = B1J(IS)
C DO CRASH FORCES
CALL CFORCE
C (20),(23),(24)

```

```

CRS07460
CRS07470
CRS07480
CRS07490
CRS07500
CRS07510
CRS07520
CRS07530
CRS07540
CRS07550
CRS07560
CRS07570
CRS07580
CRS07590
CRS07600
CRS07610
CRS07620
CRS07630
CRS07640
CRS07680
CRS07690
CRS07700
CRS07710
CRS07720
CRS07730
CRS07740
CRS07780
CRS07790
CRS07800
CRS07810
CRS07820
CRS07830
CRS07840
CRS07850
CRS07860
CRS07870
CRS07880
CRS07920
CRS07930
CRS07940
CRS07950
CRS07960
CRS07970
CRS07980
CRS08020
CRS08030
CRS08040
CRS08050
CRS08060
CRS08070
CRS08080
CRS08090
CRS08100
CRS08110
CRS08120

```

Figure 20. (Continued)

```

XA = MG7(1)-AL1F7(1)
SX = XX(1)+XA*A1(3)+XC(1)+JPX(1)
SY = XY(1)+XA*A1(6)+XC(2)+JPY(1)
SZ = XZ(1)+XA*A1(9)+XC(3)+JPZ(1)
SL = XL(1)+XC(4)+OP1(1)
SM = XM(1)+XC(5)+OPM(1)
SN = XN(1)+XC(6)+OPN(1)
C GET P,Q,R,U,V,W
PP = P(1)
QQ = Q(1)
RR = R(1)
UU = U(1)
VV = V(1)
WW = W(1)
C MASS
MGT1 = 1.0/MGT(1)
ZM = 386.0*MGT1
XACC(1) = SX*MGT1
YACC(1) = SY*MGT1
ZACC(1) = SZ*MGT1
C (25)
UOJT(1) = UOJT(1)
UOJT(1) = SX*ZM-QQ*WW+RR*VV
VOJT(1) = VOJT(1)
VOJT(1) = SY*ZM-RR*UU+PP*WW
WOJT(1) = WOJT(1)
WOJT(1) = SZ*ZM-PP*VV+QQ*UU
C (26)
T1 = -XZ(1)*PP-YZ(1)*QQ+Z(1)*RR+HEZ(1)
T2 = X(1)*PP-XY(1)*QQ-XZ(1)*RR+HEX(1)
T3 = -XY(1)*PP+Y(1)*QQ-YZ(1)*RR+HEY(1)
SL = SL-QQ*T1+RR*T3
SM = SM-RR*T2+PP*T1
SN = SN-PP*T3+QQ*T2
C (25)
DEL = DEL(1)
POJT(1) = POJT(1)
POJT(1) = DEL*(SL*X1(1)+SM*X12(1)+SN*X13(1))
QOJT(1) = QOJT(1)
QOJT(1) = DEL*(SL*X12(1)+SM*X15(1)+SN*X14(1))
ROJT(1) = ROJT(1)
ROJT(1) = DEL*(SL*X13(1)+SM*X14(1)+SN*X15(1))
IF(TIME) 2000,2000,300
300 U(1) = TT*U(1)+ET*(UCL(1)+DTHALF*(UOJT(1)+UDOT(1))
V(1) = TT*V(1)+ET*(VCL(1)+DTHALF*(VOJT(1)+VDOT(1))
W(1) = TT*W(1)+ET*(WCL(1)+DTHALF*(WOJT(1)+WDOT(1))
P(1) = TT*P(1)+ET*(POL(1)+DTHALF*(POJT(1)+PDOT(1))
Q(1) = TT*Q(1)+ET*(QCL(1)+DTHALF*(QOJT(1)+QDOT(1))
R(1) = TT*R(1)+ET*(ROLD(1)+DTHALF*(ROJT(1)+RODOT(1))
PIN(1) = TT*PIN(1)+ET*(PING(1)+DTHALF*(P(1)+POLG(1)))
DIN(1) = TT*DIN(1)+ET*(DIND(1)+DTHALF*(G(1)+GOLD(1)))
RIN(1) = TT*RIN(1)+ET*(RIND(1)+DTHALF*(R(1)+ROLD(1)))
IF (1/PEHSM(1),NE.G1,OR,11,FQ,INDP,OR,11NDP,EG,31) GO TO 2000
C
C
C
CONTROL VOLUME PENETRATION CALCULATIONS
TP1=X(1)-X(INDP)
TP2=Y(1)-Y(INDP)
TP3=Z(1)-Z(INDP)
XP1=AP(1)*TP1+AP(2)*TP2+AP(3)*TP3

```

Figure 20. (Continued)

```

YPI=AP(4)*TP1+AP(5)*TP2+AP(6)*TP3
ZPI=AP(7)*TP1+AP(8)*TP2+AP(9)*TP3
IF ((-YNBAR.GT.XPI).OR.(XPI.GT.XPBAR)) GO TO 2300
IF ((-YNBAR.GT.YPI).OR.(YPI.GT.YPBAR)) GO TO 2300
IF ((-ZNBAR.GT.ZPI).OR.(ZPI.GT.ZPBAR)) GO TO 2300
KPEV=KPEN+1
IPEV(KPEN)=I
TPEV(KPEN)=TIME
IPEVSW(I)=1
PRINT 1080, I, TIME
1080 FORMAT(1H0, ' CONTROL VOLUME PENETRATED BY MASS ', I2, '°, TIME=',
1 F10.5)
2000 CONTINUE
RETURN
END

SUBROUTINE DOAIJ
IMPLICIT REAL*8 (A-H,O-Z)
REAL*4 PLOT(3000), ZAR, TMPLT(500)
DIMENSION SF(40,3), ZAR(200), IPLOT(150), IDPLOT(150)
DIMENSION IG(80), JG(80), PHI(150), THEI(150), PSI(150), WGT(40),
1 XI(40), YI(40), ZI(40), XYI(40), YZI(40), XZI(40), HEX(40), HEY(40),
2 HEZ(40), ALIFT(40), X(40), Y(40), Z(40), PHI(40), THETA(40), PSI(40),
3 UI(40), VI(40), WI(40), PI(40), QI(40), RI(40), XDOT(40), YDOT(40), ZDOT(40),
4 PHIDOT(40), THEDOT(40), PSIDOT(40), UDOT(40), VDOT(40), WDOT(40)
DIMENSION AIJ(5), AJ(9), AJI(9), AIDOT(9), DX(40), DY(40), DZ(40),
1 DPHI(40), DTHETA(40), DPSI(40), D(6), DF(6), XX(40), XY(40), XZ(40),
2 XL(40), XM(40), XN(40), DELI(40), XI1(40), XI2(40), XI3(40),
3 XI4(40), XI5(40), XI6(40), XK(2880), FMBAR(2880), FMBAR3(6,6,80),
4 FM(2880), XKRI(10,6,80), VEE(480), VMAX(480), NN(40,3), NN2(40,3)
DIMENSION XKI3(9,6,80), BIJ(360), CIJ(360), DIJ(72), XLBAR(40,3),
1 XXLBAR(3), ISP(40,3), IISP(3), XMU(40,3), XKE(40,3), CAI(360),
2 IBS(40,3), IBS2(40,3), SI(40,3), SF(40,3), FSPDF(40,3), PHIDP(40),
3 THEDP(40), PSIDP(40), FSPBAR(40,3), FSPBA2(40,3), XLNGTH(3), XC(6),
4 XDP(40), YDP(40), ZDP(40), FM3(6,6,80), VEE2(6,80), VEEDOT(3,3)
DIMENSION PDOT(40), QDOT(40), RDOT(40), N(480), N3(30,6), DVSIGN(6),
1 XS(4320), KS(9,6,80), XKI(4320), TITLE(10)
DIMENSION XOLD(40), YOLD(40), ZOLD(40), PHIOLD(40), THEOLD(40),
1 PSIOLD(40), PCOLD(40), QOLD(40), ROLD(40), UOLD(40), VOLD(40), WOLD(40)
DIMENSION XXK(80), XXJ(80), XKY(80), XYJ(80), XZK(80), XZJ(80),
1 XLK(80), XLJ(80), XMK(80), XMJ(80), XNK(80), XNJ(80)
DIMENSION OXIJ(80), OYIJ(80), OZIJ(80)
DIMENSION PIN(40), QIN(40), RIN(40), PINO(40), QINO(40), RINO(40),
1 OPIN(40), OQIN(40), ORIN(40)
DIMENSION SINCCS(6)
DIMENSION DDI(6), DPX(40), DPY(40), DPZ(40), DPL(40), DPM(40), DPN(40)
DIMENSION XIJ(3), PRUD(9), XTHOLD(9,2), XYZIJ(9), XYZIJJ(9)
DIMENSION C(6,80), CBAR(80), DXDA(6,80)
DIMENSION XK3(6,6,80)
DIMENSION XACC(40), YACC(40), ZACC(40)
DIMENSION SUMDF(6,80), TRUPT(80), ITRUPT(80), JPUPT(80)
DIMENSION TPEN(80), IPEV(80)
DIMENSION IIPR(76)
DIMENSION AITAJ(9)
DIMENSION FSPDI(40,3), SA(40,3), SB(40,3)
DIMENSION DRI(76)
COMMON DRI
COMMON FSPDI, SA, SB
COMMON AITAJ
COMMON XNBAR, XPBAR, YNBAR, YPBAR, ZNBAR, ZPBAR, TPEN
COMMON SUMDF, TRUPT, DXDA, SC
COMMON XACC, YACC, ZACC
COMMON C, CBAR
COMMON DD, DPX, DPY, DPZ, DPL, DPM, DPN
COMMON PIN, QIN, RIN, PINO, QINO, RINO, OPIN, OQIN, ORIN
COMMON OXIJ, OYIJ, OZIJ, ZG
COMMON XXK, XXJ, XKY, XYJ, XZK, XZJ, XLK, XLJ, XMK, XMJ, XNK, XNJ
COMMON XOLD, YOLD, ZOLD, PHIOLD, THEOLD, PSIOLD, POLD, QOLD, ROLD, UOLD,
1 VOLD, WOLD, DTZ, DTHALF
COMMON PHI, THETA, PSI
COMMON BIJ, PSIDOT, THEDOT, PHIDOT, CIJ, X, Y, Z, XIJ, YIJ, ZIJ, D, DF
COMMON AI, AIDOT, AJ, AIJ, DX, DY, DZ, DPHI, DTHETA, DPSI, DVSIGN
COMMON VEE, FMBAR, FM, XK3, XKI, VMAX
COMMON XX, XY, XZ, XL, XM, XN, W3T, ALIFT, XC, P, Q, R, U, V, W
COMMON UDOT, VDOT, WDOT, XZI, YZI, ZI, HF7, XI, XYI, HEX, YI, HEY, DELI
COMMON PDOT, XI1, XI2, XI3, QDOT, XI5, XI4, RDOT, XI6, XDOT, YDOT, ZDOT

```

Figure 20. (Continued)

```

CJ44CN XLBAR,SF,FSPDF,XKE,FSPBAR,XMU,VEEDOT CRS00440
CJ44CN XGDOT,YGDOT,ZGDOT,PPR,QPR,RPR,PHIPR,THEPR,PSIPR CRS00360
CJ44CN PHIDP,THEDP,PSIDP,XDP,YDP,ZDP,OAI,DELTAT,THAX,TIME,TITLE CRS09220
CJ44CN PHITJ,THEIJ,PSITJ,XK,DIJ,XLBAR,SI,XLENGTH,IP CRS00470
CJ44CN NM,I,J,ILAST,ITABIJ,ITAB6,IJLIJ,IJLIJ,IJJK,IJL,IG,JG,ITAB,CRS09240
1 ITAB0,IJCL,ITABL1,IPRINT,ITABLE,ILINES,NPR,IGS,IISP,ISP,IBS,N,NNCRS00490
CJ44CN KRUP,T,IRUP,T,JRUP,T
CJ44CN INDP,IPEN,KPFH
CJ44CN IJPR
CJ44CN PLOT,ZAP,TMPLOT,IPLOT,IPLOT,IPLSW,IPLC,JPLOT,NPLOT,ITPLOT
EQUIVALENCE (XKS(1),XKS3(1,1,1)),(XKI(1),XKI3(1,1,1)), CRS07030
1 (XKRIN(1,1,1),FMBAR(1)),(FM(1),FM3(1,1,1)),(VEE(1),VEE2(1,1)) CRS07040
EQUIVALENCE (XTHOLD(1,1),XYZIJI(1)),(XTHOLD(1,2),XYZIJJ(1))
EQUIVALENCE (FMBAR(1),FMBAR3(1,1,1)),(N(1),N3(1,1)),(NN(1,1), CRS07050
1 NY2(1,1)),(FSPBAR(1,1),FSPBAZ(1,2)),(IBS(1,1),IBS2(1,1)) CRS07060
EQUIVALENCE (S1,SINCOS(1)),(C1,SINCOS(2)),(S2,SINCOS(3)) CRS09300
EQUIVALENCE (C2,SINCOS(4)),(S3,SINCOS(5)),(C3,SINCOS(6)) CRS09310
EQUIVALENCE (XKI(1),XKI3(1,1,1)) CRS0926
SIN(X) = DSIN(X) CRS07070
COS(X) = DCOS(X) CRS07080
SQRT(X) = DSQRT(X)
ICLD=0
DO 100 I=1,NM
ARG=PHI(I)
S1=SIN(ARG)
C1=COS(ARG)
ARG=THETA(I)
S2=SIN(ARG)
C2=COS(ARG)
ARG=PSI(I)
S3=SIN(ARG)
C3=COS(ARG)
DO 85 J=1,6
T=SINCOS(J)
IF (T) 70,85,75
70 T=-T
75 IF (T-1.E-10) 80,85,85
80 SINCOS(J)=0.
85 CONTINUE
J=9*(I-1)
C MOVE A1'S TO OLD A1'S
DO 90 JJ=1,9
90 OAI(J+JJ)=OIJ(J+JJ)
S1S2=S1*S2
C1S2=C1*S2
BIJ(J+1)=C2*C3
BIJ(J+2)=C2*S3
BIJ(J+3)=-S2
BIJ(J+4)=-C1*S2+S1S2*C3
BIJ(J+5)=C1*C3+S1S2*S3
BIJ(J+6)=S1*C2
BIJ(J+7)=S1*S3+C1S2*C3
BIJ(J+8)=-S1*C2+C1S2*S3
BIJ(J+9)=C1*C2
100 CONTINUE
C
DO 10 IJ = 1,IGS
S1 = SIN(PHITIJ(IJ)) CRS09320
C1 = COS(PHITIJ(IJ)) CRS09330
S2 = SIN(THETIJ(IJ)) CRS09340
CRS09350

```

Figure 20. (Continued)

```

C2 = COS(THETIJ(IJ))
S3 = SIN(PSIIJ(IJ))
C3 = COS(PSIIJ(IJ))
D7 40 J = 1,6
T = SINCS(J)
IF(T) 45,40,50
45 T = -T
50 IF(T-1.E-10) 55,40,40
55 SINCS(J) = 0.C
40 CONTINUE
AIJ(1) = C2*C3
AIJ(2) = C2*S3
AIJ(3) = -S2
AIJ(4) = -C1*S2+S1*S2*C3
AIJ(5) = C1*C3+S1*S2*S3
AIJ(6) = S1*C2
AIJ(7) = S1*S3+C1*S2*C3
AIJ(8) = -S1*C2+C1*S2*S3
AIJ(9) = C1*C2
I = 9*(IJ-1)
D7 15 J = 1,9
15 BIJ(I+J) = AIJ(I)
CBIJ = CBAR(IJ)
I = IG(IJ)
J = JG(IJ)
IF ((IOLD.NE.C).AND.(I.EQ.IOLD)) GO TO 120
IS=9*(I-1)
D7 110 JJ=1,9
IS=IS+1
110 AI(JJ)=BIJ(IS)
120 IOLD=I
IS=9*(J-1)
D7 125 JJ=1,9
IS=IS+1
125 AJ(JJ)=BIJ(IS)
AITAJ(1)=AI(1)*AJ(1)+AI(2)*AJ(2)+AI(3)*AJ(3)
AITAJ(2)=AI(4)*AJ(1)+AI(5)*AJ(2)+AI(6)*AJ(3)
AITAJ(3)=AI(7)*AJ(1)+AI(8)*AJ(2)+AI(9)*AJ(3)
AITAJ(4)=AI(1)*AJ(4)+AI(2)*AJ(5)+AI(3)*AJ(6)
AITAJ(5)=AI(4)*AJ(4)+AI(5)*AJ(5)+AI(6)*AJ(6)
AITAJ(6)=AI(7)*AJ(4)+AI(8)*AJ(5)+AI(9)*AJ(6)
AITAJ(7)=AI(1)*AJ(7)+AI(2)*AJ(8)+AI(3)*AJ(9)
AITAJ(8)=AI(4)*AJ(7)+AI(5)*AJ(8)+AI(6)*AJ(9)
AITAJ(9)=AI(7)*AJ(7)+AI(8)*AJ(8)+AI(9)*AJ(9)

C
C COMPUTE DAMPING COEFFICIENT MATRIX C
KCS=I
D7 312 KS=1,2
IF (KS.EQ.2) KKS=J
XTHJLD(1,KS)=XI(KKS)
XTHJLD(2,KS)=XYI(KKS)
XTHJLD(3,KS)=XZI(KKS)
XTHJLD(4,KS)=XII(KKS)
XTHJLD(5,KS)=YI(KKS)
XTHJLD(6,KS)=YZI(KKS)
XTHJLD(7,KS)=XZI(KKS)
XTHJLD(8,KS)=YZI(KKS)
312 XTHJLD(9,KS)=ZII(KKS)

C
PRDD(1)=AITAJ(1)*XYZIJJ(1)+AITAJ(4)*XYZIJJ(2)+AITAJ(7)*XYZIJJ(3)

```

CRS09360  
CRS09370  
CRS09380  
CRS09390  
CRS09400  
CRS09410  
CRS09420  
CRS09430  
CRS09440  
CRS09450  
CRS09460  
CRS09470  
CRS09480  
CRS09490  
CRS09500  
CRS09510  
CRS09520  
CRS09530  
CRS09540  
CRS09550  
CRS09560  
CRS09570  
CRS09580  
CRS09590  
CRS09600

Figure 20. (Continued)

```

PROD(2)=AITAJ(2)*XYZIJJ(1)+AITAJ(5)*XYZIJJ(2)+AITAJ(8)*XYZIJJ(3)
PROD(3)=AITAJ(3)*XYZIJJ(1)+AITAJ(6)*XYZIJJ(2)+AITAJ(9)*XYZIJJ(3)
PROD(4)=AITAJ(1)*XYZIJJ(4)+AITAJ(4)*XYZIJJ(5)+AITAJ(7)*XYZIJJ(6)
PROD(5)=AITAJ(2)*XYZIJJ(4)+AITAJ(5)*XYZIJJ(5)+AITAJ(8)*XYZIJJ(6)
PROD(6)=AITAJ(3)*XYZIJJ(4)+AITAJ(6)*XYZIJJ(5)+AITAJ(9)*XYZIJJ(6)
PROD(7)=AITAJ(1)*XYZIJJ(7)+AITAJ(4)*XYZIJJ(8)+AITAJ(7)*XYZIJJ(9)
PROD(8)=AITAJ(2)*XYZIJJ(7)+AITAJ(5)*XYZIJJ(8)+AITAJ(8)*XYZIJJ(9)
PROD(9)=AITAJ(3)*XYZIJJ(7)+AITAJ(6)*XYZIJJ(8)+AITAJ(9)*XYZIJJ(9)

```

C

```

XYZIJJ(1)=PROD(1)*AITAJ(1)+PROD(4)*AITAJ(4)+PROD(7)*AITAJ(7)
XYZIJJ(2)=PROD(2)*AITAJ(1)+PROD(5)*AITAJ(4)+PROD(8)*AITAJ(7)
XYZIJJ(3)=PROD(3)*AITAJ(1)+PROD(6)*AITAJ(4)+PROD(9)*AITAJ(7)
XYZIJJ(4)=PROD(1)*AITAJ(2)+PROD(4)*AITAJ(5)+PROD(7)*AITAJ(8)
XYZIJJ(5)=PROD(2)*AITAJ(2)+PROD(5)*AITAJ(5)+PROD(8)*AITAJ(8)
XYZIJJ(6)=PROD(3)*AITAJ(2)+PROD(6)*AITAJ(5)+PROD(9)*AITAJ(8)
XYZIJJ(7)=PROD(1)*AITAJ(3)+PROD(4)*AITAJ(6)+PROD(7)*AITAJ(9)
XYZIJJ(8)=PROD(2)*AITAJ(3)+PROD(5)*AITAJ(6)+PROD(8)*AITAJ(9)
XYZIJJ(9)=PROD(3)*AITAJ(3)+PROD(6)*AITAJ(6)+PROD(9)*AITAJ(9)
D7 314 K5=1.9

```

314

```

XYZIJJ(K5)=XYZIJJ(K5)+XYZIJJ(K5)
PROD(1)=XYZIJJ(1)*AIJ(1)+XYZIJJ(4)*AIJ(2)+XYZIJJ(7)*AIJ(3)
PROD(2)=XYZIJJ(2)*AIJ(1)+XYZIJJ(5)*AIJ(2)+XYZIJJ(8)*AIJ(3)
PROD(3)=XYZIJJ(3)*AIJ(1)+XYZIJJ(6)*AIJ(2)+XYZIJJ(9)*AIJ(3)
PROD(4)=XYZIJJ(1)*AIJ(4)+XYZIJJ(4)*AIJ(5)+XYZIJJ(7)*AIJ(6)
PROD(5)=XYZIJJ(2)*AIJ(4)+XYZIJJ(5)*AIJ(5)+XYZIJJ(8)*AIJ(6)
PROD(6)=XYZIJJ(3)*AIJ(4)+XYZIJJ(6)*AIJ(5)+XYZIJJ(9)*AIJ(6)
PROD(7)=XYZIJJ(1)*AIJ(7)+XYZIJJ(4)*AIJ(8)+XYZIJJ(7)*AIJ(9)
PROD(8)=XYZIJJ(2)*AIJ(7)+XYZIJJ(5)*AIJ(8)+XYZIJJ(8)*AIJ(9)
PROD(9)=XYZIJJ(3)*AIJ(7)+XYZIJJ(6)*AIJ(8)+XYZIJJ(9)*AIJ(9)

```

C

```

XIJJ(1)=AIJ(1)*PROD(1)+AIJ(2)*PROD(2)+AIJ(3)*PROD(3)
XIJJ(2)=AIJ(4)*PROD(4)+AIJ(5)*PROD(5)+AIJ(6)*PROD(6)
XIJJ(3)=AIJ(7)*PROD(7)+AIJ(8)*PROD(8)+AIJ(9)*PROD(9)

```

D7 20 K = 1,3

20 C(K,IJ) = .101800\*C8IJ\*SQRT(XK3(K,K,IJ)\*(WGT(I)+WGT(J)))

D7 30 K=4,6

30 C(K,IJ)=2.\*C8IJ\*SQRT(XK3(K,K,IJ)\*XIJJ(K-3))

10 CONTINUE

RETURN

END

CR509740

CR509750

CR509780

CR509790

CR509800

Figure 20. (Continued)

```

SUBROUTINE LINES
IMPLICIT REAL*8 (A-H,O-Z)
REAL*4 PLOT(30000),ZAP,YMPL(500)
DIMENSION SC(40,3),ZAR(200),IPLOT(150),IDPLOT(150)
DIMENSION IG(20),JG(80),PHI1J(80),THE1J(80),PSI1J(80),WGT(40),
1 XI(40),YI(40),ZI(40),XYI(40),YZI(40),XZI(40),HEX(40),HEY(40),
2 HEZ(40),ALIFT(40),XI(40),YI(40),Z(40),PHI(40),THEYA(40),PSI(40),
3 JI(40),VI(40),PI(40),Q(40),RI(40),XDOT(40),YDOT(40),ZDOT(40),
4 PHIDOT(40),THEDOT(40),PSIDOT(40),UDOT(40),VDOT(40),WDOT(40)
DIMENSION AIJ(5),AJ(9),AJ(9),AIDOT(9),DX(40),DY(40),DZ(40),
1 DPHI(40),DTHETA(40),DPSI(40),DI(5),DF(6),XX(40),XY(40),XZ(40),
2 XL(40),XM(40),XN(40),DELI(40),XI1(40),XI2(40),XI3(40),
3 XI4(40),XI5(40),XI6(40),XK(2880),FMBAR(2880),FMBAR3(6,6,80),
4 F4(2880),XKRIN(10,6,80),VEE(480),VMAX(480),NN(40,3),NN2(40,3)
DIMENSION XK1(9,6,80),BIJ(360),CIJ(360),DIJ(720),XLBAR(40,3),
1 XLBAR(3),ISP(40,3),IISP(3),XMU(40,3),XKE(40,3),OAI(360),
2 IRS(40,3),IRS2(40,3),SI(40,3),SF(40,3),FSPGF(40,3),PHIDP(40),
3 THEDP(40),PSIDP(40),FSPBAR(40,3),FSPBA2(40,3),XLNGTH(3),XC(6),
4 XDP(40),YDP(40),ZDP(40),FMP3(6,6,80),VEE2(6,80),VEEDOT(3,3)
DIMENSION PDOT(40),QDOT(40),RODOT(40),NI(40),N3(3,6),OVSIGN(6),
1 XCS(4320),XKS(9,6,80),XKI(4320),TITLE(10)
DIMENSION XOLD(40),YOLD(40),ZOLD(40),PHIOLD(40),THEOLD(40),
1 PSIOLD(40),PCOLD(40),QOLD(40),ROLD(40),UOLD(40),VOLD(40),WOLD(40)
DIMENSION XXK(60),XXJ(80),XYK(80),XYJ(80),XZK(80),XZJ(80),
1 XL(80),XLJ(80),XMK(80),XMJ(80),XNK(80),XNJ(80)
DIMENSION OXIJ(80),OYIJ(80),OZIJ(80)
DIMENSION PIN(40),QIN(40),RIN(40),PING(40),QINO(40),RINO(40),
1 DPIN(40),DQIN(40),DRIN(40)
DIMENSION DD(6),DPX(40),DPY(40),DPZ(40),DPL(40),DPH(40),DPN(40)
DIMENSION C(6,80),CBAR(80),DXDA(6,80)
DIMENSION XACC(40),YACC(40),ZACC(40)
DIMENSION SUMDF(6,80),TRUPT(80),TRUPT(80),JRUPT(80)
DIMENSION TPEN(80),IPEN(80)
DIMENSION IJPR(76)
DIMENSION AITAJ(9)
DIMENSION FSPDI(40,3),SA(40,3),SB(40,3)
DIMENSION DPI(76)
COMMON DJI
COMMON FSPDI,SA,SB
COMMON AITAJ
COMMON XNBAR,XPBAR,YNBAR,YPBAR,ZNBAR,ZPBAR,TPEN
COMMON SUMDF,TRUPT,DXDA,SC
COMMON XACC,YACC,ZACC
COMMON C,CBAR
COMMON DD,DPX,DPY,DPZ,DPL,DPH,DPN
COMMON PIN,QIN,RIN,PING,QINO,RINO,DPIN,DQIN,DRIN
COMMON OXIJ,OYIJ,OZIJ,ZG
COMMON XXK,XXJ,XYK,XYJ,XZK,XZJ,XLK,XLJ,XMK,XMJ,XNK,XNJ
COMMON XOLD,YOLD,ZOLD,PHIOLD,THEOLD,PSIOLD,POLO,QOLD,ROLO,UOLD,
1 VOLD,WOLD,DZ,DTHALF
COMMON PHI,THEYA,PSI
COMMON RIJ,PSIDOT,THEDOT,PHIDOT,CIJ,X,Y,Z,XIJ,YIJ,ZIJ,D,DF
COMMON AI,AIDOT,AJ,AIJ,DX,DY,DZ,DPHI,DTHETA,DPSI,OVSIGN
COMMON VEE,FMBAR,FH,XKS,XKI,VMAX
COMMON XX,XY,XZ,XL,XM,XN,WGT,ALIFT,XC,P,Q,R,U,V,W
COMMON UDOT,VDOT,WDOT,XZI,YZI,ZI,HEZ,XI,XYI,HEX,YI,HEY,DELI
COMMON PDOT,XI1,XI2,XI3,QDOT,XI5,XI4,RODOT,XI5,XDOT,YDOT,ZDOT
COMMON XLBAR,SF,FSPGF,XKE,FSPBAR,XMU,VEEDOT
COMMON XGDOT,YGDOT,ZGDOT,PPR,QPR,RPR,PHIPR,THCPR,PSIPR
COMMON PHIDP,THEDP,PSIDP,XUP,YDP,ZDP,OAI,DELTAT,TMAX,TIME,TITLE

```

CR509810

CR507310

CR507320

CR507330

CR507340

CR507350

CR507360

CR507370

CR507380

CR507390

CR507400

CR507410

CR507420

CR507430

CR507440

CR507450

CR507460

CR500180

CR507480

CR507490

CR507500

CR507510

CR507520

CR500230

CR500240

CR500250

CR500280

CR510100

CR500300

CR510130

CR510140

CR510150

CR510160

CR510170

CR510180

CR510190

CR510200

CR509400

CR510220

CR510230

CR510240

CR500440

CR500360

CR510270

Figure 20. (Continued)





```

DIMENSION DR1(16)
COMMON DR1
COMMON FSPDT, SA, SB
COMMON AITAJ
COMMON XNBAR, XPBAR, YNBAR, YPBAR, ZNBAR, ZPBAR, TPEN
COMMON SUMOF, TRUPT, DSDA, SC
COMMON XACC, YACC, ZACC
COMMON C,CBAP
COMMON DU,DYV,CY,Z,PZ,DPL,DPM,DPN
COMMON PIN,QIN,RIN,PINO,QINO,RINO,UPIN,DOIN,DRIN
COMMON OXIJ,OYIJ,OZIJ,ZG
COMMON XX,XJ,XYK,XYJ,XZK,XZJ,XLK,XLJ,XMK,XMJ,XNK,XNJ
COMMON XOLD,YOLD,ZOLD,PHIOLD,THECLO,PSIOLD,POLD,QCLD,ROLD,UOLD,
1 VOLD,WOLD,OTZ,OTHALF
COMMON PHI,THETA,PSI
COMMON RIJ,PSIDOT,THEDOT,P4IDOT,CIJ,X,Y,Z,XIJ,YIJ,ZIJ,D,DF
COMMON AI,AIDOT,AJ,AIJ,DX,DY,DZ,DPHI,DMETHA,DPSI,DYSIGN
COMMON VEE,FMBAR,FH,XKS,XKI,VMAX
COMMON XX,XY,XZ,XL,XM,XN,WGT,ALIFT,XC,P,Q,R,U,V,W
COMMON UDDT,VDDT,WDDT,XZI,YZI,ZI,HFZ,XI,XVI,HFX,YI,HEY,DELI
COMMON PDCT,XI1,XI2,XI3,QDDT,XI5,XI4,RDDT,XI6,XDDT,YDDT,ZDDT
COMMON XLBAR,SF,FSPDF,XKE,FSPBAZ,XMJ,VVEDOT
COMMON XGDCT,YGDDT,ZGDDT,PPR,QPR,KPR,P4IPR,THEPR,PSIPR
COMMON PHIDP,THEDP,PSIDP,XDP,YDP,ZDP,GAI,DELTA,TMAX,TIME,TITLE
COMMON PHIIJ,THCIJ,PSIIJ,XK,DIIJ,XLBAR,SI,XLENGTH,IP
COMMON NY,I,J,ILAST,ITAB1,ITAB6,IJLIJ,IJKLI,IJXK,IJL,IG,JG,ITAB,CRS10970
1 ITABD,IJXL,ITABL1,IPRINT,ITABLE,ILINES,NPR,IGS,IISP,ISP,IBS,N,NNCRS00490
COMMON KRUTP,IRUTP,JRUTP
COMMON INDP,ZPEN,XPEN
COMMON IJFR
COMMON PLOT,ZAR,THPLGT,IPLUT,IDPLOD,IPLSW,IPLC,JPILOT,NPILOT,ITPLOT
EQUIVALENCE (XKS(1),XKS3(1,1,1)),(XKI(1),XKI3(1,1,1)),
1 (XKRIV(1,1,1),FMBAR(1)),(FM(1),FM3(1,1,1)),(VEE(1),VEF2(1,1))
EQUIVALENCE (FMBAR(1),FMBAR3(1,1,1)),(N(1),N3(1,1)),(NH(1,1),
1 NV2(1,1)),(FSPBAR(1,1),FSPBAZ(1,1)),(IRS(1,1),IBSZ(1,1))
SORT(X) = DSORT(X)
VA(1) = X(1)
VA(2) = Y(1)
VA(3) = Z(1)
VAODT(1) = XDOT(1)
VAODT(2) = YDOT(1)
VAODT(3) = ZDOT(1)
PBAT(1) = P(1)
PBAT(2) = Q(1)
PBAT(3) = R(1)
C INITIALIZE SOME MORE
DO 10 K = 1,3
XLNGYH(K) = 0.C
IISP(K) = ISP(I,K)
XXLBAR(K) = XLBAR(I,K)
DO 15 JJ = 1,3
FSP(IJJ,K) = 0.C
15 XYDC(JJ,K) = 0.0
10 CONTINUE
C LTOP G
DO 20 K = 1,3
IF(IISPK) 25,20,25
25 ISUR = 3*K
DVC = A(IISUB)*XXLBAR(K)
WCDCT = AIDOT(ISUB)*XXLBAR(K)

```

Figure 20. (Continued)

VC = VA(3)+DVC	CRS11280
VCDOT = VADOT(3)+DVCDDT	CRS11290
C1(K) = VC/DVC	CRS11300
C2(K) = (DVC*VCDOT-VC*DVCDDT)/(DVC*DVC)	CRS11310
VC3(K) = VC	CRS11320
20 CONTINUE	CRS11330
C LOOP M	CRS11340
DO 30 M = 1,3	CRS11350
IF(IISP(K)) 35,30,35	CRS11360
35 IF(VC3(K)) 30,20,40	CRS11370
40 ISUM = 3*(K-1)	CRS11380
BARL = XLBAR(K)	CRS11390
SUM = 0.0	CRS11400
SUMD = 0.0	CRS11410
C LOOP J	CRS11420
DO 50 J = 1,3	CRS11430
ISUB = ISUM+1	CRS11440
DVC = A11ISUB*BARL	CRS11450
DVCDDT = A1DDT(ISUB)*BARL	CRS11460
DVP = C1(K)*DVC	CRS11470
DDP = C1(K)*DVCDDT+C2(K)*DVC	CRS11480
SUM = SUM+DVP*DVP	CRS11490
SUMD = SUMD+DVP*DDP	CRS11500
50 CONTINUE	CRS11510
SK = SORT(SUM)	CRS11520
S(K) = SK	CRS11530
SC(I,K) = SK	
SDDT(K) = SUMD/SK	CRS11540
C GET LENGTH	CRS11550
IF(BARL) 55,6C,60	CRS11560
- 55 T = -BARL-SK	CRS11570
IF(T) 65,65,70	CRS11580
70 T = -T	CRS11590
GO TO 65	CRS11600
60 T = BARL-SK	CRS11610
IF(T) 70,65,65	CRS11620
65 XLNGTH(K) = T	CRS11630
30 CONTINUE	CRS11640
PL(1,1) = -SDDT(1)	CRS11650
PL(2,2) = -SDDT(2)	CRS11660
PL(3,3) = -SDDT(3)	CRS11670
PL(2,1) = PBAR(3)*XLNGTH(1)	CRS11680
PL(3,1) = -PBAR(2)*XLNGTH(1)	CRS11690
PL(1,2) = -PBAR(3)*XLNGTH(2)	CRS11700
PL(3,2) = PBAR(1)*XLNGTH(2)	CRS11710
PL(1,3) = PBAR(2)*XLNGTH(3)	CRS11720
PL(2,3) = -PBAR(1)*XLNGTH(3)	CRS11730
C LOOP J	CRS11740
DO 75 JJ = 1,3	CRS11750
ISUB = JJ-3	CRS11760
VAD = VADDT(JJ)	CRS11770
C LOOP L	CRS11780
DO 80 K = 1,3	CRS11790
IF(IISP(K)) 85,80,85	CRS11800
85 IF(VC3(K)) 80,20,90	CRS11810
90 SJM = 0.0	CRS11820
C LOOP I	CRS11830
DO 95 I = 1,3	CRS11840
ISUB = ISUM+3	CRS11850
95 SJM = SUM+A11ISUB*PL(I,K)	CRS11860

Figure 20. (Continued)

```

      VEEDOT(I,J,K) = VAD*SUM
      90 CONTINUE
      75 CONTINUE
C LOOP N
      103 K = 1,3
      IF(IIS(K)) 110,105,110
      110 IF(V23(K)) 105,105,113
      115 S = S(K)
      SDIF = S - JF(I,1)
      IF(SDIF) 120,120,125
      120 IF(IIS(I,K)) 120,130,135
      125 IIS(I,K) = 1
      135 FSPJ = FSPJF(I,K)*XKE(I,K)*SDIF
      IF(FSPJ) 140,130,190
      140 FSPJ = 0.0
      130 SP = SK-FSPBAR(I,K)
C FSPBAR = SBAR-FSPDAR/KE
      IF(SP) 150,155,155
      150 FSPJ = 0.0
      160 FSPJ = 0.0
C COMPUTE FSPD PER NEW EXTERNAL SPRING LOAD-STROKE CURVES 7/25/72
      155 FSPJ=FSPJF(I,K)
      IF (SP,GE,SB(I,K)) GO TO 160
      IF (SP,GT,SA(I,K)) GO TO 157
      FSPD=FSPD(I,K)
      IF (SP,GE,SI(I,K)) GO TO 160
      FSPJ=FSPD*SP/SI(I,K)
      160 FSPJ=FSPD(I,K)+(SP-SA(I,K))*(FSPD-FSPD(I,K))/(SB(I,K)-SA(I,K))
      160 IF(SDOT(X)) 165,165,170
      170 NV(I,K) = 0
      165 IF(NV(I,K)) 190,175,190
      175 NV(I,K) = 1
      FSPBAR(I,K) = SK-FSPD/XKE(I,K)
C (ISA)
      190 XV = AI(3*K)*FSPD
      XVDC(3,K) = XV
      VI = VEEDOT(1,K)
      V2 = VEEDOT(2,K)
      V8 = SORT(V1*V1+V2*V2)
      IF(V8) 210,210,200
      200 XV = XV(I,K)*V/V8
      XVDC(1,K) = XV*VEEDOT(1,K)
      XVDC(2,K) = XV*VEEDOT(2,K)
      210 IS = 0
C LOOP J
      220 J = 1,3
      SUM = 0.0
C LOOP R
      230 L = 1,3
      IS = IS+1
      230 SUM = SUM-AI(IS)*XVDC(L,K)
      220 FSP(J,K) = SUM
C END OF LOOP N
      105 CONTINUE
C CRASH FORCES
      240 J = 1,3
      SUM = 0.0
      250 K = 1,3
      250 SUM = SUM+FSP(J,K)
      240 XC(J) = SUM
C CRASH MOMENTS
      XC(4) = FSP(3,2)*XLNGTH(2)-FSP(2,3)*XLNGTH(3)
      XC(5) = FSP(1,2)*XLNGTH(3)-FSP(3,1)*XLNGTH(1)
      XC(6) = FSP(2,1)*XLNGTH(1)-FSP(1,2)*XLNGTH(2)
C
      RETURN
      END

```

```

CRS11870
CRS11880
CRS11890
CRS11900
CRS11910
CRS11920
CRS11930
CRS11940
CRS11950
CRS11960
CRS11970
CRS11980
CRS11990
CRS12000
CRS12010
CRS12020
CRS12030
CRS12040
CRS12050
CRS12060
CRS12070
CRS12130
CRS12140
CRS12150
CRS12160
CRS12170
CRS12180
CRS12190
CRS12200
CRS12210
CRS12220
CRS12230
CRS12240
CRS12250
CRS12260
CRS12270
CRS12280
CRS12290
CRS12300
CRS12310
CRS12320
CRS12330
CRS12340
CRS12350
CRS12360
CRS12370
CRS12380
CRS12390
CRS12400
CRS12410
CRS12420
CRS12430
CRS12440
CRS12450
CRS12460
CRS12470
CRS12480
CRS12490
CRS12500
CRS12510
CRS12520

```

Figure 20. (Continued)

SUBROUTINE EULER(A,PHI,THETA,PSI)	
IMPLICIT REAL*8 (A-H,O-Z)	CRS12530
DIMENSION A(9)	
SIN(X) = DSIN(X)	CRS12540
COS(X) = DCOS(X)	CRS10010
S1 = SIN(PHI)	CRS10020
C1 = COS(PHI)	CRS12550
S2 = SIN(THETA)	CRS12560
C2 = COS(THETA)	CRS12570
S3 = SIN(PSI)	CRS12580
C3 = COS(PSI)	CRS12590
A(1) = C2*C3	CRS12600
A(2) = C2*S3	CRS12610
A(3) = -S2	CRS12620
A(4) = -C1*S3+S1*S2*C3	CRS12630
A(5) = C1*C3+S1*S2*S3	CRS12640
A(6) = S1*C2	CRS12650
A(7) = S1*S3+C1*S2*C3	CRS12660
A(8) = -S1*C3+C1*S2*S3	CRS12670
A(9) = C1*C2	CRS12680
RETURN	CRS12690
END	CRS12700
SUBROUTINE MATMUL(A,B,C)	CRS12710
IMPLICIT REAL*8 (A-H,O-Z)	CRS12720
DIMENSION A(3,3),B(3,3),C(3,3)	
C A*B	
DO 10 I = 1,3	CRS12730
DO 10 J = 1,3	CRS12740
SUM = 0.0	CRS12750
DO 20 K = 1,3	CRS12760
SUM = SUM+A(I,K)*B(K,J)	CRS12770
C(I,J) = SUM	CRS12780
RETURN	CRS12790
END	CRS12800
SUBROUTINE MATVEC(A,V,P,ISW)	CRS12810
IMPLICIT REAL*8 (A-H,O-Z)	CRS12820
DIMENSION A(3,3),V(3),P(3)	CRS12830
C A*V	
DO 10 I = 1,3	CRS12840
SUM = 0.0	CRS12850
DO 20 K = 1,3	CRS12860
IF (ISW) 40,30,40	CRS12870
SUM = SUM+A(I,K)*V(K)	CRS12880
GO TO 20	CRS12890
SUM = SUM+A(K,I)*V(K)	CRS12900
CONTINUE	CRS12910
P(I) = SUM	CRS12920
RETURN	CRS12930
END	CRS12940
	CRS12950
	CRS12960

Figure 20. (Continued)

SUBROUTINE INPLY  
 INP,ICIT,REAL\*E (A-H,O-Z)  
 REAL\*4 PLDT(3000),ZAR,TMPLDT(500)  
 DIMENSION INBUF(76)  
 DIMENSION SC(40,3),ZAR(200),IFLDT(150),IDPLOT(150)  
 DIMENSION IG(80),JG(80),PHI(100),THEIJ(80),PSI(100),MG(100),  
 1 XI(40),YI(40),ZI(40),XYI(40),YZI(40),XZI(40),HEX(40),HEY(40),  
 2 HEZ(40),ALIFT(40),PI(40),YI(40),ZI(40),PHI(40),THETA(40),PSI(40),  
 3 U(40),VI(40),W(40),P(40),Q(40),R(40),XDOT(40),YDOT(40),ZDOT(40),  
 4 PHIDOT(40),THEDOT(40),PSIDOT(40),UDOT(40),VDOT(40),WDOT(40)  
 DIMENSION AIJ(9),AJ(9),AJI(9),AIDOT(9),DX(40),DY(40),DZ(40),  
 1 PHI(40),DTHETA(40),DPSI(40),D(16),DF(16),XX(40),XY(40),XZ(40),  
 2 XL(40),XM(40),XN(40),DEL(40),XI(40),XJ(40),XK(40),XL(40),  
 3 XI(40),XJ(40),XK(40),XL(40),XM(40),XN(40),XO(40),XP(40),XQ(40),XR(40),XS(40),XT(40),XU(40),XV(40),XW(40),  
 4 FX(2880),XXRIN(10,6,80),VEE(480),VMAX(480),NN(40,3),NN2(40,3)  
 DIMENSION XKI(3,6,80),SJI(360),CIJ(360),CII(720),XIDAR(40,3),  
 1 XILAR(3),ISP(40,3),ISPI(3),XMU(40,3),XKE(40,3),NAT(360),  
 2 IS(40,3),IS2(40,3),SI(40,3),SF(40,3),FSPDF(40,3),PHIDP(40),  
 3 THEDP(40),PSIDP(40),FSPBAR(40,3),FSPBA2(40,3),XLNGTH(3),XC(16),  
 4 XDP(40),YDP(40),ZDP(40),FM3(6,6,80),VEE2(6,80),VEEDOT(3,3)  
 DIMENSION PDOT(40),QDOT(40),POOT(40),NI(480),N3(30,6),DVSIGN(16),  
 1 XCSI(4320),XKE3(9,6,80),XKI(4320),TITLE(10)  
 DIMENSION XLBAR2(40,3),ISP2(40,3),XNU2(40,3),XKE2(40,3),  
 1 XKE3(6,6,80),VMAX2(6,80)  
 DIMENSION XOLD(40),YOLD(40),ZOLD(40),PHIOLD(40),THEOLD(40),  
 1 PSIOLD(40),POLD(40),GOLD(40),ROL(40),UOLD(40),VOLD(40),WOLD(40)  
 DIMENSION XXK(80),XXJ(80),XYK(80),XYJ(80),XZK(80),XZJ(80),  
 1 XLK(80),XLJ(80),XMK(80),XMJ(80),XNK(80),XNJ(80)  
 DIMENSION CXIJ(80),CYIJ(80),CZIJ(80)  
 DIMENSION PINI(40),QINI(40),PIN(40),PINO(40),QINO(40),RINO(40),  
 1 DIPINI(40),DQINI(40),DRINI(40)  
 DIMENSION DD(6),DPX(40),DPY(40),DPZ(40),DPL(40),DPM(40),DPN(40)  
 DIMENSION C(6,80),CBAR(80),DXDA(6,80)  
 DIMENSION XACC(40),YACC(40),ZACC(40)  
 DIMENSION SUMOF(6,80),TRUPT(80),TRUPT(80),JRUPT(80)  
 DIMENSION TPEN(80),TPEN(80)  
 DIMENSION IJPR(76)  
 DIMENSION AITAJ(9)  
 DIMENSION FSPDI(40,3),SA(40,3),SB(40,3)  
 DIMENSION DRJ(76)  
 COMMON DRI  
 COMMON FSPDI,SA,SB  
 COMMON AITAJ  
 COMMON XBAR,XPBAR,YNBAR,YPBAR,ZBAR,ZPBAR,TPEN  
 COMMON SUMOF,TRUPT,DXDA,SC  
 COMMON XACC,YACC,ZACC  
 COMMON C,CBAR  
 COMMON DD,DPX,DPY,DPZ,DPL,DPM,DPN  
 COMMON PIN,QIN,RIN,PINO,QINO,RINO,DFIN,DOIN,DRIN  
 COMMON CXIJ,CYIJ,CZIJ,ZG  
 COMMON XXK,XXJ,XYK,XYJ,XZK,XZJ,XLK,XLJ,XMK,XMJ,XNK,XNJ  
 COMMON XOLD,YOLD,ZOLD,PHIOLD,THEOLD,PSIOLD,POLD,QOLD,ROL,ROLD,  
 1 VOLD,WOLD,DT2,DTHALF  
 COMMON PHI,THETA,PSI  
 COMMON BIJ,PSIDOT,THEDOT,PHIDOT,CIJ,X,Y,Z,XIJ,YIJ,ZIJ,D,DF  
 COMMON AI,AIDOT,AJ,AIJ,OX,OY,OZ,DPMI,DTHETA,DPSI,DVSIGN  
 COMMON VEE,FMBAR,FMAX,XKI,VMAX  
 COMMON XX,XY,XZ,XL,XM,XN,XO,XP,XQ,XR,XS,XT,XU,XV,XW  
 COMMON UDOT,VDOT,WDOT,XZI,YZI,ZI,HEZ,XI,XYI,HEX,YI,HEY,DEL  
 COMMON PDOT,XI1,XI2,XI3,QDOT,XI5,XI6,RODOT,XI6,XDOT,YDOT,ZDOT

CRS12970

CRS10490

CRS10500

CRS10510

CRS10520

CRS10530

CRS10540

CRS10550

CRS10560

CRS10570

CRS10580

CRS10590

CRS10600

CRS10610

CRS10620

CRS10630

CRS10640

CRS00180

CRS10660

CRS10670

CRS10680

CRS10690

CRS10700

CRS10710

CRS10720

CRS00230

CRS00240

CRS00250

CRS00280

CRS13280

CRS00300

CRS13310

CRS13320

CRS13330

CRS13340

CRS13350

CRS13360

CRS13370

CRS13380

CRS00400

CRS13400

CRS13410

CRS13420

Figure 20. (Continued)

```

CJMHQY      XLBAR,SF,FSPDF,XKE,FSPBAR,XMU,VEEDOT      CR500470
CJMHQY      XGDOT,YGDOT,ZGDOT,PPR,GPR,RPR,PHIPR,THEPR,PSIPR      CR500360
CJMHQY      PHIDP,THEOP,PSIDP,XDP,YDP,ZDP,OAL,DELTAT,TMAX,TIME,TITLE      CR513450
CJMHQY      PHIJ,TFIJ,PSIJ,XK,OTJ,XLBAR,SI,XLNGTH,IP      CR500470
CJMHQY      NY,I,J,ILAST,ITABIJ,ITAB6,IJLIJ,IJKI,IJL,IG,JG,ITAB,CR513470
1  ITABO,IJLI,ITABLI,IPRINT,ITABLE,ILINES,NPR,IGS,IISP,ISP,IIS,N,NHCR500490
CJMHQY      KRUP,T,IRUP,T,IRUP
CJMHQY      INDP,IPEN,KPEN
CJMHQY      IJPR
CJMHQY      PLDT,ZAR,TMPLOT,IPLDT,INDPLOT,IPLSK,IPLC,JPLDT,NPLGT,ITPLDT
EQUIVALENCE (XLBAR2(1,1),XLBAR(1,1)),(ISP2(1,1),ISP(1,1)),      CR510900
1  (XMU2(1,1),XMU(1,1)),(XKE2(1,1),XKE(1,1)),(XK3(1,1),XK(1,1)),      CR510910
2  (VMAX2(1,1),VMAX(1,1))      CR510920
EQUIVALENCE (XKS(1,1),XKS3(1,1,1,1)),(XKI(1,1),XKI3(1,1,1,1)),      CR510930
1  (XCRIN(1,1,1),FMBAR(1,1)),(FMI(1,1),FM3(1,1,1,1)),(VEE(1,1),VEEZ(1,1))      CR510940
EQUIVALENCE (FMBAR(1,1),FMBAR3(1,1,1,1)),(NI(1,1),N3(1,1,1,1)),(NN(1,1,1,1)),      CR510950
1  NY2(1,1,1), (FSPBAR(1,1),FSPBAR2(1,1,1,1)),(IBS(1,1),IBS2(1,1,1,1))      CR510960
READ 100, TITLE      CR513540
100 FJRHAT(10A8)      CR513550
READ 200,NY,IPRINT,ITABLE,DELTAT,TMAX      CR513560
IF(DELTAT) 17,17,18      CR511000
17 NY = 0      CR511010
GO TO 1000      CR511020
18 CONTINUE      CR511030
19 IF(NY) 1000,1CCO,16      CR511040
200 FJRHAT(313,2E12,0)      CR513570
300 FJRHAT(6E12,0)      CR513580
16 IGS = 0      CR511070
C READ THE I,J,PHIJ,THEIJ,PSIJ      CR513600
15 READ 400, I,J,PHIJ,THEIJ,PSIJ      CR513610
400 FJRHAT(213,3E12,0)      CR513620
IF(I) 50,50,2C      CR513630
20 IGS = IGS+1      CR513640
IG(IGS) = I      CR513650
JS(IGS) = J      CR513660
PHIJ(IGS) = PHIJ      CR513670
THEIJ(IGS) = THEIJ      CR513680
PSIJ(IGS) = PSIJ      CR513690
GO TO 15      CR513700
C READ HEIGHTS      CR513710
50 READ 300, (WGTH(I),I=1,NM)      CR513720
C READ MOMENTS AND INERTIA PRODUCTS      CR513730
READ 300, (XI(I),YI(I),ZI(I)),XYI(I),YXI(I),XZI(I),I=1,NM)      CR513740
C READ ANGULAR MOMENTUM COMPONENTS      CR513750
READ 300, (MEY(I),MEYI(I),MEZ(I),I=1,NM)      CR513760
C READ AERODYNAMIC LIFTS      CR513770
READ 300, (ALIFT(I),I=1,NM)      CR513780
C READ IC DATA      CR513790
READ 300, XGDOT,YGDOT,ZGDOT      CR513800
READ 300, PPR,GPR,RPR      CR513810
READ 300, PHIPR,THEPR,PSIPR,ZG      CR513820
READ 300, (XDP(I),YDP(I),ZDP(I),I=1,NM)      CR513830
READ 300, (PHIDP(I),THEOP(I),PSIDP(I),I=1,NM)      CR513840
READ 300, (XLBAR2(I,K),K=1,3),I=1,NM)      CR513850
READ 300, ((ISP2(I,K),K=1,3),I=1,NM)      CR513860
500 FJRHAT(2413)      CR513870
READ 300, ((XMU2(I,K),K=1,3),I=1,NM)      CR513880
READ 300, ((XKE2(I,K),K=1,3),I=1,NM)      CR513890
READ 300, ((XK3(I,K,IJ),I=1,6),K=1,6),IJ=1,IGS      CR513900
READ 300, ((VMAX2(I,IJ),I=1,6),IJ=1,IGS)      CR513910

```

```

C READ (R(IJL) VS. ABS(VPRIME(IJL))
READ 300, ((ID>DA(L,YJ),L=1,6),IJ=1,IGS)
READ 300,((IXKRIN(I,L,ZJ),I=1,ITABLE),L=1,6),IJ=1,IGS)
READ 300,((SI(I,K),SA(I,K),SB(I,K),SF(I,K),FSPOI(I,K),
1 FSPDF(I,K),K=1,3),I=1,NM)
READ 300, (CBAR(IJ),IJ=1,IGS)
C READ PLOT INDICATORS
NPLJT = 0
J4 = NM
D3 30 I = 1,25
IF(I.EQ.13) JM = IGS
READ 928, INBUF
928 FCR4AT(7611)
D3 40 J = 1,JM
IF (NPLJT.EQ.150) GO TO 30
IF(INBUF(I).EQ.C) GO TO 40
NPLJT = NPLJT+1
IDPLJT(INPLJT) = I
IPLJT(INPLJT) = J
40 CONTINUE
30 CONTINUE
READ 301,INDP
301 FCR4AT(4012)
IF (INDP.EQ.0) GO TO 65
READ 300, XNBAR,XPNBAR,YNBAR,YPNBAR,ZNBAR,ZPNBAR
65 READ 928, IJPR
C IF WE KNOW HOW MANY PLOTS WE WANT, WE CAN FIGURE OUT HOWMANY POINTS
C PER PLOT WE CAN HAVE, ALTHO WE DON'T WANT MORE THAN 500, BECAUSE
C WE COULDN'T NOTICE THE RESOLUTION ANYWAY.THE REST OF THIS FIGURES
C OUT HOW OFTEN TO SAVE. A TRUNCATED ITPLOT WILL TRY TO SAVE TOO MUCH
C AND THEN WE WOULDN'T GET TO TMAX, BUT IF WE WOULD ALMOST GET THERE
C IT WILL NOT BE NOTICEABLE ON THE PLOT.
IF (NPLJT.EQ.C) GO TO 60
70 IP = 30000/NPLJT
IF(IP.GT.500) IP = 500
FITER = TMAX/DELTAT+2.0
ITPLOT = FITER/IP
IF(ITPLOT.EQ.0) ITPLOT = 1
IF(FITER/(IP*ITPLOT).GT.1.002) ITPLOT = ITPLOT+1
60 CONTINUE
C*****PRINT OUT INPUT
900 FCR4AT ( ' 1',1CAB)
901 FCR4AT ( ' NM,IPRINT,ITABLE,DELTAT,TMAX')
902 FCR4AT ( 1X,315,1P2E15.5)
903 FCR4AT ( ' 1,J,PHIJ,THEIJ,PSIJ' )
904 FCR4AT ( 1X,215,1P3E15.5)
905 FCR4AT ( ' WGT' )
906 FCR4AT ( 1X,1P6E15.5)
907 FCR4AT ( ' 1,XI(1),YI(1),ZI(1),XYI(1),YZI(1),XZI(1)' )
908 FCR4AT ( 1X,15,1P6E15.5)
909 FCR4AT ( ' 1,HEX(1),MEY(1),HEZ(1)' )
910 FCR4AT(1X,15,1P3E15.5)
911 FCR4AT ( ' A,IFT' )
912 FCR4AT ( ' XGDOT,YGDOT,ZGDOT' )
913 FCR4AT ( ' PPR,OPR,RPR' )
914 FCR4AT ( ' PHIPR,THEPR,PSIPR' )
915 FCR4AT ( ' 1,XDP(1),YDP(1),ZDP(1)' )
916 FCR4AT ( ' 1,PKIDP(1),THEDP(1),PSIDP(1)' )
917 FCR4AT ( ' 1, LBAR (1,1), LBAR (1,2), LBAR (1,3)' )
918 FCR4AT ( ' 1, SP (1,1), SP (1,2), SP (1,3)' )

```

CRS13920

CRS13960

CRS13980

CRS11610

CRS11620

CRS11630

CRS11640

CRS11650

CRS11660

CRS11670

CRS11680

CRS11690

CRS11700

CRS11710

CRS11720

CRS11730

CRS11740

CRS11750

CRS11760

CRS11770

CRS11780

CRS11790

CRS11800

Figure 20. (Continued)

```

919 FPMAT ( ' I, MU (1,1), MU (1,2), MU (1,3) ' ) CRS11810
920 FPMAT ( ' I, KE (1,1), KE (1,2), KE (1,3) ' ) CRS11820
921 FPMAT ( ' IJ,K, XK(1,K,IJ), XK(2,K,IJ), XK(3,K,IJ), XK(4,K,IJ), XK(5,K,IJ), KCP(1,1,IGS) CRS11830
    L,IJ), XK(6,K,IJ) ' ) CRS11840
922 FPMAT (IX,215, IP6F,5.5 ) CRS11850
923 FPMAT ( ' I, VMAX(1,I),VMAX(2,I),VMAX(3,I),VMAX(4,I),VMAX(5,I),VCP(1,1,IGS) CRS11860
    INAX(6,I) ' ) CRS11870
924 FPMAT ( ' OX(L,IJ) FOR KR TABLES' ) CRS11880
925 FPMAT ( ' IJ,L,KR(1,L,IJ),KR(2,L,IJ),KR(3,L,IJ),KR(4,L,IJ),KR(5,L,IJ),KR(6,L,IJ),LGRS(1,1,IGS) CRS11890
    I,IJ),KR(6,L,IJ) ' ) CRS11900
926 FPMAT ( ' I,K, SI(1,K),SA(1,K),SB(1,K),SF(1,K),FSPDI(1,K),
    I FSPDF(1,K) ' )
927 FPMAT(IX,415) CRS11920
PRINT 900, TITLE CRS11930
PRINT 901 CRS11940
PRINT 902, NM, IPRINT, ITABLE, DELTAT, TMAX CRS11950
PRINT 903 CRS11960
PRINT 904, (IG(I),JG(I),PHI(IJ(I),THEI(IJ(I),PSI(IJ(I),I=1,IGS) CRS11970
PRINT 905 CRS11980
PRINT 906, (WGT(I),I=1,NM) CRS11990
PRINT 907 CRS12000
PRINT 908, (I,X(I),Y(I),Z(I),XT(I),YT(I),ZT(I),I=1,NM) CRS12010
PRINT 909 CRS12020
PRINT 910, (I,PEX(I),HEY(I),HEZ(I),I=1,NM) CRS12030
PRINT 911 CRS12040
PRINT 906, (ALIFT(I),I=1,NM) CRS12050
PRINT 912 CRS12060
PRINT 906, XGDOT,YGDOT,ZGDOT CRS12070
PRINT 913 CRS12080
PRINT 906, PPR,QPR,RPR CRS12090
PRINT 914 CRS12100
PRINT 906, DMIPR,THEPR,PSIPR CRS12110
PRINT 915 CRS12120
PRINT 910, (I,XCP(I),YCP(I),ZCP(I),I=1,NM) CRS12130
PRINT 916 CRS12140
PRINT 910, (I,PHIOP(I),THEOP(I),PSIOP(I),I=1,NM) CRS12150
PRINT 917 CRS12160
PRINT 910, (I,(XLBAR2(I,K),K=1,3),I=1,NM) CRS12170
PRINT 918 CRS12180
PRINT 927, (I,(ISP2(I,K),K=1,3),I=1,NM) CRS12190
PRINT 919 CRS12200
PRINT 910, (I,(XHU2(I,K),K=1,3),I=1,NM) CRS12210
PRINT 920 CRS12220
PRINT 910, (I,(XKE2(I,K),K=1,3),I=1,NM) CRS12230
PRINT 921 CRS12240
PRINT 922, (I,IJ,K,(XK3(I,K,IJ),I=1,6),K=1,6),IJ=1,IGS) CRS12250
PRINT 923 CRS12260
PRINT 908, (I,(VMAX2(I,I),L=1,6),I=1,IGS) CRS12270
PRINT 924 CRS12280
PRINT 906, ((DMA(L,IJ),L=1,6),IJ=1,IGS) CRS12290
PRINT 925 CRS12300
PRINT 922, ((IJ,L,(XKRIN(I,L,IJ),I=1,(TABLE),L=1,6),IJ=1,IGS) CRS12310
PRINT 926 CRS12320
PRINT 922, ((I,K,SI(I,K),SA(I,K),SB(I,K),SF(I,K),FSPDI(I,K),
    I FSPDF(I,K),K=1,3),I=1,NM)
PRINT 931
931 FPMAT ( ' I,J,CBAR(J) ' )
PRINT 924, (IG(I),JG(I),CBAR(I),I=1,IGS)
929 FPMAT (IX,215,IP6F,5)
IF (INDP.EQ.0) GO TO 1000
PRINT 930
930 FPMAT ( ' >,XNBAR,XPBAR,YNBAR,YPBAR,ZNBAR,ZPBAR ' )
PRINT 908, INDP,XNBAR,XPBAR,YNBAR,YPBAR,ZNBAR,ZPBAR
1000 RTN
END

```

Figure 20. (Continued)



```

SUBROUTINE IC
IMPLICIT REAL*E (A-H,O-Z)
REAL*4 PLDT(3000),ZAR,TMPLOT(500)
DIMENSION SC(40,3),ZAR(200),IPLOT(150),IDPLOT(150)
DIMENSION IGI(80),JG(80),PHI IJ(80),THE IJ(80),PSI IJ(80),WGT(40),
1 XI(40),YI(40),ZI(40),XYI(40),YZI(40),XZI(40),HEX(40),HEY(40),
2 HEZ(40),ALIFT(40),X(40),Y(40),Z(40),PHI(40),THETA(40),PSI(40),
3 U(40),V(40),W(40),P(40),Q(40),R(40),XDOT(40),YDOT(40),ZDOT(40),
4 PHIDOT(40),THEDOT(40),PSIDOT(40),UDOT(40),VDOT(40),WDOT(40)
DIMENSION AIJ(9),AJ(9),AJ(9),AIJOT(9),DX(40),DY(40),DZ(40),
1 DPHI(40),DTHETA(40),DPSI(40),D(6),DF(6),XX(40),XY(40),XZ(40),
2 XL(40),XM(40),XN(40),DELI(40),XI1(40),XI2(40),XI3(40),
3 XI4(40),XI5(40),XI6(40),XK(2880),FMRAR(2880),FMBAR3(6,6,80),
4 F4(2880),XKR IN(10,6,80),VFF(480),VMAX(480),NN(40,3),NN2(40,3)
DIMENSION XKI(315,6,80),BIJ(360),CIJ(360),DIJ(720),XLBAR(40,3),
1 XXLBAR(3),ISP(40,3),IISP(3),XMU(40,3),XKE(40,3),OAI(360),
2 IDS(40,3),IBS2(40,3),SI(40,3),SF(40,3),FSPDF(40,3),PHIDP(40),
3 THEDP(40),PSIDP(40),FSPBAR(40,3),FSPBAZ(40,3),XNGTH(3),XC(6),
4 XOP(40),YOP(40),ZOP(40),FM3(6,6,80),VEE2(6,80),VEEDOT(3,3)
DIMENSION PDOT(40),ODOT(40),RODT(40),NI(480),N3(80,6),DVSIGN(6),
1 XKSI(4320),XKSI(9,6,80),XKI(4320),TITLE(10)
DIMENSION ABARPP(3,3),APR(3,3),XPPP(3),ANGDPR(3),DPR(3,3),
1 ADP(3,3),AIC(3,3),VIP(3),XV(3),ADPR(3,3),VJPI(40,3)
DIMENSION ISP2(40,3),XLBAR2(40,3)
DIMENSION XOLD(40),YOLD(40),ZOLD(40),PHIOLD(40),THEOLD(40),
1 PSICLD(40),PCLD(40),QCLD(40),ROLD(40),UOLD(40),VOLD(40),WOLD(40)
DIMENSION XXX(80),XXJ(80),XYK(80),XYJ(80),XZK(80),XZJ(80),
1 XLK(80),XLJ(80),XMK(80),XMJ(80),XNK(80),XNJ(80)
DIMENSION DXIJ(80),OYIJ(80),OZIJ(80)
DIMENSION PIN(40),QIN(40),RIN(40),PINO(40),QINO(40),RINO(40),
1 DPIN(40),DQIN(40),DRIN(40)
DIMENSION DP(6),DPX(40),DPY(40),DPZ(40),DPL(40),DPM(40),DPN(40)
DIMENSION C(6,6),CHAR(80),DXDA(6,80)
DIMENSION XACC(40),YACC(40),ZACC(40)
DIMENSION SUMDF(6,80),TRUPT(80),IRUPT(80),JRUPT(80)
DIMENSION TPEN(80),IPEN(80)
DIMENSION IJPR(76)
DIMENSION AITAJ(9)
DIMENSION FSPDI(40,3),SA(40,3),SB(40,3)
DIMENSION DRI(76)
COMMON DRI
COMMON FSPDI,SA,SB
COMMON AITAJ
COMMON XNBAR,XPRAR,YNBAR,YPRAR,ZNBAR,ZPRAR,TPEN
COMMON SUMDF,TRUPT,DXDA,SC
COMMON XACC,YACC,ZACC
COMMON C,CHAR
COMMON DP,DPX,DPY,DPZ,DPL,DPM,DPN
COMMON PIN,QIN,RIN,PINO,QINO,DPIN,DQIN,DRIN
COMMON OXIJ,OYIJ,OZIJ,ZC
COMMON XXX,XXJ,XYK,XYJ,XZK,XZJ,XLK,XLJ,XMK,XMJ,XNK,XNJ
COMMON XOLD,YOLD,ZOLD,PHIOLD,THEOLD,PSICLD,POLD,QOLD,ROLD,UOLD,
1 VOLD,WOLD,DTZ,DTHALF
COMMON PHI,THETA,PSI
COMMON BIJ,PSIDOT,THEDOT,PHIDOT,CIJ,X,Y,Z,XIJ,YIJ,ZIJ,D,DF
COMMON AI,AIDOT,AJ,AIJ,DX,DY,DZ,DPHI,DTHETA,DPSI,DVSIGN
COMMON VFE,FMRAR,F4,XKS,XKI,VMAX
COMMON XX,XY,XZ,XL,XM,XN,W,Z,ALIFT,XC,P,Q,R,U,V,W
COMMON UDOT,VDOT,WDOT,XZI,YZI,ZI,HFZ,XI,XYI,HLX,YI,HEY,DFLI
COMMON PDOT,XI1,XI2,XI3,ODOT,XI5,XI4,PDOT,XI6,XDOT,YDOT,ZDOT

```

CRS14010

CRS12380

CRS12390

CRS12400

CRS12410

CRS12420

CRS12430

CRS12440

CRS12450

CRS12460

CRS12470

CRS12480

CRS12490

CRS12500

CRS12510

CRS12520

CRS12530

CRS00180

CRS12550

CRS12560

CRS12570

CRS12580

CRS12590

CRS12600

CRS12610

CRS12620

CRS00230

CRS00240

CRS00250

CRS00280

CRS14330

CRS00300

CRS14360

CRS14370

CRS14380

CRS14390

CRS14400

CRS14410

CRS14420

CRS14430

CRS00400

CRS14450

CRS14460

CRS14470

Figure 20. (Continued)

```

CJMMJN      XLBAR,SF,FSPDF,XKE,FSBAR,XMU,VEEDOT      CRS00440
CJMMJN XGDOT,YGDOT,ZGDOT,PPR,QPR,RPR,PHIPR,THEPR,PSIPR      CRS00360
CJMMJN PHIDP,THEDP,PSIDP,XDP,YDP,ZDP,OAI,DELTAT,TMAX,TIME,TITLE      CRS14500
CJMMJN PHIIJ,THEIJ,PSIIJ,XK,DIJ,XLBAR,SI,XLNGYH,IP      CPS00470
CJMMJN NM,I,J,ILAST,ITABIJ,ITAB6,IJLIJ,IJLIJ,IJKK,IJL,IG,JG,ITAB,CPS14520
1 ITABD,IJKL,ITABL1,IPRINT,ITABLE,ILINES,NPK,IGS,IISP,ISP,IBS,N,HNCRS00490
CJMMJN KRUP,T,IRUP,T,IRUP,T
CJMMJN INDP,IPEN,KPFN
CJMMJN IJPR
CJMMJN PLOT,ZAR,TMPLOT,IPLDT,IDPLOT,IPLSW,IPLC,JPLOT,NPLOT,ITPLOT
EQUIVALENCE (PPR,XMPR(1)),
1 (PHIDPR,ANGDPR(1)),(THEDPR,ANGDPR(2)),(PSIDPR,ANGDPR(3))      CRS12800
EQUIVALENCE (XKS(1),XKS3(1,1,1)),(XKI(1),XKI3(1,1,1)),      CRS12810
1 (XKRI(1,1,1),FMBAP(1)),(FMI(1),FMI3(1,1,1)),(VEE(1),VEE2(1,1))      CRS12820
EQUIVALENCE (FMBAR(1),FMBAR3(1,1,1)),(N(1),N3(1,1)),(NN(1,1)),      CRS12830
1 VV2(1,1)),(FSPBAR(1,1),FSPBAR2(1,1)),(IBS(1,1),IBS2(1,1))      CRS12840
EQUIVALENCE (XLBAR2(1,1),XLBAR(1,1)),(ISP2(1,1),ISP(1,1))      CRS12850
SIN(X) = DSIN(X)      CRS12860
COS(X) = DCOS(X)      CRS12870
SQR(X) = DSQR(X)      CRS12880
ARSIN(X) = DAR SIN(X)      CRS12890
ATAN2(Y,X) = DATAN2(Y,X)      CRS12900
WTOT = 0.0      CRS12910
D1 10 I = 1,NM      CRS14600
10 WTOT = WTOT+WGT(I)      CRS14610
XGDP = 0.0      CRS14620
YGDP = 0.0      CRS14630
ZGDP = 0.0      CRS14640
D1 20 I = 1,NM      CRS14650
XGDP = XGDP+WGT(I)*XDP(I)      CRS14660
YGDP = YGDP+WGT(I)*YDP(I)      CRS14670
20 ZGDP = ZGDP+WGT(I)*ZDP(I)      CRS14680
XGDP = XGDP/WTOT      CRS14690
YGDP = YGDP/WTOT      CRS14700
ZGDP = ZGDP/WTOT      CRS14710
C APPRIME AND ABARPRIME (3)      CRS14720
CALL EULER(AOR,PHIPR,THEPR,PSIPR)      CRS14730
S1 = SIN(PHIPR)      CRS14740
C1 = COS(PHIPR)      CRS14750
S2 = SIN(THEPR)      CRS14760
C2 = COS(THEPR)      CRS14770
C NOW ABARPRIME (4)      CRS14780
ABARPR(1,1) = 1.0      CRS14790
ABARPR(2,1) = 0.0      CRS14800
ABARPR(3,1) = 0.0      CRS14810
ABARPR(1,2) = S1*S2/C2      CRS14820
ABARPR(2,2) = C1      CRS14830
ABARPR(3,2) = S1/C2      CRS14840
ABARPR(1,3) = C1*S2/C2      CRS14850
ABARPR(2,3) = -S1      CRS14860
ABARPR(3,3) = C1/C2      CRS14870
C ANGLE DOT PRIMES (4)      CRS14880
CALL MATVEC(ABARPR,XMPR,ANGDPR,0)      CRS14890
C D PRIME (7)      CRS14900
DPR(1,1) = 0.0      CRS14910
DPR(1,2) = THEDPR*S1-PSIDPR*C1*C2      CRS14920
DPR(1,3) = THEDPR*C1+PSIDPR*S1*C2      CRS14930
DPR(2,1) = -DPR(1,2)      CRS14940
DPR(2,2) = 0.0      CRS14950
DPR(2,3) = -PHIDPR+PSIDPR*S2      CRS14960

```

Figure 20. (Continued)

OPR(3,1) = -OPR(1,3)	CRS14980
OPR(3,2) = -OPR(2,3)	CRS14990
OPR(3,3) = 0.0	CRS15000
C A DOT PRIME (8)	CRS15010
CALL MATMUL(APR,OPR,ADPR)	CRS15020
ZCMAX = 0.0	CRS15030
C LOOP A	CRS15040
DO 40 I = 1,NM	CRS15050
C AI DOUBLE PRIME (9)	CRS15060
CALL EULER(AIDP,PHIDP(I),THEDP(I),PSIDP(I))	CRS15070
C AI (10)	CRS15080
CALL MATMUL(APR,AIDP,AIC)	CRS15090
THETA(I) = -ARCSIN(AIC(3,1))	CRS13420
CT = 1.0/COS(THETA(I))	CRS13430
PHI(I) = ARCSIN(AIC(3,2)*CT)	CRS13440
PSI(I) = ARCSIN(AIC(3,1)*CT)	CRS13450
C (12)	CRS15180
VJP(I,1) = XGOP-XDP(I)	CRS15190
VJP(I,2) = YGOP-YDP(I)	CRS15200
VJP(I,3) = ZGOP-ZDP(I)	CRS15210
---C LOOP B	CRS15220
DO 50 K = 1,3	CRS15230
IF(ISP2(I,K)) 40,50,60	CRS15240
60 VC = AIC(3,K)*LBAR2(I,K)	CRS15250
DO 70 L = 1,3	CRS15260
70 VC = VC+APR(3,L)*VJP(I,L)	CRS15270
IF(VC-ZCMAX) 50,50,80	CRS15280
80 ZCMAX = VC	CRS15290
50 CONTINUE	CRS15300
C END OF LOOP A	CRS15310
40 CONTINUE	CRS15320
IF(ZG) 220,210,220	CRS15330
210 ZG = -ZCMAX-.00100	CRS15340
C SEE IF PHI'', ETC. ARE ALL ZERO	CRS15350
220 DO 100 I = 1,NM	CRS15360
IF(PHIDP(I)) 150,110,150	CRS15370
110 IF(THEDP(I)) 150,120,150	CRS15380
120 IF(PSIDP(I)) 150,100,150	CRS15390
100 CONTINUE	CRS15400
C IF WE GET HERE WE COMPUTE NEW THETA(I,J) AND PSI(I,J)	CRS15410
PI = 3.1415926535897932400	
PI2 = .500*PI	
DO 200 IJ = 1,IGS	CRS15430
I = IG(IJ)	CRS15440
J = JG(IJ)	CRS15450
XIJP = VJP(J,1)-VJP(I,1)	CRS15460
YIJP = VJP(J,2)-VJP(I,2)	CRS15470
ZIJP = VJP(J,3)-VJP(I,3)	CRS15480
IF(YIJP) 140,130,140	CRS15490
130 IF(XIJP) 180,170,180	CRS15500
180 PSI(IJ(IJ)) = 0.0	CRS15510
THET(IJ(IJ)) = -ATAN2(ZIJP,XIJP)	CRS13800
GO TO 200	CRS15530
170 PSI(IJ(IJ)) = 0.0	CRS15540
THET(IJ(IJ)) = -PI2	CRS15550
IF(ZIJP) 160,200,200	CRS15560
160 THET(IJ(IJ)) = PI2	CRS15570
GO TO 200	CRS15580
140 PSI(IJ(IJ)) = ATAN2(YIJP,XIJP)	CRS13870
THET(IJ(IJ)) = -ATAN2(ZIJP,SQRT(XIJP*XIJP+YIJP*YIJP))	CRS13880

Figure 20. (Continued)

200 CONTINUE	CRS15610
C LOOPC	CRS15620
150 DO 90 I = 1,NM	CRS15630
VIP(1) = VJP(I,1)	CRS15640
VIP(2) = VJP(I,2)	CRS15650
VIP(3) = VJP(I,3)	CRS15660
C (14)	CRS15670
CALL MATVEC(APRVIP,XV,0)	CRS15680
XV(3) = XV(3)+ZG	CRS15690
X(1) = XV(1)	CRS15700
Y(1) = XV(2)	CRS15710
Z(1) = XV(3)	CRS15720
C (15)	CRS15730
CALL MATVEC(ADPR,VIP,XV,0)	CRS15740
XV(1) = XV(1)+XGDOT	CRS15750
XV(2) = XV(2)+YGDOT	CRS15760
XV(3) = XV(3)+ZGDOT	CRS15770
XDOT(1) = XV(1)	CRS15780
YDOT(1) = XV(2)	CRS15790
ZDOT(1) = XV(3)	CRS15800
C (16)	CRS15810
CALL MATVEC(AIC,XV,VIP,1)	CRS15820
U(1) = VIP(1)	CRS15830
V(1) = VIP(2)	CRS15840
W(1) = VIP(3)	CRS15850
C (17)	CRS15860
CALL MATVEC(AIDP,XMPR,VIP,1)	CRS15870
P(1) = V(1)	CRS15880
Q(1) = V(2)	CRS15890
R(1) = V(3)	CRS15900
C ATBAR (18)	CRS15910
S1 = SIN(PHI(1))	CRS15920
C1 = COS(PHI(1))	CRS15930
S2 = SIN(THETA(1))	CRS15940
C2 = COS(THETA(1))	CRS15950
ABARPR(1,2) = S1*S2/C2	CRS15960
ABARPR(2,2) = C1	CRS15970
ABARPR(3,2) = S1/C2	CRS15980
ABARPR(1,3) = C1*S2/C2	CRS15990
ABARPR(2,3) = -S1	CRS16000
ABARPR(3,3) = C1/C2	CRS16010
C (19)	CRS16020
CALL MATVEC(ABARPR,VIP,XV,0)	CRS16030
PHIDOT(1) = XV(1)	CRS16040
THEDOT(1) = XV(2)	CRS16050
PSIDOT(1) = XV(3)	CRS16060
C END LOOP C	CRS16070
90 CONTINUE	CRS16080
PRINT 301	
301 FORMAT(1H,'IJ,THEIJ(IJ),PSIIJ(IJ)')	
PRINT 300,(IJ,THEIJ(IJ),PSIIJ(IJ),IJ=1,IGS)	
300 FORMAT(1H,'IS,IPZ(15,5)')	
RETURN	CRS16090
END	CRS16100

Figure 20. (Continued)

```

SUBROUTINE PRINT
IMPLICIT REAL*8 (A-H,O-Z)
REAL*4 PLOT(3000),ZAR,TMPLOT(500)
DIMENSION SC(4,3),ZAR(200),IPLOT(150),IDPLOT(150)
DIMENSION IG(80),JS(80),PHIJ(80),THEIJ(80),PSIJ(80),WG(40),
1 XI(40),YI(40),ZI(40),XYI(40),YZI(40),XZI(40),HEX(40),HEY(40),
2 HEZ(40),ALIFT(40),X(40),Y(40),Z(40),PHI(40),THETA(40),PSI(40),
3 U(40),V(40),W(40),P(40),Q(40),R(40),XDOT(40),YDOT(40),ZDOT(40),
4 PHIDOT(40),THEDOT(40),PSIDOT(40),UDOT(40),VDOT(40),WDOT(40)
DIMENSION AIJ(5),AJ(9),AI(9),AIDOT(9),DX(40),DY(40),DZ(40),
1 DPHI(40),DTHETA(40),DPSI(40),DI(6),DF(6),XX(40),XY(40),XZ(40),
2 XL(40),XM(40),XN(40),DELI(40),XII(40),XIZ(40),XIS(40),
3 XIS(40),XIS(40),XIS(40),XK(2880),FMBAR(2880),FMBAR3(6,6,80),
4 F4(2880),XKRIN(10,6,80),VEE(480),VMAX(480),NN(40,3),NN2(40,3)
DIMENSION XKI(9,6,80),DIJ(360),CIJ(360),DIJ(720),XLBAR(40,3),
1 XLBAR(3),ISPI(40,3),IISPI(3),XMU(40,3),XKF(6,3),DAI(360),
2 IS(40,3),IS2(40,3),SI(40,3),SF(40,3),FSPDF(6,3),PHIDP(40),
3 THEDP(40),PSIDP(40),FSPBP(40,3),FSPBZ(40,3),XLNGTH(3),XC(6),
4 XDP(40),YDP(40),ZDP(40),F3(6,6,80),VEE2(6,80),VEEDOT(3,3)
DIMENSION PDOT(40),DDOT(40),MDOT(40),N(480),N3(80,6),OVSIGN(6),
1 XCS(4320),XKS(9,6,80),XKI(4320),TITIE(10)
DIMENSION XOLD(40),YOLD(40),ZOLD(40),PHICLD(40),THECLD(40),
1 PSICLD(40),PCLD(40),QCLD(40),RCLD(40),UCLD(40),VCLD(40),WCLD(40)
DIMENSION XX(80),XXJ(80),XYK(80),XYJ(80),XZK(80),XZJ(80),
1 XLK(80),XLJ(80),XMK(80),XMJ(80),XNK(80),XNJ(80)
DIMENSION OXIJ(80),OYIJ(80),OZIJ(80)
DIMENSION PIN(40),QIN(40),RIN(40),PINO(40),QINO(40),RINO(40),
1 DIN(40),DOIN(40),DRIN(40)
DIMENSION DO(6),DPXI(40),DPY(40),DPZ(40),DPL(40),DPM(40),DPN(40)
DIMENSION C(6,80),CBAR(80),DXDA(6,80)
DIMENSION XACC(40),YACC(40),ZACC(40)
DIMENSION SUMDF(6,80),TRUPT(80),TRUPT(80),JRUPT(80)
DIMENSION TPEN(80),IPEN(80)
DIMENSION IJPR(76)
DIMENSION AITAJ(9)
DIMENSION FSPDI(40,3),SA(40,3),SB(40,3)
DIMENSION DRI(76)
COMMON DRI
COMMON FSPDI,SA,SB
COMMON AITAJ
COMMON XNBAR,XPRAR,YNBAR,YPRAR,ZNBAR,ZPRAR,TPEN
COMMON SUMDF,TRUPT,DXDA,SC
COMMON XACC,YACC,ZACC
COMMON C,CBAR
COMMON DO,DPX,DPY,DPZ,DPL,DPM,DPN
COMMON PIN,QIN,RIN,PINO,QINO,RINO,DOIN,DRIN
COMMON OXIJ,OYIJ,OZIJ,ZG
COMMON AXK,XXJ,XYK,XYJ,XZK,XZJ,XLK,XLJ,XMK,XMJ,XNK,XNJ
COMMON XOLD,YOLD,ZOLD,PHICLD,THECLD,PSICLD,PCLD,QCLD,RCLD,UCLD,
1 VCLD,WCLD,DZ,DTHALF
COMMON PHI,THETA,PSI
COMMON SIJ,PSIDOT,THEDOT,PHIDOT,CIJ,X,Y,Z,XIJ,YIJ,ZIJ,D,DF
COMMON AI,AIDOT,AJ,AIJ,DX,DY,DZ,DPHI,DTHETA,DPSI,CVSIGH
COMMON VEE,FMBAR,FM,XKS,XAI,VMAX
COMMON XX,XY,XZ,XL,XM,XN,WJT,ALIFT,XC,P,G,R,U,V,W
COMMON UDOT,VDOT,WDOT,XZI,YZI,ZZI,HEZ,XI,XYI,MYI,MEY,DEI
COMMON PDOT,XI1,XI2,XI3,ZDOT,XI5,XI4,PDOT,XI5,XDOT,YDOT,ZDOT
COMMON XLBAR,SF,FSPDF,XKF,FSPBP,XMU,VEEDOT
COMMON XGDOT,YGDOT,ZGDOT,PPR,PPF,PPR,P4IPR,THEPR,PSIPR
COMMON PHIDP,THEDP,PSIDP,XDP,YDP,ZDP,DAI,DELIAT,TMAX,TIME,TITLE

```

CRS16110

CRS14410

CRS14420

CRS14430

CRS14440

CRS14450

CRS14460

CRS14470

CRS14480

CRS14490

CRS14500

CRS14510

CRS14520

CRS14530

CRS14540

CRS14550

CRS14560

CRS00180

CRS14580

CRS14590

CRS14600

CRS14610

CRS14620

CRS00230

CRS00240

CRS00250

CRS00280

CRS16400

CRS00300

CRS16430

CRS16440

CRS16450

CRS16460

CRS16470

CRS16480

CRS16490

CRS16500

CRS00400

CRS16520

CRS16530

CRS16540

CRS00440

CRS00460

CRS16570

Figure 20. (Continued)

```

CJ44JN PHIJ,THEIJ,PSIJ,XK,DIJ,XXLBAR,SI,XLNGTH,IP          CFS00470
CJ44JN NY,I,J,ILAST,ITABIJ,ITAB6,IJLIJ,IJLIJ,IJKK,IJL,IG,JG,ITAB,CRS16590
1 ITABD,IJCL,ITABLI,IPRINT,ITABLE,ILINES,NPP,IGS,IISP,ISP,IBS,N,NWCRS00490
CJ44JN KRUP,T,IRUP,T,IRUP,T
CJ44JN INDP,IPEN,KPEN
CJ44JN IJUR
CJ44JN PLOT,ZAR,THPLOT,IPLOT,IPLOT,IPLOT,IPLOT,IPLOT,IPLOT,IPLOT
EQUIVALENCE (XKSI(1),XKSI(1,1,1)),(XKI(1),XKI(1,1,1)),          CRS14800
1 (XKRI(1,1,1),FMBAR(1)),(FM(1),FM3(1,1,1)),(VEE(1),VEE2(1,1)) CRS14810
EQUIVALENCE (FMBAR(1),FMBAR3(1,1,1)),(N(1),N3(1,1)),(NN(1,1), CRS14820
1 NV2(1,1)),(FSPBA1(1,1),FSPBA2(1,1)),(BS(1,1),BS2(1,1))      CRS14830
ILINES = 60
IPL = 6
ITTL = 9
C FORCE NEW PAGE
NPR = 1000
DO 99 I = 1,NM
IF (ILINES-NPP-IPL) 10,20,20
10 PRINT 100, TITLE
100 FPRMAT(IH1,10AE,/)
PRINT 200, TIME
200 FPRMAT(IH,6HTIME*,F9.5,/)
PRINT 300
PRINT 400
PRINT 500
PRINT 600
PRINT 900
300 FPRMAT(IH,18X,1HX,14X,1HY,14X,1H2,13X,3HPHI,11X,5HMETHA, CRS16790
1 11X,3HPSI)
400 FPRMAT(IH,17X,4HXDOT,11X,4HYDOT,11X,4HZDOT,10X,5HPHIDOT, CRS16800
1 8X,8HMETADOT,3X,6HPSIDOT)
500 FPRMAT(IH,18X,1HU,14X,1HV,14X,1HW,14X,1HP,14X,1HQ,14X,1HR) CRS16810
600 FPRMAT(IH,17X,4HVDOT,11X,4HVDOT,11X,4HVDOT,11X,4HVDOT,11X, CRS16820
1 4HVDOT,11X,4HVDOT)
900 FPRMAT(IH,16X,6HXACCEL,9X,6HYACCEL,9X,5HZACCEL,/)
NPR = ITTL
20 NPR = NPR+IPL
PRINT 700, I,X(I),Y(I),Z(I),PHI(I),THETA(I),PSI(I)
PRINT 800, XDOT(I),YDOT(I),ZDOT(I),PHIDOT(I),THEDOT(I),PSIDOT(I)
PRINT 800, U(I),V(I),W(I),P(I),O(I),R(I)
PRINT 800, UDOT(I),VDOT(I),WDOT(I),PDOT(I),QDOT(I),RDOT(I)
PRINT 800, XACC(I),YACC(I),ZACC(I)
PRINT 800
700 FPRMAT(IH,5HMASS,72,2X,1P6F15.5)
800 FPRMAT(IH,9X,1P6E15.5)
99 CONTINUE
PRINT 830
830 FPRMAT(IH,'IG(IJ),JG(IJ),SUMOF(1,IJ),SUMOF(2,IJ),SUMOF(3,IJ),'
1 'SUMOF(4,IJ),SUMOF(5,IJ),SUMOF(6,IJ)')
PRINT 810,(IG(IJ),JG(IJ),(SUMOF(K,IJ),K=1,6),IJ=1,IGS)
PRINT 831
831 FPRMAT(IH,'IG(IJ),JG(IJ),VEE2(1,IJ),VEE2(2,IJ),VEE2(3,IJ),VEE2(4,
1 IJ),VEE2(5,IJ),VEE2(6,IJ)')
PRINT 810,(IG(IJ),JG(IJ),(VEE2(K,IJ),K=1,6),IJ=1,IGS)
810 FPRMAT(IH,1X,12,2X,12,2X,1P6E15.5)
PRINT 832
832 FPRMAT(IH,'I,SC(I,1),SC(I,2),SC(I,3)')
DO 50 I = 1,NM
DO 50 J = 1,3
IF (ISP(I,J),NE,Q) GO TO 60

```

Figure 20. (Continued)

```

50 CONTINUE
60 GO TO 60
80 PRINT 820, I, (SC(I,J), J=1,3)
820 FORMAT(1H, I7, 3X, 1P3E15.3)
40 CONTINUE
ISET=0
DO TO I=1,76
IF (IJPRI(I).EQ.0) GO TO 70
IF (ISET.EQ.1) GO TO 65
PRINT 821
821 FORMAT(1H, //1X, 'MASS', 7X, 'CRI')
ISET=1
65 PRINT 822, JG(I), DRI(I)
70 CONTINUE
822 FORMAT(1H, 1X, 12, 3X, 1P3E15.3)
RETURN
END
SUBROUTINE SAVE
IMPLICIT REAL*8 (A-H,O-Z)
REAL*4 PLOT(3000), ZAR, TMPLGT(500)
DIMENSION SC(4,3), ZAR(200), IPLDT(150), IDPLOT(150)
DIMENSION IG(20), JG(20), PHI(1,100), THE(1,100), PSI(1,100), WGT(40),
1 XI(40), YI(40), ZI(40), XYI(40), YZI(40), XZI(40), HEX(40), HEY(40),
2 HEZ(40), ALIFT(40), X(40), Y(40), Z(40), PHI(40), THE(40), PSI(40),
3 UI(40), VI(40), W(40), PI(40), Q(40), R(40), XDOT(40), YDOT(40), ZDOT(40),
4 PHIDOT(40), THEDOT(40), PSIDOT(40), UDOT(40), VDOT(40), WDOT(40)
DIMENSION AIJ(5), AJ(9), AIDOT(9), DX(40), DY(40), DZ(40),
1 DPHI(40), DTHE(40), DPSI(40), D(6), DF(6), XX(40), XY(40), XZ(40),
2 XL(40), XM(40), XN(40), DELT(40), XI1(40), XI2(40), XI3(40),
3 XI4(40), XI5(40), XI6(40), XKI(280), FMBAR(280), FMBAR3(6,6,80),
4 F4I(280), XKRI(10,6,80), VEE(480), VMAX(480), NN(40,3), NN2(40,3)
DIMENSION XKI(219,6,80), XIJ(360), CIJ(360), DIJ(720), XLBAR(40,3),
1 XLBARP(3), ISPI(40,3), IISPI(3), XMU(40,3), XKE(40,3), OAI(360),
2 IBS(40,3), IBS2(40,3), SI(40,3), SF(40,3), FSPDF(40,3), PHIDP(40),
3 THEDP(40), PSIDP(40), FSPBAR(40,3), FSPBA2(40,3), XLNGTH(3), XC(6),
4 XDP(40), YDP(40), ZDP(40), FM3(6,6,80), VEE2(6,80), VEEDOT(3,3)
DIMENSION PDDT(40), QDDT(40), RDDT(40), NI(80), NI2(80,6), DVSIGN(6),
1 XKSI(4320), XKSI2(9,6,80), XKSI(4320), TITLE(10)
DIMENSION XOLD(40), YOLD(40), ZOLD(40), PHIOLD(40), THEOLD(40),
1 PSIOLD(40), PCOLD(40), QOLD(40), POLD(40), UOLD(40), VOLDD(40), WOLD(40)
DIMENSION XXX(60), XXJ(80), XYK(80), XYJ(80), XZK(60), XZJ(80),
1 XL(80), XLJ(80), XMK(80), XMJ(80), XNK(80), XNJ(80)
DIMENSION OXIJ(80), OYIJ(80), OZIJ(80)
DIMENSION PIN(40), DIN(40), PIN(40), QINO(40), FIND(40),
1 OPIN(40), OQIN(40), OPIN(40)
DIMENSION DD(6), DPX(40), DPY(40), DPZ(40), DPL(40), DPM(40), DPN(40)
DIMENSION C(6,80), CBAR(80), DXDA(6,80)
DIMENSION XACC(40), YACC(40), ZACC(40)
DIMENSION SUMDF(6,20), TRUPT(80), ITRUPT(80), JRUPT(80)
DIMENSION TPEN(80), IPEN(80)
DIMENSION IJPRI(76)
DIMENSION AITAJ(9)
DIMENSION FSPDI(40,3), SA(40,3), SB(40,3)
DIMENSION DRI(76)
COMMON DRI
COMMON FSPDI, SA, SB
COMMON AITAJ
COMMON XNBAR, XNBAR, YNBAR, YNBAR, ZNBAR, ZNBAR, TPEN
COMMON SUMDF, TRUPT, DMDA, SC
COMMON XACC, YACC, ZACC
COMMON C, CBAR
COMMON DD, DPX, DPY, DPZ, DPL, DPM, DPN
COMMON PIN, DIN, RIN, PINO, QINO, RINO, OPIN, OQIN, ORIN
COMMON OXIJ, OYIJ, OZIJ, ZG
COMMON XXX, XXJ, XYK, XYJ, XZK, XZJ, XLK, XLJ, XMK, XMJ, XNK, XNJ
COMMON XOLD, YOLD, ZOLD, PHIOLD, THEOLD, PSIOLD, FOLD, GULD, RULD, UOLD,
1 VOLD, WOLD, DT2, DTHALF
COMMON PHI, THEIA, PSI
COMMON BIJ, PSIDOT, THEDOT, PHIDOT, CIJ, X, Y, Z, XIJ, YIJ, ZIJ, D, DF
COMMON AI, AIDOT, AJ, AIJ, DX, DY, DZ, DPHI, DTHE, DPSI, DVSIGN
COMMON VEE, FMBAR, FM, XKI, VMAX
COMMON XX, XY, XZ, XL, XM, XN, WGT, ALIFT, XC, P, Q, R, U, V, W
COMMON UDOT, VDOT, WDOT, XZI, YZI, ZI, HEZ, XI, XYI, HEX, YI, HFI, DELT
COMMON PDDT, XI1, XI2, XI3, QDDT, XI5, XI4, PDDT, XI5, XDOT, YDOT, ZDOT
COMMON XLBAR, S, FSPDF, XKE, FSPBAR, XMU, VEEDOT
COMMON XDDT, YDDT, ZDDT, PPR, QPR, RPR, PHIPR, THEPR, PSIPR
COMMON PHIDP, THEDP, PSIDP, XDP, YDP, ZDP, CAI, CELTAT, TMAX, TIME, TITLE

```

Figure 20. (Continued)

```

COMMON PHIJ,THEIJ,PSIJ,XK,DIJ,XXLMAR,SI,XLNGTH,IP
COMMON N4,I,J,ILAST,ITABIJ,ITAB6,IJLIJ,IJLIIJ,IJL,IG,JG,ITAB,CRS00470
1 ITABD,IJL,ITABL,IPRINT,ITABLE,ILINES,NPR,IGS,IISP,ISP,IBS,N,NMCRS00480
COMMON KRUP,T,IPLUT,JRUPT
COMMON INDP,IPEN,KPEN
COMMON IJPR
COMMON PLOT,ZAR,TMPLT,IPLT,IPLOT,IPLOT,IPLOT,IPLOT,IPLOT,IPLOT,IPLOT
EQUIVALENCE (XKSI(1),XKSI(1,1,1)),(XKSI(1),XKSI(1,1,1)),
1 (XKSI(1,1,1),FMBAR(1)),(FMBAR(1),FMBAR(1,1,1)),(VEE(1),VEE(1,1)) CRS00410
EQUIVALENCE (FMBAR(1),FMBAR(1,1,1)),(FMBAR(1),FMBAR(1,1,1)),(INN(1,1),
1 VV2(1,1)),(FSPBAR(1,1),FSPBAR(1,1)),(IBS(1,1),IBS(1,1)) CRS00420
IPLC = 0
JPLT = JPLT+1
IF(JPLT,GT,IP) RETURN
TMPLT(:PLOT) = TIME
DO 30 I = 1,NPLOT
IS = IPLT(I)
IO = IPLOT(I)
DO 12 (1,2,3,4,5,6,7,8,9,10,11,12,13,14,15,16,17,18,19,20,21,
1 22,23,24,25), IO CRS00430
1 T = X(IS)
GO TO 30
2 T = Y(IS)
GO TO 30
3 T = Z(IS)
GO TO 30
4 T = XDOT(IS)
GO TO 30
5 T = YDOT(IS)
GO TO 30
6 T = ZDOT(IS)
GO TO 30
7 T = XACC(IS)
GO TO 30
8 T = YACC(IS)
GO TO 30
9 T = ZACC(IS)
GO TO 30
10 T = SC(15,1)
GO TO 30
11 T = SC(15,2)
GO TO 30
12 T = SC(15,3)
GO TO 30
13 T = VEE2(1,15)
GO TO 30
14 T = VEE2(2,15)
GO TO 30
15 T = VEE2(3,15)
GO TO 30
16 T = VEE2(4,15)
GO TO 30
17 T = VEE2(5,15)
GO TO 30
18 T = VEE2(6,15)
GO TO 30
19 T = SUMDF(1,15)
GO TO 30
20 T = SUMDF(2,15)
GO TO 30
21 T = SUMDF(3,15)
GO TO 30
22 T = SUMDF(4,15)
GO TO 30
23 T = SUMDF(5,15)
GO TO 30
24 T = SUMDF(6,15)
GO TO 30
25 T=OR(15)
30 PLOT(IP=(1-1)+JPLT) = T
RETURN
END

```

Figure 20. (Continued)



```

SUBROUTINE PRINTM(A,IO,ILINE)
IMPLICIT REAL*8 (A-H,O-Z)
DIMENSION A(3,3)
PRINT 100, IO, ILINE
100 FORMAT(1H, 'MATRIX ', A4, ' ON PAGE ', I3)
PRINT 200, ((A(I,J), J=1,3), I=1,3)
200 FORMAT(1H, 'P2E20.10')
RETURN
END

SUBROUTINE TOLP
IMPLICIT REAL*8 (A-H,O-Z)
REAL*4 PLOT(3000), ZAR, THPLOT(500)
REAL*4 DELX, DELY, DLX, DLY, X=MT, Y=PT, YMIN, YMAX, XMIN, XMAX
DIMENSION SC(4,3), ZAR(200), IYCHAR(3), LIT(3), NAMES(25),
1 I PLOT(150), IDPLOT(150)
DIMENSION IG(80), JS(20), PHITJ(80), THEITJ(80), PSTIJ(80), WGT(40),
1 XI(40), YI(40), ZI(40), XVI(40), YZI(40), XZI(40), HEX(40), HEY(40),
2 HEZ(40), ALIFT(40), X(40), Y(40), Z(40), PHI(40), THETA(40), PSI(40),
3 UI(40), VI(40), XI(40), PI(40), Q(40), R(40), XDOT(40), YDOT(40), ZDOT(40),
4 PHIDOT(40), THEDOT(40), PSIDOT(40), UDOT(40), VDOT(40), WDOT(40)
DIMENSION AIJ(5), AI(9), AJ(9), AIDOT(9), DX(40), DY(40), DZ(40),
1 DPHI(40), DTHETA(40), DPSI(40), D(6), DF(6), XX(40), XY(40), XZ(40),
2 XL(40), XM(40), XN(40), DELI(40), XI1(40), XI2(40), XI3(40),
3 XI4(40), XI5(40), XI6(40), XKI(2880), FMBAR(2880), FMBAR3(6,6,80),
4 F(2880), XKRINI(10,6,80), VEE(480), VMAX(480), NN(40,3), NN2(40,3)
DIMENSION XKI(219,6,80), UIJ(360), CIJ(360), DIJ(720), XLBAR(40,3),
1 XXLBAR(3), ISP(40,3), IIS(3), XMU(40,3), XKF(40,3), DAI(360),
2 IS(40,3), IS2(40,3), SI(40,3), SF(40,3), FSPDF(40,3), PHIDP(40),
3 THEDP(40), PSIDP(40), FSPBAR(40,3), FSPBA2(40,3), XLNGTH(3), XC(6),
4 XDP(40), YDP(40), ZDP(40), FM3(6,6,80), VEE2(6,80), VEEODT(3,3)
DIMENSION PDOT(40), QDOT(40), RDOT(40), NI(480), NI2(80,6), DVSIGM(6),
1 XKS(4320), XKS3(6,6,80), XKI(4320), TITLE(10)
DIMENSION XOLD(40), YOLD(40), ZOLD(40), PHICLD(40), THECLD(40),
1 PSTCLD(40), PCLD(40), QOLD(40), ROLD(40), UOLD(40), VOLD(40), WOLD(40)
DIMENSION XXX(80), XXJ(80), XYK(80), XYJ(80), XZK(80), XZJ(80),
1 XL(80), XLJ(80), XMK(80), XMJ(80), XNK(80), XNJ(80)
DIMENSION OXIJ(80), OYIJ(80), OZIJ(80)
DIMENSION PIN(40), QIN(40), RIN(40), PINO(40), QENO(40), RINO(40),
1 OPIN(40), OQIN(40), ORIN(40)
DIMENSION DDI(6), DPX(40), DPY(40), DPZ(40), DPL(40), DPH(40), DPN(40)
DIMENSION C(6,80), CBAR(80), DXDA(6,80)
DIMENSION XACC(40), YACC(40), ZACC(40)
DIMENSION SUMDF(6,80), TRUPT(80), TRUPT(80), JRUPT(80)
DIMENSION TPEN(80), IPEN(80)
DIMENSION IJPR(76)
DIMENSION AITAJ(9)
DIMENSION FSPDI(40,3), SA(40,3), SS(40,3)
DIMENSION DR(76)
COMMON ORI
COMMON FSPDI, SA, SS
COMMON AITAJ
COMMON XNBAR, XPNAR, YNBAR, YPNAR, ZNBAR, ZPNAR, TPEN
COMMON SUMDF, TRUPT, DXDA, SC
COMMON XACC, YACC, ZACC
COMMON C, CBAR
COMMON DD, DPX, DPY, DPZ, DPL, DPH, DPN
COMMON PIN, QIN, RIN, PINO, QINO, RINO, OPIN, OQIN, ORIN
COMMON OXIJ, OYIJ, OZIJ, ZG
COMMON XXX, XXJ, XYK, XYJ, XZK, XZJ, XLK, XLJ, XMK, XMJ, XNK, XNJ
COMMON XOLD, YOLD, ZOLD, PHICLD, THECLD, PSTCLD, POLD, QOLD, ROLD, UOLD,
1 VOLD, WOLD, DTZ, DTHALF
COMMON PHI, THETA, PSI
COMMON BIJ, PSIDOT, THEDOT, PHIDOT, CIJ, X,Y,Z, XIJ, YIJ, ZIJ, D, DF
COMMON AI, AIDOT, AJ, AIDOT, DX, DY, DZ, DPHI, DTHETA, DPSI, DVSIGM
COMMON VEE, FMBAR, FM, XKS, XKI, VMAX
COMMON XX, XY, XZ, XL, XM, XN, WJ, ALIFT, XC, F, Q, R, U, V, W
COMMON UDOT, VDOT, WDOT, XZI, YZI, ZI, HEZ, XI, XVI, HEX, YI, HEY, DELI
COMMON PDOT, XI1, XI2, XI3, PDOT, XI5, XI4, PDOT, XI6, XDOT, YDOT, ZDOT
COMMON XLBAR, SF, FSPDF, XKE, FSPBAR, XMU, VEEDOT

```

Figure 20. (Continued)



```

YMAX = YMIN
DO 40 J = 2, JPLOT
YMIN = AMIN(YMIN, PLOT(IP*(I-1)+J))
40 YMAX = AMAX(YMAX, PLOT(IP*(I-1)+J))
IF(YMIN.EQ.YMAX) GO TO 10
CALL SUBJEG(ZAR, XMIN, YMIN, XMAX, YMAX)
CALL SETUPG(ZAR, 1, DELX, DELY, IXTM, JYTH, DLX, DLY, XFMT, YFMT)
DO 60 J = 106, 109
60 ZAR(J) = 0.0
CALL GRIDG(ZAR, DELX, DELY, IXTM, JYTH)
CALL SETSMG(ZAR, 45, 1, 0)
CALL LABELG(ZAR, 0, DLX, 0, XFMT)
CALL LABELG(ZAR, 1, DLY, 0, YFMT)
CALL SETSMG(ZAR, 45, 1, 5)
CALL TITLEG(ZAR, 14, 14*TIME (SECONDS), NY, IYCHAR, 70, TITLE)
CALL LINESG(ZAR, JPLOT, YMPLOT, PLOT(IP*(I-1)+1))
C NEW FRAME
CALL PAGEG(ZAR, 0, 1, 1)
10 CONTINUE
RETURN
END

```

Figure 20. (Continued)

## TEST DATA

### RECORDED DATA

The acceleration and strain gage data recorded on the Central Data System (CDS) are presented in Figures 21 through 46. The CDS sample is at a rate of 1500 per sec. This provides 5 samples per cycle for a 300-Hz signal. The list of acceleration channels is presented in Volume I, Table IX. Channels 61 and 62 represent the strain gage data near the leading edge of the forward and aft landing skid struts, respectively. The time of impact is zero (0) on the time scale. Positive times occur after impact.

### 100-CPS LOW-PASS FILTERED TEST DATA

Thirteen acceleration data channels were recorded on FM tape while the full complement of data was being recorded simultaneously in CDS. The channels that were recorded on tape are:

<u>Channel No.</u>	<u>Identification</u>
07	Pilot Seat Pan Vertical Acceleration
08	Pilot Seat Pan Lateral Acceleration
09	Copilot Seat Pan Vertical Acceleration
10	Copilot Seat Pan Lateral Acceleration
30	Copilot Floor Vertical Acceleration
31	Copilot Floor Lateral Acceleration
36	Passenger Floor Vertical Acceleration
40	Transmission Vertical Acceleration
41	Transmission Lateral Acceleration
42	Transmission Axial Acceleration
43	Engine Vertical Acceleration
44	Engine Lateral Acceleration
45	Engine Axial Acceleration

Figures 47 through 59 show the filtered data.

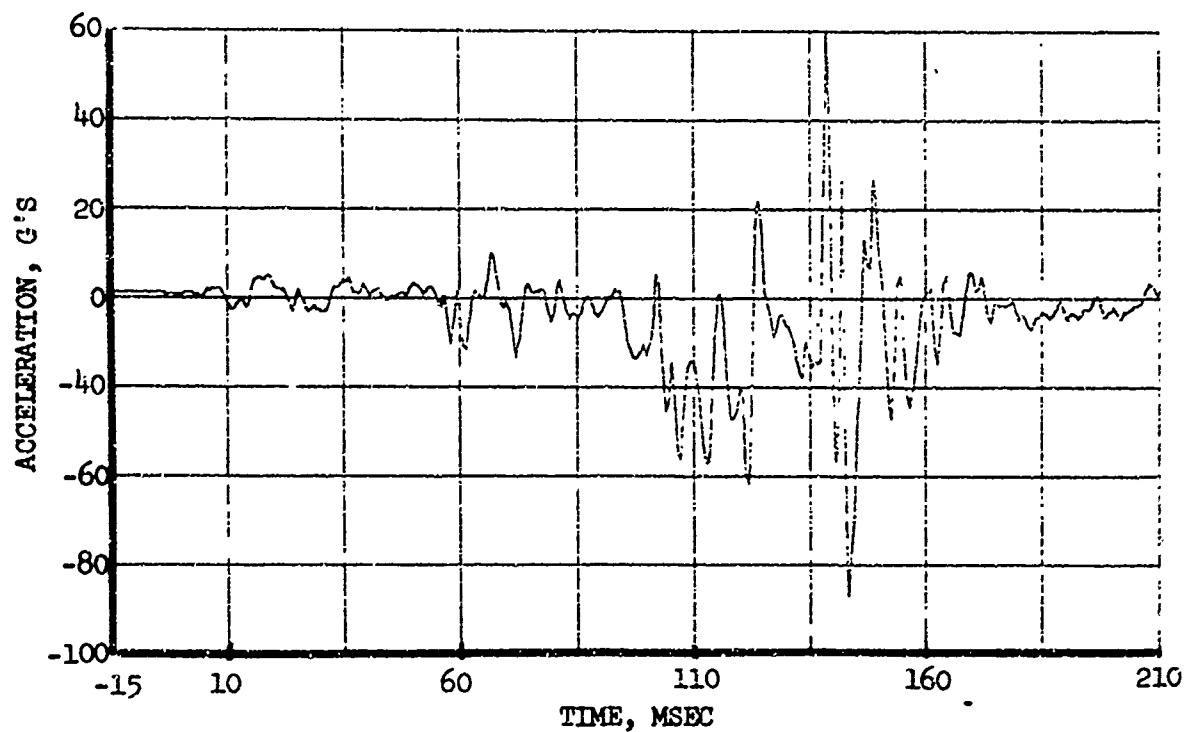


Figure 21. Recorded Time History, Pilot Seat Pan,  
Vertical Acceleration (Channel 07).

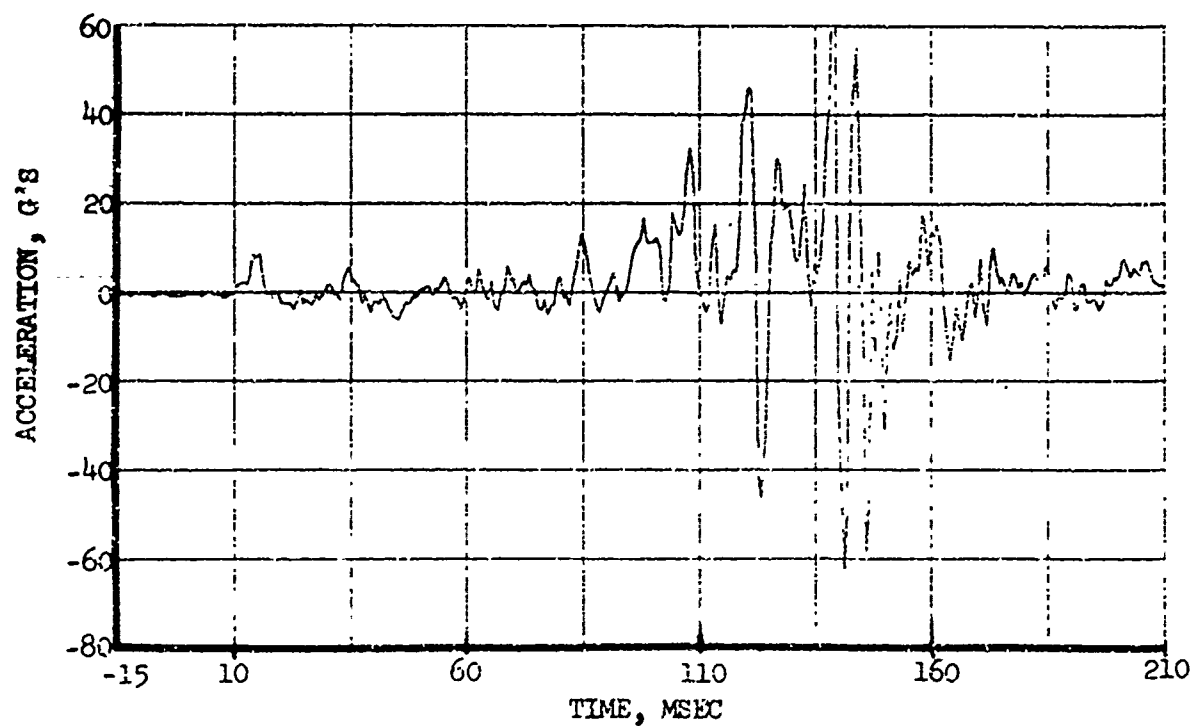


Figure 22. Recorded Time History, Pilot Seat Pan,  
Lateral Acceleration (Channel 08).

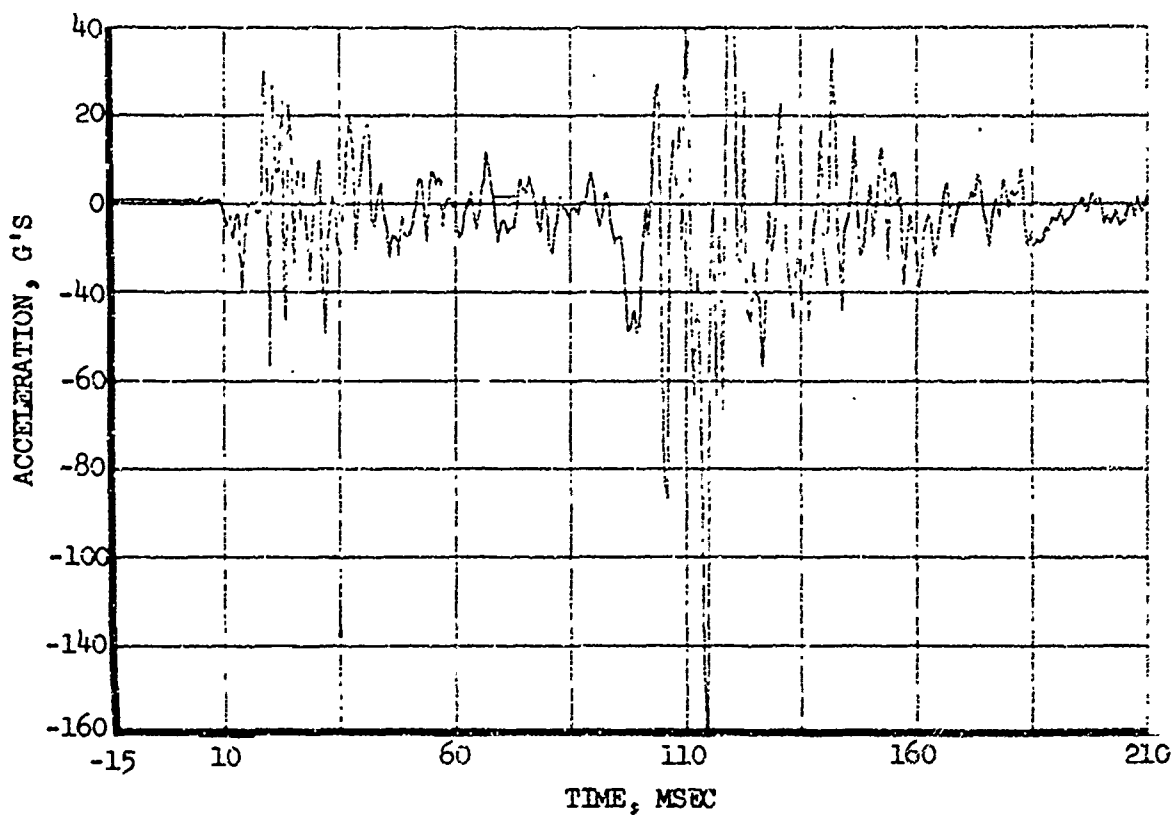


Figure 23. Recorded Time History, Copilot Seat Pan,  
Vertical Acceleration (Channel 09).

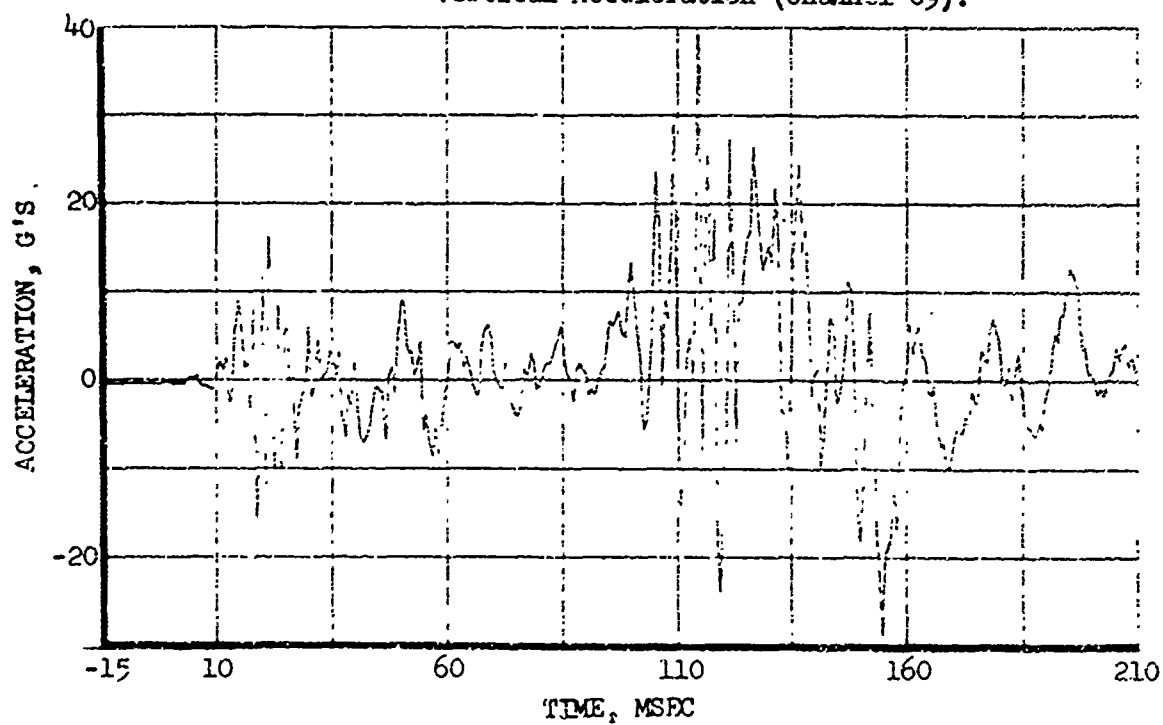


Figure 24. Recorded Time History, Copilot Seat Pan,  
Lateral Acceleration (Channel 10).

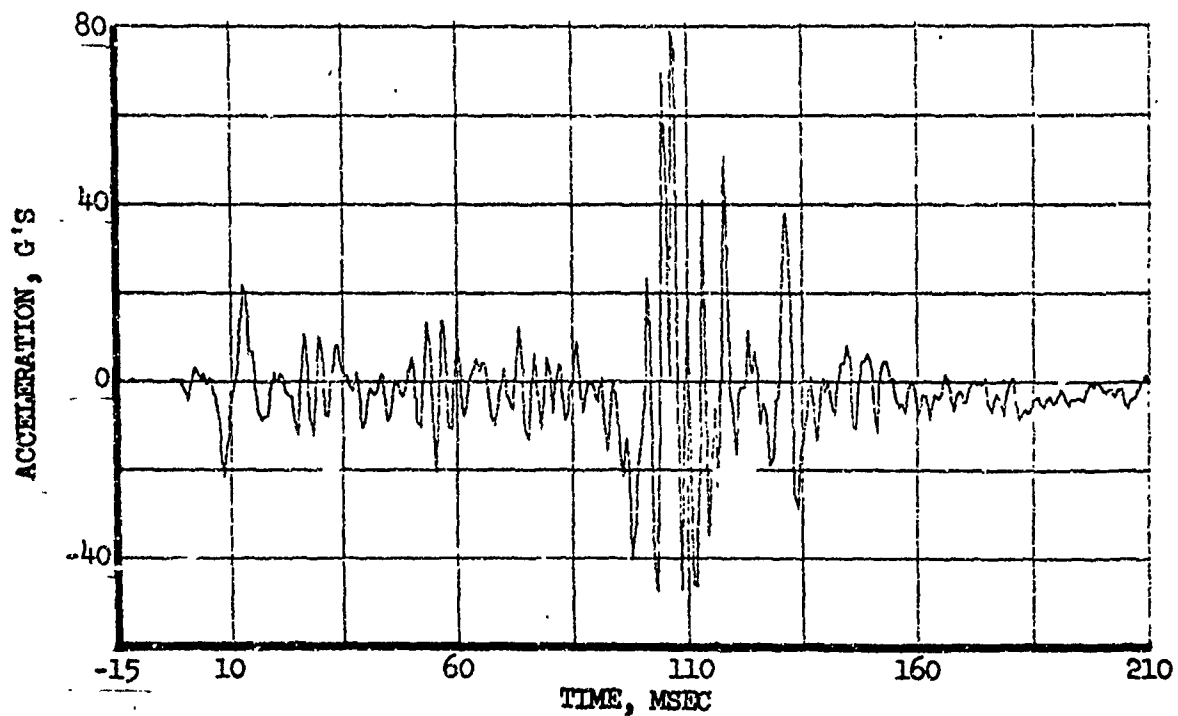


Figure 25. Recorded Time History, Floor Copilot Location, Vertical Acceleration (Channel 30).

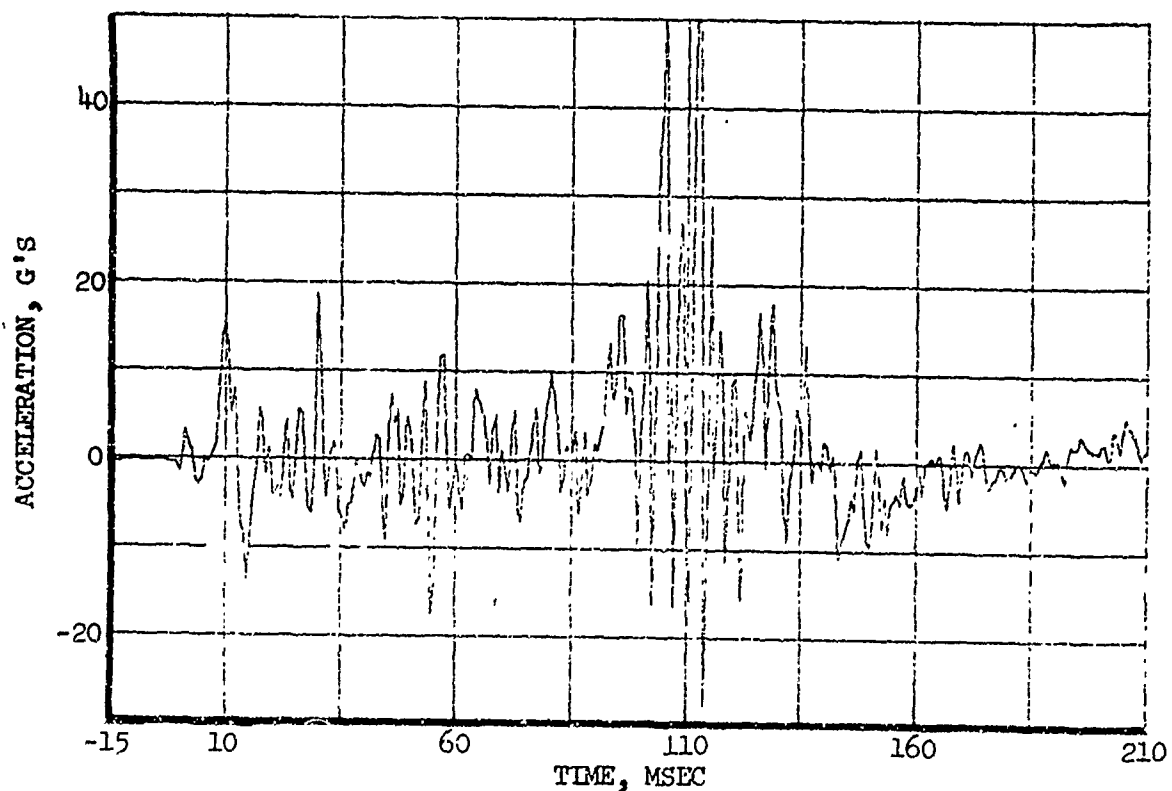


Figure 26. Recorded Time History, Floor Copilot Location, Lateral Acceleration (Channel 31).

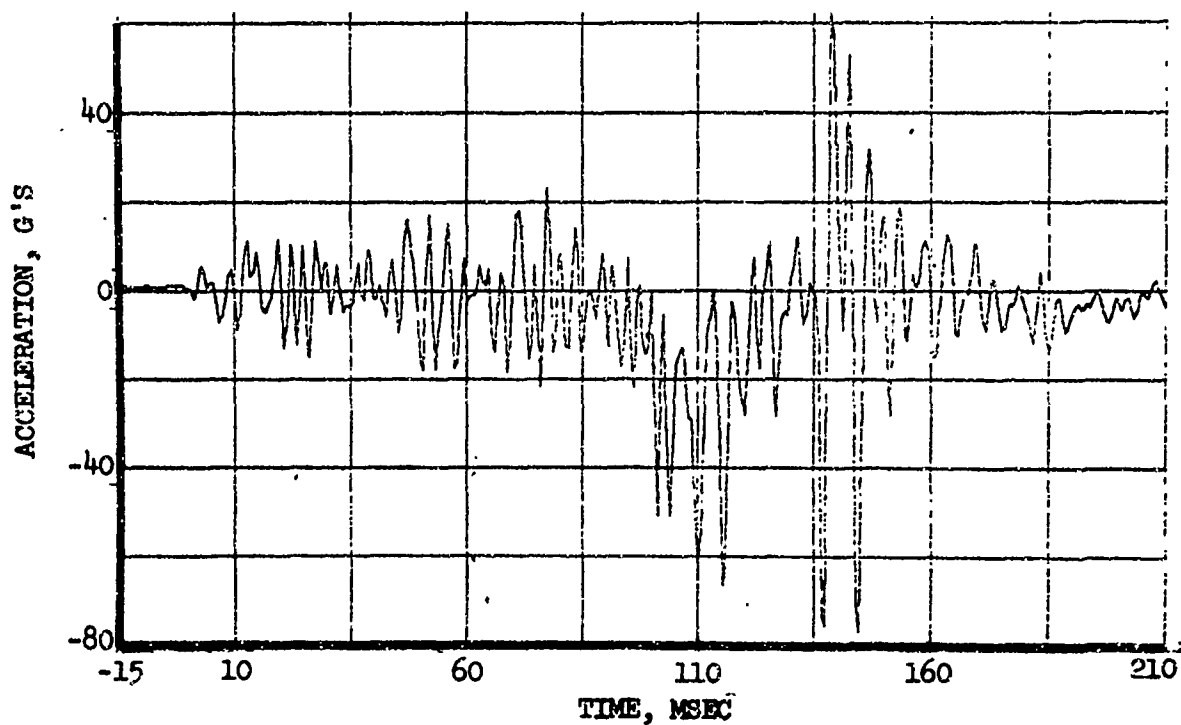


Figure 27. Recorded Time History, Floor Pilot Location, Vertical Acceleration (Channel 32).

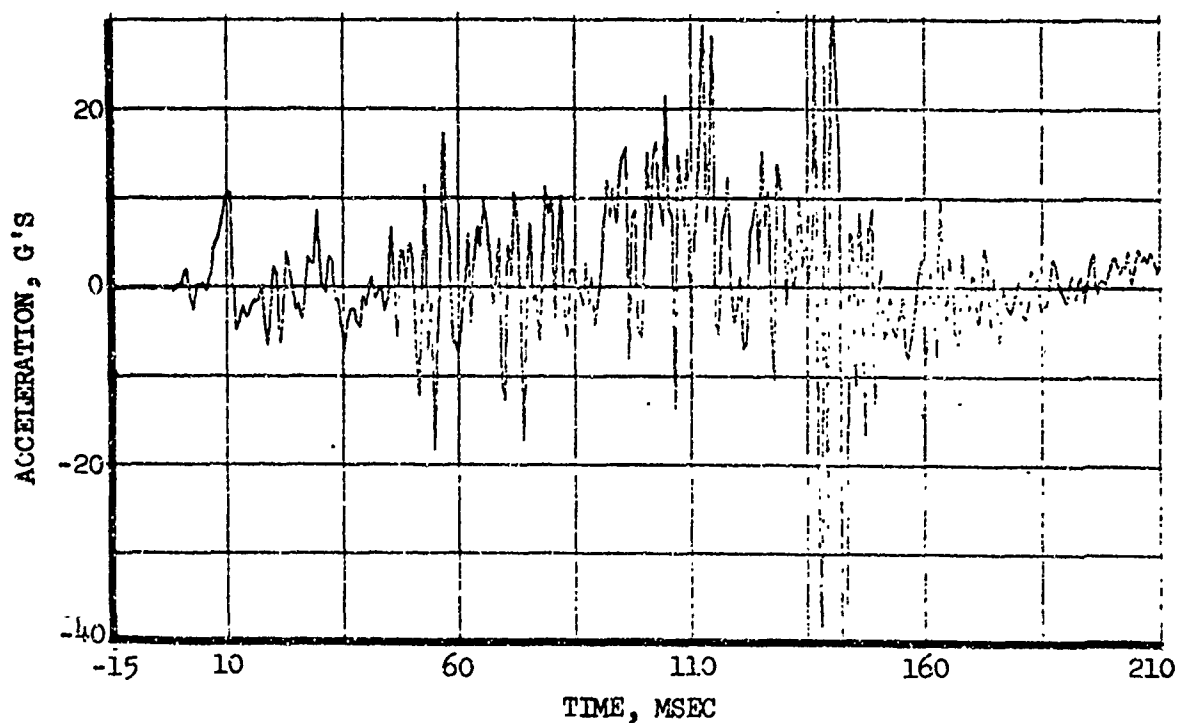


Figure 28. Recorded Time History, Floor Pilot Location, Lateral Acceleration (Channel 33).



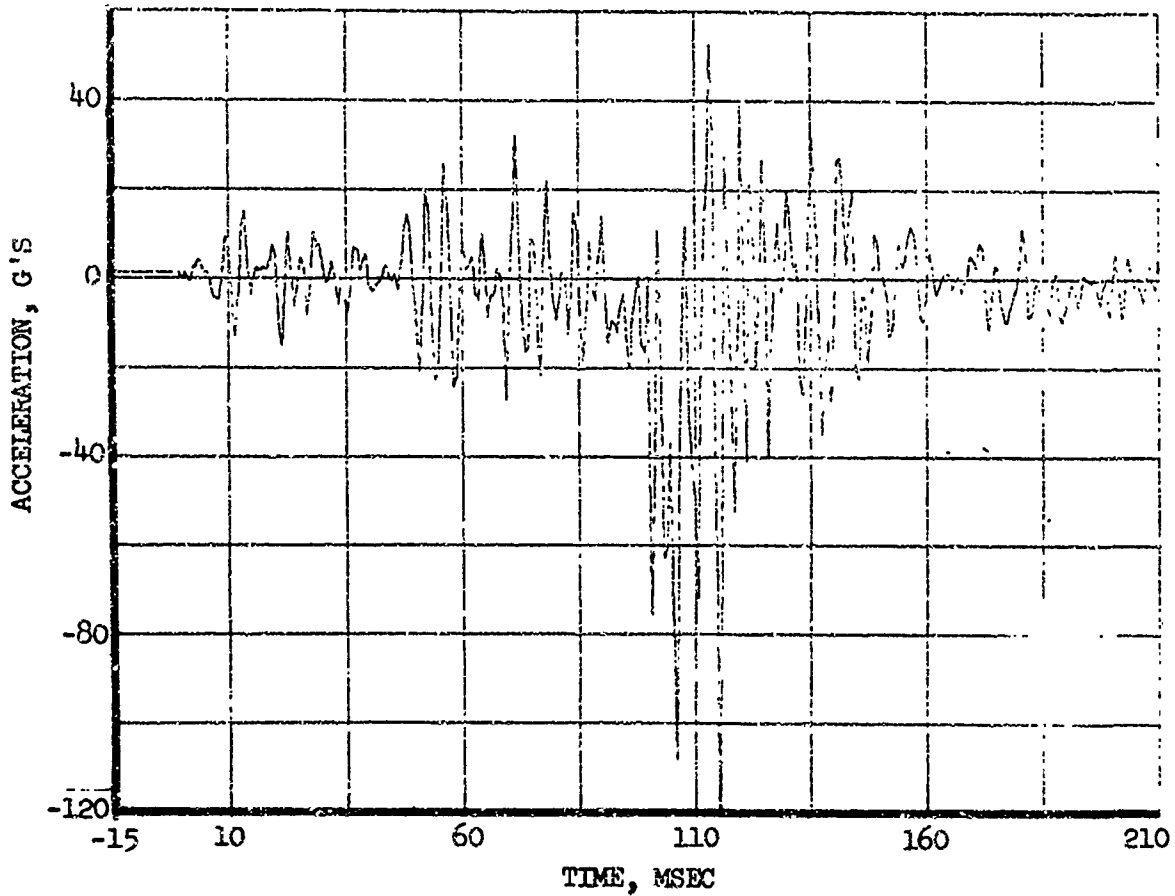


Figure 29. Recorded Time History, Cargo Floor Forward Right, Vertical Acceleration (Channel 34).

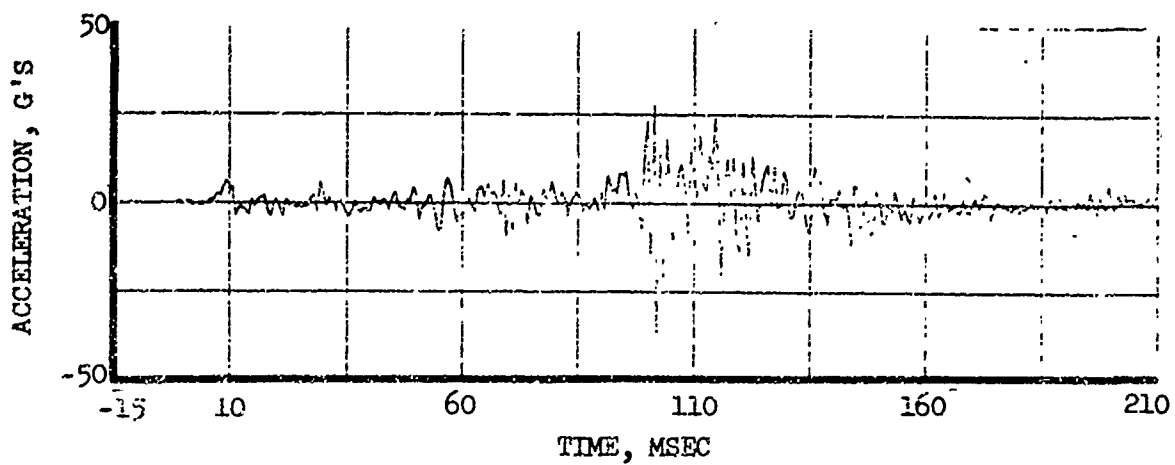


Figure 30. Recorded Time History, Cargo Floor Forward Right, Lateral Acceleration (Channel 35).

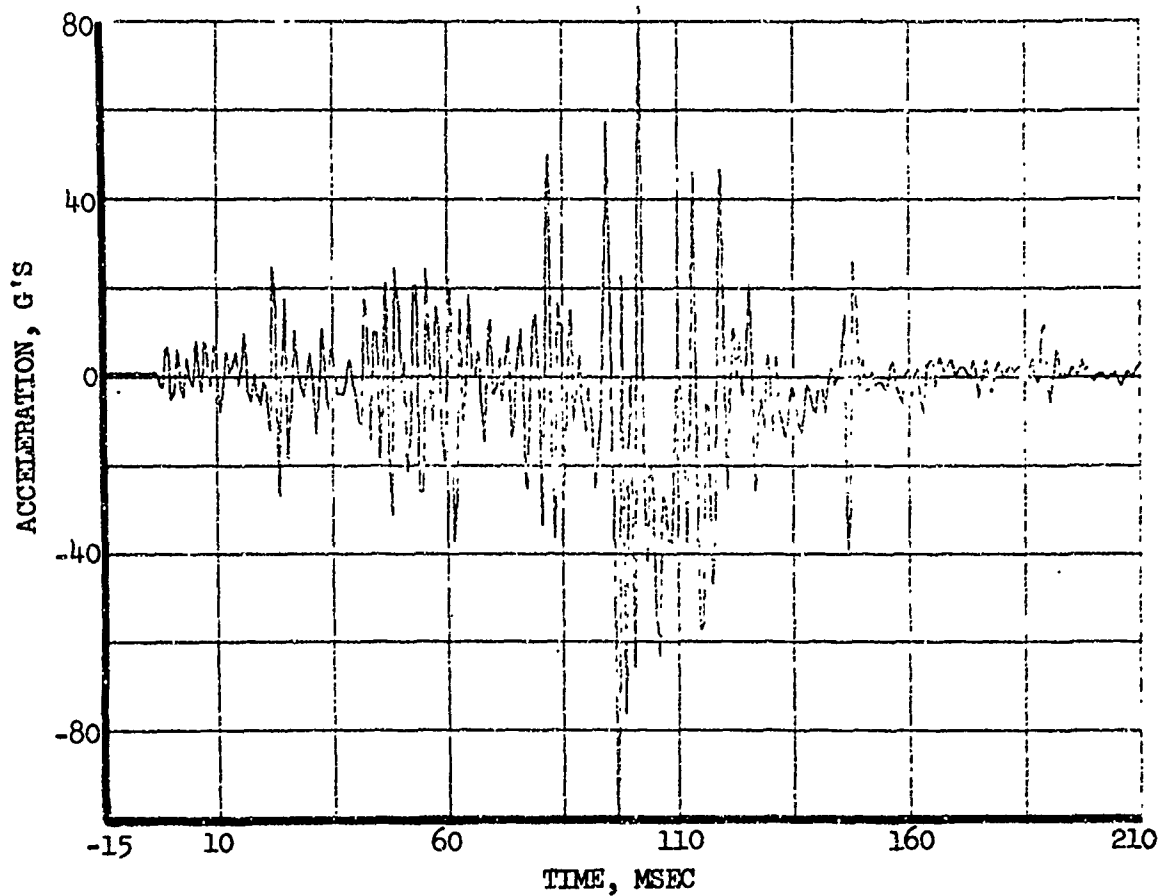


Figure 31. Recorded Time History, PAX Floor Rear Left, Vertical Acceleration (Channel 36).

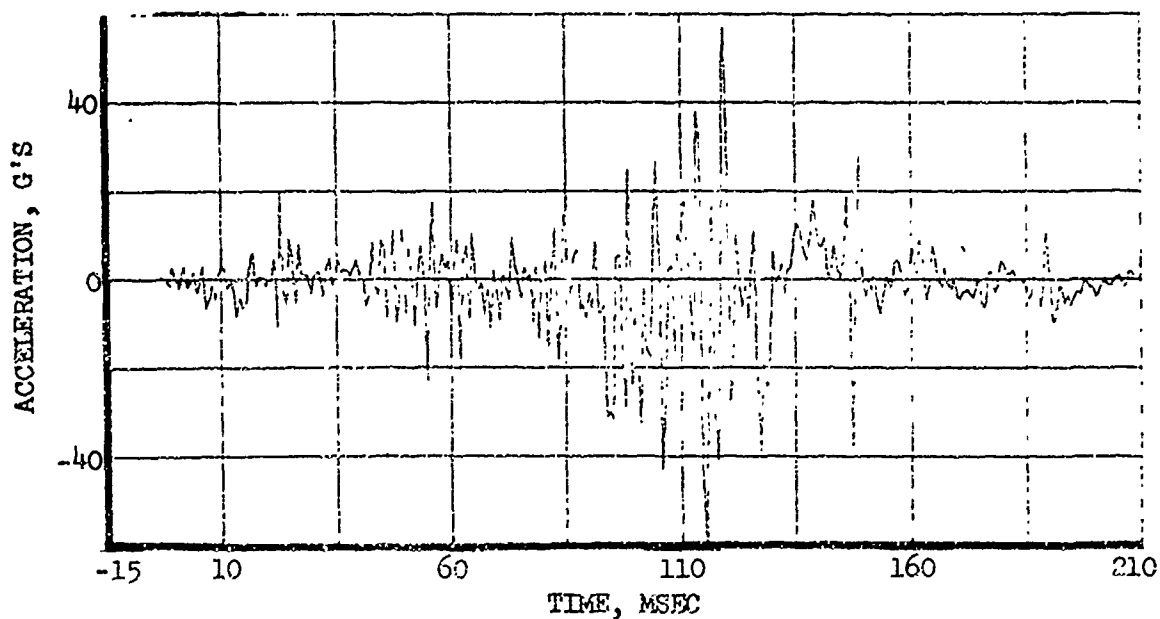


Figure 32. Recorded Time History, PAX Floor Rear Left, Lateral Acceleration (Channel 37).

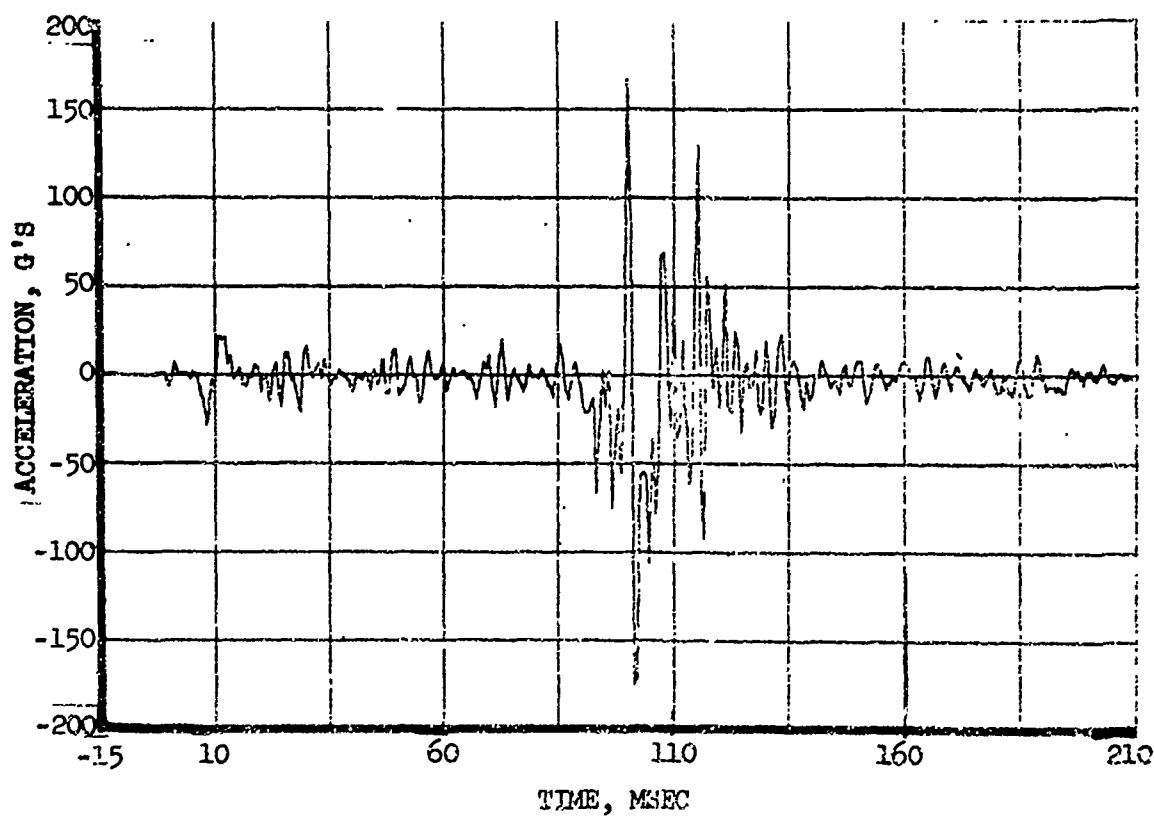


Figure 33. Recorded Time History, Cargo Floor Forward Left, Vertical Acceleration (Channel 38).

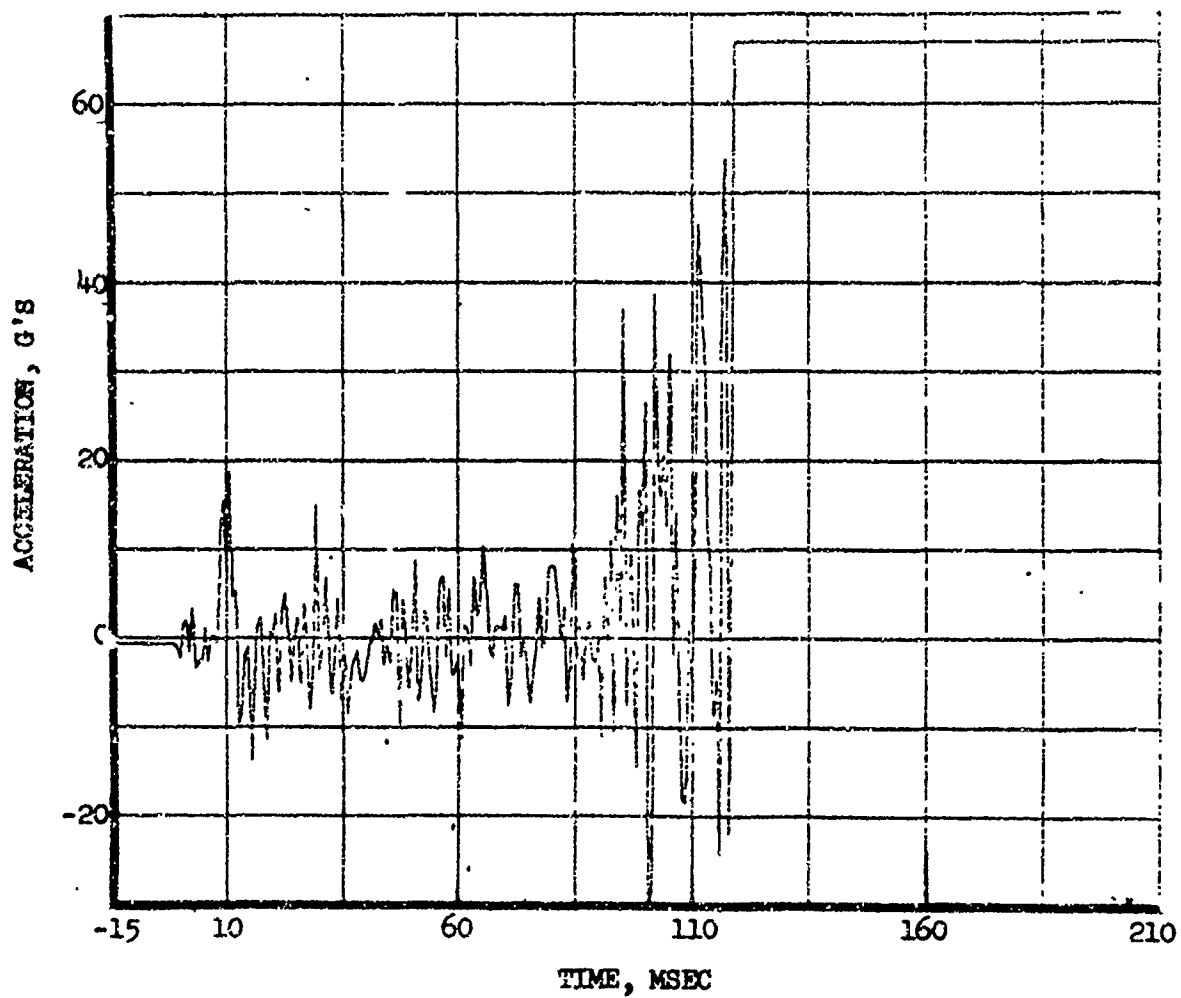


Figure 34. Recorded Time History, Cargo Floor- Forward Left, Lateral Acceleration (Channel 39).

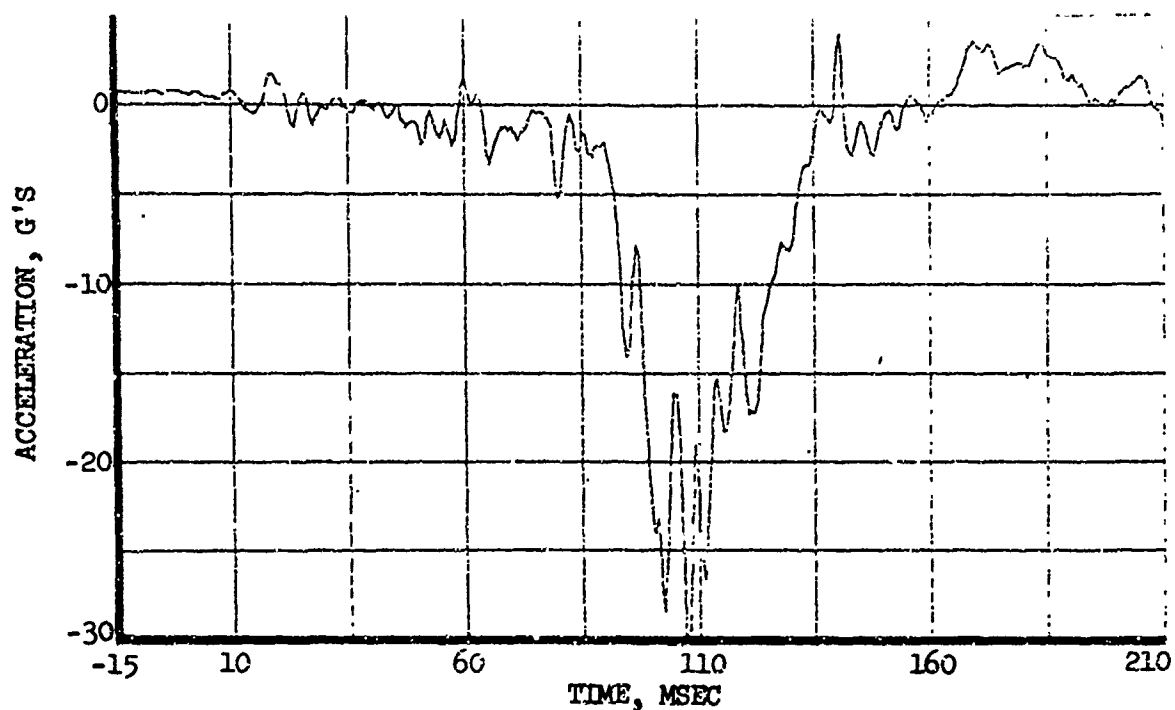


Figure 35. Recorded Time History, Transmission Rotor Housing, Vertical Acceleration (Channel 40).

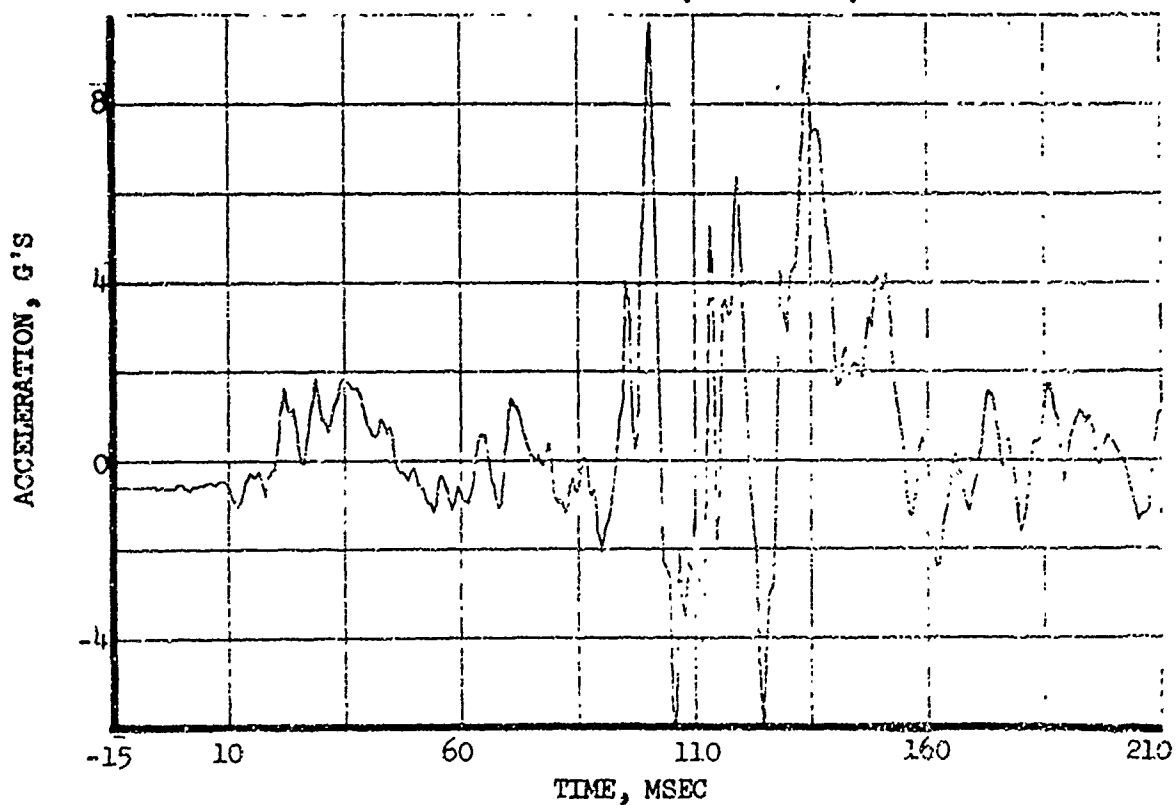


Figure 36. Recorded Time History, Transmission Rotor Housing, Lateral Acceleration (Channel 41).

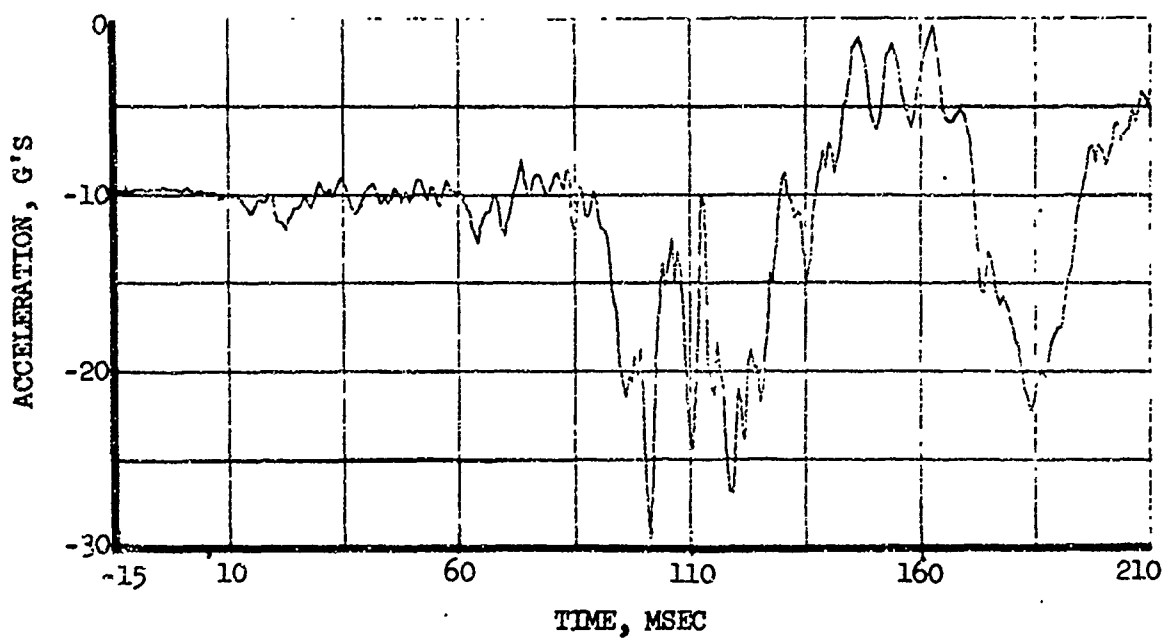


Figure 37. Recorded Time History, Transmission Rotor Housing, Axial Acceleration (Channel 42).

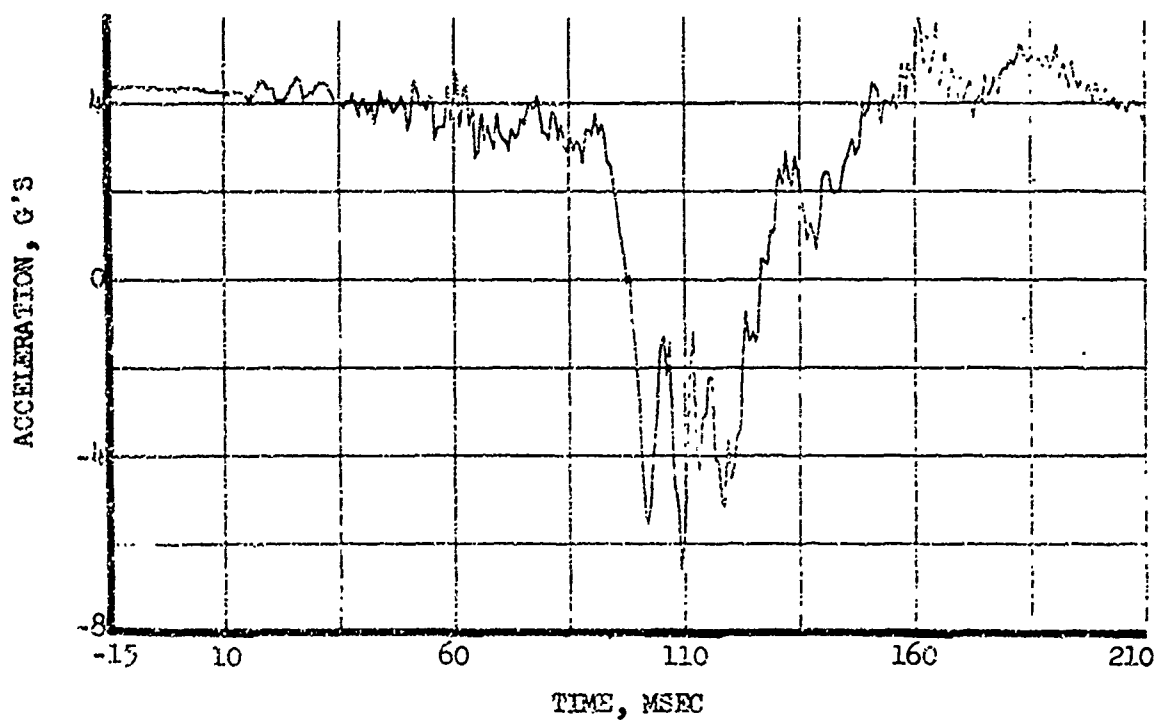


Figure 38. Recorded Time History, Engine, Vertical Acceleration (Channel 43).

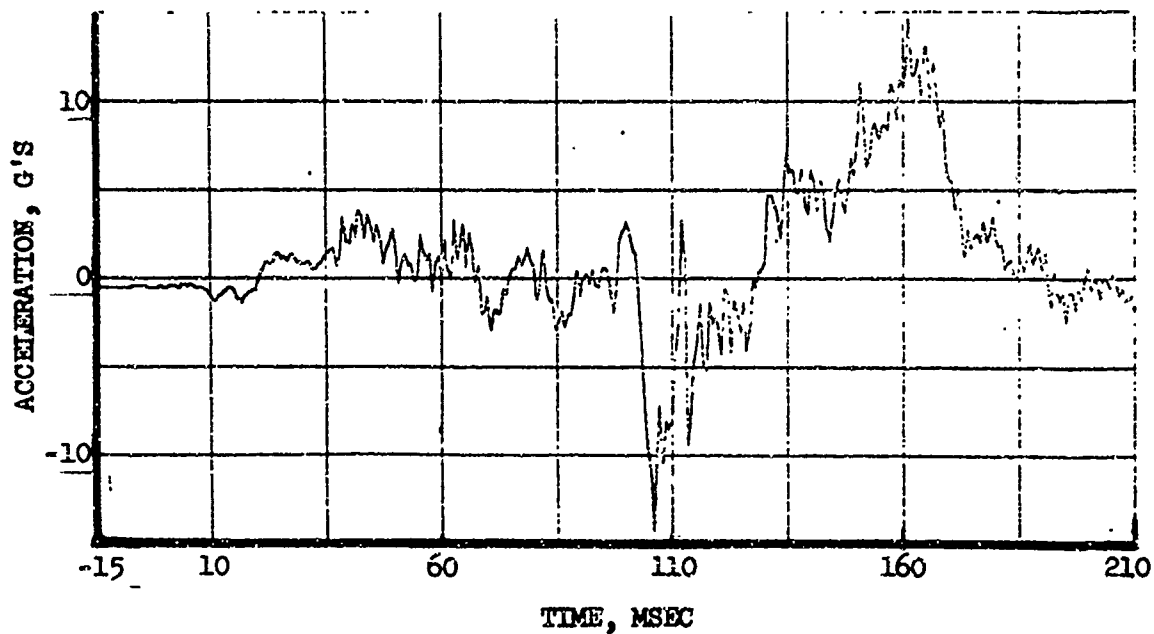


Figure 39. Recorded Time History, Engine, Lateral Acceleration (Channel 44).

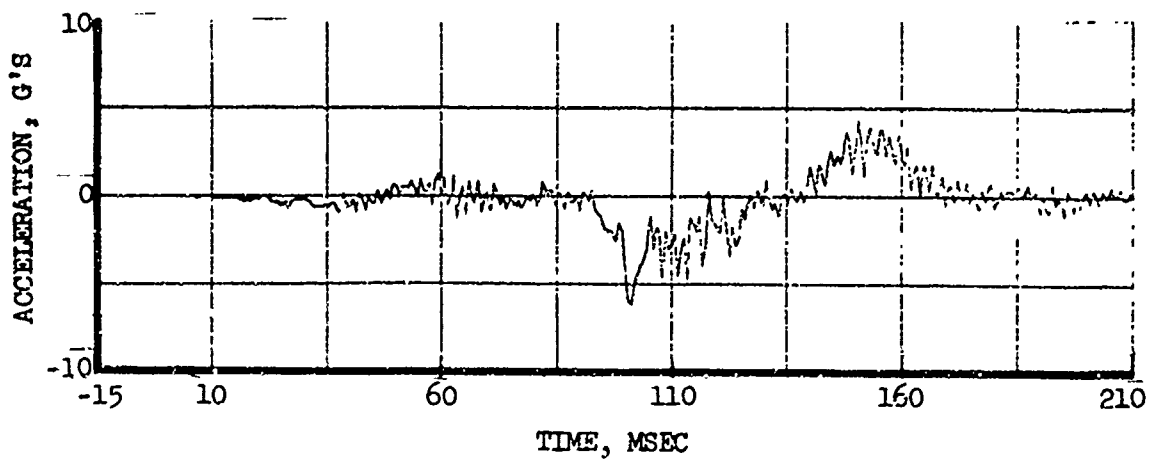


Figure 40. Recorded Time History, Engine, Axial Acceleration (Channel 45).

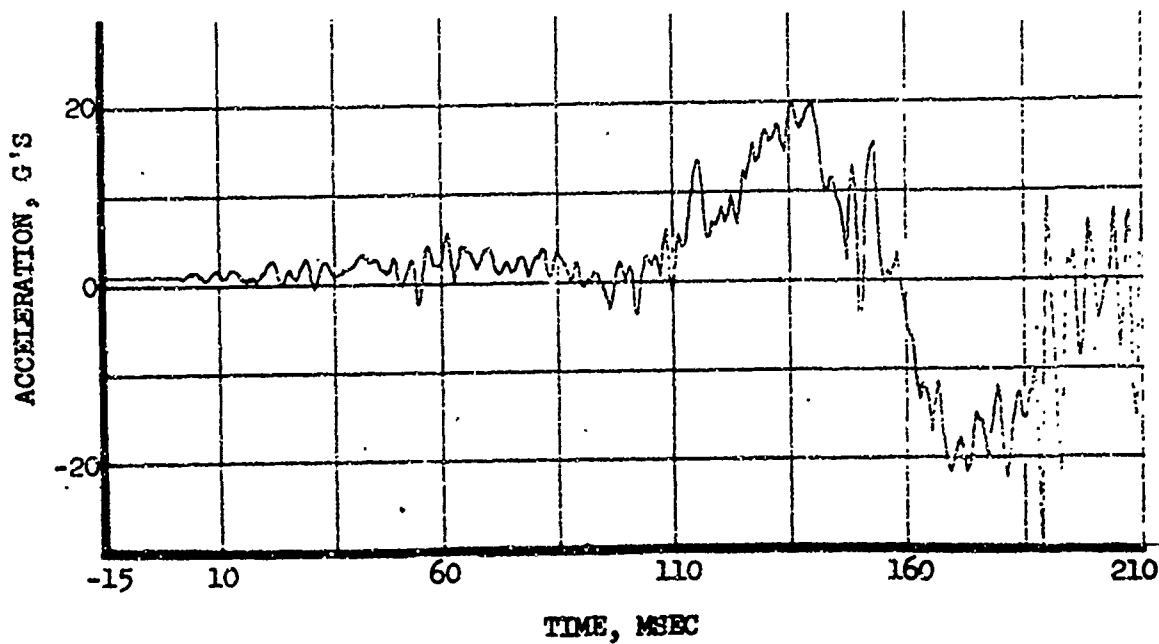


Figure 41. Recorded Time History, Tail Rotor Gearbox, Vertical Acceleration (Channel 46).

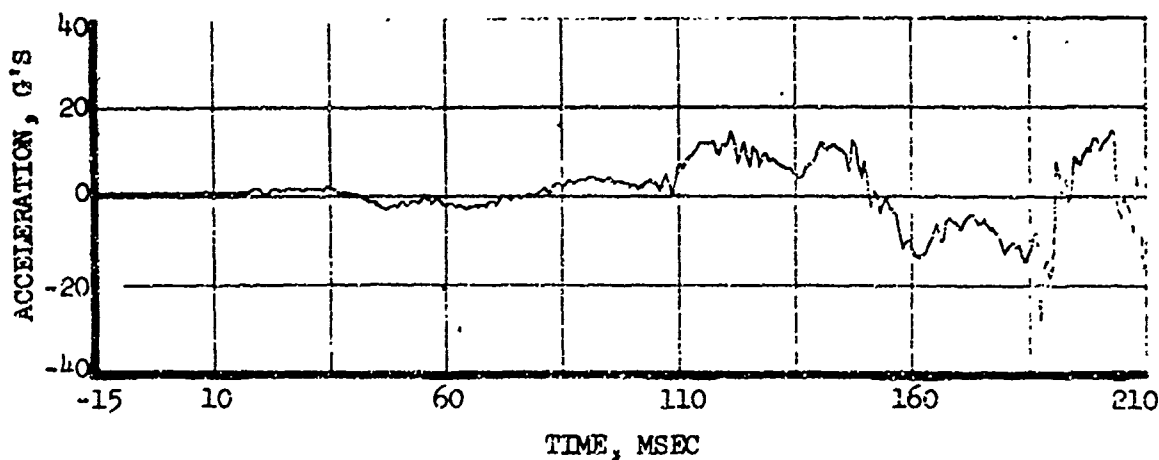


Figure 42. Recorded Time History, Tail Rotor Gearbox, Lateral Acceleration (Channel 47).



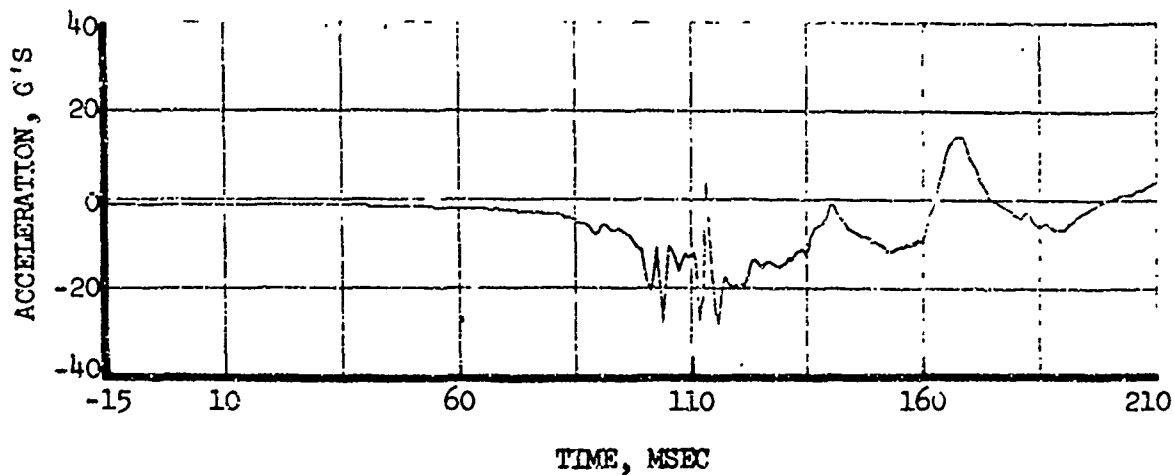


Figure 43. Recorded Time History, Passenger Pelvic, Vertical Acceleration (Channel 48).

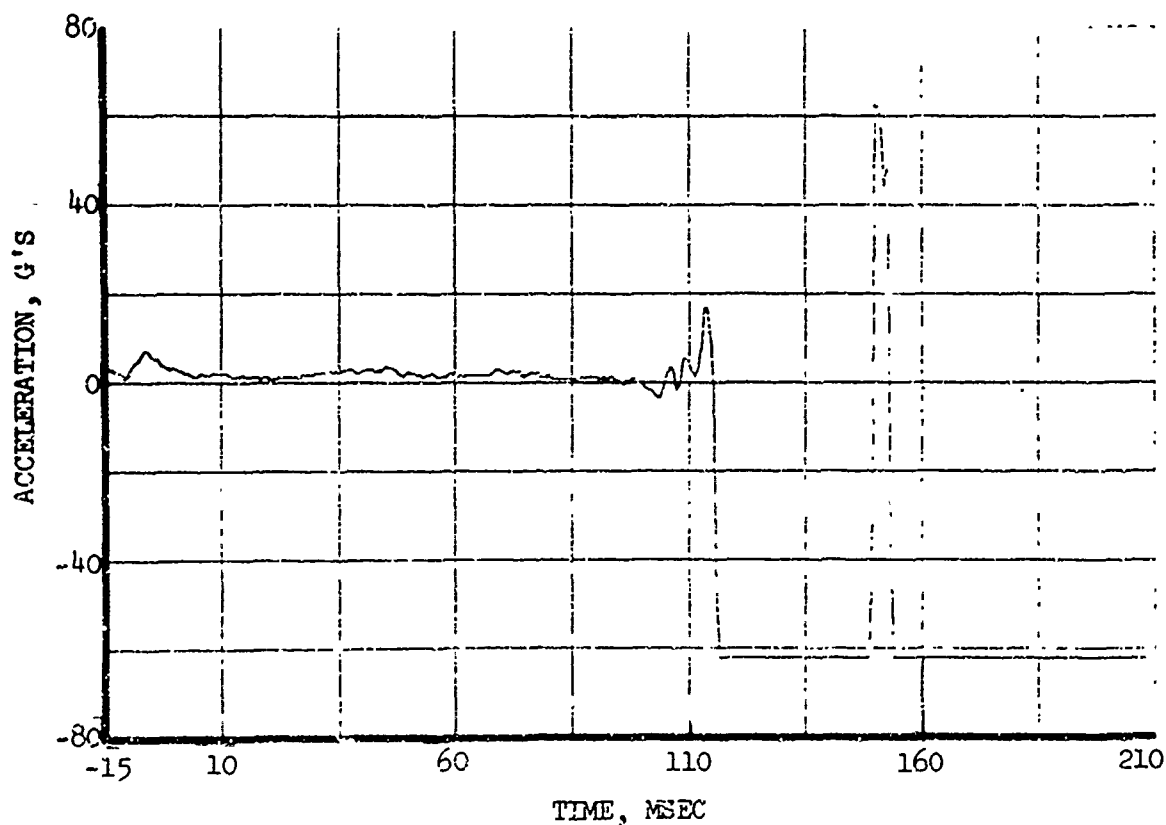


Figure 44. Recorded Time History, Passenger Pelvic, Lateral Acceleration (Channel 60).

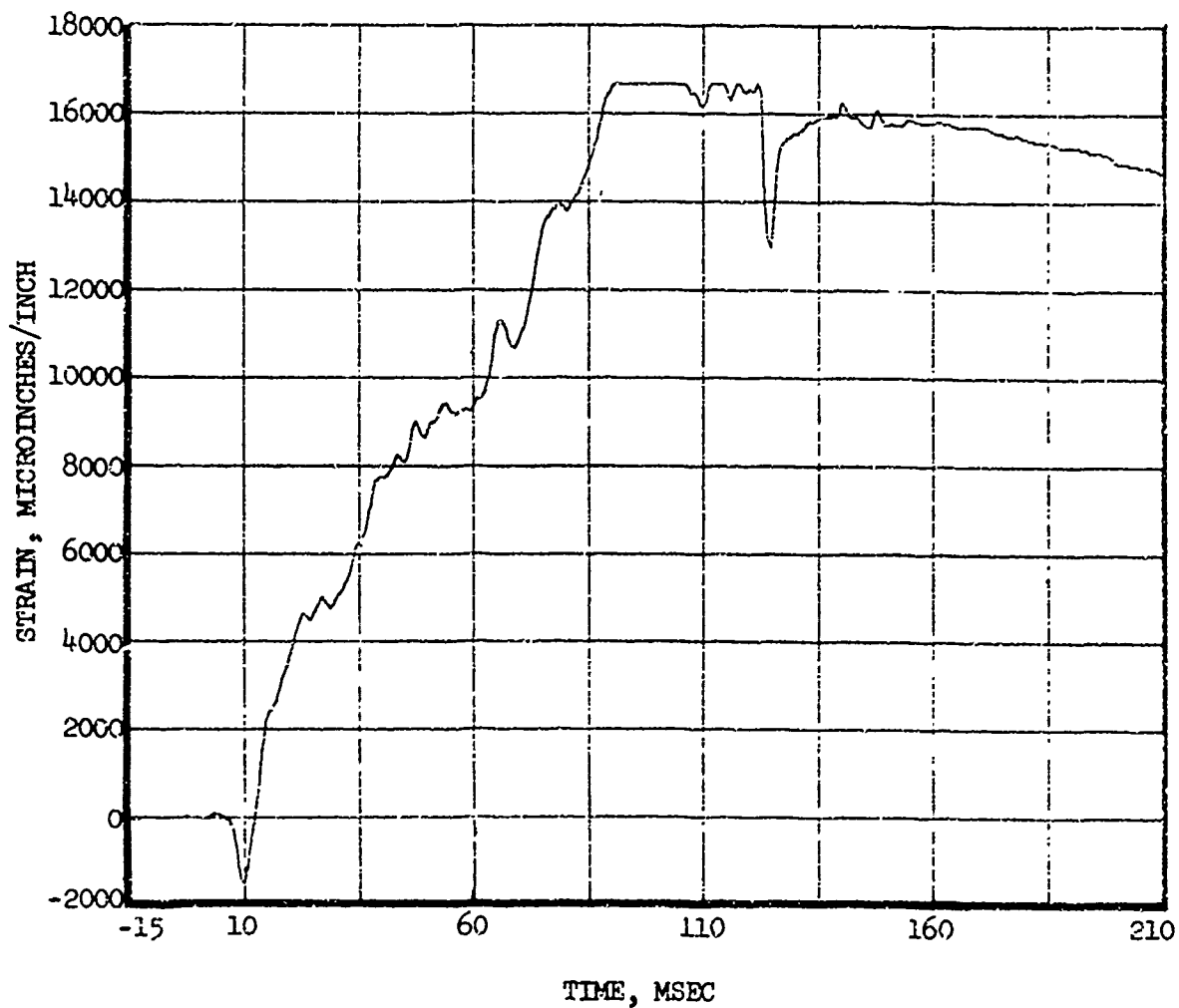


Figure 45. Recorded Time History, Forward Strut, Left Side Strain Gage (Channel 61).

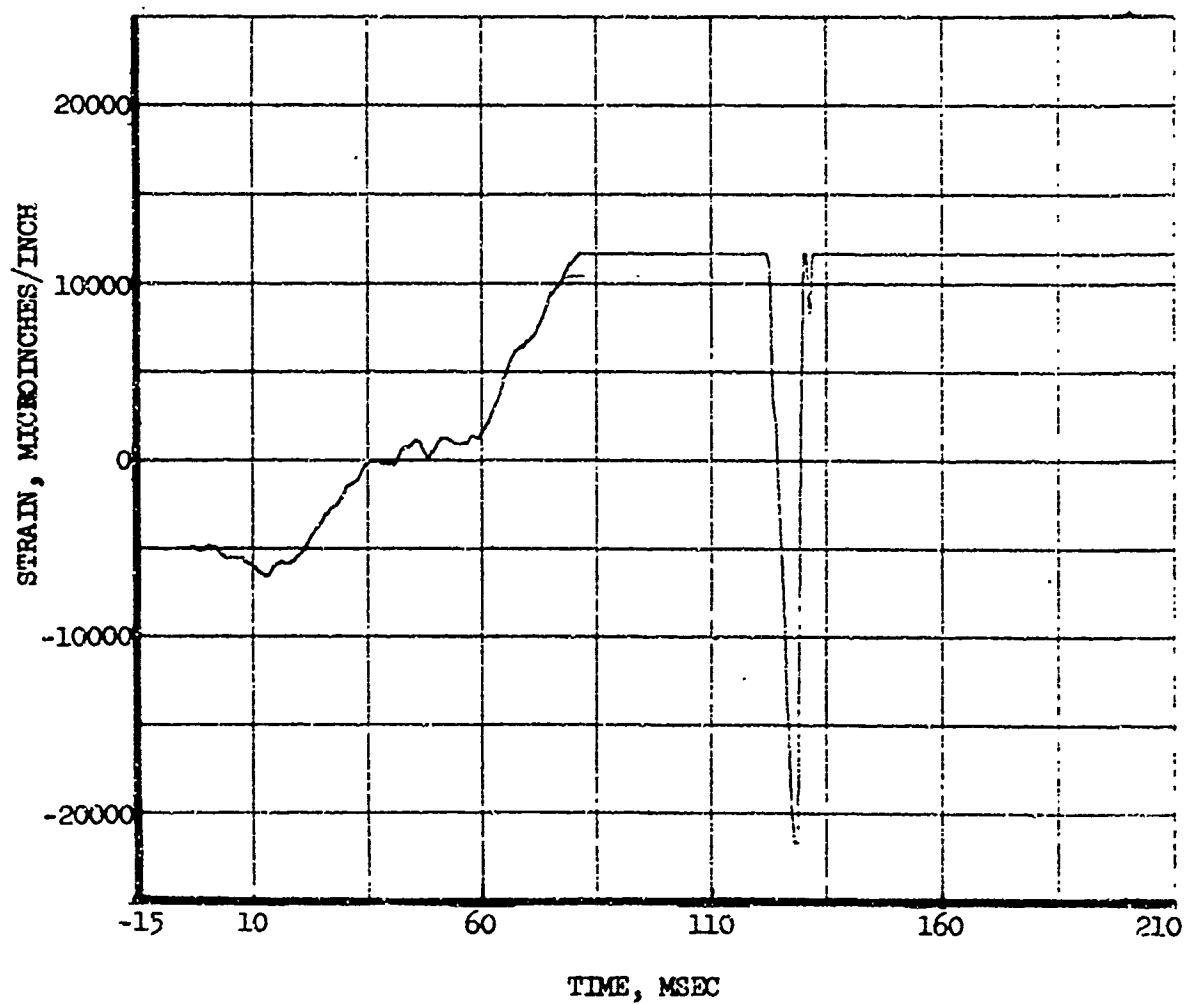


Figure 46. Recorded Time History, Rear Strut, Left Side, Strain Gage (Channel 62).

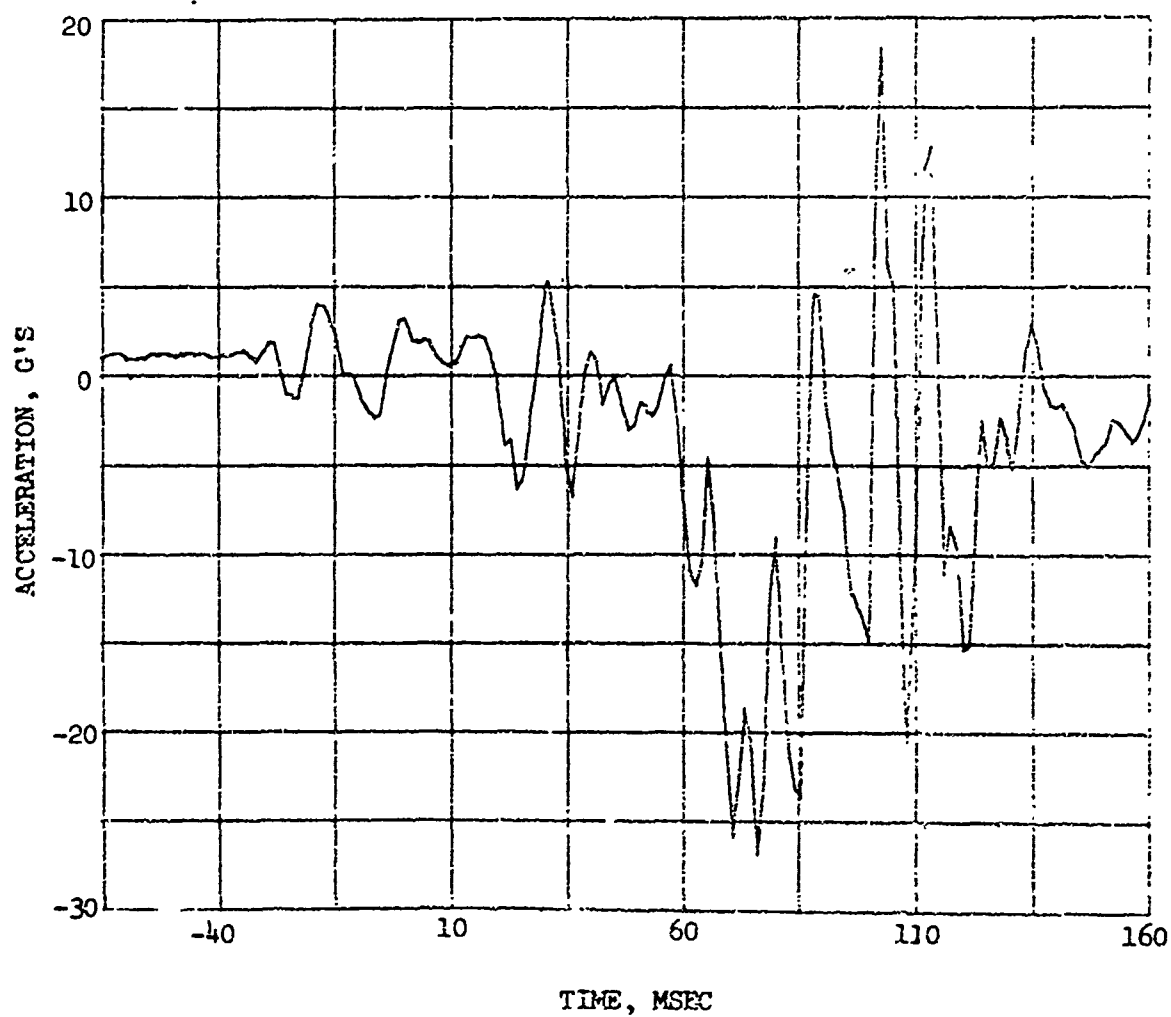


Figure 47. 100-CPS Low-Pass Filtered Test Data, Pilot Seat Pan, Vertical Acceleration (Channel 07).

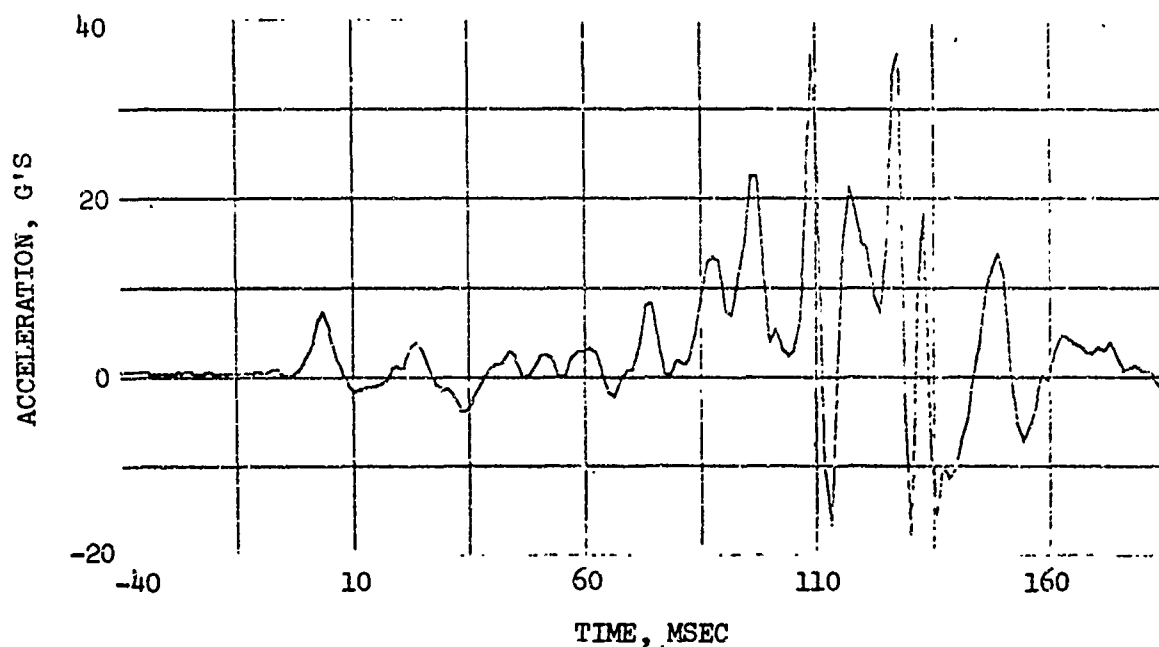


Figure 48. 100-CPS Low-Pass Filtered Test Data, Pilot Seat Pan, Lateral Acceleration (Channel 08).

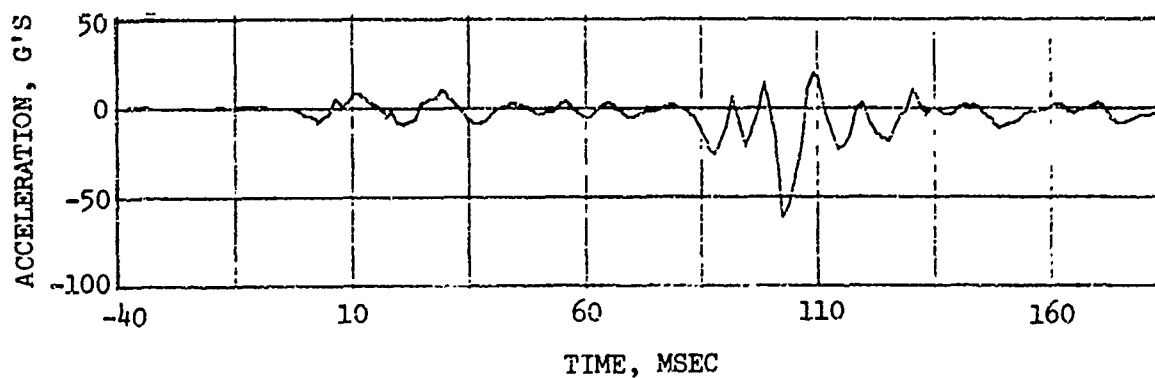


Figure 49. 100-CPS Low-Pass Filtered Test Data, Copilot Seat Pan Vertical Acceleration (Channel 09).

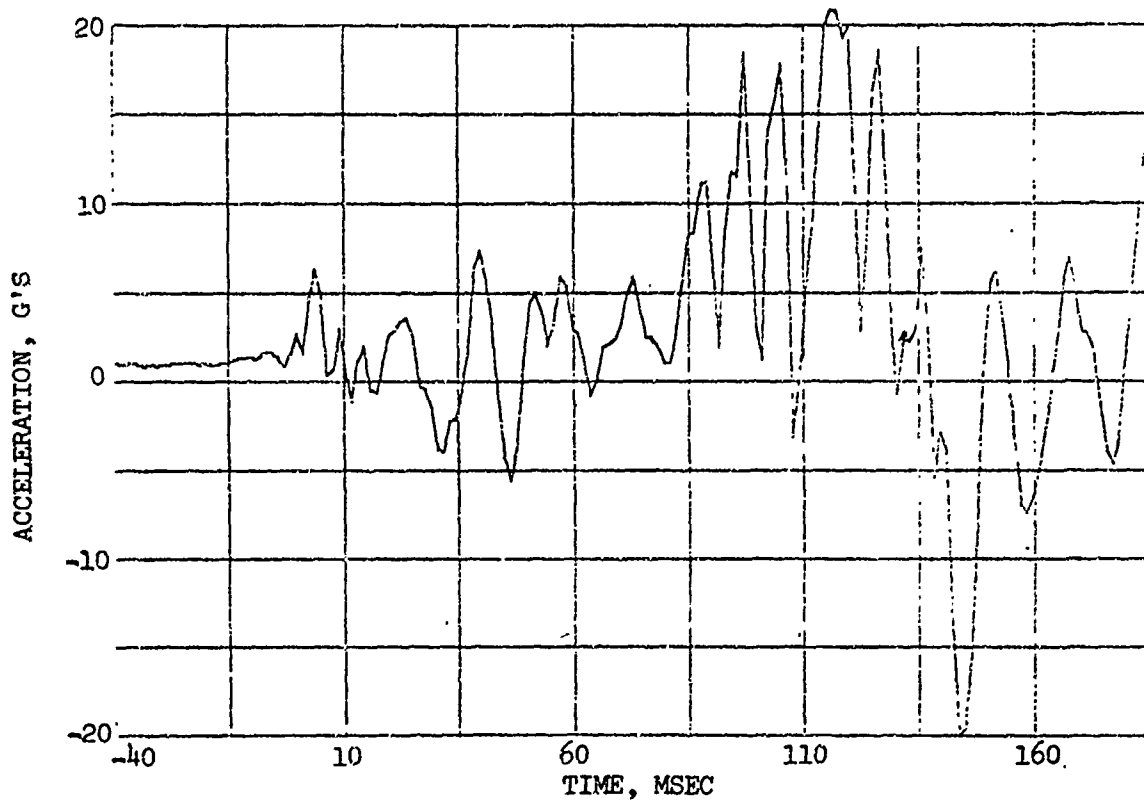


Figure 50. 100-CPS Low-Pass Filtered Test Data, Copilot Seat Pan, Lateral Acceleration (Channel 10).

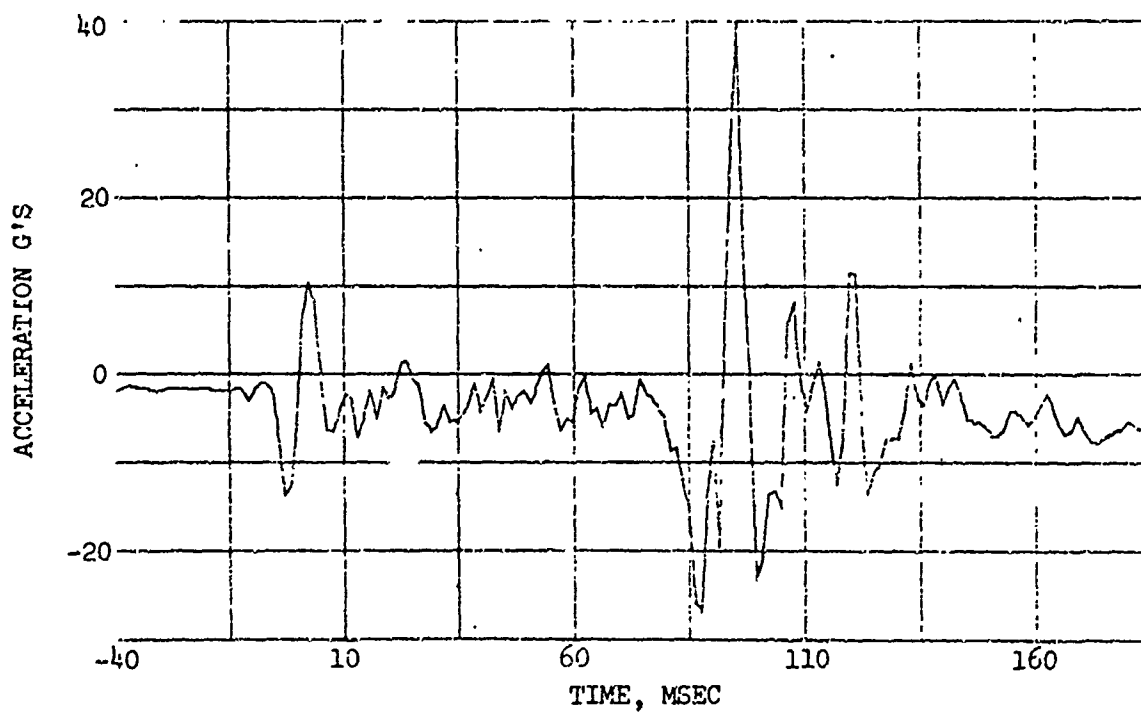


Figure 51. 100-CPS Low-Pass Filtered Test Data, Copilot Floor, Vertical Acceleration (Channel 3G).

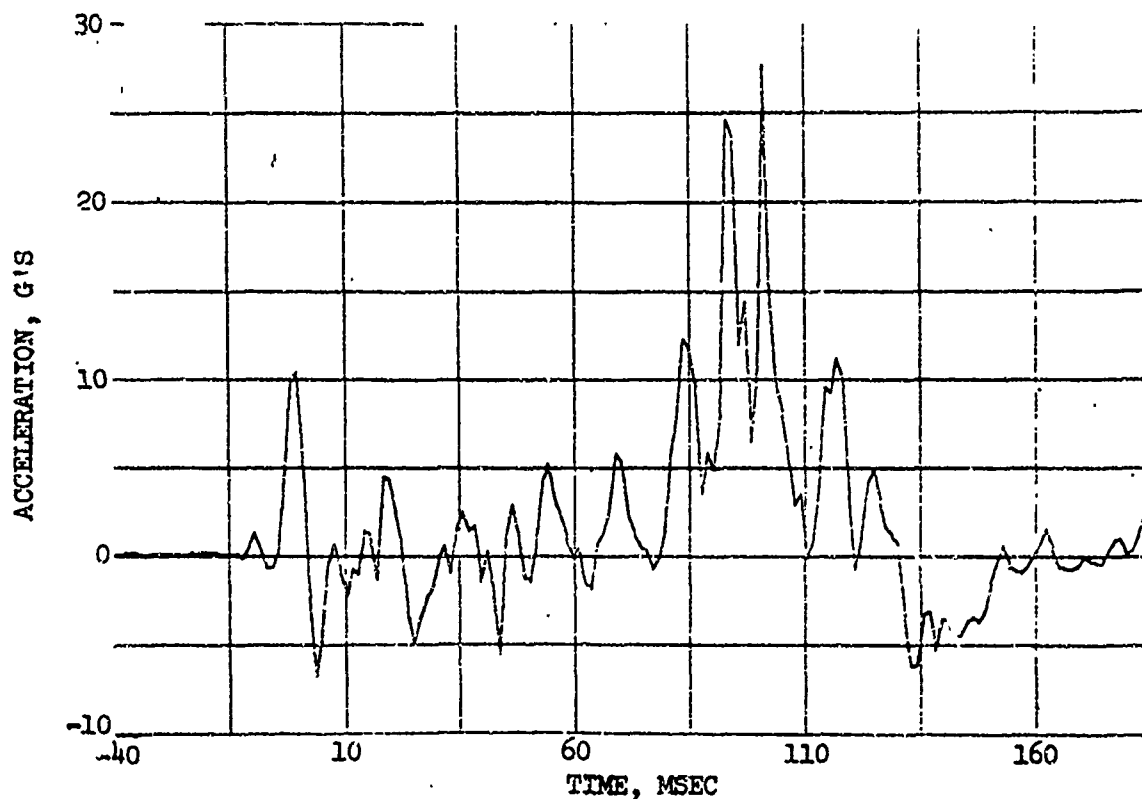


Figure 52. 100-CPS Low-Pass Filtered Test Data, Copilot Floor,  
Lateral Acceleration (Channel 31).

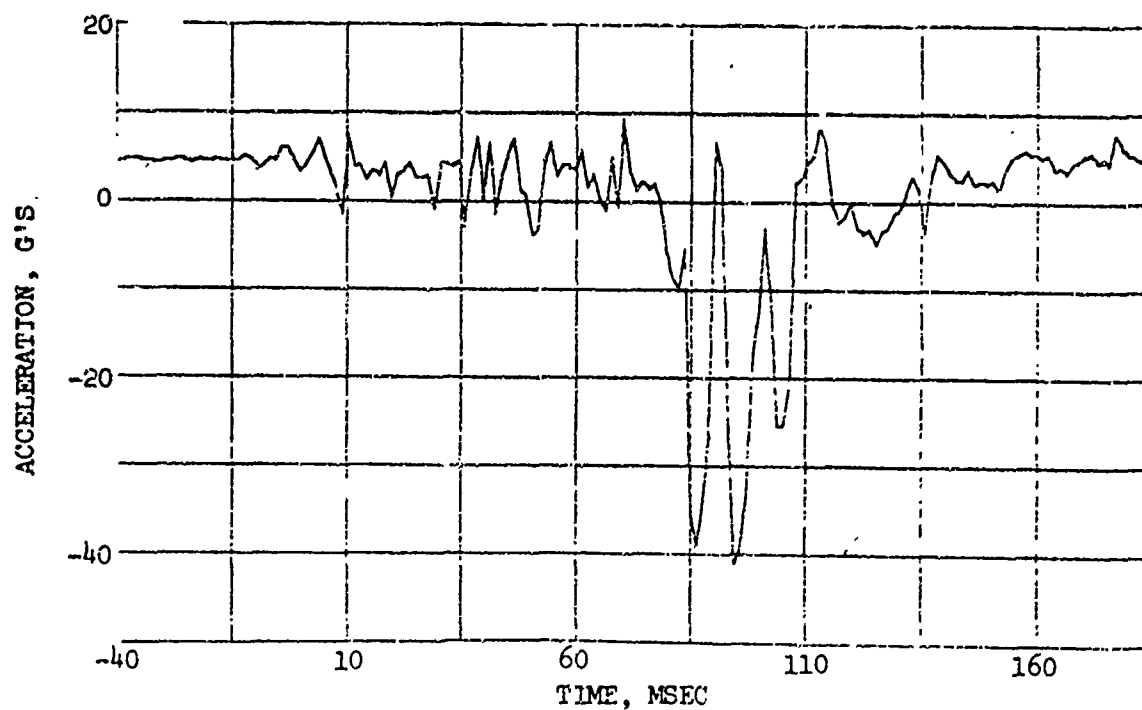


Figure 53. 100-CPS Low-Pass Filtered Test Data, Passenger Floor,  
Vertical Acceleration (Channel 36).

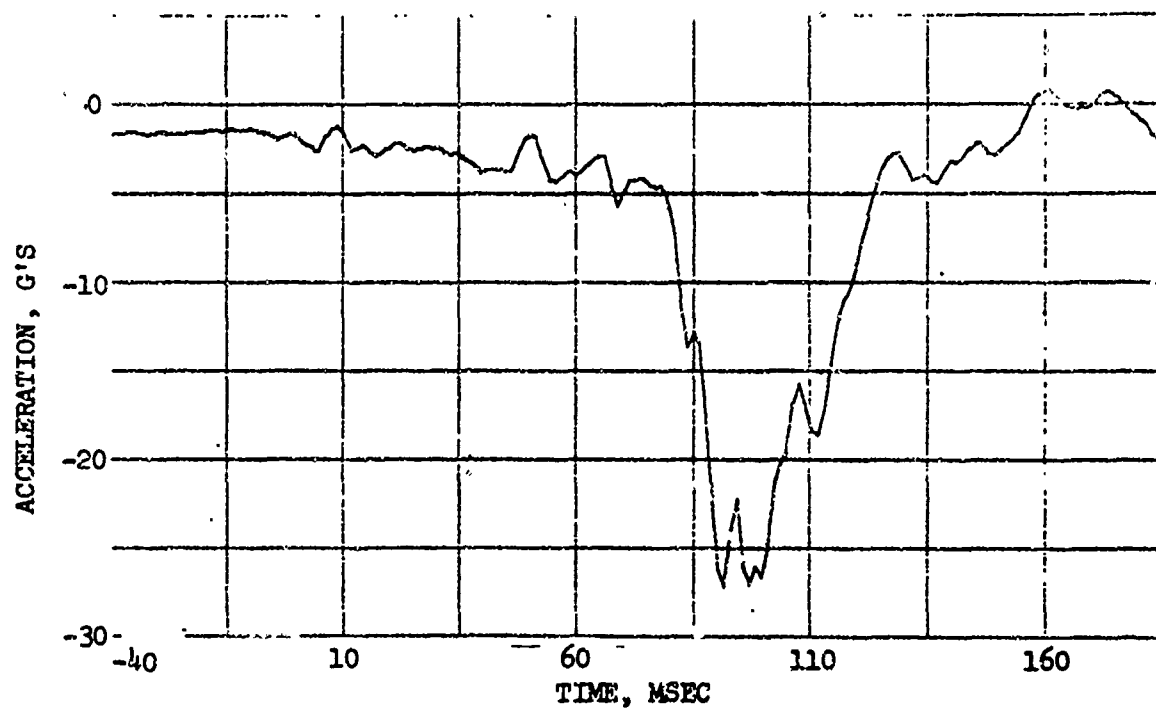


Figure 54. 100-CPS Low-Pass Filtered Test Data, Transmission Rotor Housing, Vertical Acceleration (Channel 40).

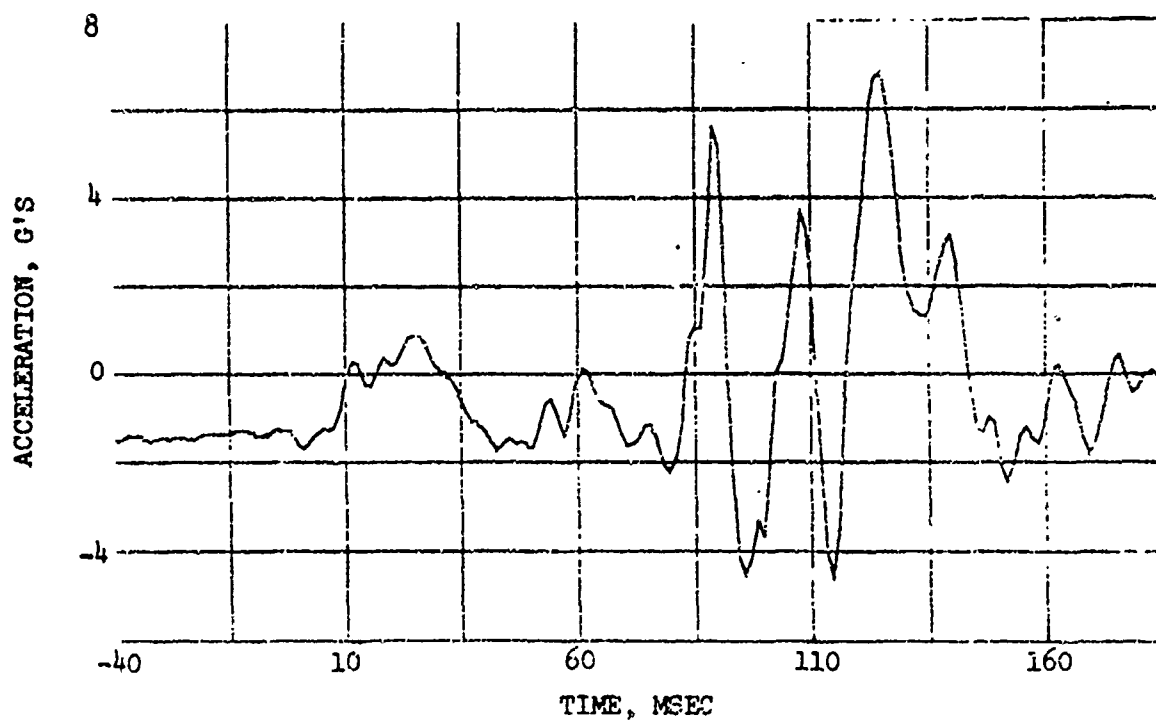


Figure 55. 100-CPS Low-Pass Filtered Test Data, Transmission Rotor Housing, Lateral Acceleration (Channel 41).



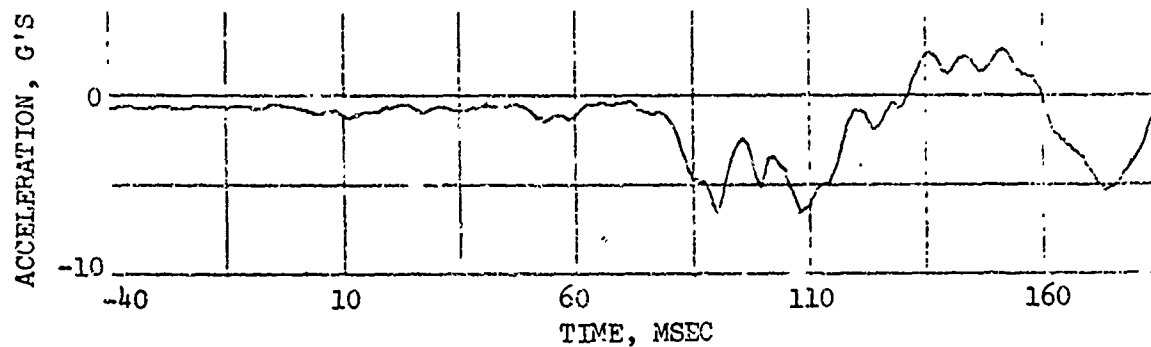


Figure 56. 100-CPS Low-Pass Filtered Test Data, Transmission Rotor Housing, Axial Acceleration (Channel 42).

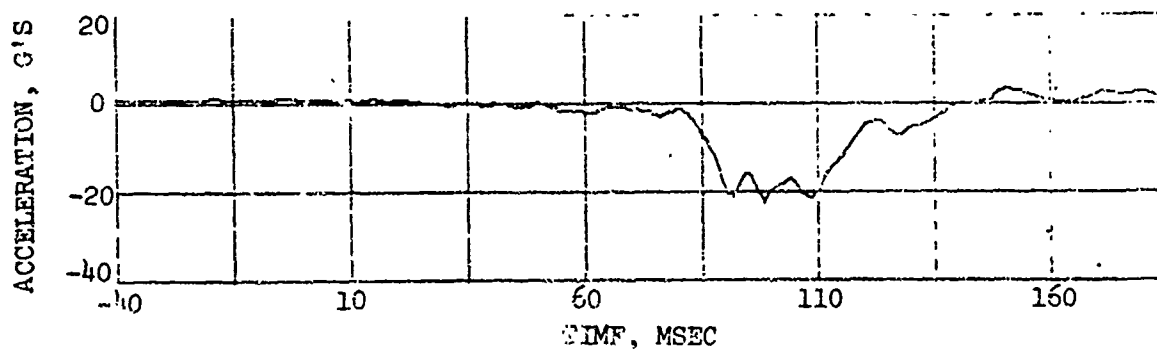


Figure 57. 100-CPS Low-Pass Filtered Test Data, Engine, Vertical Acceleration (Channel 43).

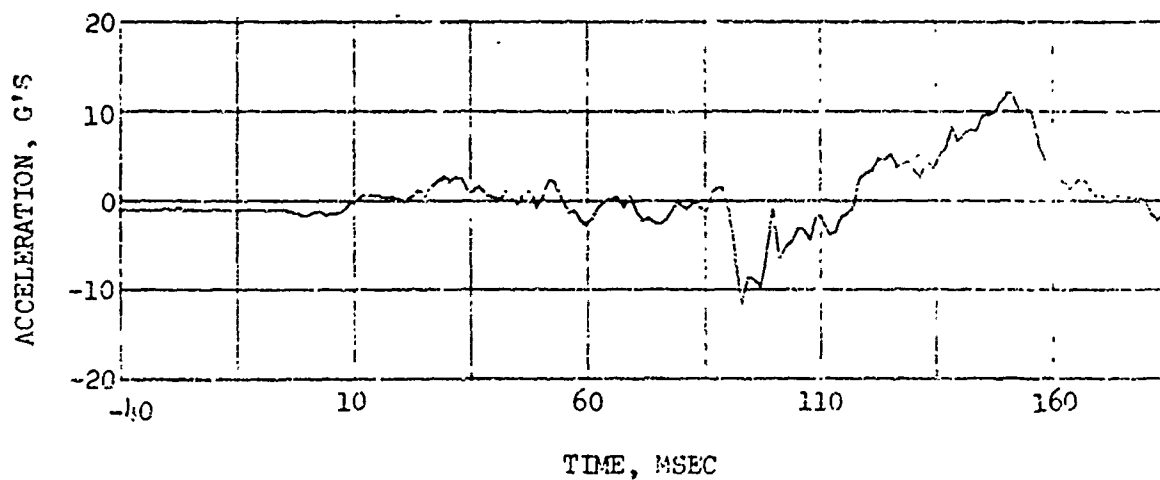


Figure 58. 100-CPS Low-Pass Filtered Test Data, Engine, Lateral Acceleration (Channel 44).

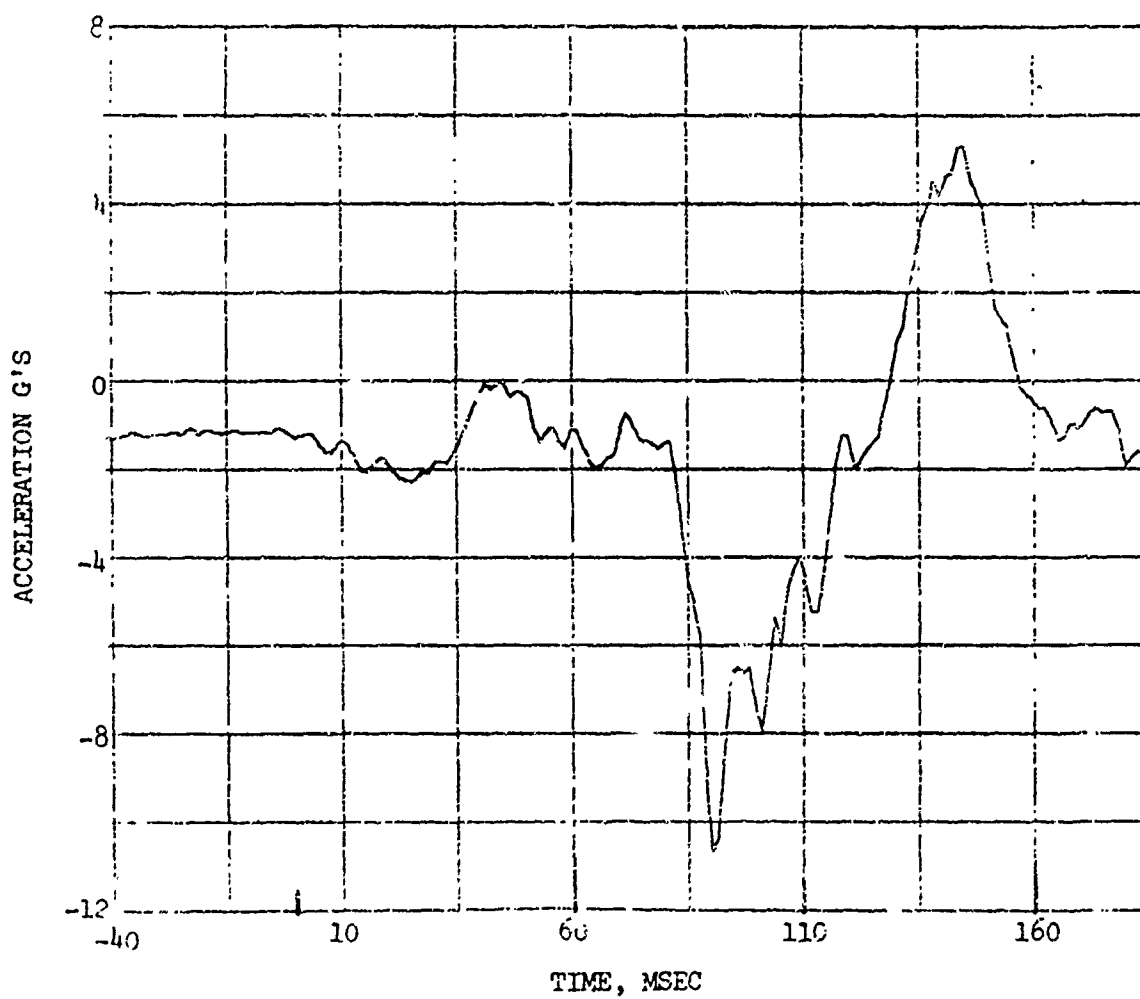


Figure 59. 100-CPS Low-Pass Filtered Test Data, Engine, Axial Acceleration (Channel 45).

#### TIME HISTORIES OF INTEGRATED DATA

The integrated velocities and displacements were obtained from the recorded accelerations. A digital program was written which numerically integrated the acceleration time histories using a trapezoidal rule and an integration time interval of .0008. The acceleration data was adjusted to account for channel noise, offset accelerations due to initial swing positions, and post-test position changes resulting from one or more of the following sources: structural damage, seat collapse, floor buckling, and passenger movement. The velocities obtained from integrating the accelerations are shown in Figures 60 through 70. The displacements obtained from the integrated velocities are shown in Figures 71 through 82.

#### IMPACT VELOCITY DATA

Figures 83 through 87 are obtained from analysis of the high speed film and show the sequence of events and the vertical and lateral velocities and displacements.

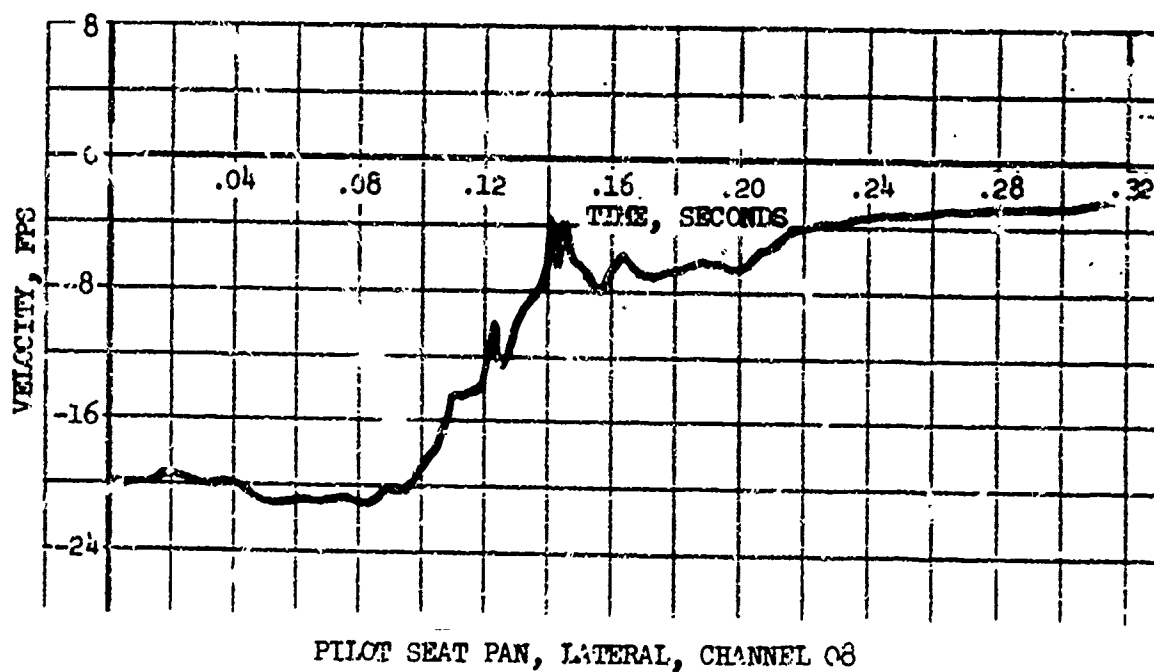
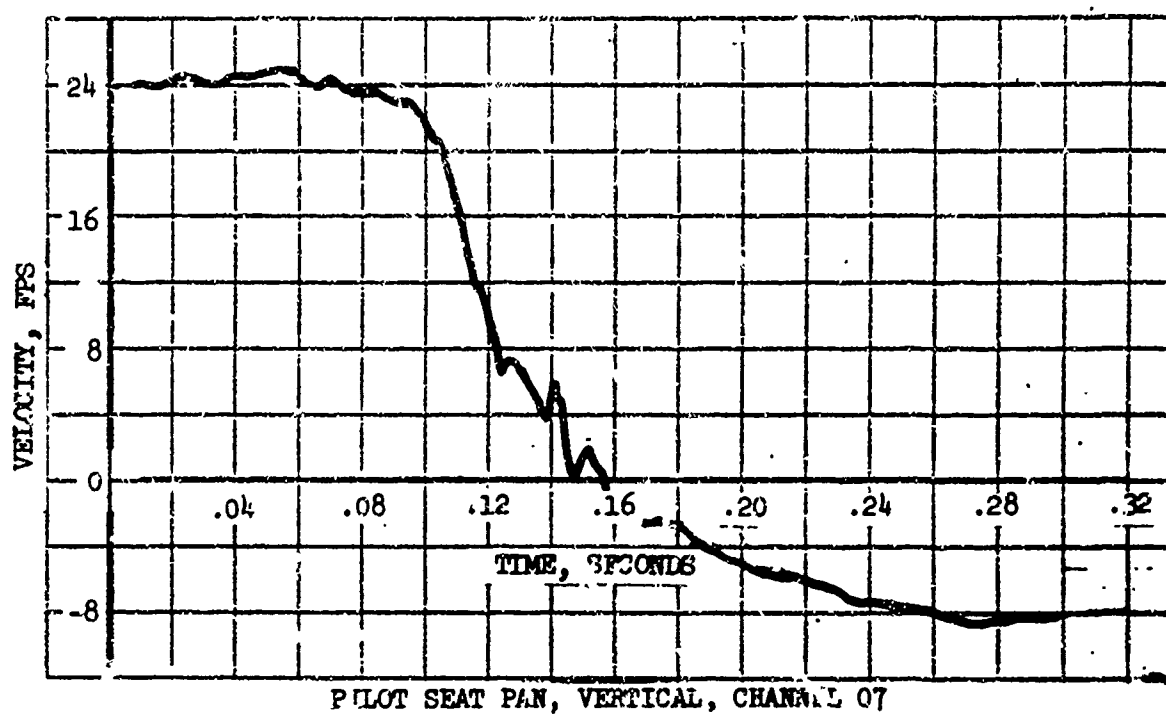


Figure 60. Integrated Velocities, Pilot Seat Pan.

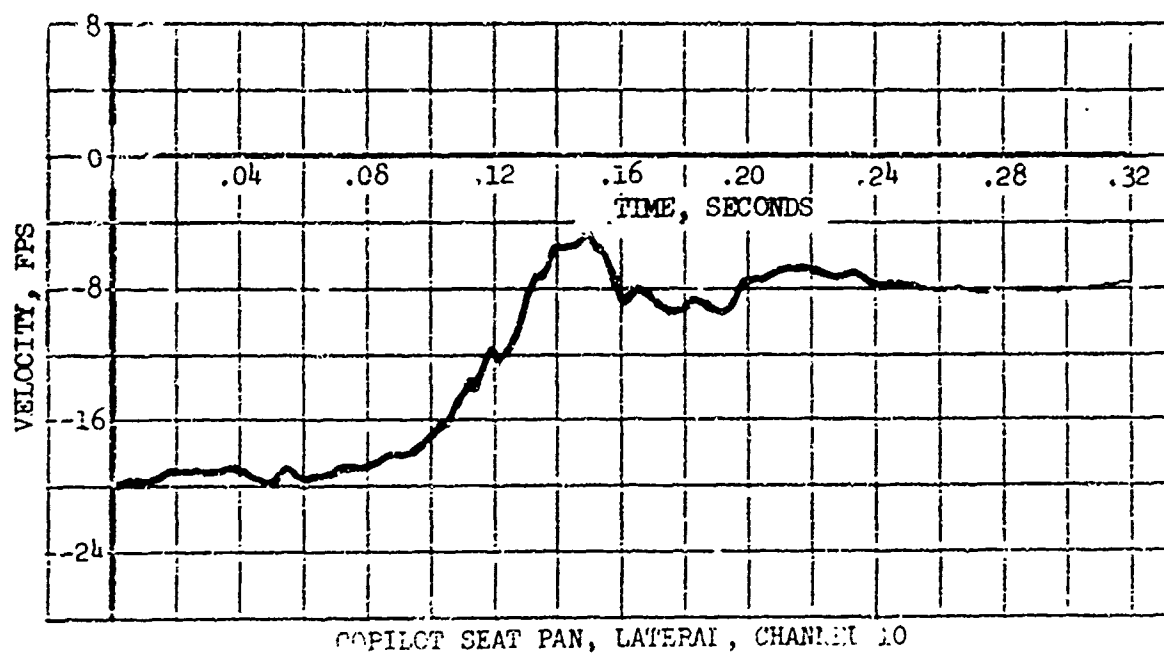
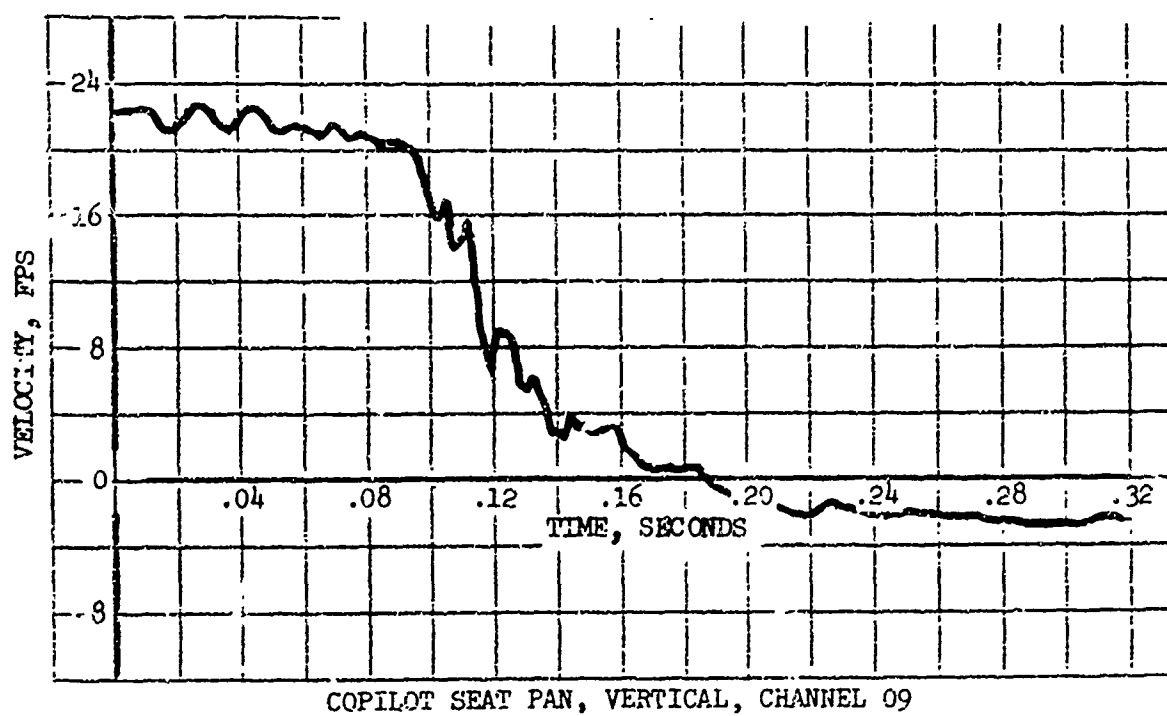
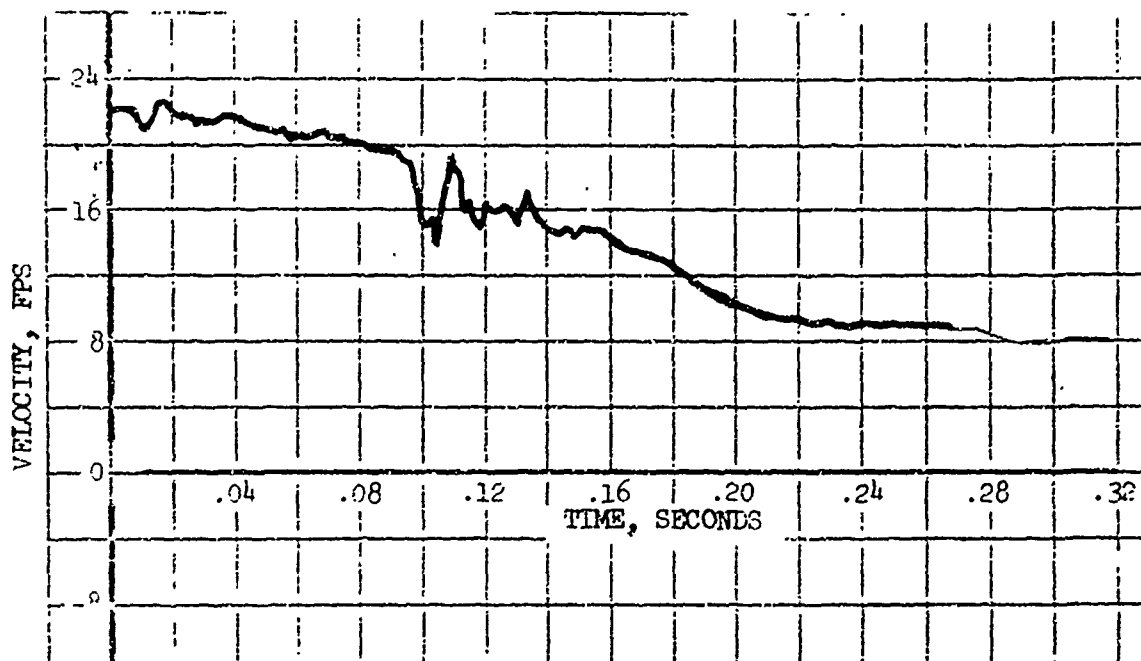
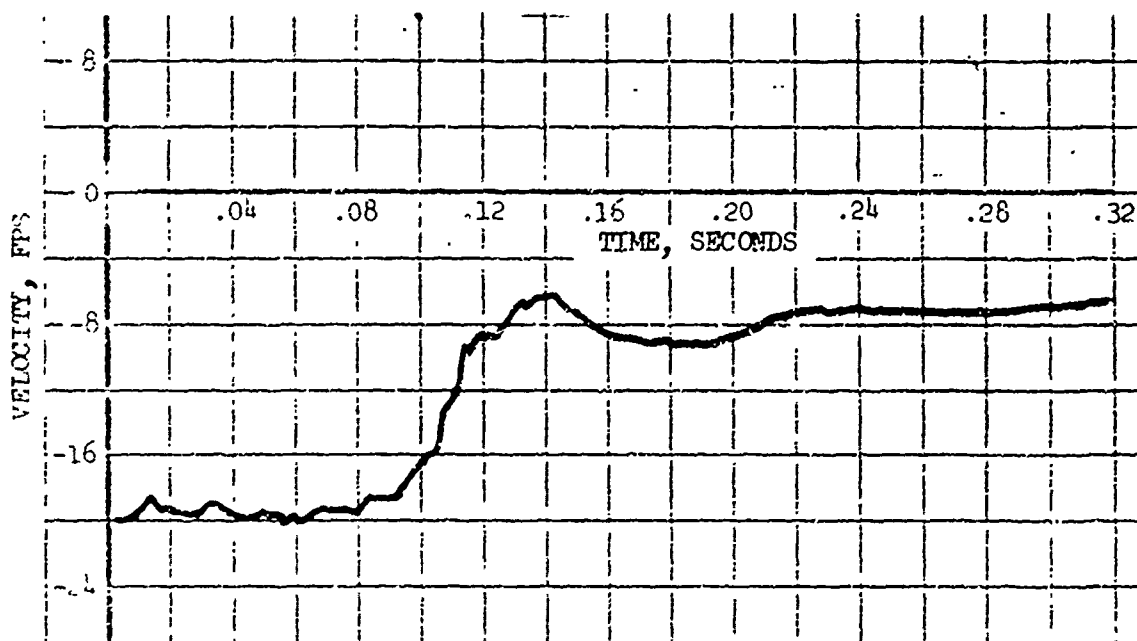


Figure 61. Integrated Velocities, Copilot Seat Pan.

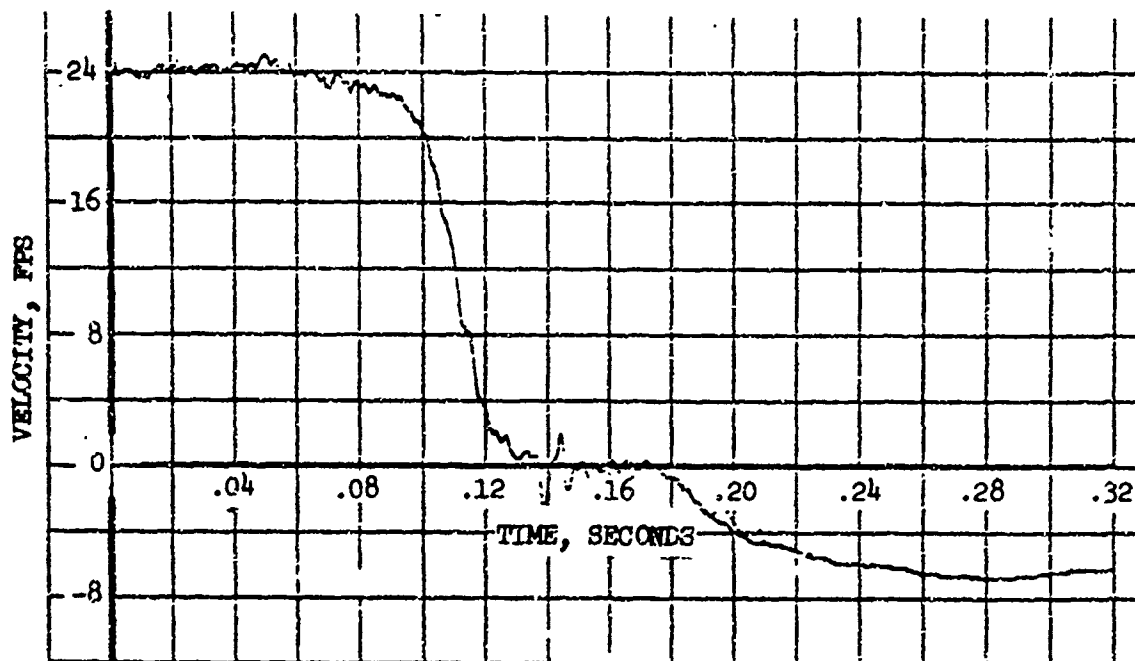


FLOOR, PILOT LOC., VERTICAL, CHANNEL 32

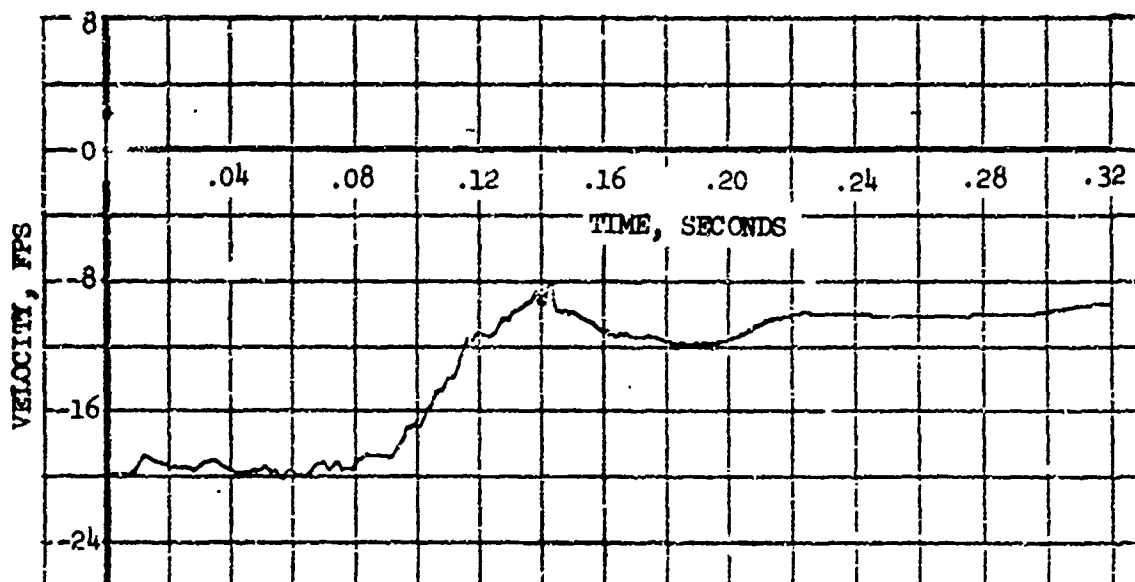


FLOOR, PILOT LOC., LATERAL, CHANNEL 33

Figure 6A. Integrated Velocities, Floor, Copilot Location

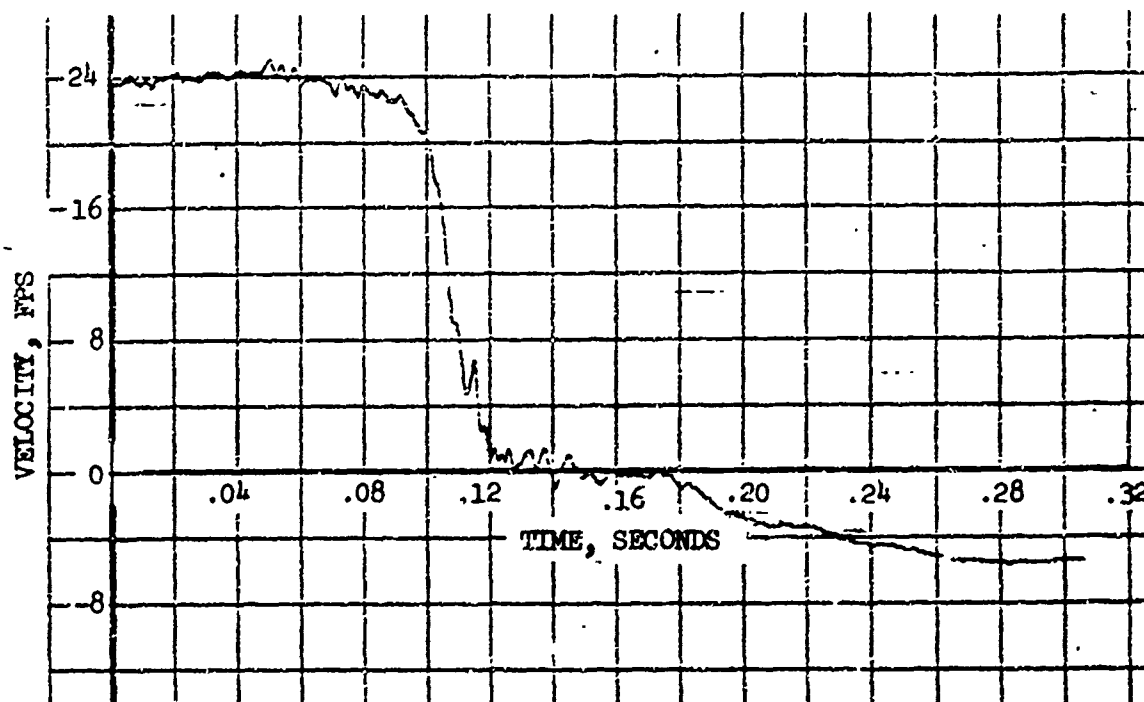


FLOOR, PILOT LOC., VERTICAL, CHANNEL 32

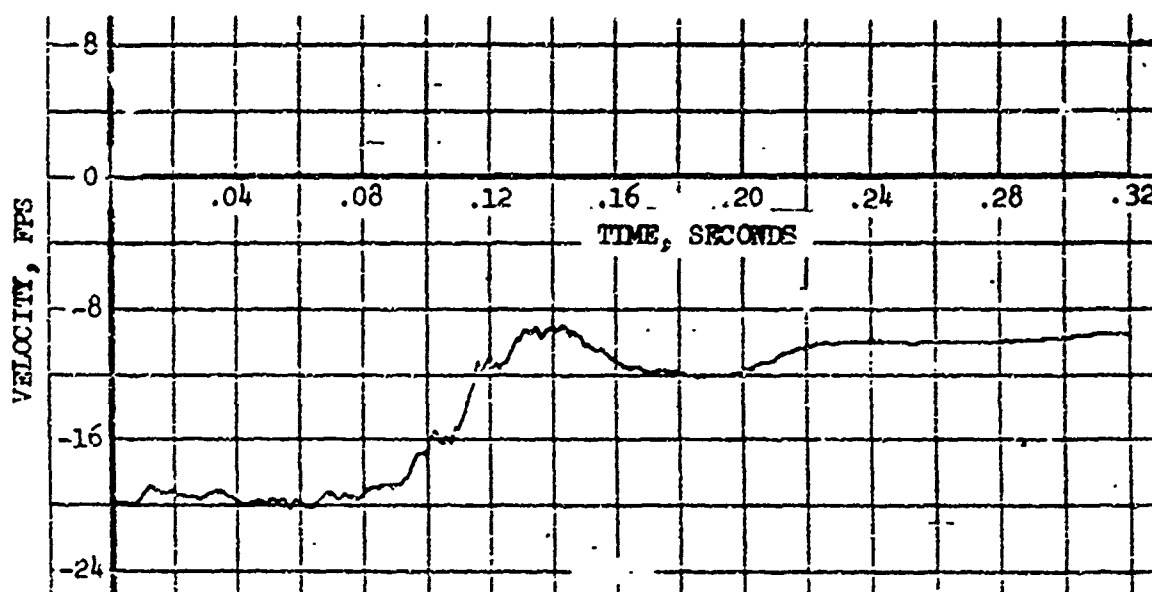


FLOOR, PILOT LOC., LATERAL, CHANNEL 33

Figure 63. Integrated Velocities, Floor, Pilot Location



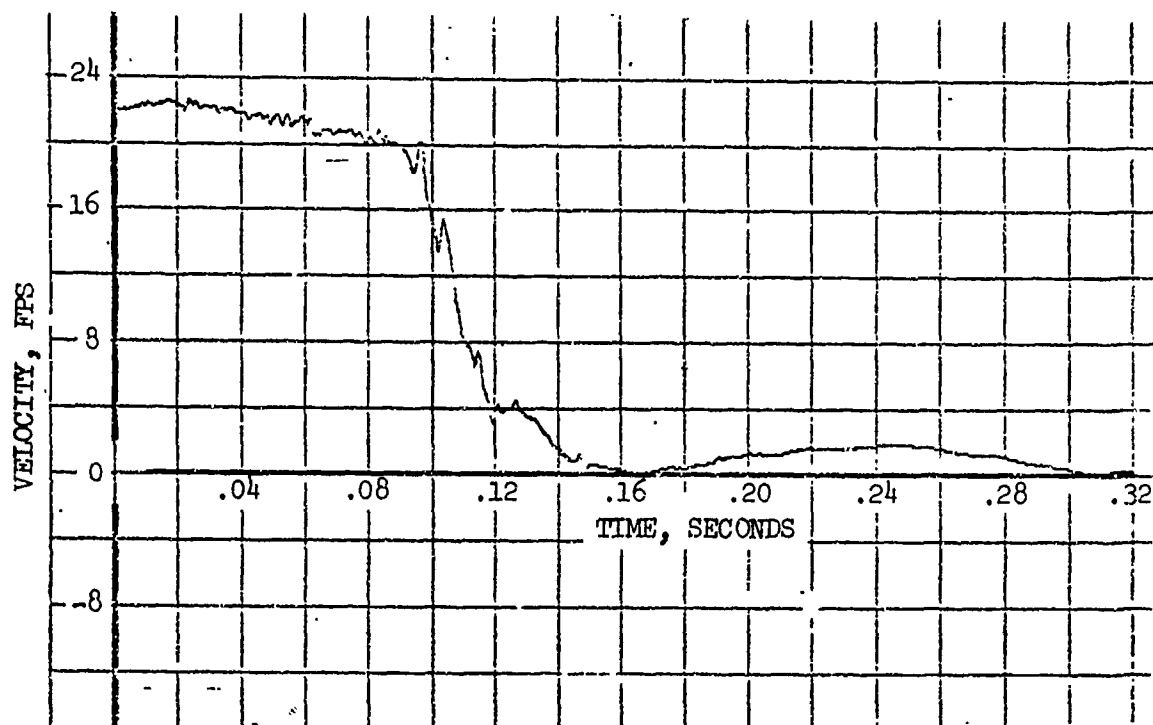
CARGO FLOOR, FWD. RIGHT, VERTICAL, CHANNEL 34



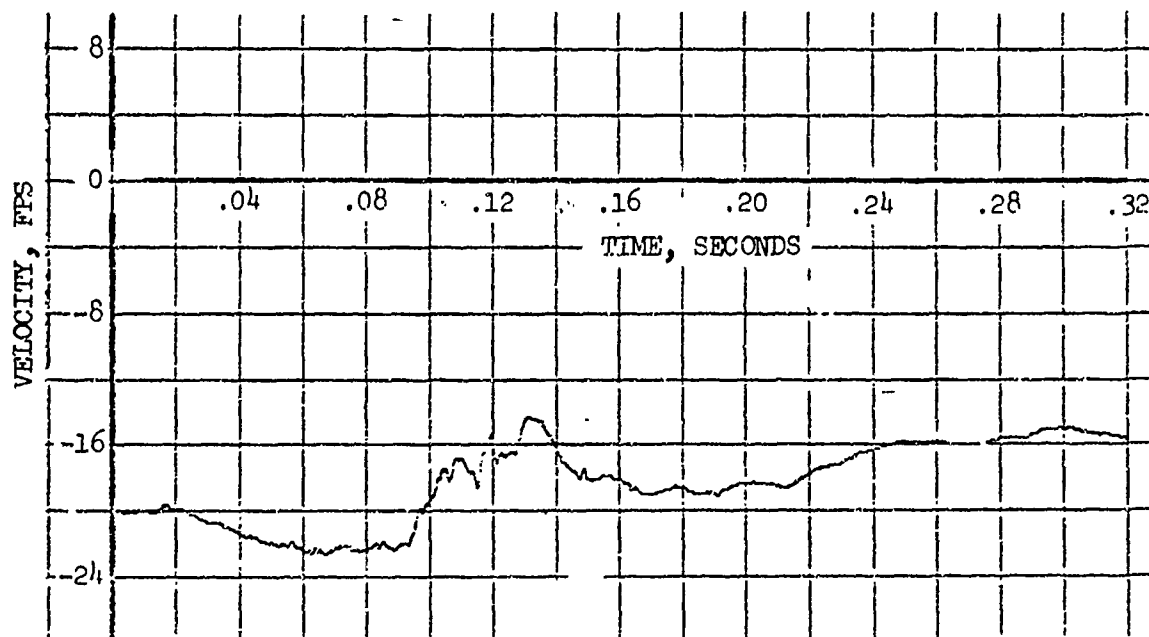
CARGO FLOOR, FWD. RIGHT, LATERAL, CHANNEL 35

Figure 64. Integrated Velocities, Cargo Floor, Forward Right.



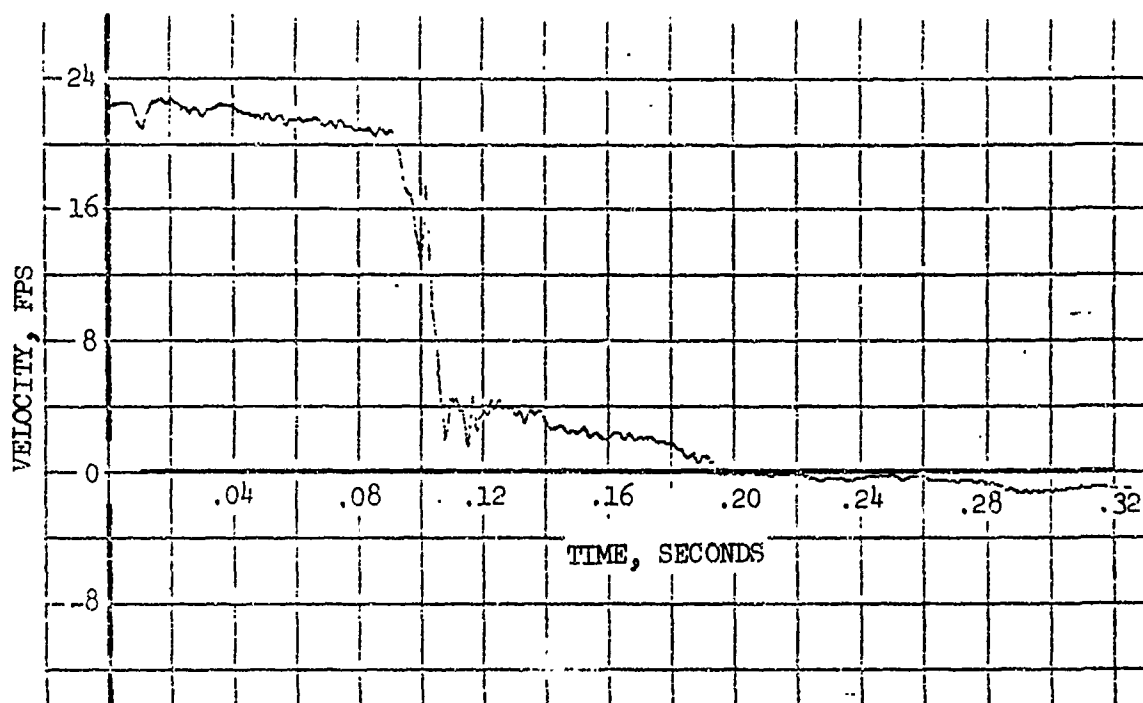


PAX FLOOR, REAR, LEFT, VERTICAL, CHANNEL 36

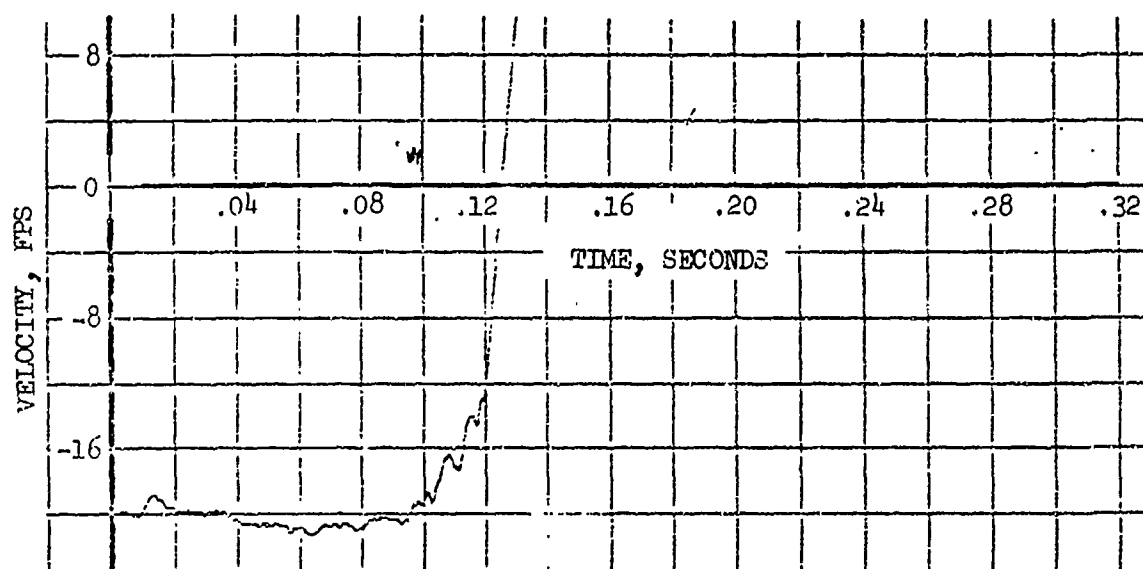


PAX FLOOR, REAR, LEFT, LATERAL, CHANNEL 37

Figure 65. Integrated Velocities, Passenger Floor, Rear Left.

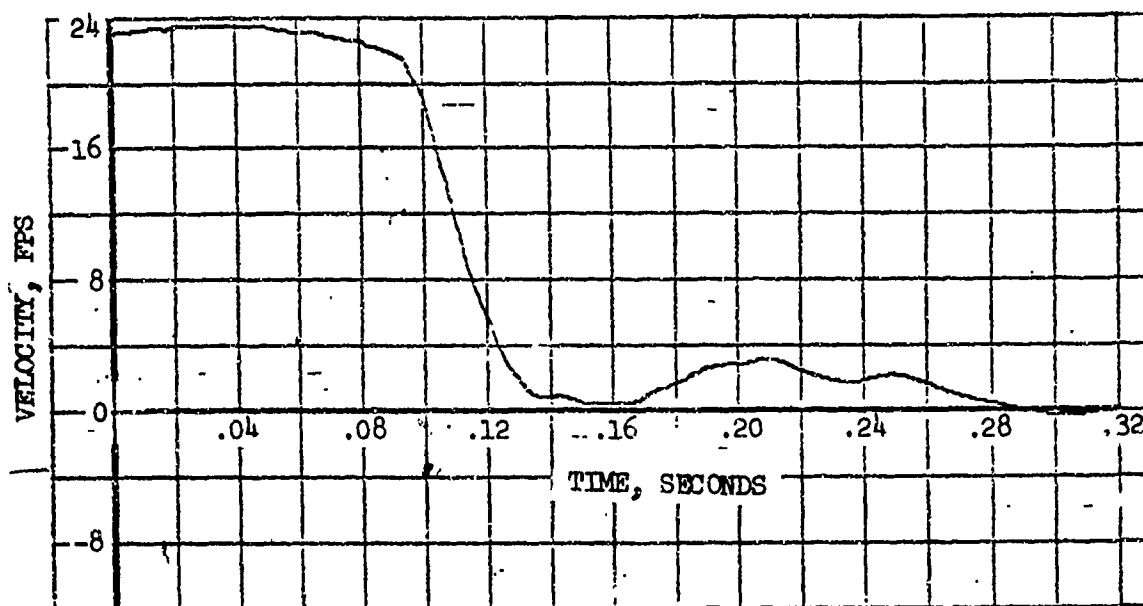


CARGO FLOOR, FWD. LEFT, VERTICAL, CHANNEL 38

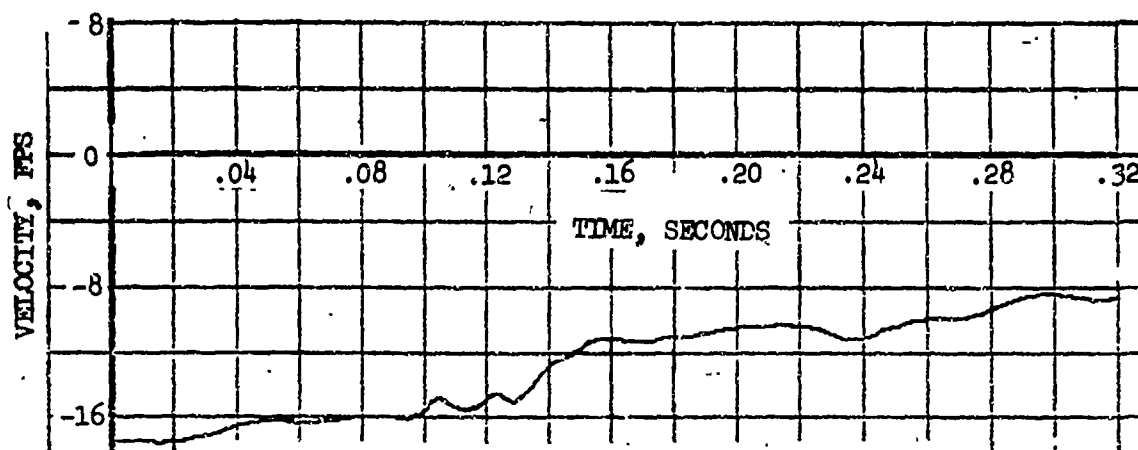


CARGO FLOOR, FWD. LEFT, LATERAL, CHANNEL 39

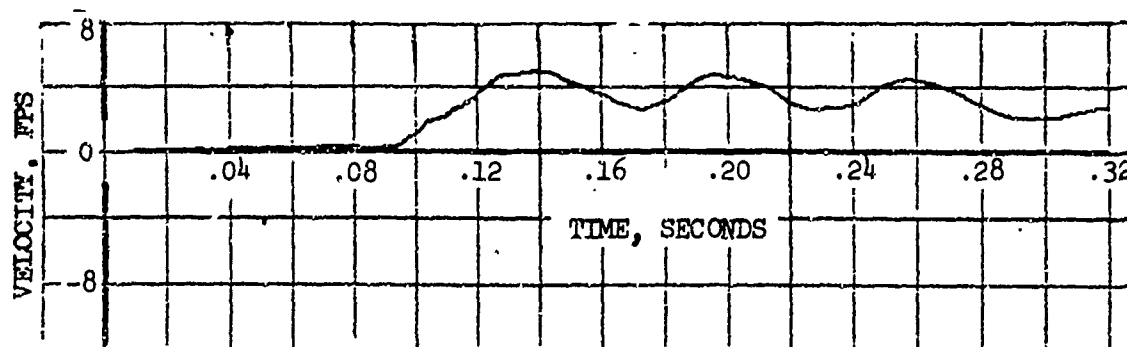
Figure 66. Integrated Velocities. Cargo Floor, Forward Left.



TRANSMISSION ROTOR HOUSING, VERTICAL, CHANNEL 40

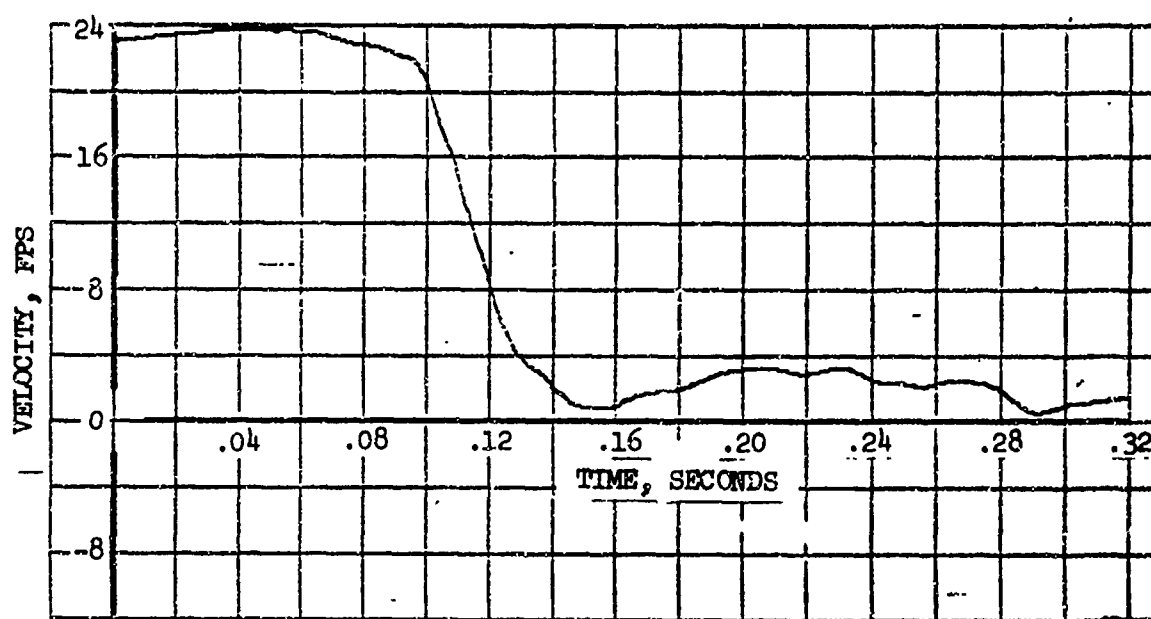


TRANSMISSION ROTOR HOUSING, LATERAL, CHANNEL 41

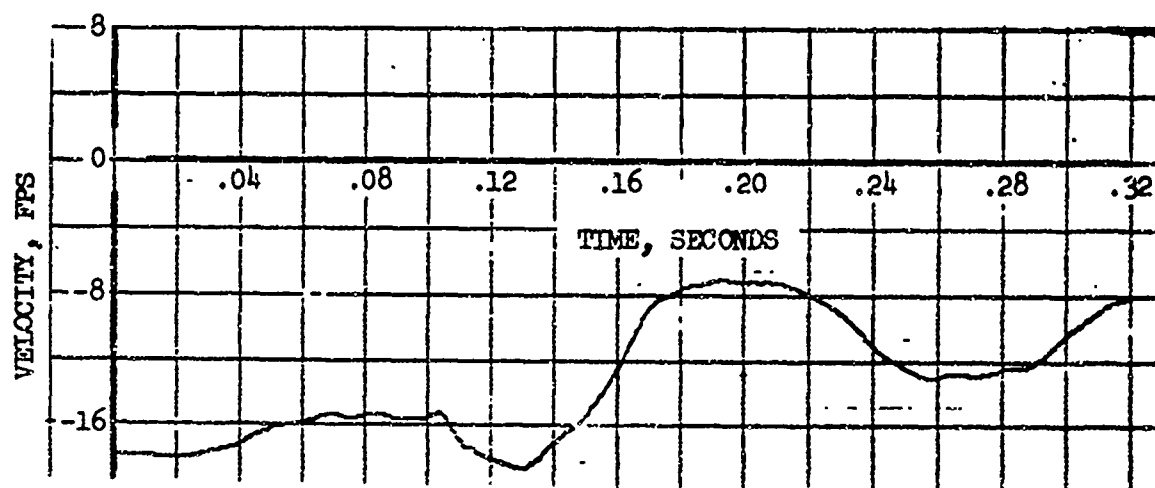


TRANSMISSION, ROTOR HOUSING, AXIAL, CHANNEL 42

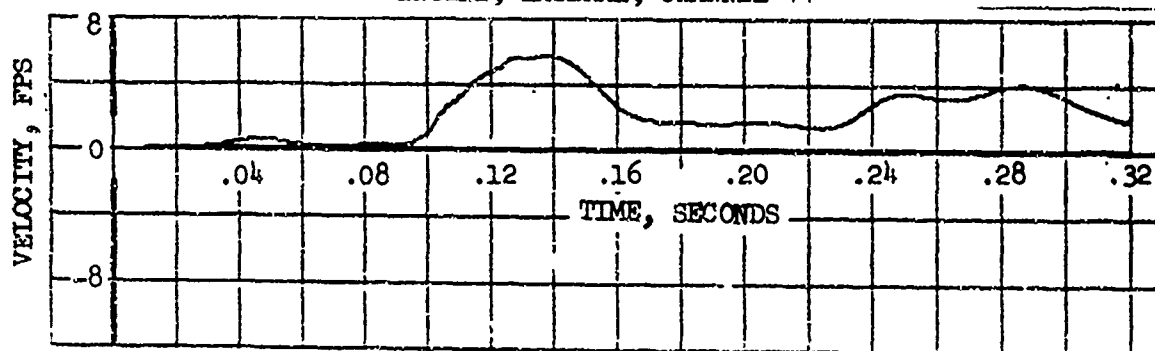
Figure 67. Integrated Velocities, Transmission Rotor Housing.



ENGINE, VERTICAL, CHANNEL 43

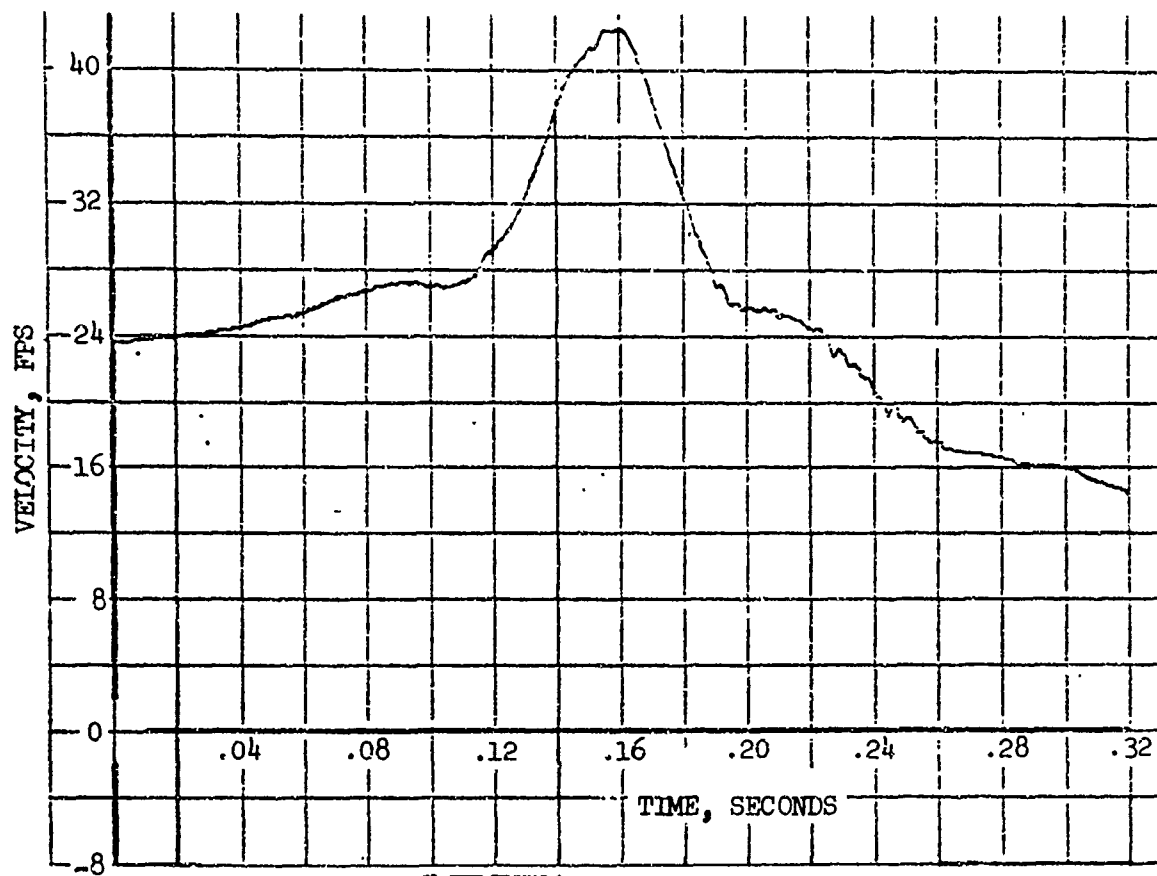


ENGINE, LATERAL, CHANNEL 44

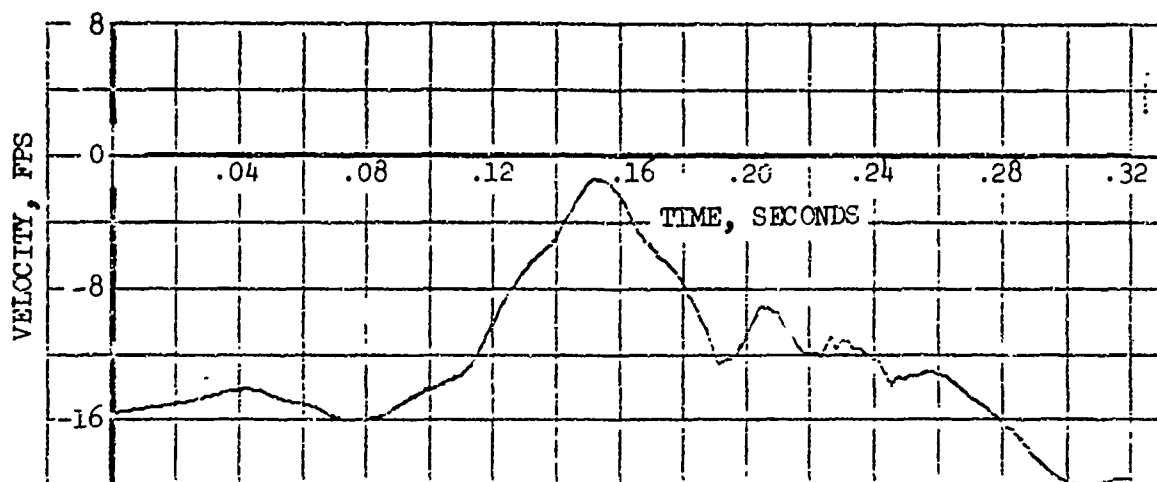


ENGINE, AXIAL, CHANNEL 45

Figure 68. Integrated Velocities, Engine.

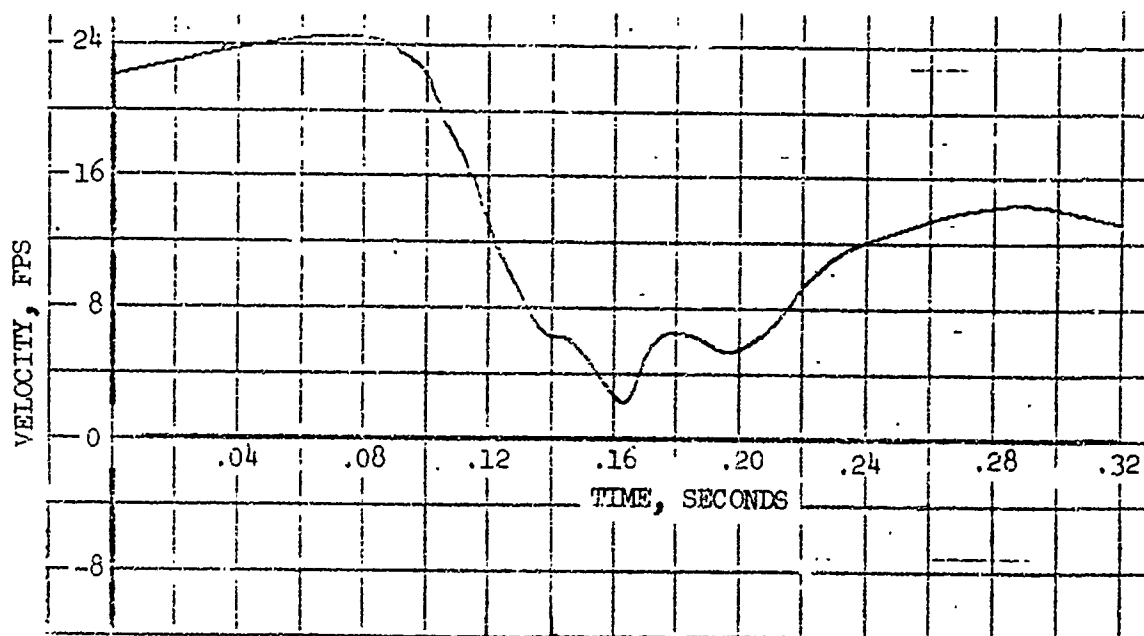


TAIL ROTOR GEARBOX, VERTICAL, CHANNEL 46

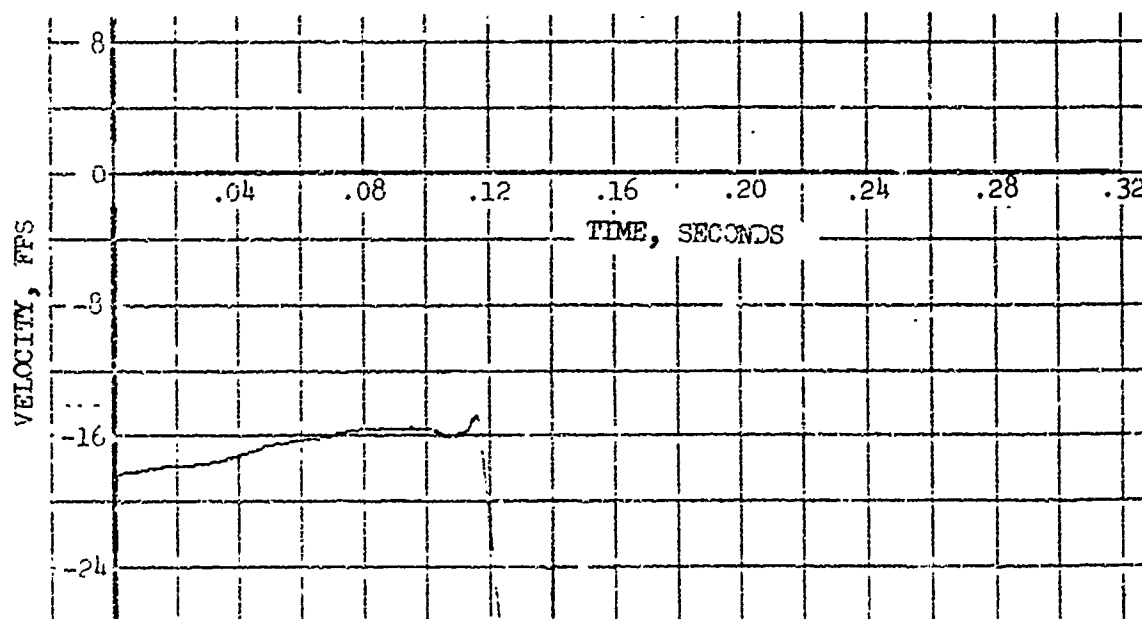


TAIL ROTOR GEARBOX, LATERAL, CHANNEL 47

Figure 69. Integrated Velocities, Tail Rotor Gearbox.

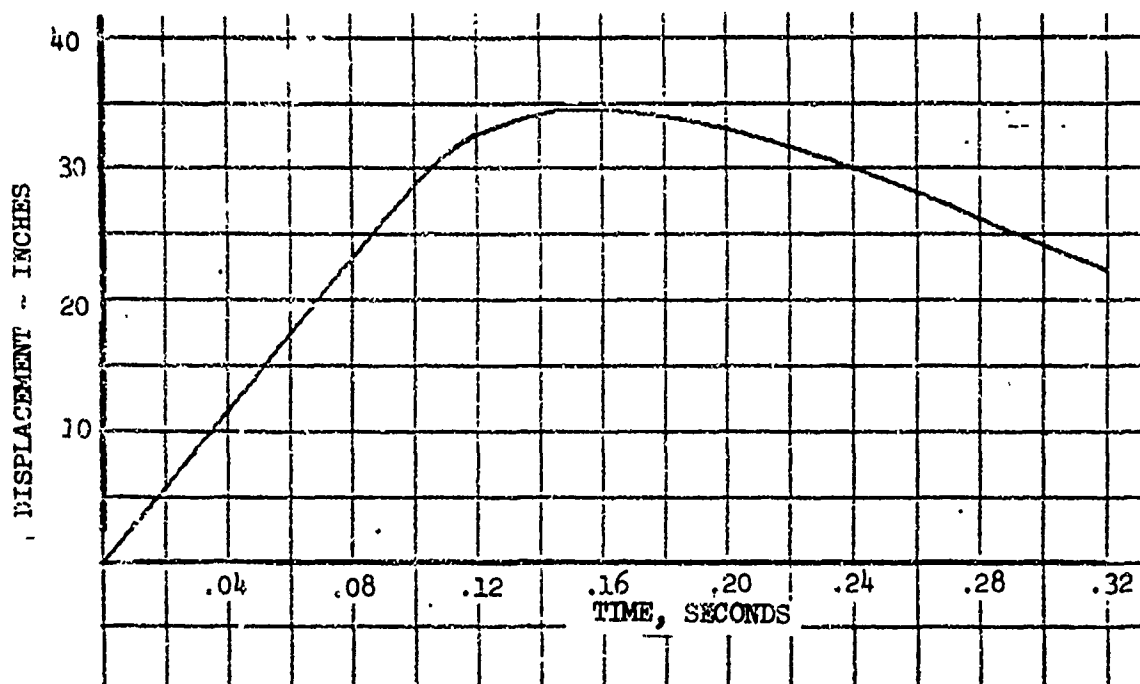


PAX PELVIC, VERTICAL, CHANNEL 48

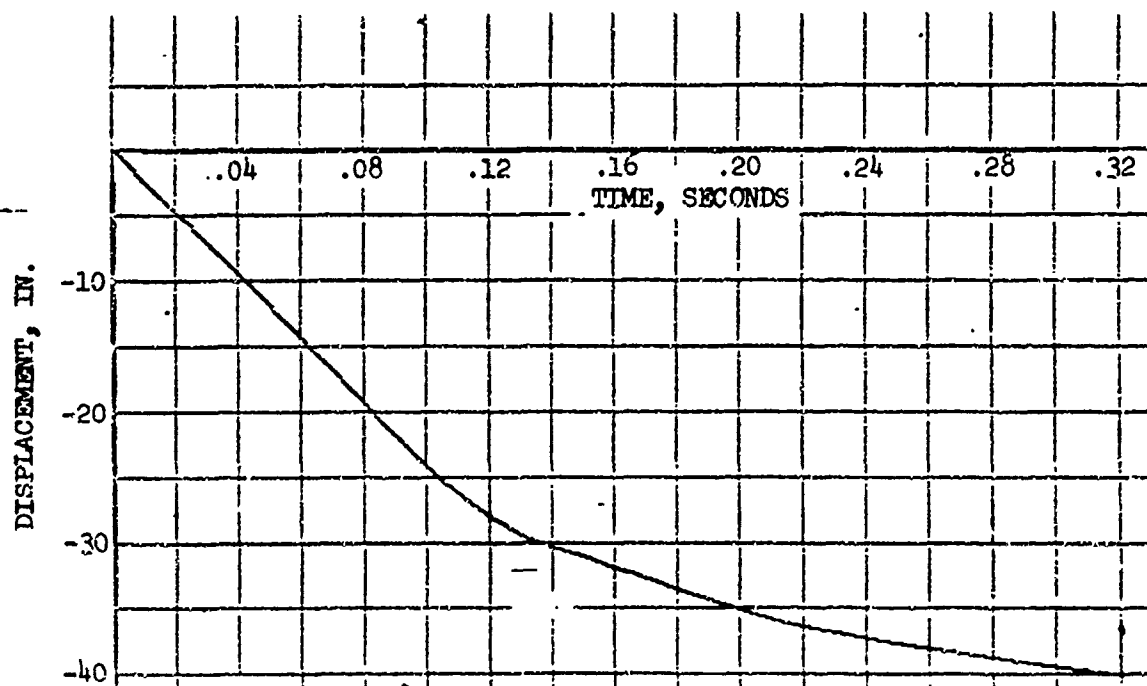


PAX PELVIC, LATERAL, CHANNEL 60

Figure 70. Integrated Velocities, Passenger Pelvic.

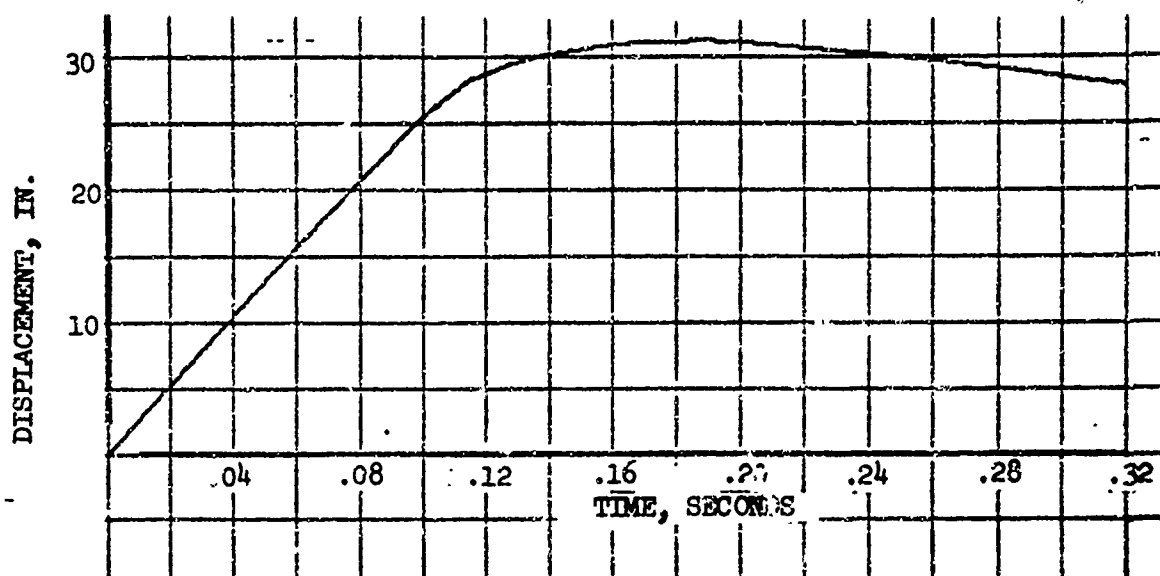


PILOT SEAT PAN, VERTICAL, CHANNEL 07

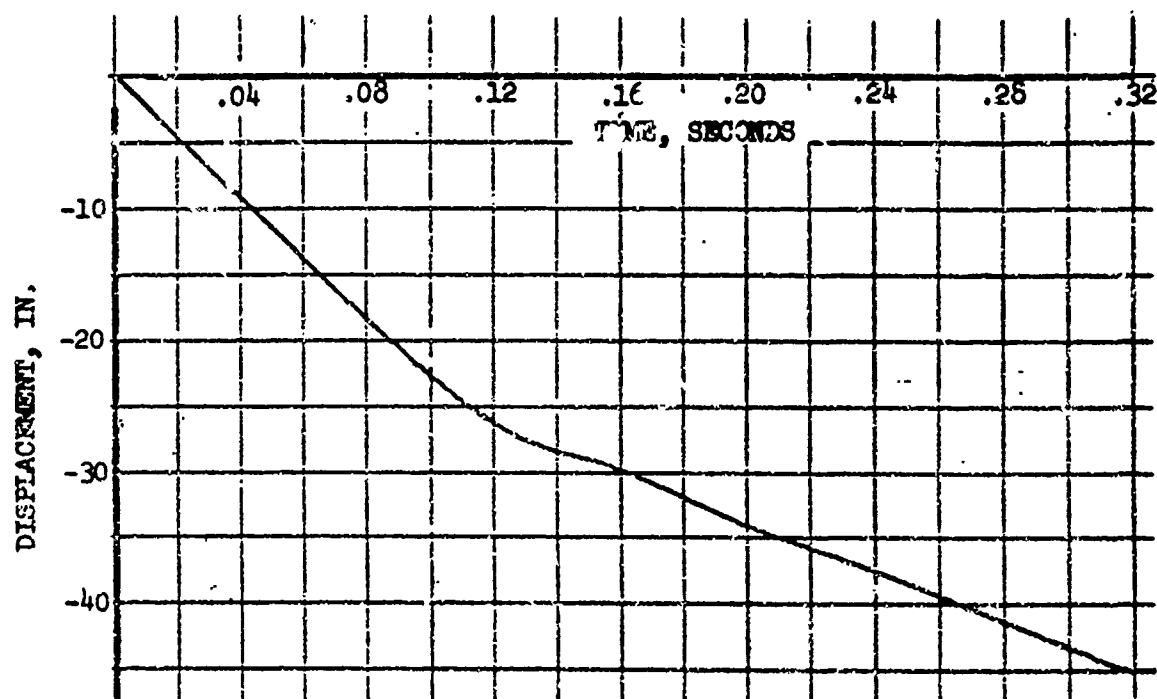


PILOT SEAT PAN, LATERAL, CHANNEL 08

Figure 71. Integrated Displacements, Pilot Seat Pan.



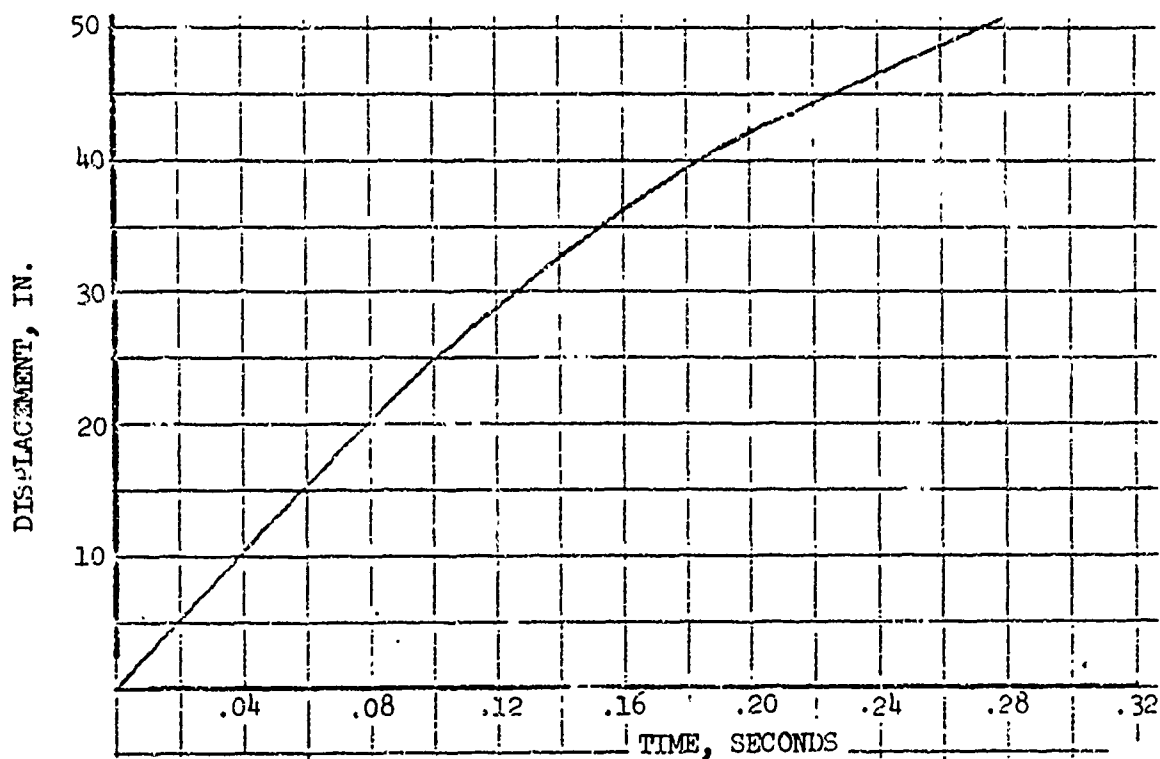
COPILOT SEAT PAN. VERTICAL, CHANNEL 09



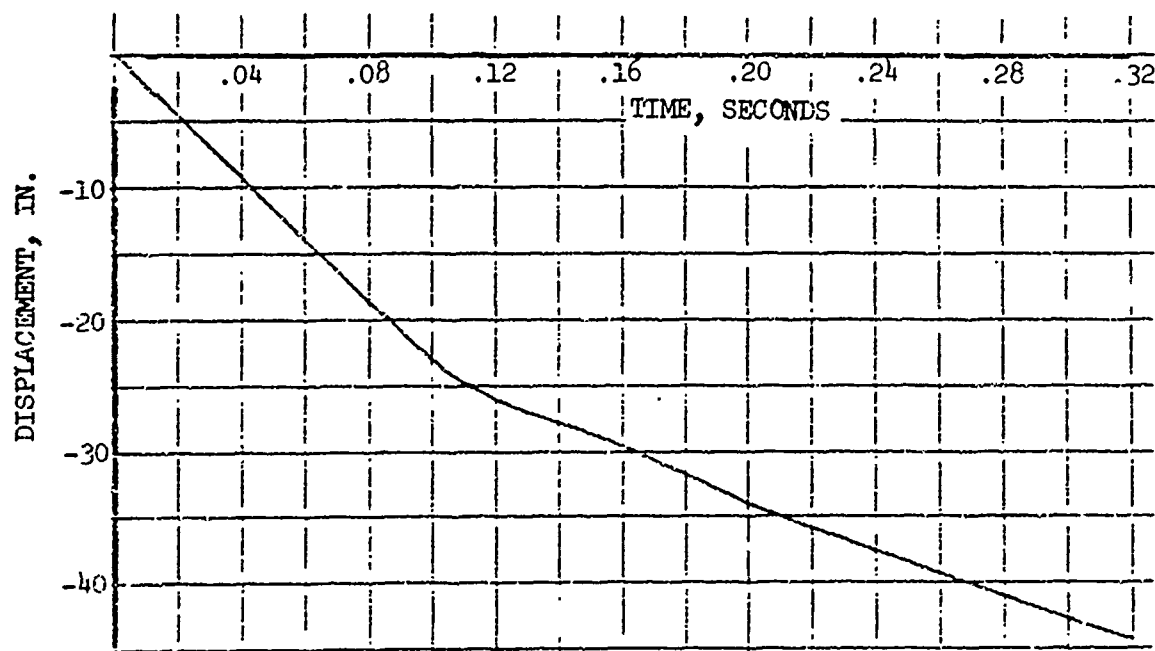
COPILOT SEAT PAN, LATERAL, CHANNEL 10

Figure 72. Integrated Displacements, Copilot Seat Pan.



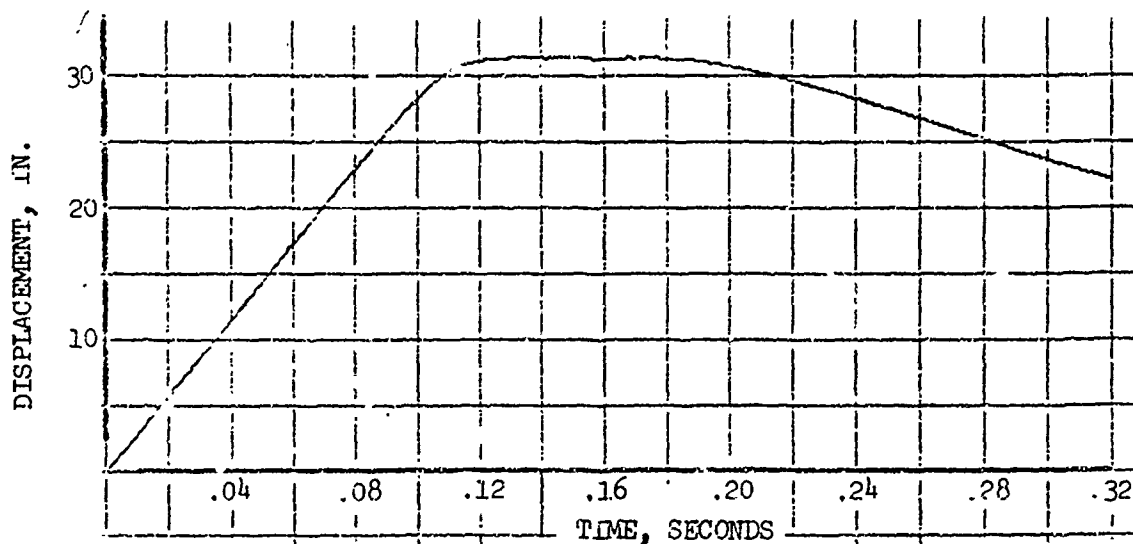


FLOOR, COPILOT LOC., VERTICAL, CHANNEL 30

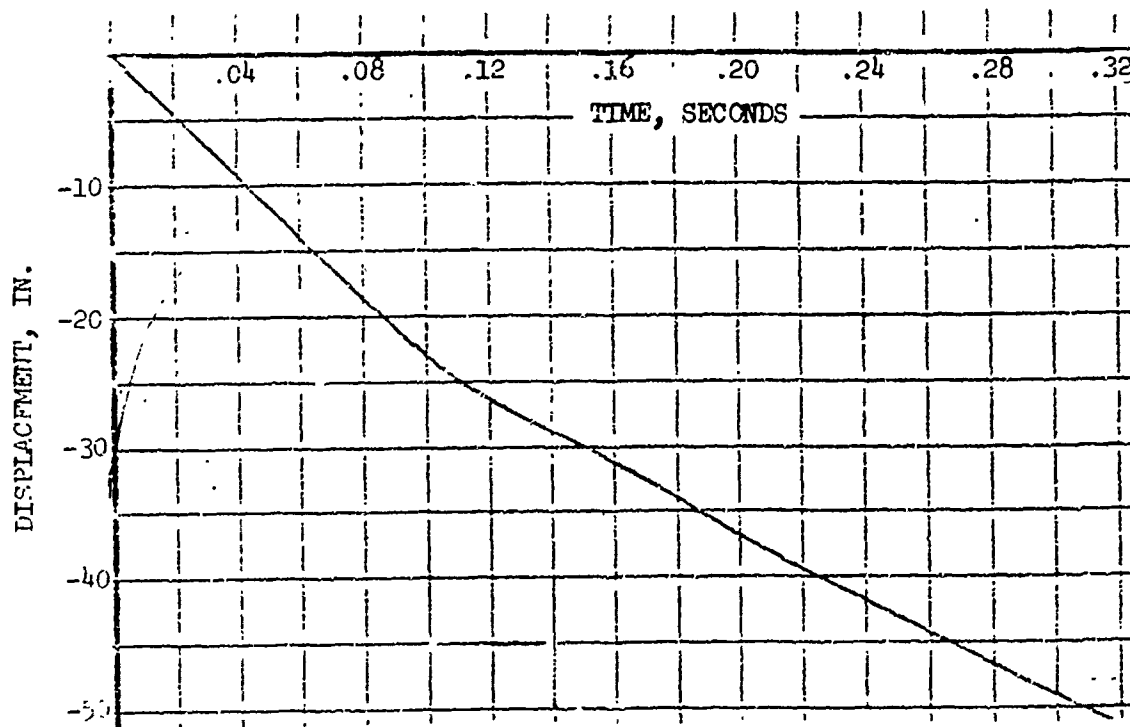


FLOOR, COPILOT LOC., LATERAL, CHANNEL 31

Figure 7b. Integrated Displacements, Floor, Copilot Location.

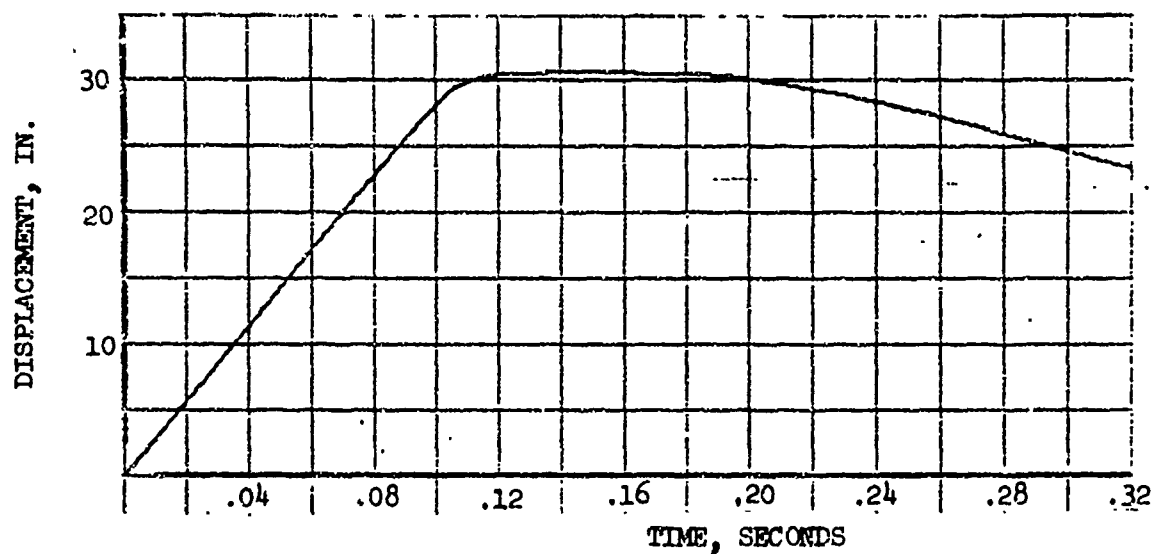


FLOOR, PILOT LOC., VERTICAL, CHANNEL 32

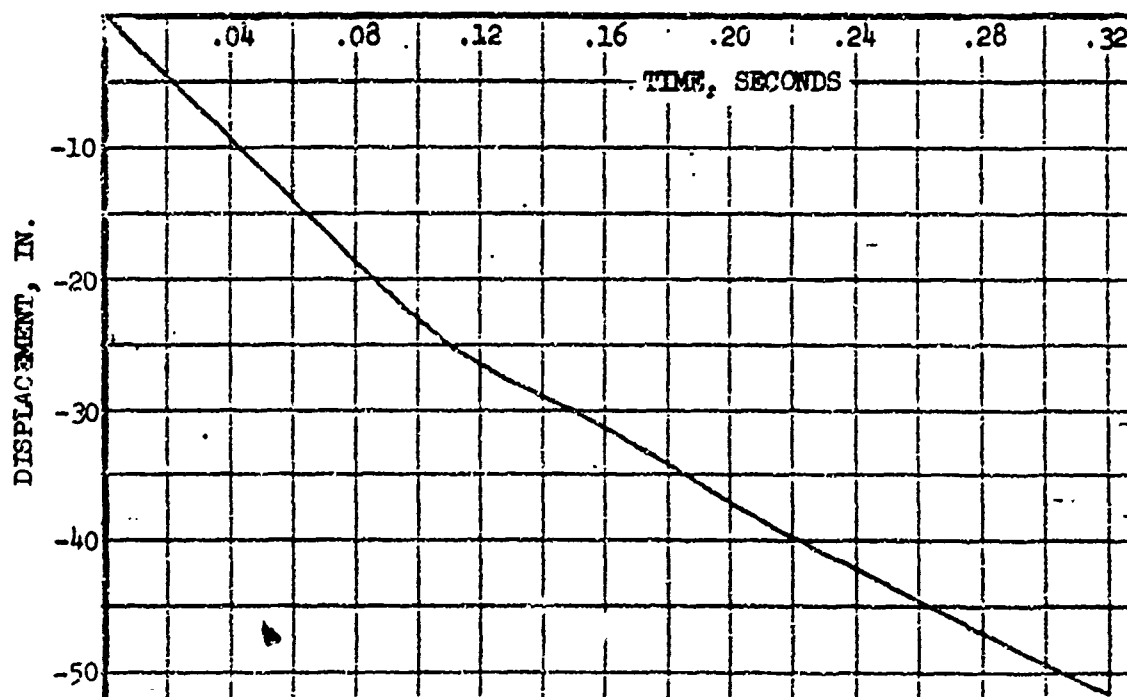


FLOOR, PILOT LOC., LATERAL, CHANNEL 33

Figure 7. Integrated Displacements, Floor, Pilot Location.

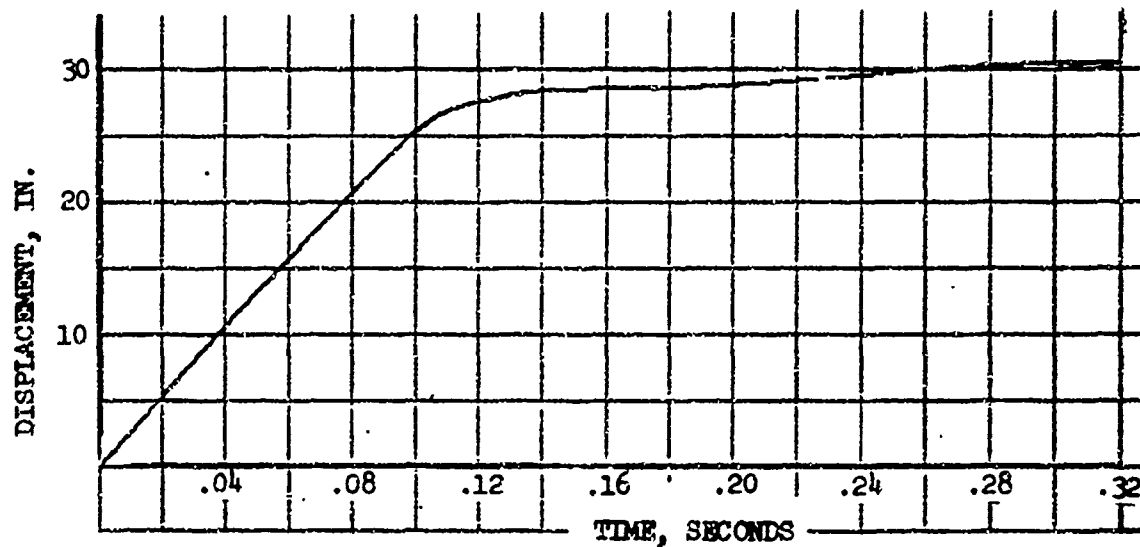


CARGO FLOOR, FWD. RIGHT, VERTICAL, CHANNEL 34

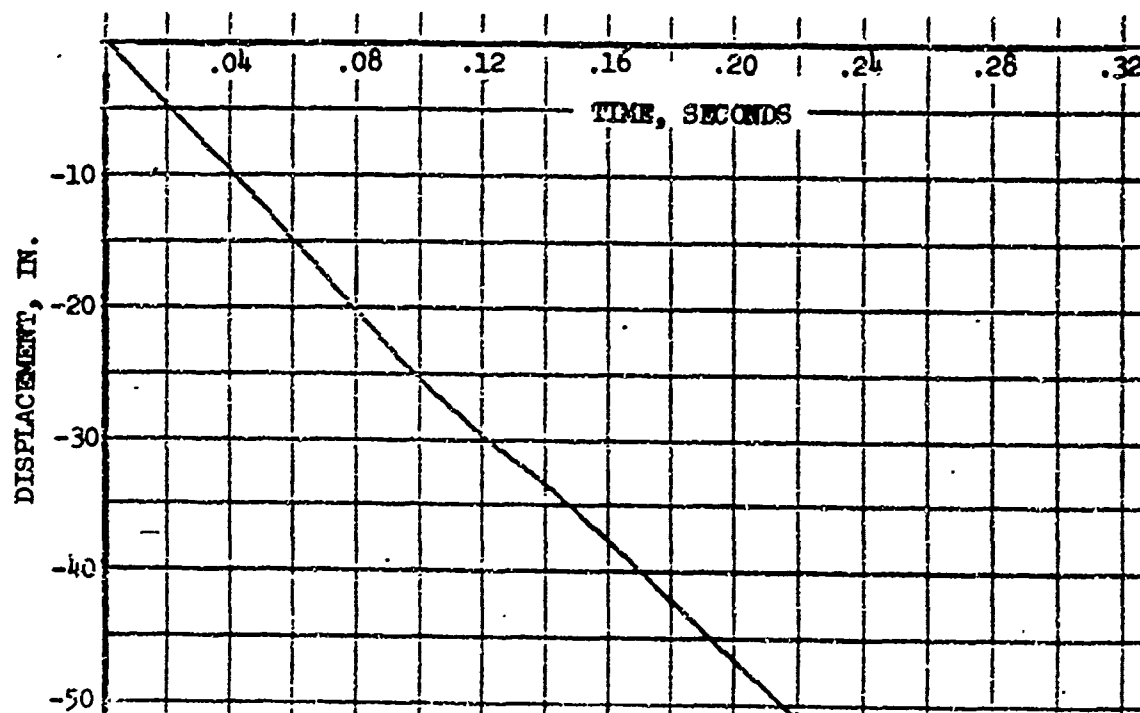


CARGO FLOOR, FWD. RIGHT, LATERAL, CHANNEL 35

Figure 75. Integrated Displacements, Cargo Floor Forward Right.

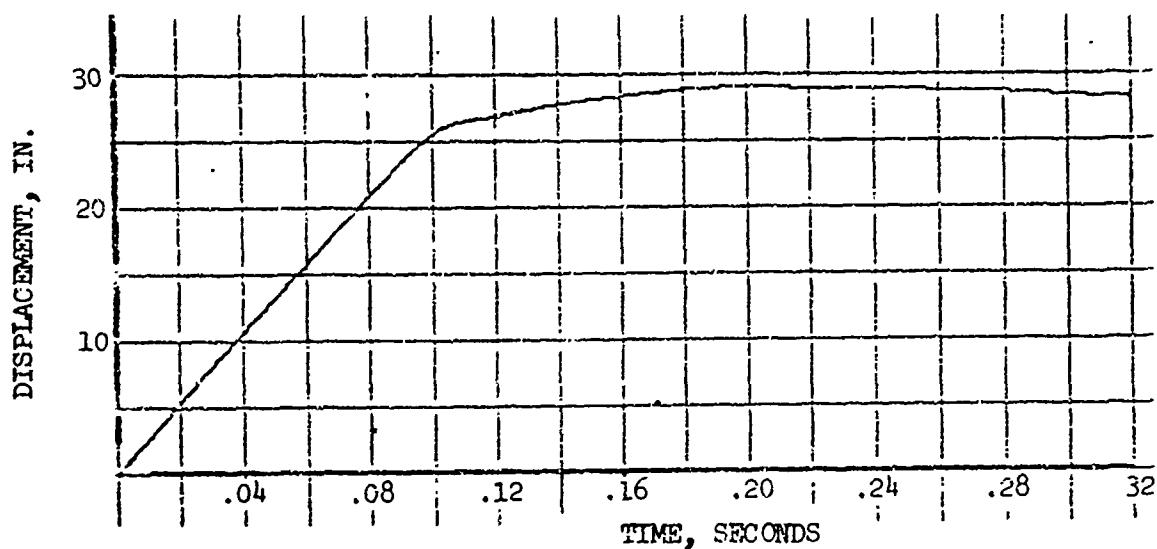


PAX FLOOR, REAR, LEFT, VERTICAL, CHANNEL 36

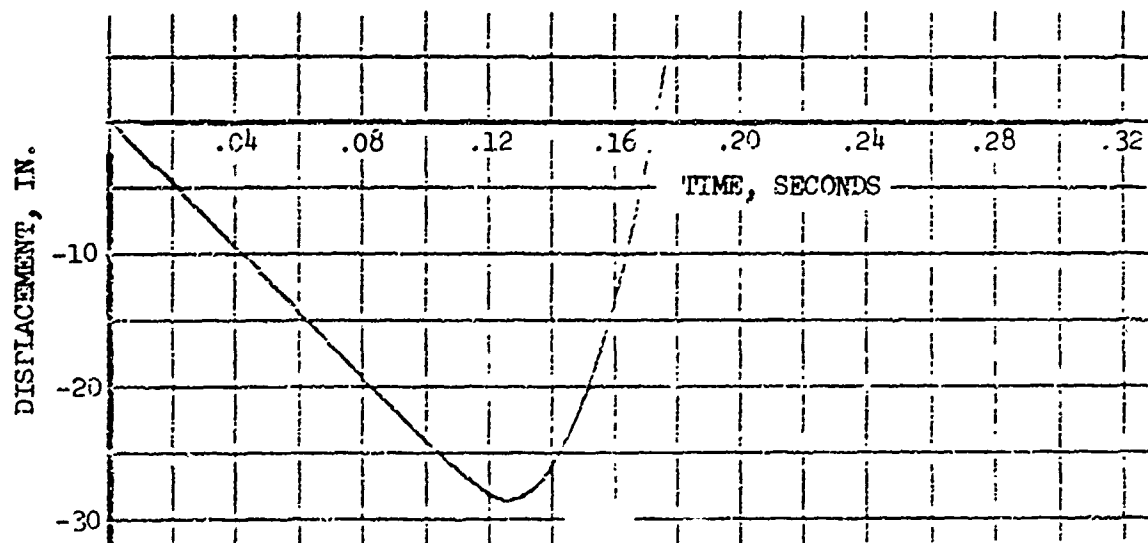


PAX FLOOR, REAR, LEFT, LATERAL, CHANNEL 37

Figure 76. Integrated Displacements, Passenger Floor Rear Left.



CARGO FLOOR, FWD. LEFT, VERTICAL, CHANNEL 38



CARGO FLOOR, FWD. LEFT, LATERAL, CHANNEL 39

Figure 77. Integrated Displacements, Cargo Floor Forward Left.

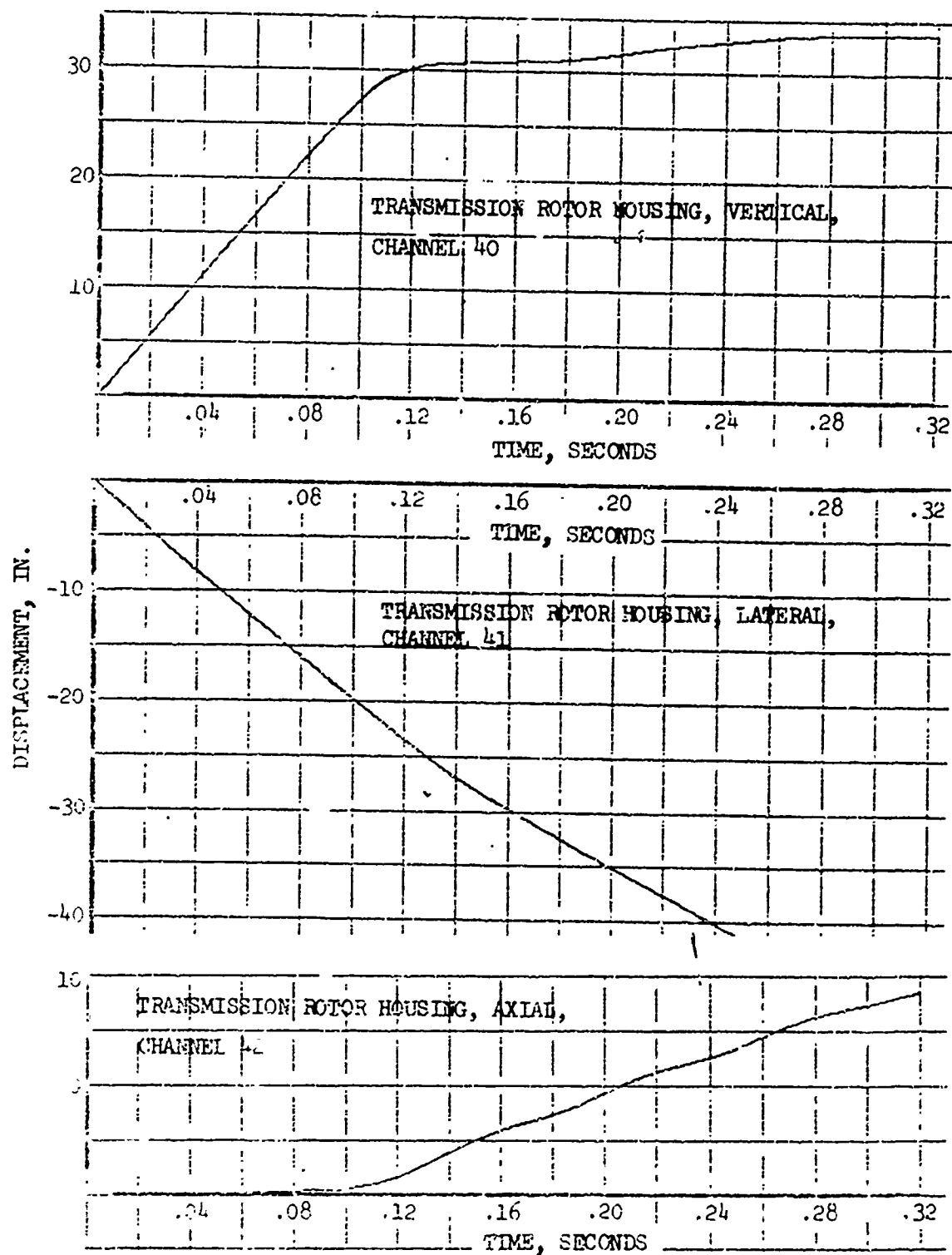


Figure 77. Integrated Displacements, Transmission Rotor Housing.

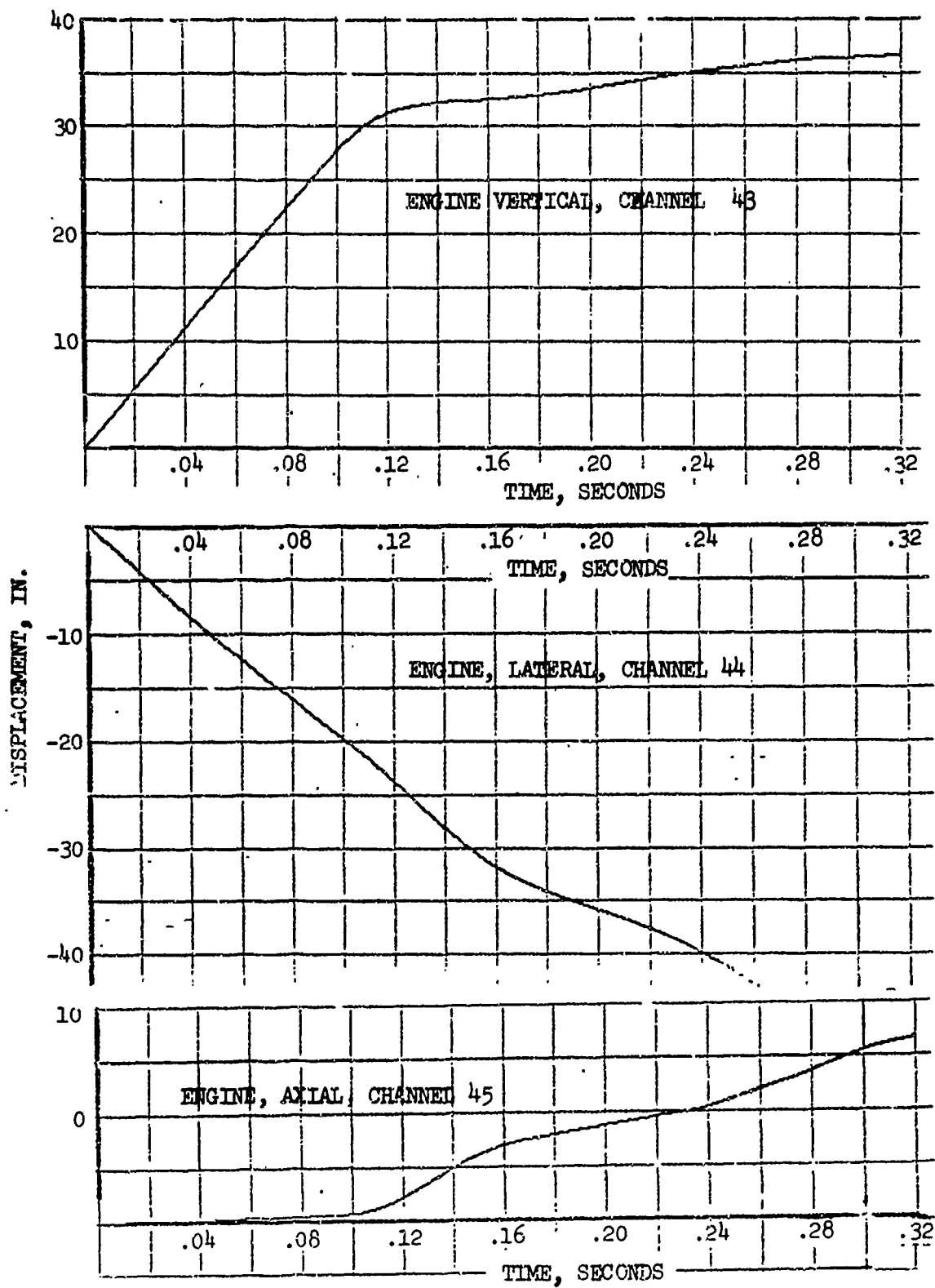


Figure 79. Integrated Displacements, Engine.

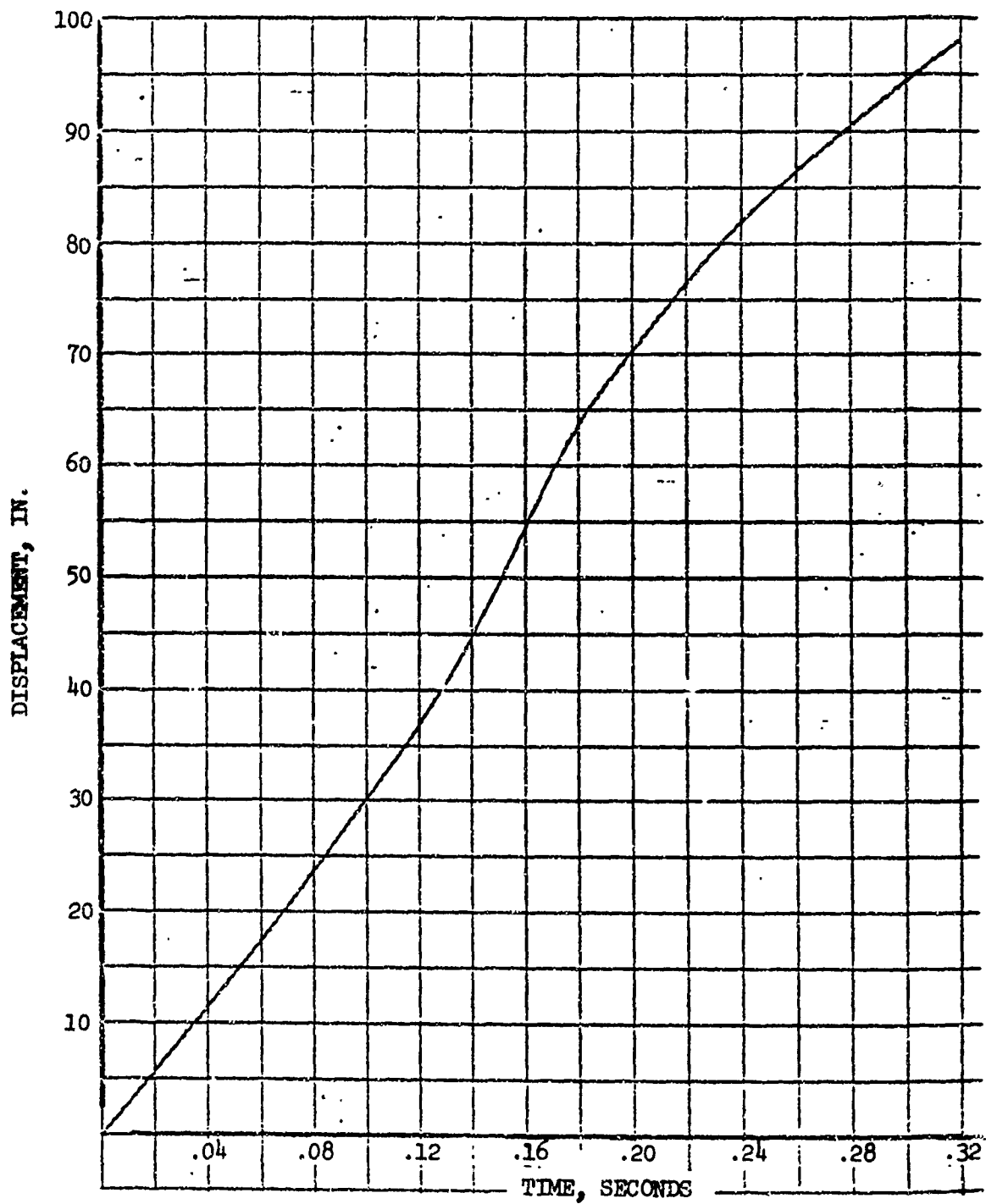


Figure 80. Integrated Displacement, Tail Rotor Gearbox, Vertical, Channel 46.



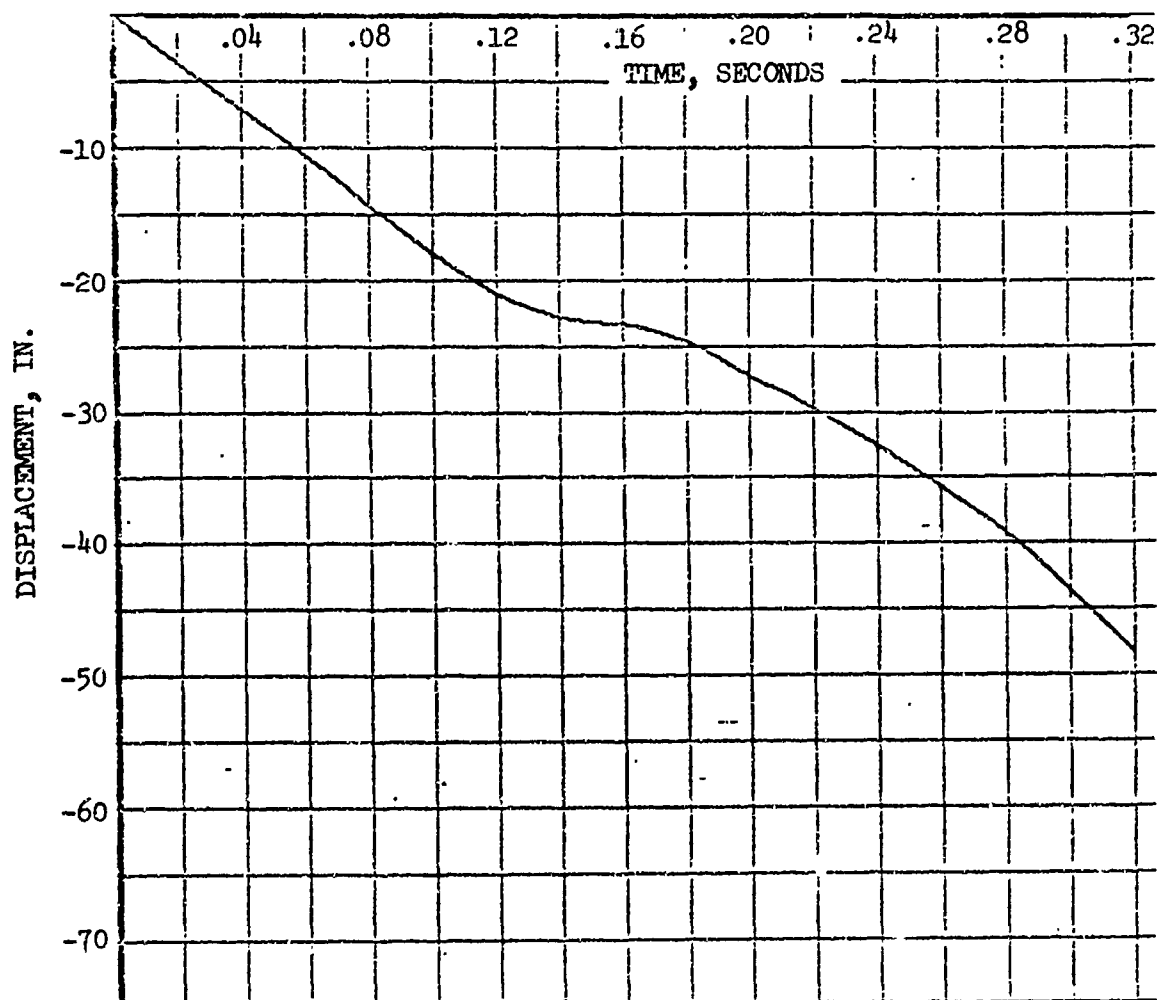
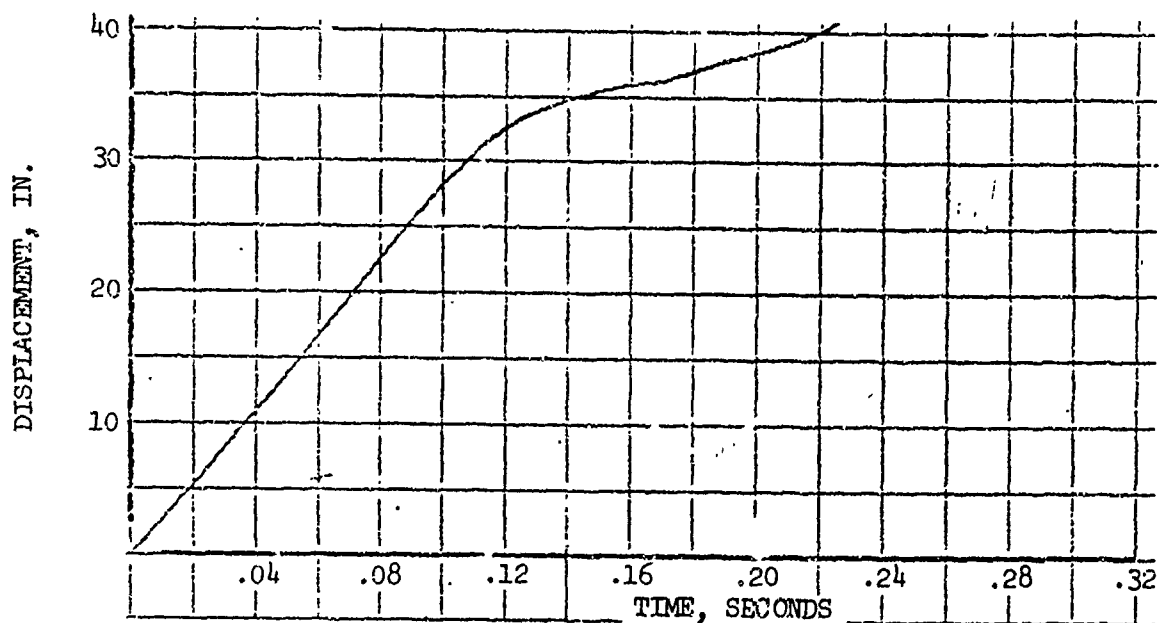
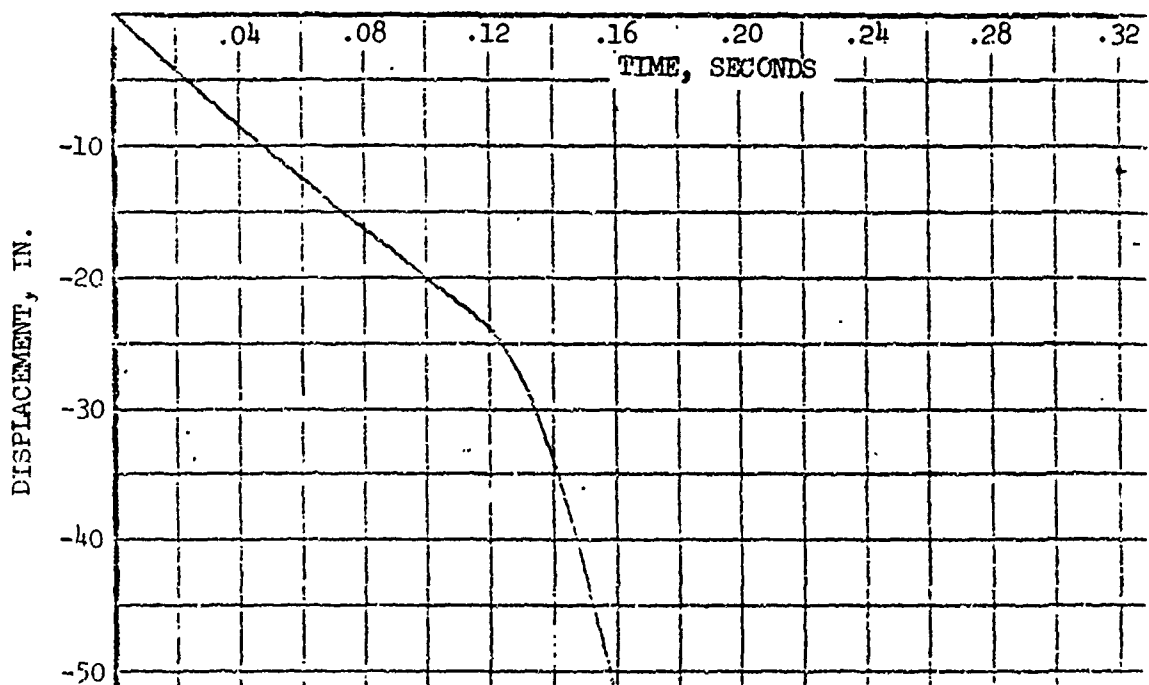


Figure 81. Integrated Displacement, Tail Rotor Gearbox,  
Lateral, Channel 47.



PAX PELVIC, VERTICAL, CHANNEL 48



PAX PELVIC, LATERAL, CHANNEL 60

Figure 82. Integrated Displacement, Passenger Pelvic.

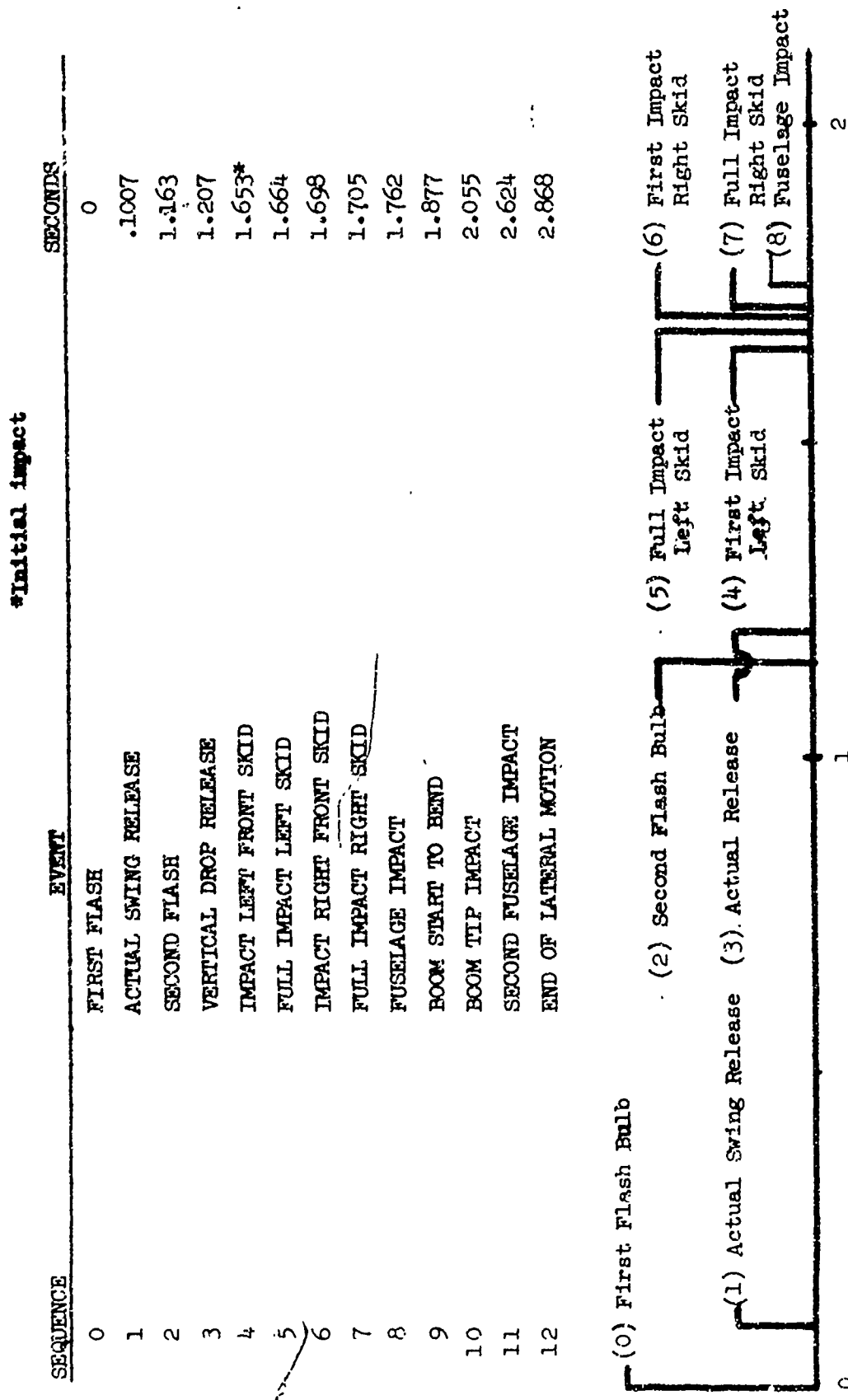


Figure 83. Sequence of Events - Film Data.

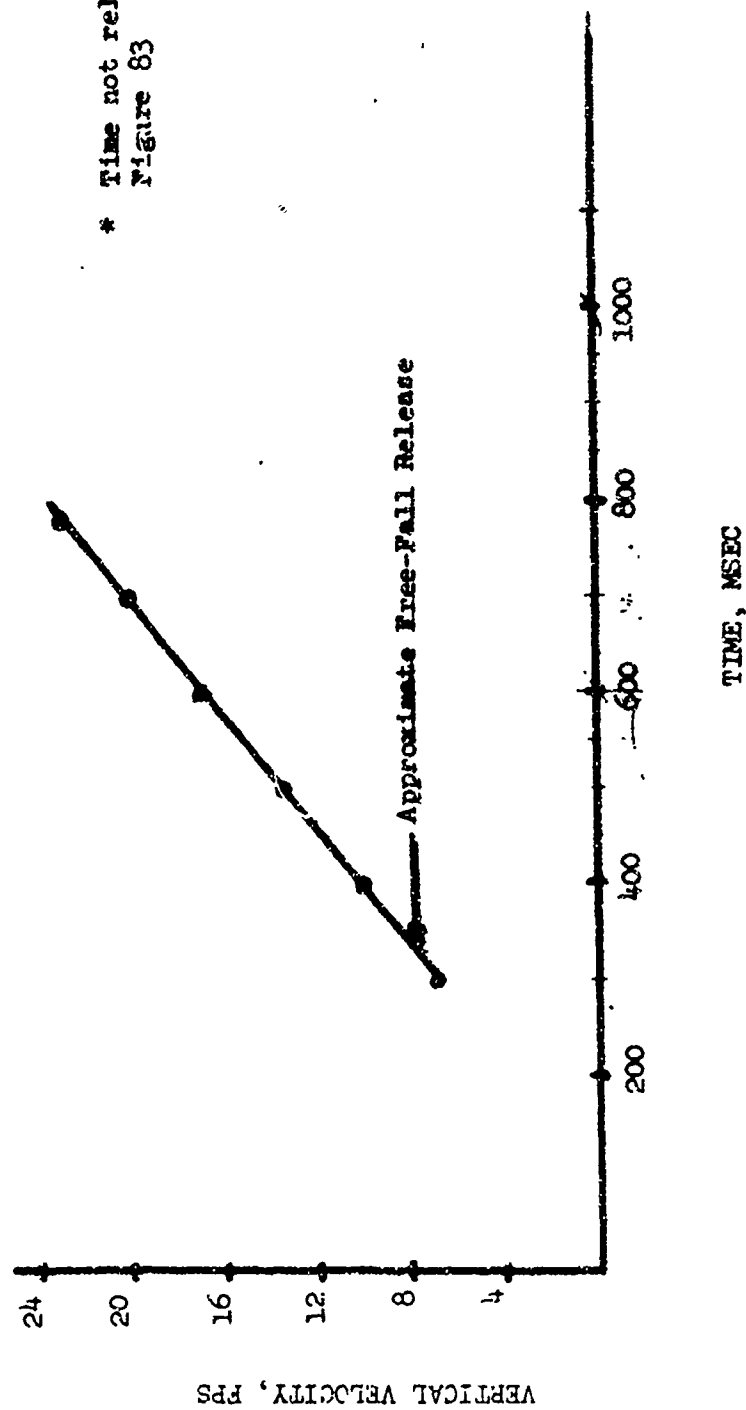
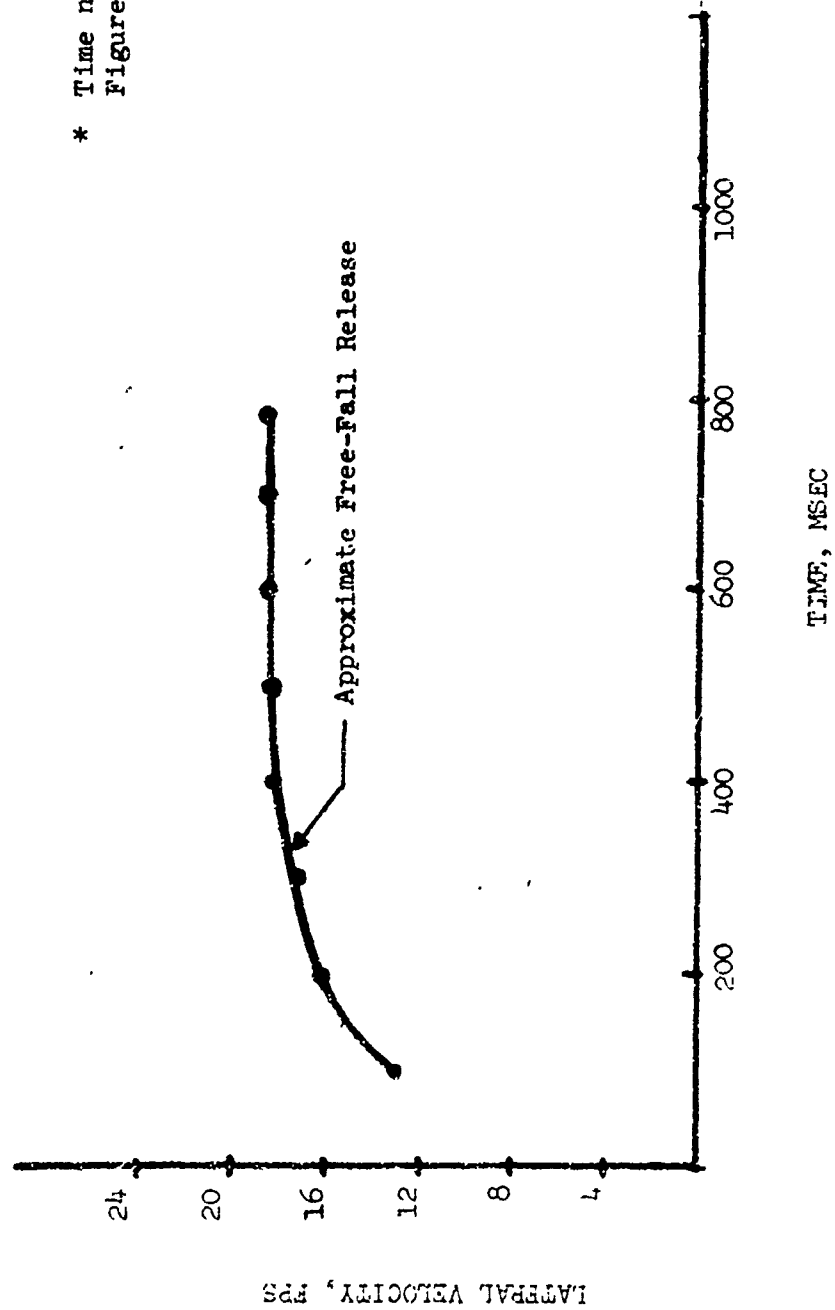


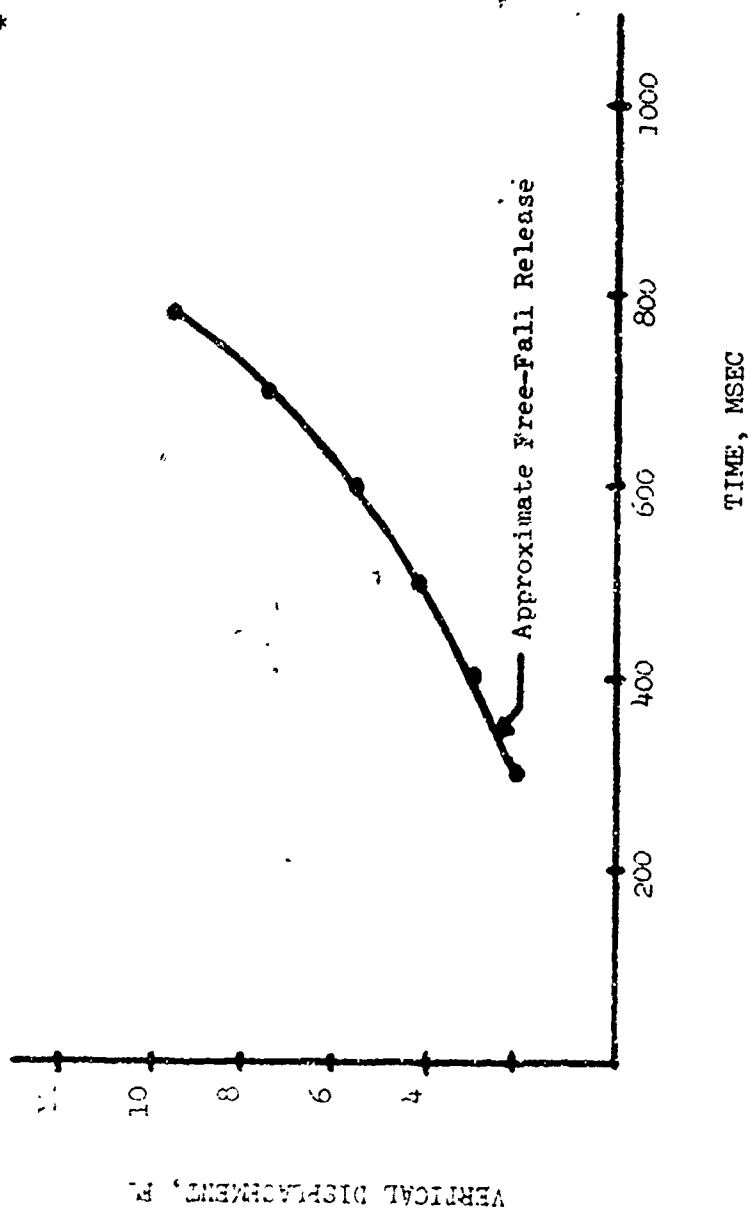
Figure 84. Vertical Impact Velocity - Film Data.



\* Time not related to  
Figure 83

Figure 85. Lateral Impact Velocity - Film Data

\* Time not related to  
Figure 83



FILE

Figure 86. Vertical Displacement - Film Data

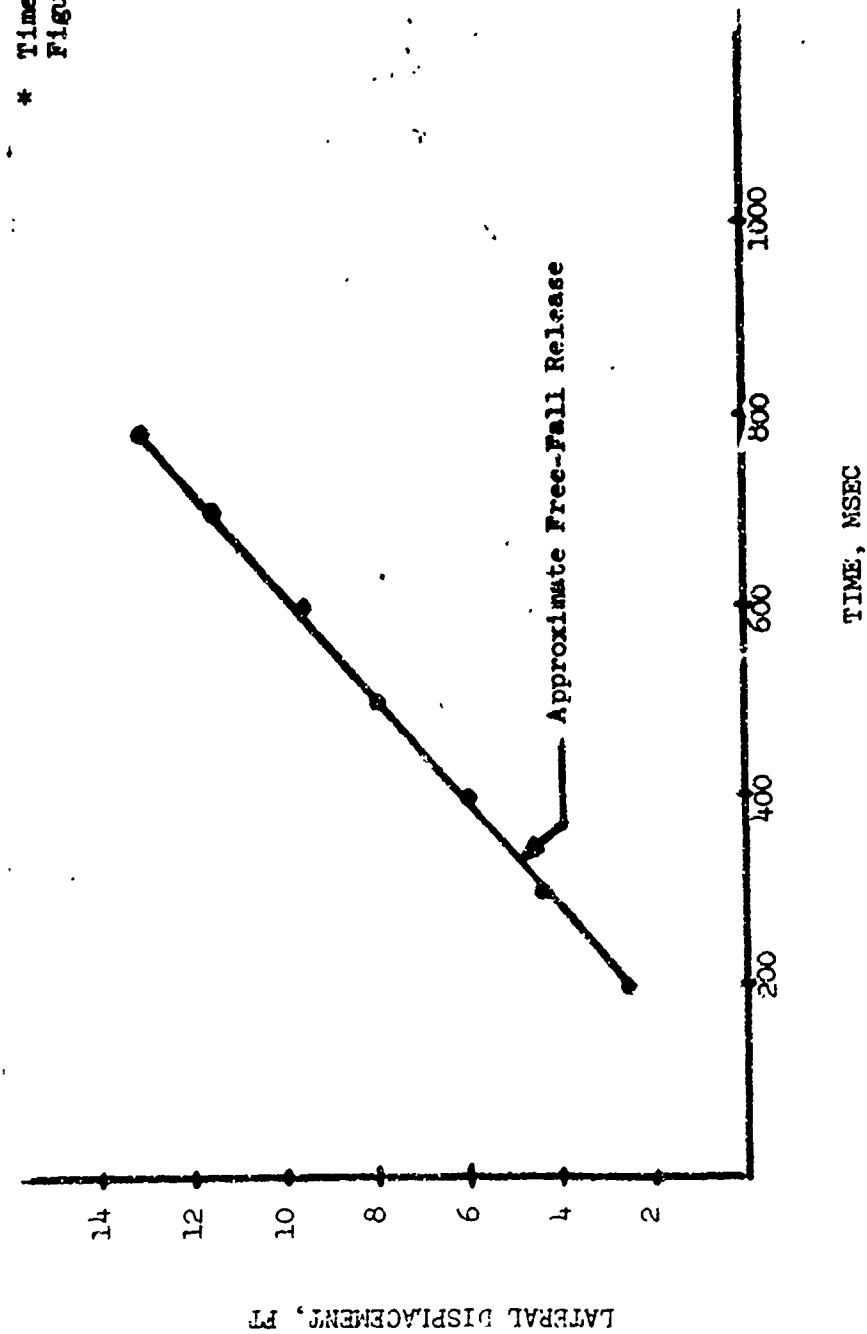


Figure 87. Lateral Displacement - Film Data

## CALCULATED TEST IMPACT VELOCITIES

### APPROACH NO. 1

#### 1. Position (1) Cable Load ( $P_c$ )

$$P_c = 8600 \text{ lb}$$



#### 2. Position (2) $40^\circ$ Rotation for Initial Swing Release

$$P_c = 8600 \cos 40^\circ$$

$$P_s = 8600 \sin 40^\circ$$

$$\cos 40^\circ = .77$$

$$\sin 40^\circ = .64$$

$$P_c = 8600 \times .77 = 6700 \text{ lb}$$

$$P_s = 8600 \times .64 = 5500 \text{ lb}$$

#### 3. Position (3) $24^\circ$ Rotation; Release for Free Fall

$$P_c = 8600 \times \cos 24^\circ$$

$$P_c = 8600 \times .91$$

$$P_c = 7800 \text{ lb}$$

$$\text{K.E.} = \text{P.E.}$$

$$\frac{W}{g} \frac{V^2}{2} = Wh$$

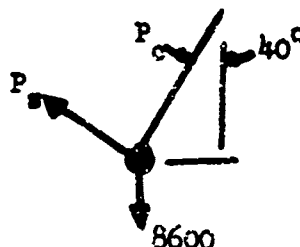
$$V = \sqrt{(2gh)}$$

$$V = [2 \times 32.2 (18.2 - 11.6)]^{\frac{1}{2}}$$

$$V = 20.2 \text{ fps}$$

$$V_h = 20.2 (.92) = 18.6$$

$$V_v = V (.405) = 8.20$$





#### 4. Position (4)

$$h_4 = 50 \sin 10^\circ + 48 \cos 10^\circ$$

$$\sin 10^\circ = .1736$$

$$\cos 10^\circ = .9848$$

$$h_4 = (50 \times .1736 + 48 \times .9848) 1/12$$

$$h_4 = (8.63 + 47.5) 1/12$$

$$h_4 = 4.65 \text{ ft.}$$

$$h_4 = \frac{1}{2} g t^2 + v_v t = 4.65$$

$$h = 11.6 - 4.65 = 6.95$$

$$16.1 t^2 + 8.2 t - 6.95 = 0$$

$$t = \frac{-b + \sqrt{b^2 - 4ac}}{2a}$$

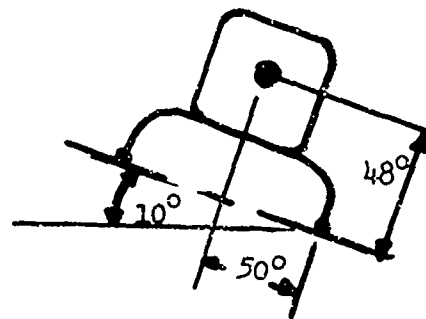
$$t = .5 \text{ sec}$$

$$V = \sqrt{v_o^2 + (2 gh)}$$

$$= \sqrt{(8.2)^2 + (64.4 \times 6.95)}$$

$$V = 22.8 \text{ fps}$$

$$Sh = 18.6 \times .5 = 9.3 \text{ ft (lateral horizontal displacement of vehicle)}$$



#### APPROACH NO. 2

$$KE = (1/2) I \omega^2 = Wh$$

$$I_x = 33034 \text{ lb-in.-sec}^2 (\text{Roll})$$

$$W_t = 8600 \text{ lb}$$

$$= 8600 (12 \times 6.6) = 680,000 \text{ in.-lb}$$

$$h = 18.2 - 11.6 = 6.6$$

$$I_{xt} = I_x + (M_o d^2) = 33034 + \left[ \frac{8600}{386} \times (42 \times 12^2) \right] =$$

$$= 33034 + (6,050,000) = 6.1 (10^6)$$

$I_{xt}$  refers to fulcrum point at 46 ft from CG

APPROACH NO. 2 (Cont'd)

$$I_{xt} = 0.1 (10^6) \text{ lb-in.-sec}^2$$

$$\omega = \sqrt{\frac{2 \cdot KE}{I}} = \sqrt{\frac{2 \times 680,000}{6.1 (10)^6}} = .48 \text{ rad/sec}$$

$$V_t = R\omega = (42 \times 12) .48 = 240 \text{ in./sec}$$

$$V_t = \text{Tangential Vel} = 20 \text{ ft/sec}$$

$$V_v = V_t (\sin \quad) = 240 (.405) = 8.1 \text{ ft/sec}$$

$$V_h = V_t (\cos \quad) = 240 (.92) = 18.4 \text{ ft/sec}$$

Assume that at ground the CG is 4.7 ft from the ground level.

The free vertical distance is: (11.6 - 4.7)

The final vertical velocity is:

$$V_{v4} = \sqrt{V_{v3}^2 + 2gh} = 22.6 \text{ ft/sec}$$

1

The time for the free-fall portion is:

$$t = \frac{S_v}{V_v \text{ avg.}} = .48 \text{ sec}$$

Assuming that the lateral (horizontal) velocity is constant, the lateral horizontal displacement of the body is:

$$S_h = V_{h_{3-4}} (t) = 18.4 (.48) = 8.9 \text{ ft}$$

1 The vertical velocity stated in the test plan was based on expressing the final velocity as  $\sqrt{2gh + v^1}$

$v^1$  = vertical velocity component at initiation of free fall

## ANALYTICAL DATA

### COMPUTER OUTPUT CORRELATION RUN

The results of the analysis using a 31-mass model to correlate with the drop test data are presented in the section in Volume I entitled CORRELATION. The following output plots representing a cross section of the time histories are presented in Figures 88 through 100:

- Aft Fuselage Lateral Velocity
- Forward Fuselage Lateral Velocity
- Aft Fuselage Vertical Velocity
- Forward Fuselage Vertical Velocity
- Engine Lateral Acceleration
- Transmission Rotor Housing Lateral Acceleration
- Mid Fuselage Lateral Acceleration
- Engine Vertical Acceleration
- Transmission Rotor Housing Vertical Acceleration
- Mid Fuselage Vertical Acceleration
- Engine Mount Vertical Deflection
- Transmission Mount Vertical Deflection
- Forward Occupant Vertical Deflection

### COMPARISON OF ANALYTICAL AND TEST RESULTS - AXIAL RESPONSES

Figures 101 through 106 show comparisons of analytical and test axial responses for the engine and transmission. Accelerations, velocities and displacements are presented. No attempt was made to obtain good correlation with the axial responses, since the objective was to obtain good correlation of a combined vertical-lateral drop. However, the acceleration results are still close to the right magnitude, although the analytical results appear to lag behind the test results by 30-50 milliseconds. The velocities and displacements show consistent trends, but the magnitudes are off. It is felt that the results shown are quite reasonable for a first approximation of the input data, and that acceptable correlation of the axial responses could be obtained with a little additional effort.

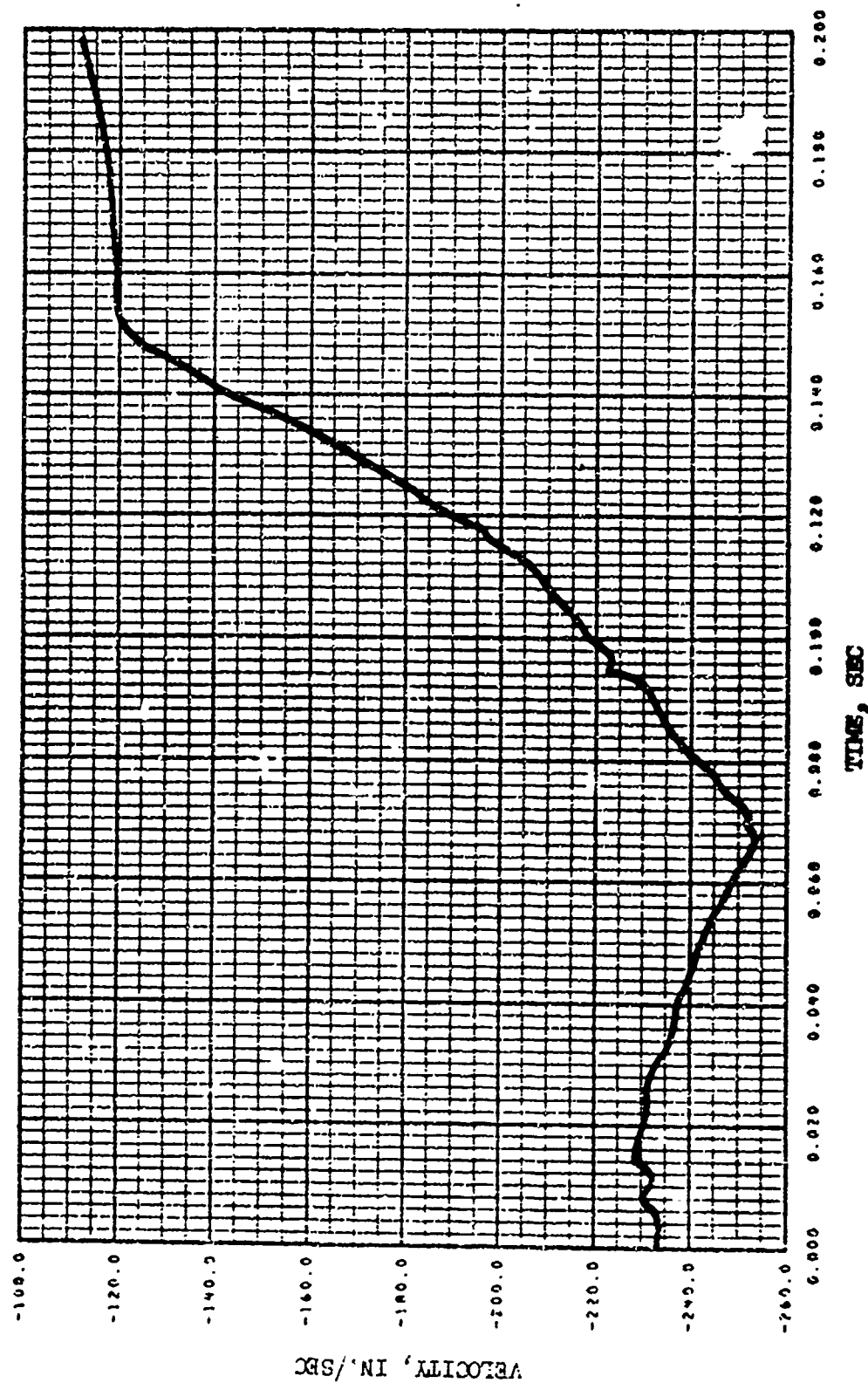


Figure 88. Correlation Run Analysis Output, Aft Floor, Lateral Velocity Time History.

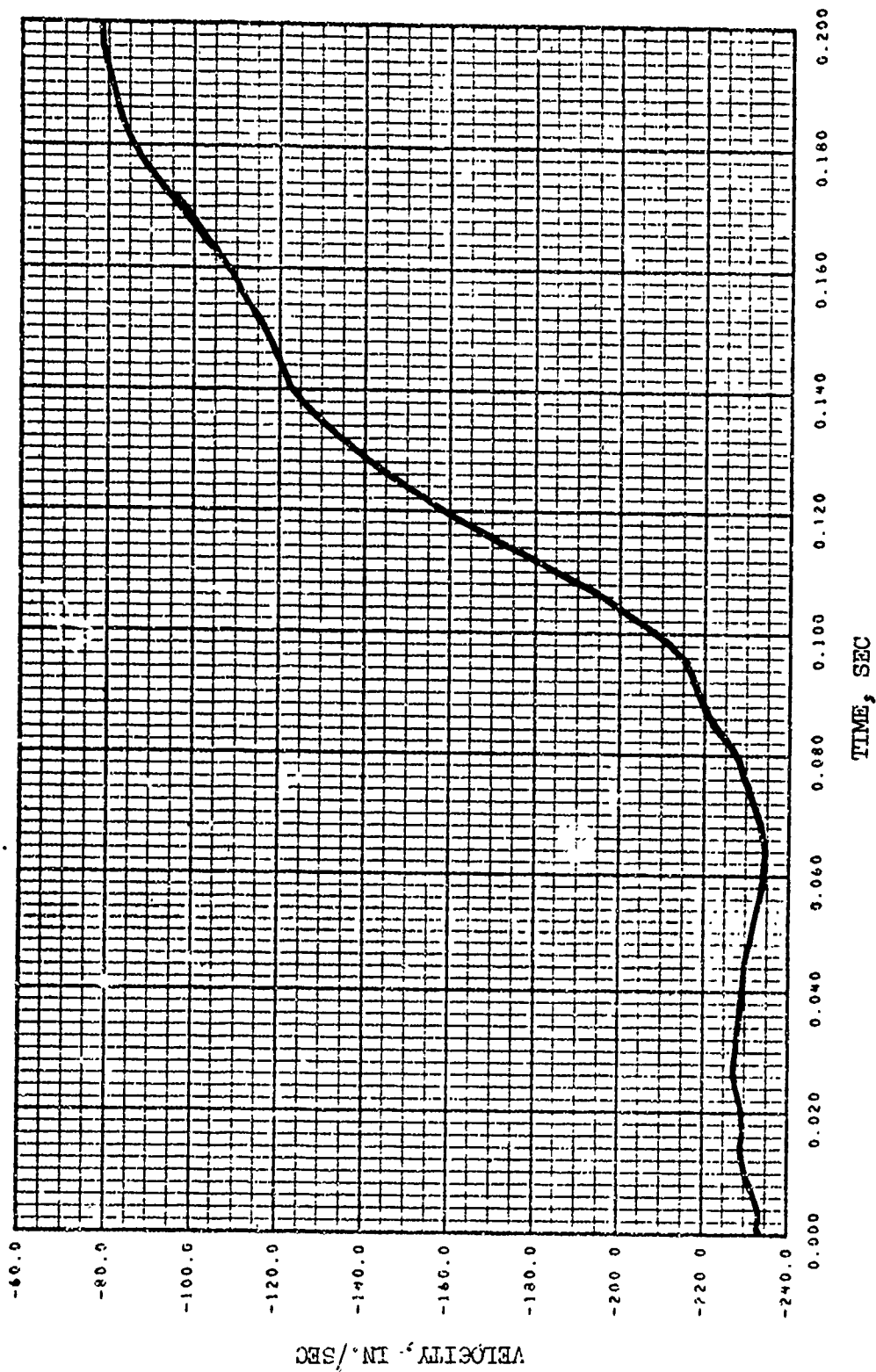


Figure 89. Correlation Run Analysis Output, Forward Floor, Lateral Velocity Time History.

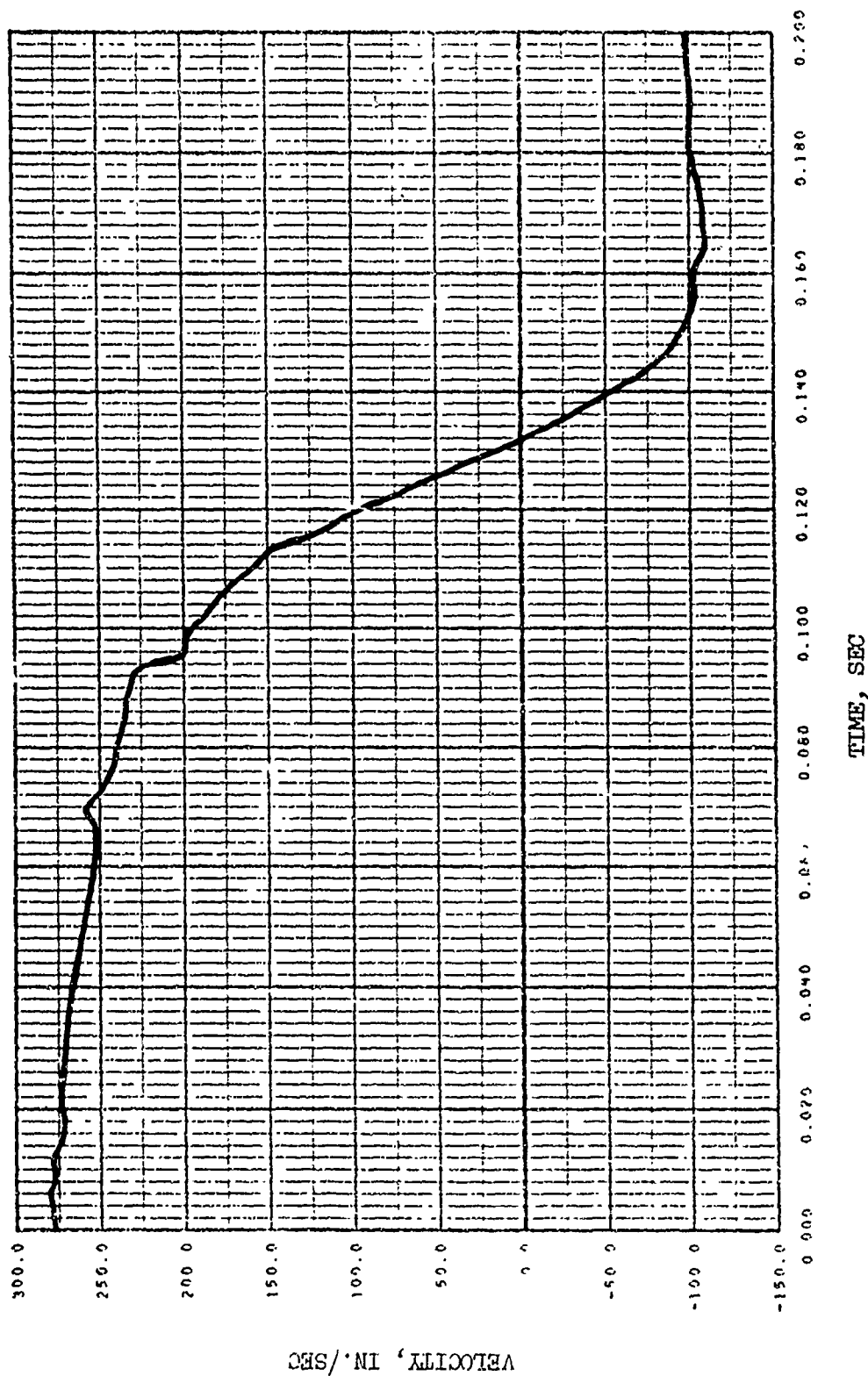


Figure 90. Correlation Run Analysis Output, Aft Floor, Vertical Velocity Time History.

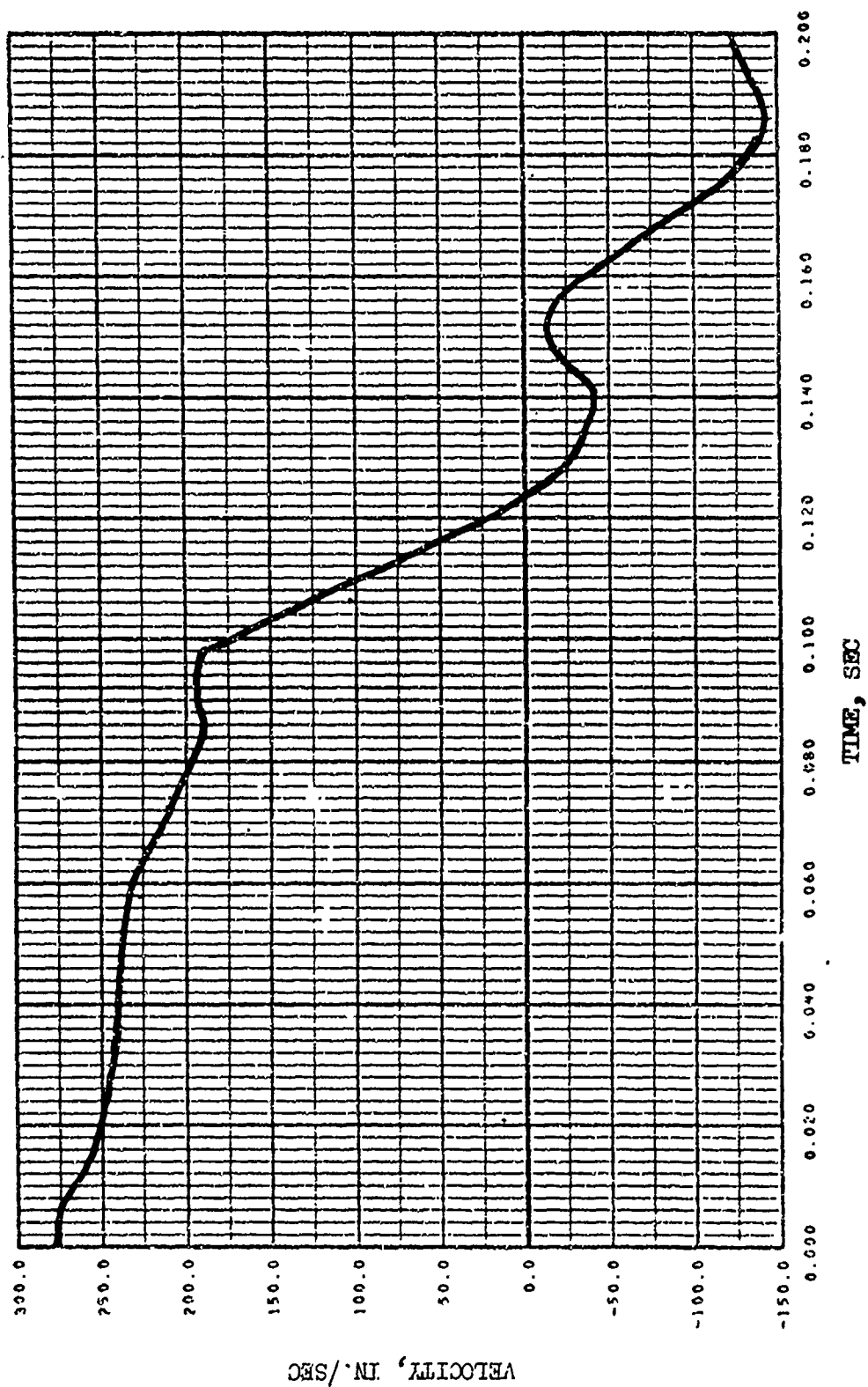


Figure 91. Correlation Run Analysis Output, Forward Floor, Vertical Velocity Time History.

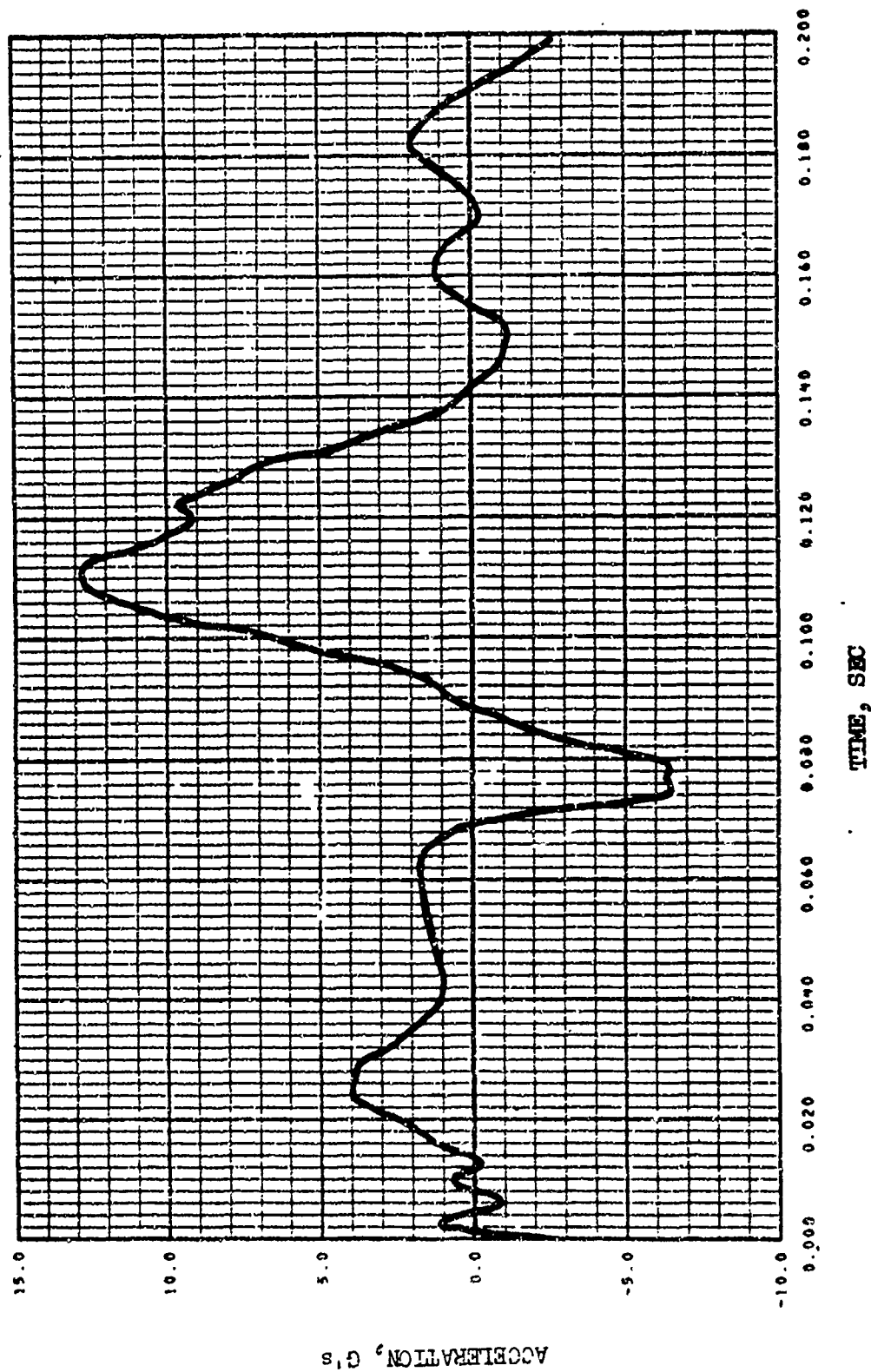


Figure 92. Correlation Run Analysis Output, Engine, Lateral Acceleration Time History.



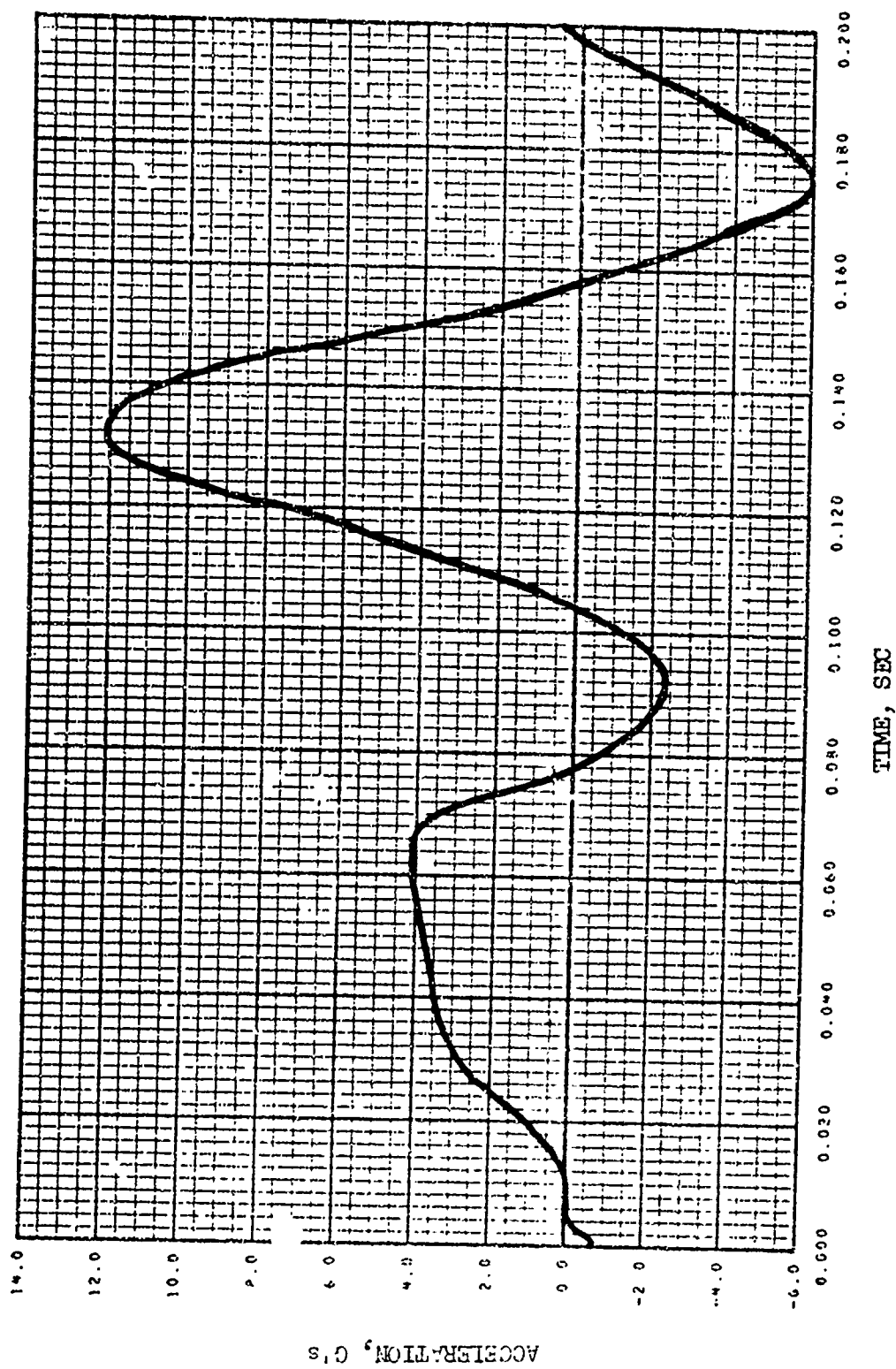


Figure 93. Correlation Run Analysis Output, Transmission Rotor Housing, Lateral Acceleration Time History.

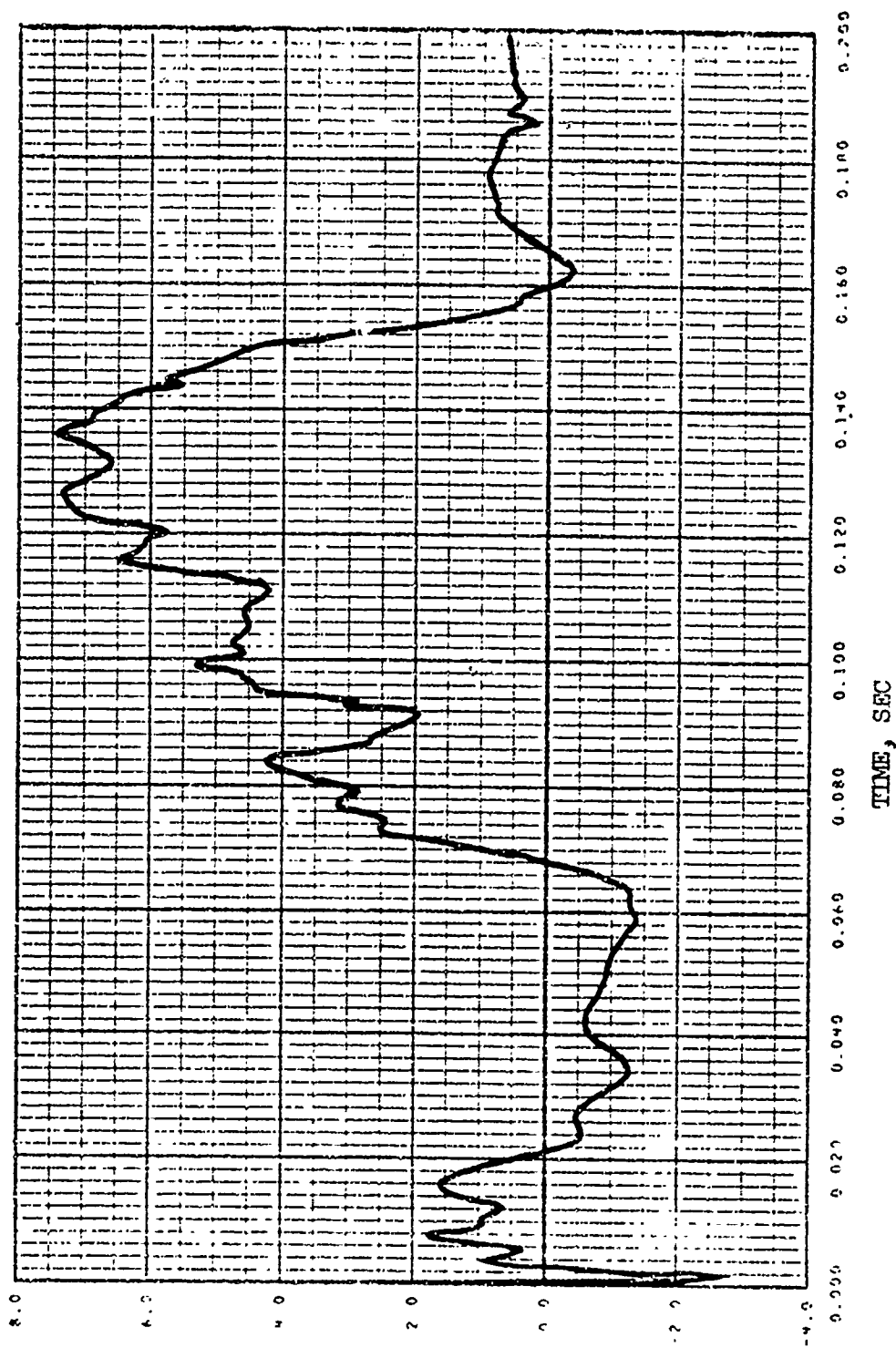


Figure 9h. Correlation Run Analysis Output, Mid-Floor, Lateral Acceleration Time History.

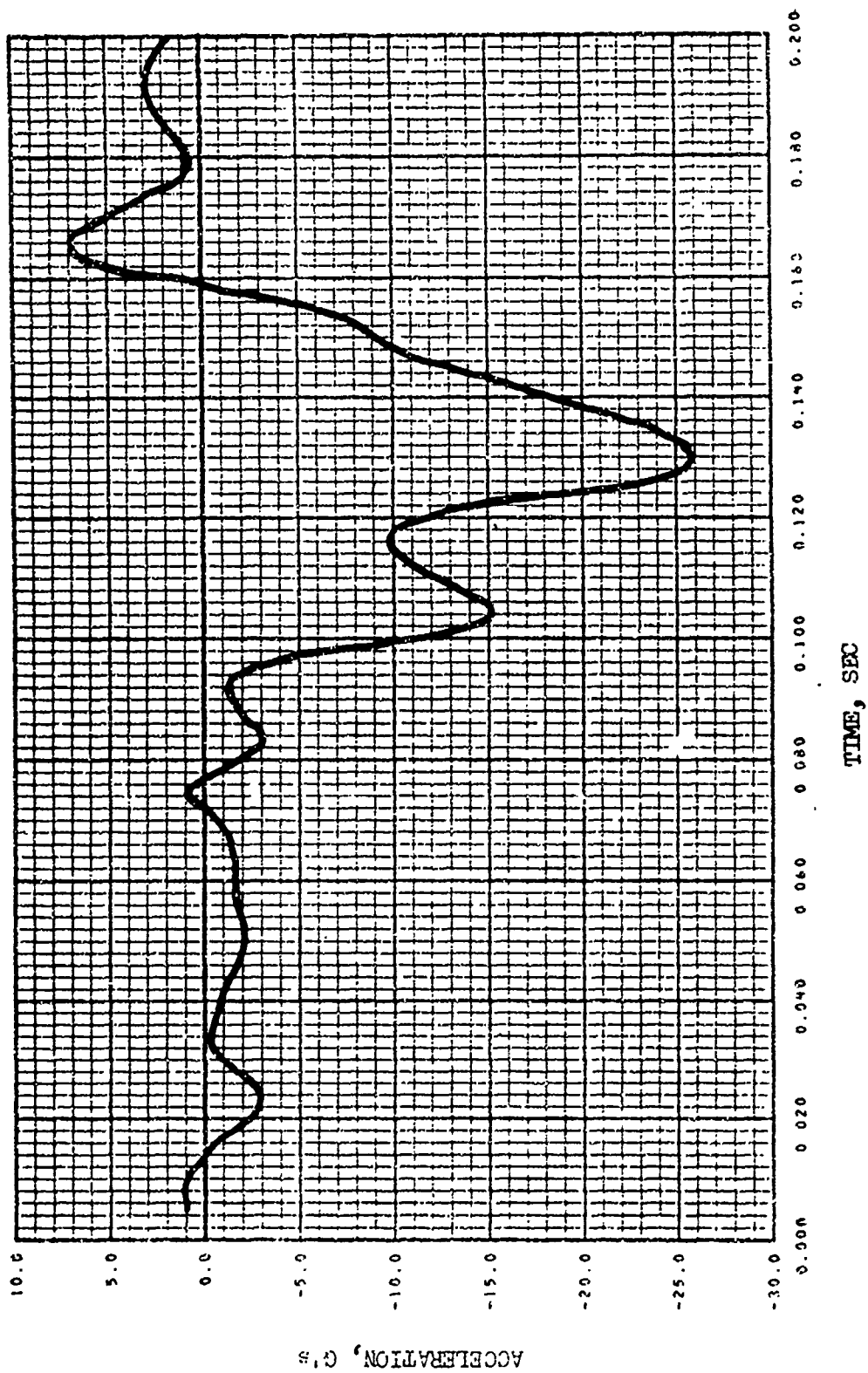


Figure 95. Correlation Run Analysis Output, Engine, Vertical Acceleration Time History.

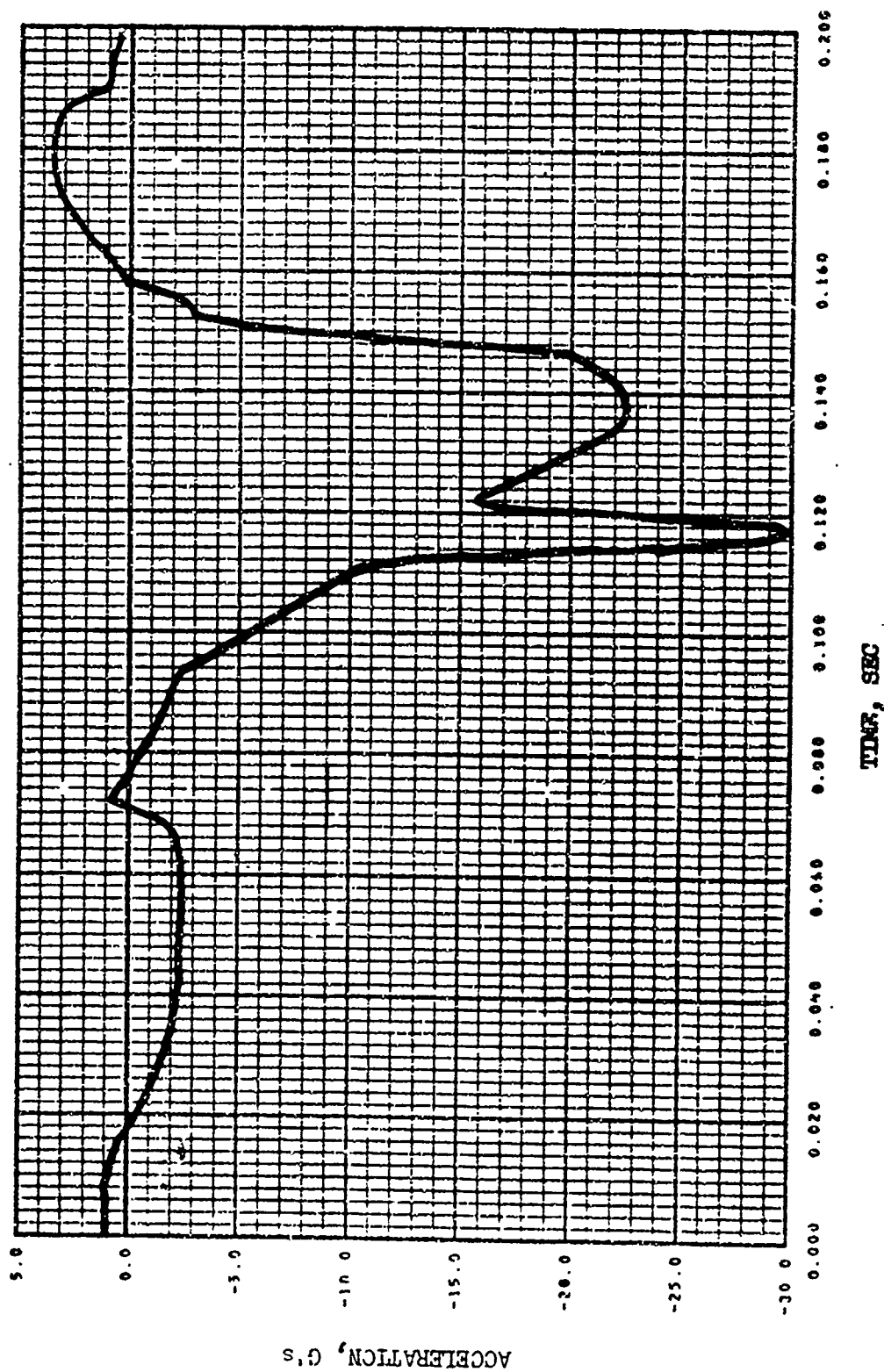


Figure 96. Correlation Run Analysis Output, Transmission Rotor Housing, Vertical Acceleration Time History.

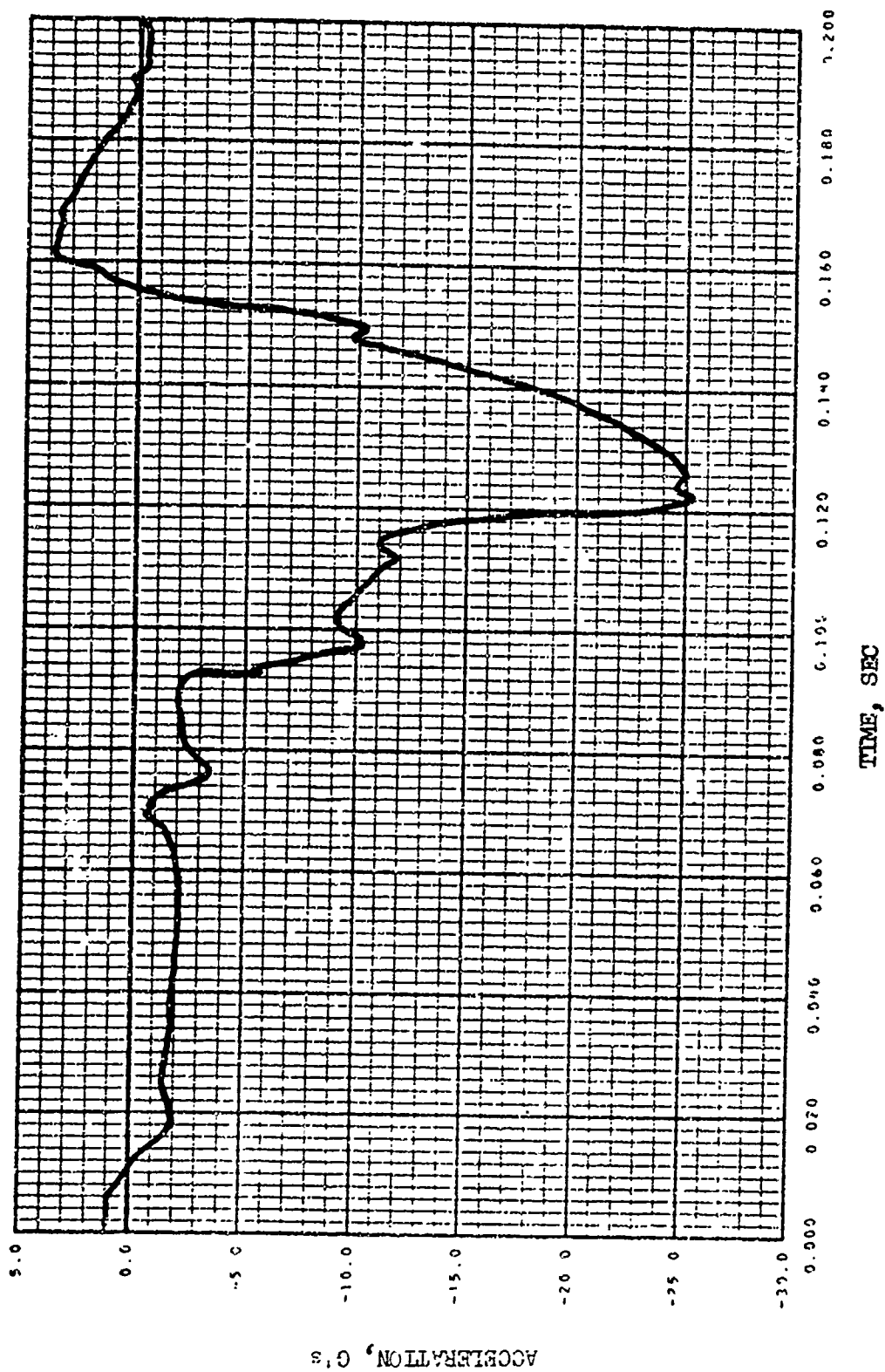


Figure 97. Correlation Run Analysis Output, Mid-Floor, Vertical Acceleration Time History.

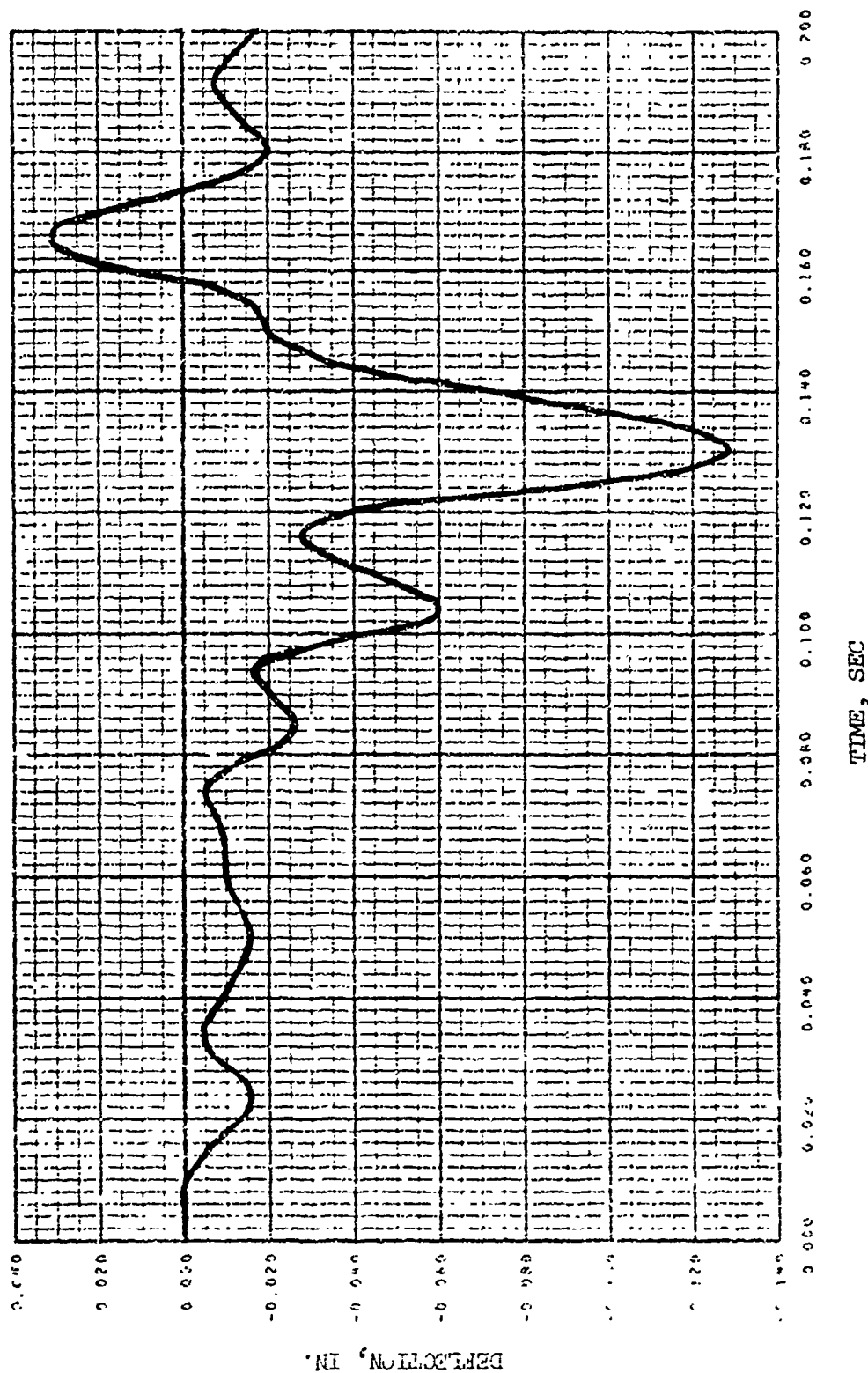


Figure 98. Correlation Run Analysis Output, Engine Mount, Vertical Deflection Time History.

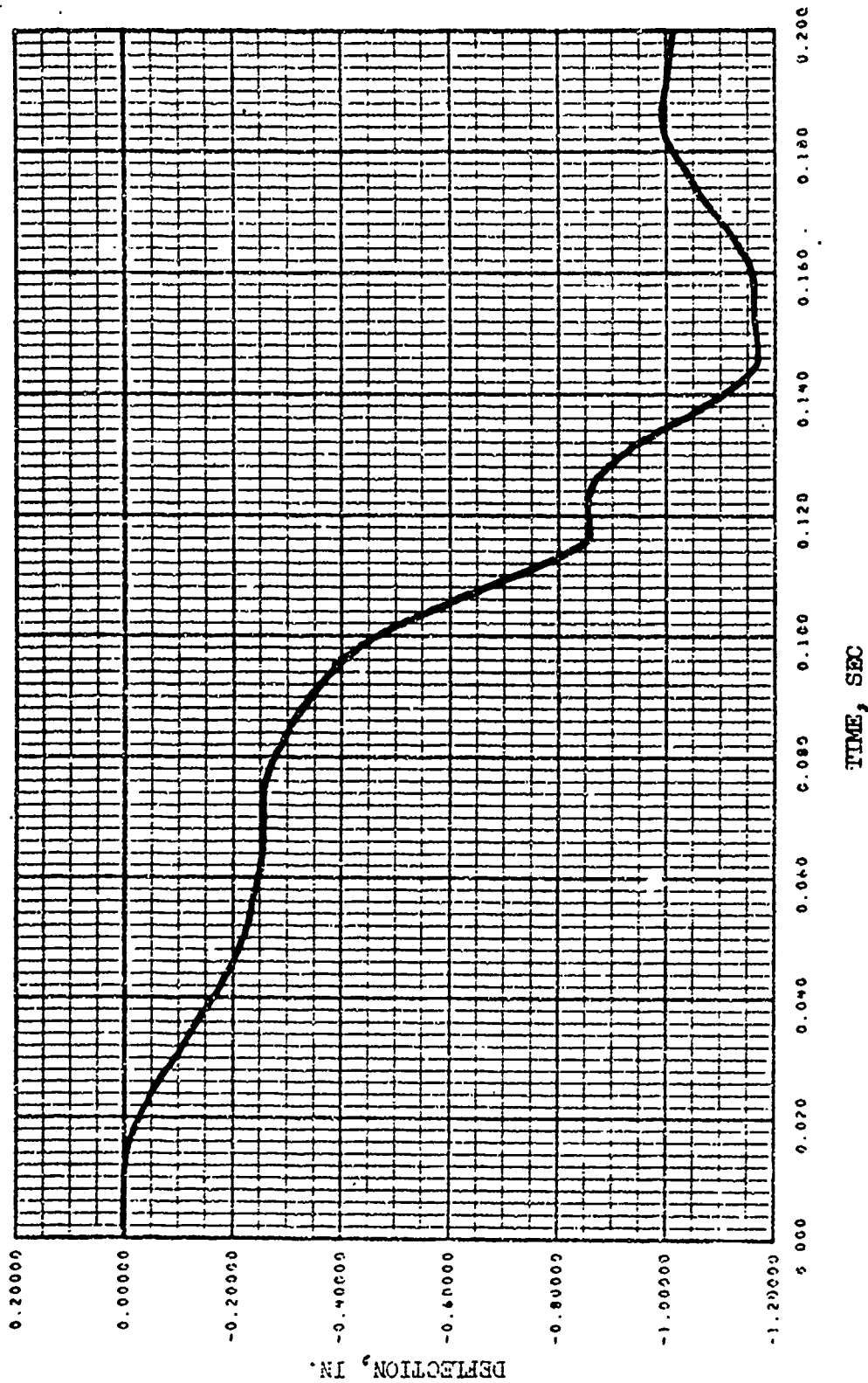


Figure 99. Correlation Run Analysis Output, Transmission Mount, Vertical Deflection Time History.

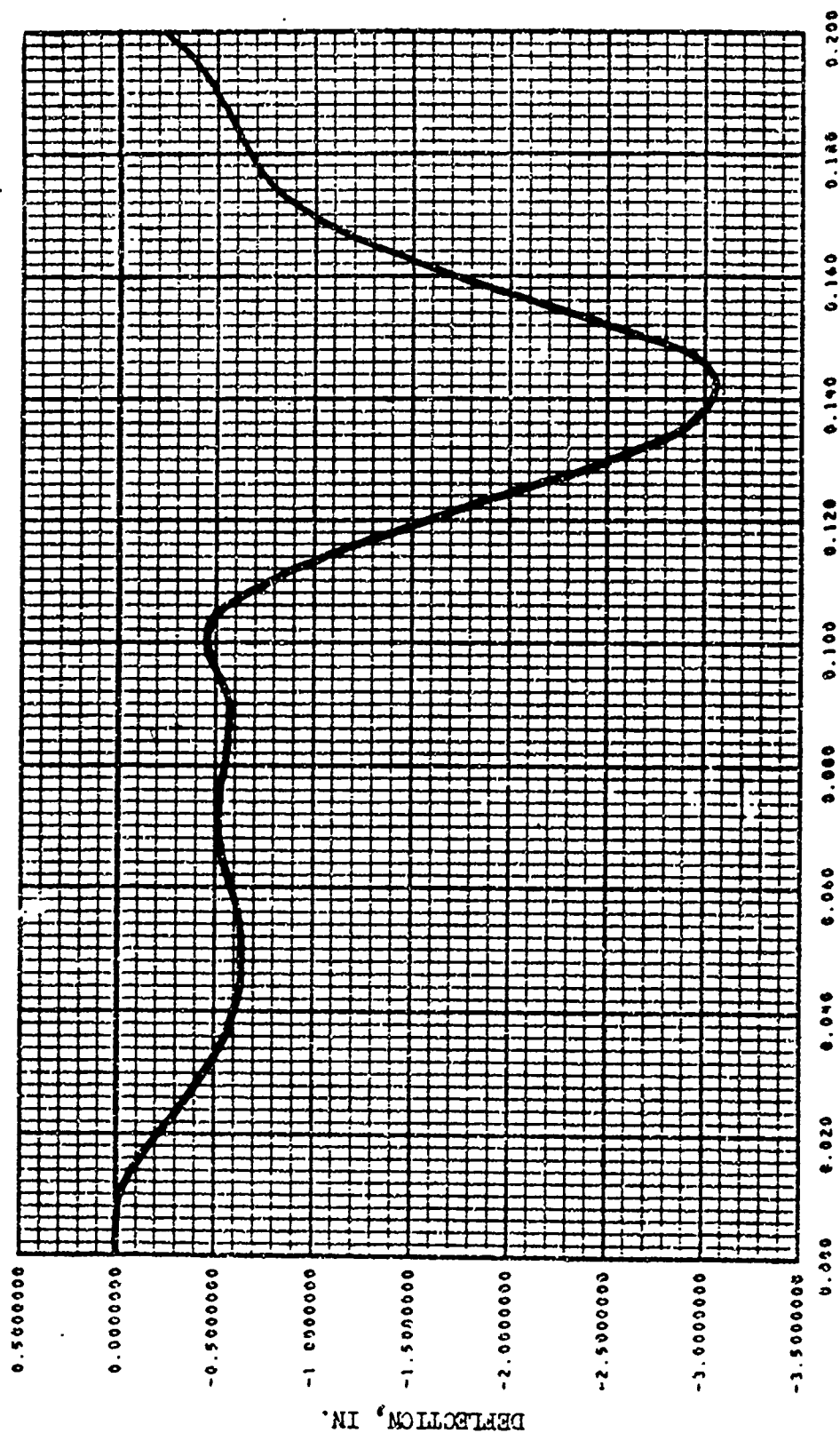


Figure 100. Correlation Run Analysis Output, Forward Seated Occupant, Vertical Deflection Time History.



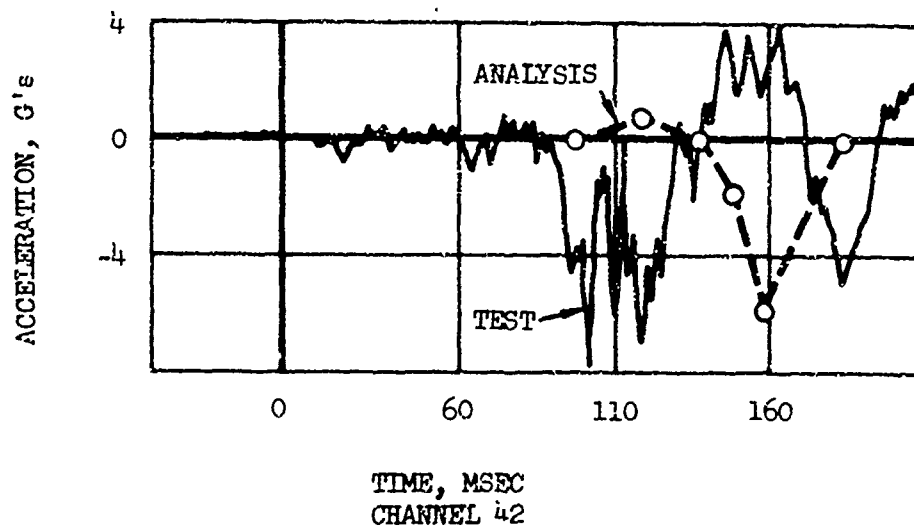


Figure 101. Correlation, Transmission Rotor Housing Axial Acceleration.

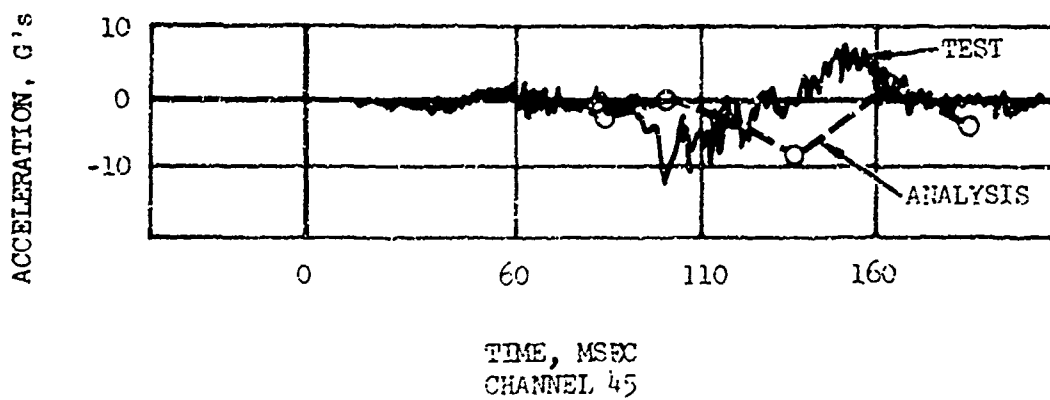


Figure 102. Correlation, Engine Axial Acceleration.

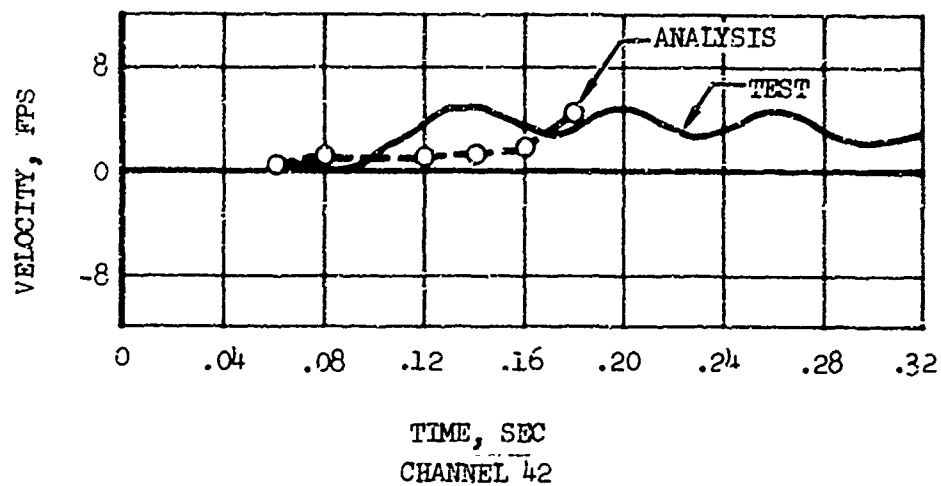


Figure 103. Correlation, Transmission Rotor Housing Axial Velocity.

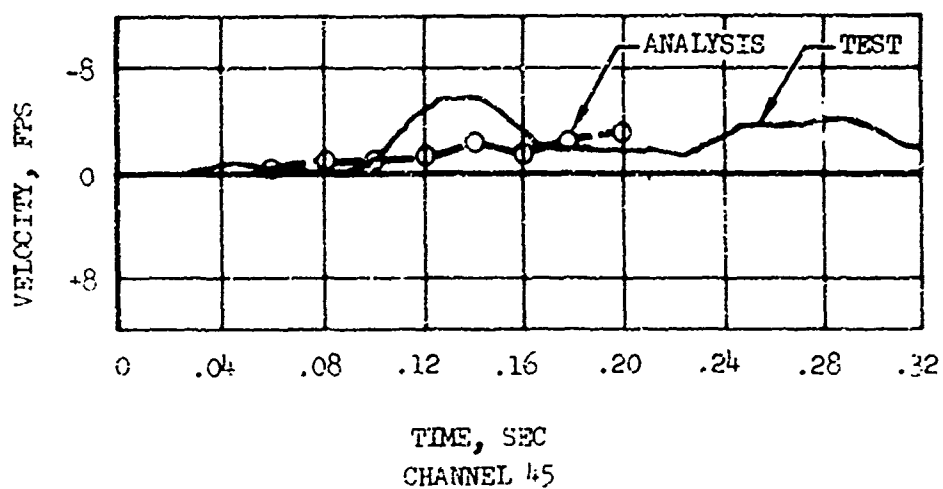


Figure 104. Correlation, Engine Axial Velocity.

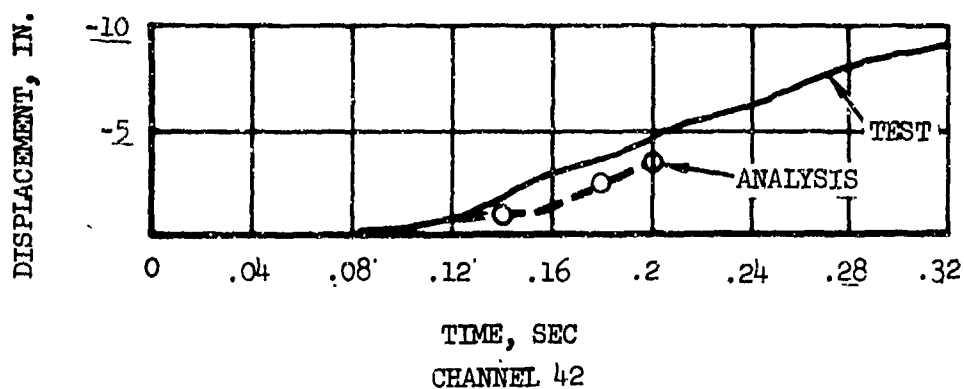


Figure 105. Correlation, Transmission Rotor Housing Axial Displacement.

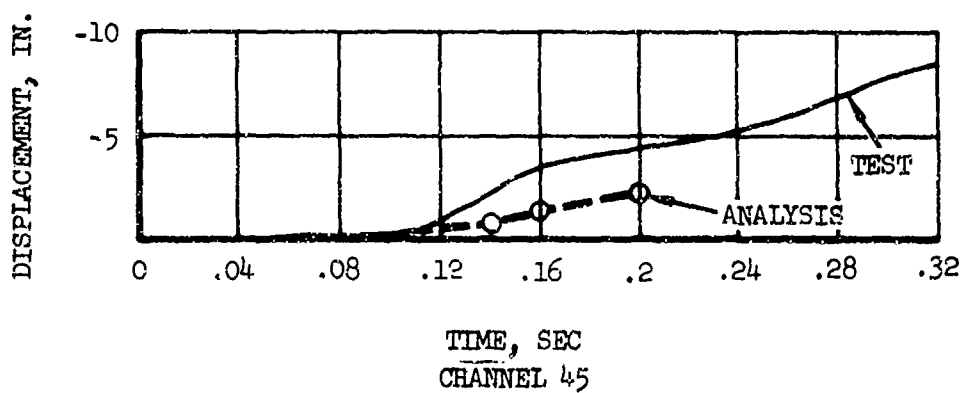


Figure 106. Correlation, Engine Axial Displacement.

### LITERATURE CITED

1. Reed, William, Avery, James Ph.D., PRINCIPALS FOR IMPROVING STRUCTURAL CRASHWORTHINESS FOR STOL AND CTOL AIRCRAFT, Aviation Safety Engineering and Research; USAAVIABS Technical Report 66-39, U. S. Army Aviation Materiel Laboratories, Fort Eustis, Virginia, June 1966, AD 637133.
2. Turnbow, J. W., Carrol, D. F., Haley, J. L., Jr Robertson, S. N., CRASH SURVIVAL DESIGN GUIDE, Dynamic Science; USAAVIABS Technical Report 70-22, U.S. Army Aviation Materiel Laboratories, Fort Eustis, Virginia August 1969, AD 695648. (Most recent revision is USAAMFDL TR 71-22, AD 733358).
3. Gatlin, Califfor; Goebel, Donald; and Larsen, Stuart; ANALYSIS OF HELICOPTER STRUCTURAL CRASHWORTHINESS, Dynamic Science; USAAVIABS Technical Report 70-71, Eustis Directorate, U. S. Army Air Mobility Research and Development Laboratory, Fort Eustis, Virginia, January 1971, AD 880680 and AD880678.
4. Greer, D. L., et al, CRASHWORTHY DESIGN PRINCIPLES, General Dynamics, Convair; FAA Technical Report ADS-24, Federal Aviation Administration, Washington, D. C., November 1965, AD 623575.
5. Reed, W. H., et al, FULL SCALE DYNAMIC CRASH TEST OF A DOUGLAS DC-7 AIRCRAFT, Aviation Safety Engineering and Research; FAA Technical Report ADS-37, Federal Aviation Administration, Washington, D. C., April 1965, AD 624051.
6. Reed, W. H., et al, FULL-SCALE DYNAMIC CRASH TEST OF A LOCKHEED CONSTELLATION MODEL 1649 AIRCRAFT, Aviation Safety Engineering and Research; FAA Technical Report ADS-38, Federal Aviation Administration, Washington, D. C., October 1965.
7. Fitzgibbon, Donald P., et al, CRASH LOADS ENVIRONMENT STUDY, Mechanics Research, Inc.; FAA Technical Report DS-67-2, Federal Aviation Administration, Washington, D.C., February 1967, AD 655920.
8. Greer, D. L., et al, DESIGN STUDY AND MODEL STRUCTURES TEST PROGRAM TO IMPROVE FUSELAGE CRASHWORTHINESS, General Dynamics, Convair; FAA Report DS-67-20, Federal Aviation Administration, Washington, D. C., October 1967.
9. Bigham, James P., and Bingham, William W., THEORETICAL DETERMINATION OF CRASH LOADS FOR A LOCKHEED 1649 AIRCRAFT IN A CRASH TEST PROGRAM, Boeing Airplane Company; FAA Technical Report ADS-15, Federal Aviation Administration, Washington, D. C., July 1964.

LITERATURE CITED (CONTINUED)

10. Turnbow, J. W., Ph.D., A DYNAMIC TEST OF AN H-25 HELICOPTER, Aviation Crash Injury Research Division; SAE Report 517A, National Aeronautic Meeting, April 1962.
11. Ieredaht, B. H., et al, SOME NOTES ON THE PHYSIOLOGICAL TOLERANCE TO ACCELERATION, Douglas Aircraft Company, Report ES 40253, February 1961.
12. Stech, Ernest, and Payne, Peter, DYNAMIC MODELS OF THE HUMAN BODY, Frost Engineering Development Company; AMRL-TR-66-157, Aerospace Medical Research Laboratory, Wright-Patterson Air Force Base, Ohio, November 1969, AD 701 383.
13. PERSONNEL RESTRAINT SYSTEMS STUDY, BASIC CONCEPTS, Flight Safety Foundation; TCREC Technical Report 62-94, Task 9R95-20-001-01, U. S. Army Transportation Research Command, Fort Eustis, Virginia, December 1962.
14. Coleman, Rolf R., THE MECHANICAL IMPEDANCE OF THE HUMAN BODY IN SITTING AND STANDING POSITION AT LOW FREQUENCIES, Biomedical Laboratory; ASD Technical Report 61-492, Aeronautical Systems Division, Wright-Patterson Air Force Base, Ohio, September 1961.
15. Eiband, Martin A., HUMAN TOLERANCE TO RAPIDLY APPLIED ACCELERATIONS: A SUMMARY OF THE LITERATURE, Lewis Research Center, NASA Memo 5-19-59E, National Aeronautics and Space Administration, Washington, D.C., June 1959.
16. O'Bryan, Thomas, and Hatch, Howard, Jr., LIMITED INVESTIGATION OF CRUSH-ABLE STRUCTURES FOR ACCELERATION PROTECTION OF OCCUPANTS OF VEHICLES AT LOW IMPACT SPEEDS, Langley Research Center, NASA-TN-D-158, National Aeronautics and Space Administration, Washington, D. C., October 1959.
17. UH-1 ACCIDENT SUMMARY, USABAAR Report, U. S. Army Board for Aviation Accident Research, Ft. Rucker, Alabama, 1963.
18. Mattox, Kenneth L., INJURY EXPERIENCE IN ARMY HELICOPTER ACCIDENTS, U. S. Army Board for Aviation Accident Research, Ft. Rucker, Alabama, September 1967, AD 658079.
19. Turnbow, James W., and Haley, J. L., Jr., A REVIEW OF CRASHWORTHY SEAT DESIGN PRINCIPLES, Arizona State University and AVSER Flight Safety Foundation, SAE Paper 851A, Air Transport and Space Meeting, April 1964.
20. Rich, M. J., VULNERABILITY AND CRASHWORTHINESS IN THE DESIGN OF ROTARY WING VEHICLE STRUCTURES, SAE Paper 680673, 1968.

LITERATURE CITED (CONTINUED)

21. Moseley, Harry, Colonel, et al, RELATION OF INJURY TO FORCES AND DIRECTION OF DECELERATION IN AIRCRAFT ACCIDENTS, Journal of Aviation Medicine, Vol. 29, October 1958.
22. Brinkley, James W., DEVELOPMENT OF AEROSPACE ESCAPE SYSTEMS, Air University Review, July-August 1968.
23. Weinberg, L. W. T., CRASHWORTHINESS EVALUATION OF AN ENERGY ABSORPTION EXPERIMENTAL TROOP SEAT CONCEPT, Aviation Safety Engineering and Research; USATRECOM Technical Report 65-6, U. S. Army Transportation Research Command, Fort Eustis, Virginia, February 1965, AD 614582.
24. Bruggink, G. M., and Schneider, D. J., M.D., LIMITS OF SEAT BELT PROTECTION DURING CRASH DECELERATIONS, Aviation Crash Injury Research; TCREC 61-115, U. S. Army Transportation Research Command, Fort Eustis, Virginia, September 1961, AD 265868.
25. Haley, J. L., HELICOPTER STRUCTURAL DESIGN FOR IMPACT SURVIVAL, U. S. Army Board of Aviation Accident Research, Ft. Rucker, Ala., November 1970.
26. Smith, H. G., and McDermott, J. M., DESIGNING FOR CRASHWORTHINESS AND SURVIVABILITY, Hughes Tool Co., American Helicopter Society Proceedings, November 1968.
27. Thompson, A. B., A PROPOSED NEW CONCEPT FOR ESTIMATING THE LIMIT OF HUMAN TOLERANCE TO IMPACT ACCELERATION, Aerospace Medical Journal, Vol. 33, No. 11, November 1962.
28. MIL-S-9479A, A GENERAL SPECIFICATION FOR AIRCRAFT UPWARD EJECTION SEAT SYSTEM, Amended December 1969.
29. MIL-T-27422B AIRCRAFT CRASH RESISTANT FUEL TANK MILITARY SPECIFICATION, Amended February 1970.
30. MIL-S-8698, HELICOPTER STRUCTURAL DESIGN REQUIREMENTS MILITARY SPECIFICATION, July 1954.
31. MIL-S-58095, GENERAL MILITARY SPECIFICATION FOR AIRCREW NON EJECTION CRASHWORTHY SEAT SYSTEM, August 1971.
32. Haley, J., PRELIMINARY DRAFT, COST EFFECTIVENESS OF CRASHWORTHY STRUCTURAL FEATURES IN A 9-13 PLACE HELICOPTER, USAAAVG, Technical Report 72-1, U.S. Army Agency for Aviation Safety, Ft. Rucker, Ala.

LITERATURE CITED (CONTINUED)

33. Haley, J., ANALYSIS OF HELICOPTER ACCIDENTS TO DEFINE IMPACT INJURY PROBLEMS, USAAAVS Report To Be Published, U. S. Army Agency For Aviation Safety.
34. STATIC TEST OF FUSELAGE TAIL BUMPER, Lockheed Aircraft Corporation, SRM 148, August 1948.
35. Phillips, N. S., A STATISTICAL EVALUATION OF THE INJURY POTENTIAL OF A "SQUARE WAVE" ENERGY ABSORBER, Beta Industries, USAAMRDL Technical Report 72-9, U. S. Army Air Mobility Research and Development Laboratory, Ft. Eustis, Virginia.
36. Carr, R. W., Phillips, N. S., DEFINITION OF DESIGN CRITERIA FOR ENERGY ABSORPTION SYSTEMS, Beta Industries Inc., NADC Report AC-7010, Naval Air Devel. Center, Johnsville, Warminster, Pa., June 1970, AD 871-040.
37. RFP DAAJ02-72-R-0254 UTILITY TACTICAL TRANSPORT AIRCRAFT SYSTEM, U. S. Army Aviation Systems Command, St. Louis, Mo., December 1971.
38. Timoshenko, S. P., THEORY OF ELASTIC STABILITY, McGraw-Hill Book Company, 1961.
39. Hoff, N. J., THE DYNAMICS OF THE BUCKLING OF ELASTIC COLUMNS, Journal of Applied Mechanics, March 1951, pages 68 - 74, Vol. 18.
40. Bell Helicopter Company Report 205-099-004, UNIT INERTIA LOADS - WEIGHT AND INERTIA DISTRIBUTION DATA.
41. Harris, C. M., Crede, C. E., VIBRATION AND SHOCK HANDBOOK, VOLUME 1, Chapter 8, McGraw Hill Book Company, 1961.
42. Lockheed Missile and Space Company, Inc. (IMSC), STAG'S USERS MANUAL, 0032008.
43. Etkin, B., DYNAMICS OF FLIGHT, John Wiley and Sons, Inc., 1959.
44. Bell Helicopter Company Report 205-099-403, STATIC TESTS OF THE UH-1D.
45. Bell Helicopter Company Report 205-099-991, BASIC STRUCTURAL DESIGN CRITERIA.
46. Bell Helicopter Company Report 205-099-003, STRUCTURAL DESCRIPTION REPORT.
47. Bell Helicopter Company Report 205-099-007, STRESS AND LOADS ANALYSIS.
48. Bell Helicopter Company Report 205-099-401, SKID GEAR DROP TESTS.